Effect of induced condensing agents on ethylene polymerization in gas-phase reactors

Amel Ben Mrad

N°d'ordre NNT : 2020LYSE1312

THESE de DOCTORAT DE L'UNIVERSITE DE LYON
opérée au sein de
l'Université Claude Bernard Lyon 1

Ecole Doctorale ED206
Chimie de Lyon

Spécialité de doctorat : Polyolefin Reaction Engineering
Discipline : Génie des procédés

Soutenue publiquement le 11/12/2020, par :
Amel BEN MRAD

Effect of Induced Condensing Agents on Ethylene Polymerization in Gas-Phase reactors

---

Devant le jury composé de :

KIPARISSIDES, Costas Professeur, Université Aristote de Thessalonique, Grèce	**Rapporteur**
MORENO VOZMEDIANO, Jovita Professeure, Université Rey Juan Carlos, Espagne	**Rapporteure**
CERMELLI, Isabelle Directrice R&D, Ineos (Martigues), France	**Examinatrice**
FONGARLAND, Pascal Professeur, Université Lyon 1, CNRS, France	**Examinateur**
MCKENNA, Timothy Directeur de recherche, CNRS, France	**Directeur de thèse**
SHEIBAT-OTHMAN, Nida Directrice de recherche, CNRS, France	**Co-directrice de thèse**

Université Claude Bernard – LYON 1

Administrateur provisoire de l'Université	M. Frédéric FLEURY
Président du Conseil Académique	M. Hamda BEN HADID
Vice-Président du Conseil d'Administration	M. Didier REVEL
Vice-Président du Conseil des Etudes et de la Vie Universitaire	M. Philippe CHEVALLIER
Vice-Président de la Commission de Recherche	M. Jean-François MORNEX
Directeur Général des Services	M. Pierre ROLLAND

COMPOSANTES SANTE

Département de Formation et Centre de Recherche en Biologie Humaine	Directrice : Mme Anne-Marie SCHOTT
Faculté d'Odontologie	Doyenne : Mme Dominique SEUX
Faculté de Médecine et Maïeutique Lyon Sud - Charles Mérieux	Doyenne : Mme Carole BURILLON
Faculté de Médecine Lyon-Est	Doyen : M. Gilles RODE
Institut des Sciences et Techniques de la Réadaptation (ISTR)	Directeur : M. Xavier PERROT
Institut des Sciences Pharmaceutiques et Biologiques (ISBP)	Directrice : Mme Christine VINCIGUERRA

COMPOSANTES & DEPARTEMENTS DE SCIENCES & TECHNOLOGIE

Département Génie Electrique et des Procédés (GEP)	Directrice : Mme Rosaria FERRIGNO
Département Informatique	Directeur : M. Behzad SHARIAT
Département Mécanique	Directeur M. Marc BUFFAT
Ecole Supérieure de Chimie, Physique, Electronique (CPE Lyon)	Directeur : Gérard PIGNAULT
Institut de Science Financière et d'Assurances (ISFA)	Directeur : M. Nicolas LEBOISNE
Institut National du Professorat et de l'Education	Administrateur Provisoire : M. Pierre CHAREYRON
Institut Universitaire de Technologie de Lyon 1	Directeur : M. Christophe VITON
Observatoire de Lyon	Directrice : Mme Isabelle DANIEL
Polytechnique Lyon	Directeur : Emmanuel PERRIN
UFR Biosciences	Administratrice provisoire : Mme Kathrin GIESELER
UFR des Sciences et Techniques des Activités Physiques et Sportives (STAPS)	Directeur : M. Yannick VANPOULLE
UFR Faculté des Sciences	Directeur : M. Bruno ANDRIOLETTI

Remerciements

Je souhaiterai en premier lieu remercier le laboratoire CP2M de m'avoir accueillie ainsi que l'Agence Nationale de la Recherche (ANR) pour le financement de cette thèse.

Je souhaite également remercier les membres du jury d'avoir accepté de faire partie du jury et d'avoir contribué à une discussion très enrichissante. Je remercie infiniment M. Costas Kiparissides ainsi que Mme Jovita Moreno Vozmediano d'avoir accepté d'examiner mon travail de thèse, Mme Isabelle Cermelli d'avoir accepté de participer à la soutenance de thèse et M. Pascal Fongarland d'avoir accepté de présider le jury et d'avoir évaluer mon travail.

Cette thèse intitulée « Thermopoly » a fait l'objet d'une collaboration Franco-Suisse avec l'ETH Zurich, que je tiens aussi à remercier. Je remercie en particulier à M. Guiseppe Storti et M. Tommaso Casalini pour cette collaboration et pour vos idées fructueuses.

Je tiens aussi à remercier Dr. Michael Bartke de m'avoir acceuilli dans son laboratoire à Martin-Luther Universität à Halle en Allemagne et de m'avoir permis de faire des expériences sur une balance magnétique à suspension. Je tiens en particulier à remercier ses doctorants, Jorik Hill et Sina Valaei qui m'ont formé et rendu la vie moins compliquée à Halle. Merci pour tous vos conseils et votre bonne humeur.

J'adresse maintenant mes remerciements les plus sincères à mes encadrants de thèse sans qui rien de tout cela n'aurait été accompli. Je vous remercie pour votre implication, vos conseils et votre grande disponibilité. Je vous suis tellement reconnaissante pour la formation que vous m'avez offerte. Tim, je te remercie d'avoir été non seulement un encadrant de thèse mais aussi un ami. Merci pour tous les moments qu'on a partagés, toutes ces réunions toutes aussi enrichissantes les unes que les autres, tous les conseils que tu m'as donné, et surtout merci de m'avoir permis d'avoir confiance en moi. Merci aussi pour ton côté humain, tes conseils qui m'ont permis de me forger petit à petit et surtout merci d'être venu à mon mariage à Lyon et à Tunis, ce geste m'a beaucoup touché. Nida, je te remercie pour tout ton dévouement pendant ma thèse, ta passion pour mon sujet. Tu m'as appris tant de choses, et surtout en modélisation et je t'en remercie. Tu as toujours su avoir les bons mots pour m'encourager, féliciter mon travail lorsqu'il le fallait.

Ce travail n'aurait pas été possible sans Sebastien Norsic, mon bff, que je remercie infiniment. Tu as participé grandement au projet, humainement et scientifiquement, et je t'en suis reconnaissante. Je te remercie de m'avoir formée à souffrir, et le tout dans la bonne humeur. Aujourd'hui, je sais monter des réacteurs, et faire de la tuyauterie grâce à toi.

Je tiens à remercier tous les membres du CP2M grâce à qui j'ai vécu une expérience humaine inoubliable. Merci pour tous ces moments qu'on a partagés, l'amigo-secreto, les repas de Noël, la chandeleur, les escapes-game, le ski, les repas internationaux, les restos, les bowlings, les soirées vin/fromage, les sorties au parc, les afterworks et toutes les soirées.

Je remercie tout d'abord Nathalie, la petite maman du labo qui prend soin de tout le monde. Merci pour toutes les discussions qu'on a eues, tu as toujours eu de bons conseils. Merci aussi de m'avoir fait connaitre les animaux de la ferme, je transmettrai ça à mes enfants !

Je remercie également mes co-bureau pour cette bonne humeur et tous les agréables moments passés ensembles. Merci à Rita avec qui on a partagé beaucoup de moments ensembles, beaucoup de discussions scientifiques aussi. Merci de m'avoir formé au départ, tu m'as appris tellement de choses. Je te remercie aussi car j'avais continuellement un modèle de force et de courage à mes côtés. Saches que je serais toujours là pour toi. Je n'oublierais jamais tous les moments et les voyages qu'on a fait ensemble (Amsterdam, Maastricht, Hambourg). Je remercie également Manel pour tous les moments passés ensembles, ces discussions qui pouvaient durer des après-midis. Ces trois années de thèse auraient été bien plus tristes sans toi dans ce bureau. Tu m'as toujours réconforté et donné de bons conseils, et surtout fait rire. Merci pour tout, tu vas me manquer. Enfin, merci à Frank pour toute cette bonne humeur au bureau, pour tous ces moments de partage. On t'aura apporté toute la chaleur tunisienne avec Manel, j'espère que ça ne va pas trop te manquer. Merci aussi à Kusuma, que j'ai connu malheureusement trop tard, pour ta gentillesse. Enfin un grand merci à Camille, arrivée bien trop tard au bureau, mais avec qui j'ai eu d'agréable discussions, et beaucoup de fous-rires. Merci pour ta bonne humeur.

Je tiens à remercier tous les doctorants du laboratoire, et en particulier « les vrais », Doudou, James, Rémi, Florian, Paul et Mathieu. Ma thèse n'aurait pas été pareil sans vous. Merci pour tous ces bons moments passés ensembles, les pauses café, toutes ces soirées à pas d'heure, tous ces afterworks. Je vous remercie pour votre gentillesse, votre bienveillance et votre bonne humeur. Je tiens aussi à remercier Priscilla, sans qui ma thèse et surtout ma dernière année aurait été bien plus déprimante. Merci d'avoir été là pour moi, de m'avoir entendu râler tellement de fois, de m'avoir remonté le moral et merci aussi pour ta bonne humeur. Merci à Aurélien pour ta gentillesse et ton sens du partage. Merci à Priss, Aurélien, Cédric et Rémi pour toutes les soirées jeux où je vous ai gagné et vu ragé. Je tiens à remercier Astrid pour la bonne ambiance au labo, et pour ta joie de vivre. Merci à Mathieu, Juliette et Maxime pour toutes ces soirées qu'on a passé ensemble. Merci à Fabiana et Yashmin d'avoir été là pendant ces trois ans, j'ai vécu plein de bons moments avec vous. Merci à Alice, Marie, Ambroise pour toutes les pauses café et les afterworks. Je remercie également Raman pour ta gentillesse et ta bienveillance, merci d'avoir toujours su trouver les mots justes, tu as été une belle découverte. Merci à Niyi avec qui j'ai beaucoup travaillé, merci d'avoir accepté de faire des expériences pour moi à la dernière minute, et j'espère que mon bébé réacteur se porte bien avec toi. Je remercie également Léo qui a fait un stage sur une partie de mon sujet de thèse, et qui m'a aidé à générer d'avantages de résultats, merci pour ton travail. Enfin merci à Anderson, Barbara et Aaron avec qui j'ai commencé ma thèse, on a passé tellement de moments agréables ensemble, surtout à Maastricht. Je remercie également tous les autres doctorants et post-doc pour cette bonne ambiance au laboratoire.

Enfin je tiens à remercier tous les permanents du laboratoire ; Jean, Damien, Vincent, Olivier, Frank, Muriel, Christophe, Elodie, Pierre-Yves et Fabrice. Vous avez tous participé directement ou indirectement à la réalisation de ma thèse. Merci de m'avoir aidé quand j'en avais besoin, de m'avoir écouté ou de m'avoir fait rire. Enfin, merci Edgar pour ta bienveillance inconditionnelle.

Avec toute la reconnaissance du monde, je souhaite dédier cette thèse à ma mère et mon père sans qui rien de tout cela n'aurait été possible. Ils m'ont donné toute la force et le courage pour ne jamais baisser les bras et toujours donner le meilleur de moi-même. Le maître mot a toujours

été le travail, et je vous remercie de m'avoir inculqué ces valeurs. Tout ce travail je l'ai fait grâce à vous, et il n'y a rien de plus beau que la fierté des parents.

Je tiens à remercier mes sœurs, Ines et Imen, qui ont toujours eu les mots juste pour me pousser à aller de l'avant et à puiser dans mes ressources sans jamais abandonner. Je vous remercie de m'avoir toujours encouragé et soutenu dans tout ce que j'ai entrepris, d'avoir toujours pu compter sur vous, et de voir toute la fierté que vous me portez au quotidien. Vous êtes mes piliers.

Je remercie également mon mari, Ouassim, qui a toujours été là pour moi pendant ces trois ans. Tu as vécu tous les bons et mauvais côtés de cette thèse, et je te remercie d'avoir toujours su comment me remonter le moral et d'avoir autant pris soin de moi.

Je remercie ma tante, Samia, avec qui j'ai commencé cette aventure en France. Merci d'avoir toujours été là pour moi, de faire autant attention à moi, et merci pour tout l'amour que tu me portes.

Enfin, je tiens à remercier toutes les personnes qui, de près ou de loin, ont contribué à la réalisation et à la concrétisation de ce projet. Je tiens à remercier Amina, ma troisième sœur, qui a toujours été là pour moi, et qui m'a toujours soutenu. Je tiens aussi à remercier mes ami(e)s, et en particulier Lina, Yasmine, Ines, Sirine, Akram pour vos encouragements et votre soutien au quotidien qui m'ont permis de finaliser mes travaux malgré les moments de difficultés rencontrés. Merci aussi pour tous ces moments qu'on a vécu durant ma thèse qui m'ont permis de m'évader (mon mariage, mon EVJF, toutes les soirées..)

ABSTRACT

An experimental and theoretical study of the impact of induced condensing agents (ICAs) on ethylene polymerization in gas phase reactors is presented. In order to overcome the lack of thermodynamic data for multicomponent systems, a novel approach is proposed for the estimation of the Sanchez-Lacombe interaction parameters. This method is based on combining total solubility measurements with estimates of the compressibility factor of gas mixtures using the Peng-Robinson Equation of State (PR EoS). Following this, a new experimental set-up based on the pressure decay method was built to estimate the partial solubilities of each component in ternary and quaternary (and higher order) systems in order to show the impact of both ICAs and comonomers on ethylene polymerization in gas phase. The quaternary Sanchez-Lacombe model has been validated with experimental data through gravimetric (total solubilities) and pressure decay (partial solubilities) methods.

Subsequently, the overall diffusivity of ternary and quaternary systems have been measured with the gravimetric method, and fitted to Crank's solution to Fick's law using a two-level particle representation. Individual solubilities are used to calculate multicomponent diffusivities through Vrentas and Duda model, in order to validate the experimental data.

All these thermodynamic data are incorporated into a single particle model. The random pore polymer flow model (RPPFM) has been developed in order to look at the impact of different ICAs on the temperature and concentration gradients throughout the growing polymer particles, as well as the reaction rate. The Sanchez-Lacombe EoS has been used in this model in order to calculate the solubility in multicomponent systems, and together with the multicomponent diffusivities, it allowed us to show the impact of the gas phase composition (i.e. ICA, hydrogen) on kinetics and molecular weight distributions.

Finally, the thermodynamics of ethylene polymerization in slurry phase has also been studied, since as in gas phase systems, the polymerizing particles will swell in the slurry phase. An experimental study has been performed in order to measure the solubility and the swelling in presence of different diluents (C4-C10) in various polymer grades.

Key words: polyethylene, Induced Condensing Agents (ICA), Sanchez-Lacombe equation of state (SL EoS), solubility, diffusivity, Random-Pore Polymer Flow model (RPPFM), quaternary systems

RÉSUMÉ

Une étude expérimentale et théorique de l'impact des agents de condensation induits (ICA) sur la polymérisation de l'éthylène dans les réacteurs en phase gazeuse est présentée. Afin de pallier le manque de données thermodynamiques concernant les systèmes à plusieurs composants, une nouvelle approche est proposée permettant l'estimation des paramètres d'interaction de Sanchez-Lacombe. Cette méthode est basée sur la combinaison de mesures de solubilité totale avec des estimations du facteur de compressibilité des mélanges de gaz en utilisant l'équation d'état de Peng-Robinson (PR EoS). Suite à cela, une méthode expérimentale basée sur la perte de charge a été développée afin d'estimer les solubilités partielles des différents composés dans les systèmes ternaires et quaternaires (et d'ordre supérieur) afin de montrer l'impact des ICAs et des comonomères sur la polymérisation de l'éthylène en phase gazeuse. Le modèle quaternaire de Sanchez-Lacombe a été validé avec des données expérimentales par des méthodes gravimétriques (solubilités totales) et de perte de charge (solubilités partielles).

Par la suite, la diffusivité globale des systèmes ternaires et quaternaires a été mesurée avec la méthode gravimétrique et ajustée à la solution de Crank à la loi de Fick en utilisant une représentation de particules à deux niveaux. Les solubilités individuelles sont utilisées pour calculer les diffusivités à plusieurs composants à travers le modèle de Vrentas et Duda, afin de valider les données expérimentales.

Toutes ces données thermodynamiques sont incorporées dans un modèle de particule. Le modèle d'écoulement de polymère à pores aléatoires (RPPFM) a également été développé afin d'examiner l'impact de différents ICAs sur les gradients de température et de concentration à travers les particules de polymère en croissance, ainsi que sur la vitesse de la réaction. L'équation d'état de Sanchez-Lacombe a été utilisée dans ce modèle afin de calculer la solubilité dans des systèmes à plusieurs composants, et avec les diffusivités des systèmes à plusieurs composants, ils ont permis de montrer l'impact de la composition de phase gazeuse (i.e. ICA, hydrogène) sur la cinétique et la distribution des masses molaires.

Enfin, la thermodynamique de la polymérisation de l'éthylène en suspension a également été étudiée, car comme dans les systèmes en phase gazeuse, les particules de polymères sont supposées gonfler en présence de diluant liquides. Une étude expérimentale a été réalisée afin de mesurer la solubilité et le gonflement en présence de différents diluants liquides (C_4-C_{10}) dans divers types de polymères.

Mots-clés: polyéthylène, agents de condensation induits (ICA), équation d'état de Sanchez-Lacombe (SL EoS), solubilité, diffusivité, modèle d'écoulement de polymère à pores aléatoires (RPPFM), systèmes quaternaires

Résumé en français

En 2020, les polyoléfines sont la famille de polymères la plus utilisée au monde puisqu'ils représentent environ 45% de la production de matières plastiques dans le monde. Le marché mondial du polyéthylène devrait augmenter substantiellement à environ 150 millions de tonnes d'ici 2027[1,2]. En effet, le polyéthylène, objet de la thèse actuelle, est le polymère le plus produit sur la planète en raison de sa large gamme de propriétés et d'utilisations, de son faible coût de production et d'un impact environnemental relativement faible. Les polyéthylènes sont utilisés dans de nombreux domaines essentiels, comme par exemple l'électricité et l'électronique, l'emballage, l'automobile, les produits pharmaceutiques, le bâtiment et la construction[3].

Le polyéthylène peut être fabriqué dans des procédés en solution, en suspension et en phase gazeuse en utilisant de l'éthylène et très souvent un comonomère α-oléfine[4]. La polymérisation de l'éthylène sur un catalyseur supporté dans des réacteurs à lit fluidisé (FBRs) en phase gazeuse est le procédé prédominant pour la production d'environ 75% de polyéthylène linéaire basse densité (LLDPE) et 25% de polyéthylène haute densité (HDPE) dans le monde. Cependant, en raison de la nature hautement exothermique de la polymérisation, la vitesse maximale à laquelle cette chaleur peut être éliminée du réacteur est clairement une étape limitante dans la vitesse de production du polymère dans les réacteurs en phase gazeuse[5]. Le procédé en mode condensé est utilisé afin d'augmenter la capacité d'évacuation de la chaleur, permettant ainsi d'optimiser la productivité. En effet, en mode de fonctionnement condensé, en plus d'injecter de l'éthylène, de l'hydrogène, de l'azote, et éventuellement un comonomère; des solvants inertes, qui sont principalement des alcanes comme le propane, l'isobutane, le n-pentane ou le n-hexane, sont utilisés comme agents de condensation induits (ICAs)[6]. Ces alcanes permettent principalement d'évacuer la chaleur générée à l'intérieur du réacteur puisqu'ils sont partiellement liquéfiés dans un échangeur de chaleur externe puis pulvérisés à l'intérieur du réacteur. Toutes ces espèces présentes dans la phase gazeuse, inertes ou non, diffuseront dans la phase amorphe du polymère. Ils modifieront donc la structure physique et éventuellement chimique du polymère produit, qui à son tour peut influencer des paramètres importants tels que la vitesse de la réaction, par le biais du changement de la solubilité et de la diffusivité de ces espèces[7,8]. Afin de mieux contrôler et comprendre le processus de polymérisation, il est évidemment assez important de connaître avec précision la solubilité ainsi que la diffusivité des espèces individuelles dans la phase amorphe du polymère.

Jusqu'à présent, la plupart des études expérimentales de solubilité sont réduites aux systèmes binaires (pénétrant - PE), avec un nombre limité de systèmes ternaires (pénétrant 1 - pénétrant 2 - PE). Cependant, la plupart des études ternaires mesurent la solubilité globale du mélange

gazeux dans la phase amorphe du polymère. Les modèles thermodynamiques, permettant de calculer la solubilité totale mais aussi partielle des différentes molécules composant le mélange gazeux, sont donc très important à développer. Évidemment, cela signifie que ces modèles thermodynamiques doivent être appropriés, c'est-à-dire prendre en considération les interactions entre les différentes molécules dans le mélange. Il est clair que l'on ne peut pas utiliser des modèles de solubilité binaires pour prédire les solubilités individuelles des molécules de pénétrant dans les systèmes à plusieurs composants, puis estimer la solubilité globale en additionnant simplement les solubilités partielles[9].

L'équation d'état de Sanchez-Lacombe (SL EoS) est l'un des modèles thermodynamiques les plus couramment utilisés dans le domaine des polyoléfines[10]. Par contre, cette équation d'état doit être ajustée aux données de solubilité expérimentales afin d'identifier des paramètres d'interactions relatifs à SL, et ces données font cruellement défaut pour les systèmes à plusieurs composants dans des conditions similaires à celles utilisées dans un processus de polymérisation industriel. Actuellement, les expériences basées sur la méthode gravimétrique utilisant une balance à suspension magnétique (MSB) sont peut-être la technique la plus utilisée pour ce type de mesure de solubilité en raison de leur relative simplicité et de leur haute précision. Un grand nombre d'études ont utilisé cette méthode pour étudier l'impact des pressions partielles et de la température sur la solubilité et la diffusivité des systèmes (principalement) binaires et (très occasionnellement) ternaires. Cependant, ces expériences n'aboutissent souvent qu'à l'obtention de données thermodynamiques globales d'un mélange donné dans un polymère, et des étapes supplémentaires sont nécessaires afin d'estimer les solubilités partielles.

Afin de surmonter le manque de données de solubilités individuelles dans les systèmes à plusieurs composants, une nouvelle approche permettant l'estimation des paramètres d'interaction de Sanchez-Lacombe est proposée. En effet, cette méthode est basée sur la combinaison de mesures expérimentales de solubilité totale avec des estimations du facteur de compressibilité des mélanges gazeux à travers l'équation d'état de Peng-Robinson[11]. Ces deux données seront alors ajustées à SL EoS afin de déterminer les paramètres d'interactions spécifiques à un système donné. Cette nouvelle approche permet donc de calculer les solubilités individuelles des deux pénétrants dans un système ternaire non idéal où la troisième phase est le polyéthylène.

En raison du manque important de données de solubilité dans des conditions industrielles, la méthode expérimentale de perte de charge a été employée afin de mesurer expérimentalement

les solubilités globales et individuelles des systèmes à plusieurs composants. Les solubilités individuelles et globales ternaires et quaternaires ont été mesurées grâce à cette méthode et les solubilités globales ont été validées avec la technique gravimétrique. Ensuite, ces systèmes ont été modélisés à partir de l'équation d'état de Sanchez-Lacombe. En effet, pour la première fois à notre connaissance, l'application de l'équation d'état de Sanchez-Lacombe est étendue du système ternaire au système quaternaire, comprenant donc trois pénétrants et un polymère. L'effet des ICAs ainsi que du comonomère sur la solubilité de l'éthylène dans la phase amorphe du polymère a été étudié. Les effets de co-solubilité, entrainant une augmentation de la solubilité de l'éthylène en présence de composés plus lourds, ainsi que les effets anti-solvants, provoquant une baisse de la solubilité des composés lourds en présence d'éthylène, ont été mis en évidence.

De plus, un manque significatif de données concernant la diffusivité des mélanges à plusieurs composants en phase gazeuse est également observé dans la littérature. Cette information est cruciale car il a été montré que la prise en compte de la co-solubilité ainsi que des effets de co-diffusion ont un impact notable sur le transfert de masse et de chaleur et donc sur la vitesse de polymérisation. Il est donc important d'obtenir d'avantage d'études expérimentales et théoriques sur la diffusion des mélanges de pénétrants dans la phase amorphe du polymère. La diffusivité globale des systèmes binaires, ternaires et quaternaires sera donc mesurée par la méthode gravimétrique, et analysée à partir de la solution de Crank à la loi de Fick en utilisant une représentation des particules à deux niveaux [12]. En effet, ce modèle suppose que la particule de polymère est constituée de deux tailles de granulés de polymère compact, avec des fractions différentes. Les effets de co-diffusion ont été démontré dans les systèmes ternaires par l'augmentation de la diffusivité globale en présence de composés plus lourds (i.e. ICAs, comonomère). Les diffusivités quaternaires sont quant à elles assez proches des diffusivités ternaires dans la gamme de pression analysée.

La connaissance de ces données thermodynamiques est essentielle pour décrire la polymérisation de l'éthylène en phase gazeuse puisque les propriétés physiques et chimiques du polymère seront fortement influencées par la variation de la composition de la phase gazeuse. En effet, lors de la polymérisation de l'éthylène, la particule de catalyseur est d'abord injectée dans le réacteur. Le monomère diffuse de la phase continue du réacteur, et dans les pores de la particule supportée, où se trouvent les sites actifs du catalyseur. Lorsque le monomère entre en contact avec les sites actifs de la particule de catalyseur, la formation de polymère a lieu. A mesure que le polymère s'accumule au niveau des sites actifs, la structure initiale de la particule

subit une accumulation de contraintes conduisant au processus de fragmentation. La formation continue de polymère, qui se déposera sur la surface et dans les pores du catalyseur, entraine une adsorption et une diffusion du monomère à travers cette couche de polymère pour atteindre les sites actifs, où la polymérisation a lieu. Au fur et à mesure que la réaction se déroule, la particule continue de se dilater et le volume de polymère continue de croître[13,14]. Cela se traduira par des gradients de température et de concentration à travers la particule de polymère en croissance conduisant à des variations des vitesses de réaction locales et des propriétés du polymère. Ainsi, pour décrire la réaction de polymérisation, il est impératif de pouvoir prédire les dynamiques de transfert de matière et de chaleur dans la particule en croissance.

Un modèle de croissance des particules, tenant compte des limitations de masse et de transfert de chaleur se produisant pendant la croissance d'un catalyseur Ziegler-Natta lors de réaction de polymérisation en phase gazeuse, est développé. Le "Random-Pore Polymer Flow Model" (RPPFM)[15] sera adapté afin d'estimer les vitesses de polymérisation ainsi que l'évolution temporo-spatiale des profils de concentration et de température dans la particule de polymère et la distribution de masse molaire. Evidemment, la détermination précise à la fois de la concentration des pénétrants dans la phase amorphe du polymère et du coefficient de diffusion des pénétrants est cruciale dans toute étude de modélisation de la croissance des particules. En incorporant un modèle thermodynamique précis, le RPPFM est donc capable de prédire l'impact de la composition de la phase gazeuse (ICA, hydrogène) sur la polymérisation de l'éthylène en phase gazeuse.

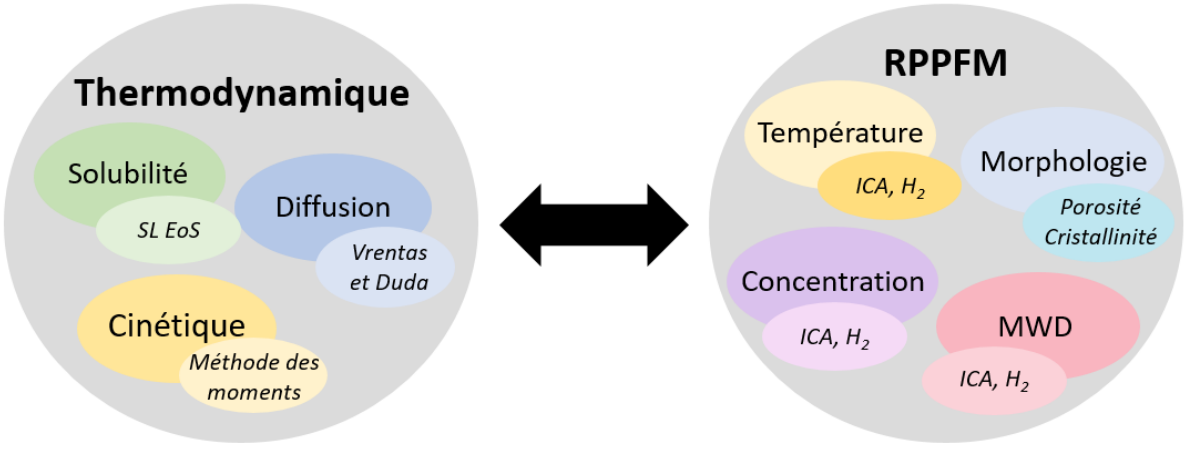

Figure 1. Schéma représentant les différents paramètres à prendre en compte lors de la modélisation d'une particule de polymère en croissance

Il a été conclu que le comportement inverse a été observé pour l'ICA et l'hydrogène. En effet, une augmentation de la pression partielle de l'hydrogène entraine une diminution de la vitesse de polymérisation ainsi que de la distribution de la masse molaire alors qu'une augmentation de la pression partielle de l'ICA entraine le comportement inverse.

Enfin, il convient de rappeler que les procédés en phase gazeuse ne sont pas les seuls utilisés pour la production du polyéthylène. Etant donné l'impact des différentes espèces utilisées dans la phase gazeuse, il est raisonnable de supposer que les particules de polymère gonfleront aussi dans les réacteurs en suspension. La façon dont ils gonflent dépendra ainsi du diluant utilisé, de la température du réacteur et des propriétés du polymère. Comme pour les systèmes en phase gazeuse, les données thermodynamiques concernant les systèmes binaires diluants liquides/PE liés à la polymérisation en suspension ne sont pas suffisamment courantes dans la littérature[16]. La connaissance de ces données thermodynamiques est cruciale si l'on a besoin de contrôler la masse molaire du polymère produit ou d'optimiser le processus de dégazage. En outre, ceci est d'autant plus important que ces diluants liquides modifieront les propriétés physiques du polymère produit en provoquant son gonflement et son ramollissement en raison de leur forte solubilité dans la phase amorphe du polymère. Une étude expérimentale a donc été réalisée afin de mesurer la solubilité et le gonflement de la phase amorphe du polymère en présence de différents diluants liquides dans des conditions industrielles avec différents grades de polyéthylène. Nous avons conclu que la solubilité ainsi que le gonflement augmentent lorsque l'on augmente la température ou que l'on diminue la longueur de la chaine carbonée des diluants liquides et la cristallinité du polymère. Il est aussi important de noter que le taux de gonflement du polymère en présence de diluants liquides légers (i.e. n-pentane, n-hexane) peut atteindre 57 %vol à 90°C. Cette augmentation drastique du gonflement est une propriété très importante à contrôler dans les réacteurs industriels afin d'éviter un encrassement du réacteur dû à la plastification du polymère[17].

Toutes ces données thermodynamiques, aussi bien en phase gazeuse qu'en suspension, doivent être soigneusement prises en compte, car elles sont un outil important pour comprendre l'évolution de la particule de polymère en croissance au cours de la réaction de polymérisation de l'éthylène permettant ainsi une modélisation précise des réacteurs industriels.

Références:

1. S&P Global Plantts, ‘Petrochemicals infographic: What’s in store for global polyethylene and polypropylene out to 2027?’ - The barrel Blog [Accessed 15 March 2020]. https://blogs.platts.com/2017/09/07/infographic-whats-store-global-polyethylene-polypropylene-2027/ (2017).

2. Plastics Market Size, Share & Trends Report, 2020-2027 [Accessed 09 June 2020]. https://www.grandviewresearch.com/industry-analysis/global-plastics-market.

3. Hassan, A., Bagherzadeh, E., Anthony, R. G., Borsinger, G. & Hassan, A. System and process for production of polyethylene and polypropylene. (2011).

4. Polyolefin Microstructural Modeling. in *Polyolefin Reaction Engineering* 187–269 (Wiley-VCH Verlag GmbH & Co. KGaA, 2012). doi:10.1002/9783527646944.ch6.

5. McKenna, T. F. L. Condensed Mode Cooling of Ethylene Polymerization in Fluidized Bed Reactors. *Macromol. React. Eng.* **13**, 1800026 (2019).

6. Alizadeh, A. Study of sorption, heat and mass transfer during condensed mode operation of gas phase ethylene polymerization on supported catalyst. (Departement of Chemical Engineering, Queen’s University, 2014).

7. Alizadeh, A. *et al.* Modeling Condensed Mode Operation for Ethylene Polymerization: Part I. Thermodynamics of Sorption. *Ind. Eng. Chem. Res.* **56**, 1168–1185 (2017).

8. Alizadeh, A. & McKenna, T. F. L. Condensed Mode Cooling for Ethylene Polymerization: The Influence of the Heat of Sorption: Condensed Mode Cooling for Ethylene Polymerization …. *Macromol. React. Eng.* **8**, 419–433 (2014).

9. Bashir, M. A., Al-haj Ali, M., Kanellopoulos, V. & Seppälä, J. Modelling of multicomponent olefins solubility in polyolefins using Sanchez–Lacombe equation of state. *Fluid Phase Equilibria* **358**, 83–90 (2013).

10. Sanchez, I. C. & Lacombe, R. H. An elementary molecular theory of classical fluids. Pure fluids. *J. Phys. Chem.* **80**, 2352–2362 (1976).

11. Peng, D.-Y. & Robinson, D. B. A New Two-Constant Equation of State. *Ind. Eng. Chem. Fund.* **15**, 59–64 (1976).

12. Bobak, M., Gregor, T., Bachman, B. & Kosek, J. Estimation of Morphology Characteristics of Porous Poly(propylene) Particles from Degassing Measurements. *Macromolecular Reaction Engineering* **2**, 176–189 (2008).

13. McKenna, T. F. L., Di Martino, A., Weickert, G. & Soares, J. B. P. Particle Growth During the Polymerisation of Olefins on Supported Catalysts, 1 - Nascent Polymer Structures. *Macromol. React. Eng.* **4**, 40–64 (2010).

14. Alizadeh, A. & McKenna, T. F. L. Particle Growth during the Polymerization of Olefins on Supported Catalysts. Part 2: Current Experimental Understanding and Modeling Progresses on Particle Fragmentation, Growth, and Morphology Development. *Macromol. React. Eng.* **12**, 1700027 (2018).

15. Kanellopoulos, V., Dompazis, G., Gustafsson, B. & Kiparissides, C. Comprehensive Analysis of Single-Particle Growth in Heterogeneous Olefin Polymerization: The Random-Pore Polymeric Flow Model. 4 (2004).

16. Krajakova, L., Laskova, M., Chmelar, J., Jindrova, K. & Kosek, J. Sorption of Liquid Diluents in Polyethylene: Comprehensive Experimental Data for Slurry Polymerization. *Ind. Eng. Chem. Res.* **58**, 7037–7043 (2019).

17. Fouarge, L., Lewalle, A., Auwera, M. V. D. & Brande, F. V. D. Swell control in slurry loop reactor. (2005).

Table of Contents

List of Abbreviations and Symbols

List of Abbreviations

CCD	Chemical Composition Distribution
CSTR	Continuous Stirred Tank Reactor
EoS	Equation of State
FBR	Fluidized Bed Reactor
FRP	Free Radical Polymerization
HDPE	High-Density Polyethylene
ICA	Induced Condensing Agent
IGA	Intelligent Gravimetric Analyzer
HiPP	High impact Polypropylene
iPP	impact Polypropylene
LCB	Long Chain Branches
LCST	Lower Critical Solution Temperature
LDPE	Low-Density Polyethylene
LLDPE	Linear Low-Density Polyethylene
MFI	Melt Flow Index
MGM	Multigrain Model
MSB	Magnetic Suspension Balance
MWD	Molecular Weight Distribution
PSD	Particle Size Distribution
PC SAFT	Perturbated-Chain Statistical Associating Fluid Theory
PE	Polyethylene
PFM	Particle Flow Model
PI	Polydispersity
PP	Polypropylene
PR	Peng-Robinson
PSD	Particle Size Distribution
SCB	Short Chain Branches
SL	Sanchez-Lacombe

SPM	Single Particle Model
ZN	Ziegler-Natta

List of Symbols

A	surface area of contact between the exchanger wall (m^2)
a	attractive forces between molecules
b	co-volume occupied molecules
C^*	concentration of active sites at the surface of the catalyst (mol.site.m^{-3}cata)
C_{d}	concentration of deactivated catalyst site (mol.m^{-3})
C_{ICA}	ICA concentration (mol.m^{-3})
C_{M}	monomer concentration (mol.m^{-3})
$C_{p,\mathrm{ov}}$	overall heat capacity of the particle (J.kg^{-1}.K^{-1})
$C_{p\mathrm{g,in}}$	heat capacity of the inlet gas stream (J.K^{-1}.mol^{-1})
$[C_i]^{\mathrm{eq}}$	equilibrium concentration of component *i* in the particle (mol.m^{-3})
$[C_i]$	concentration of component *i* (mol.m^{-3})
$D_{i,\mathrm{ov}}$	overall (or effective) diffusivity of component *i* (m^2. s^{-1})
D_r	concentration of dead polymer chains (mol.m^{-3})
D	diffusion coefficient (m^2.s^{-1})
D_0	pre-exponential factor of Vrentas and Duda (m^2.s^{-1})
E_{a}	diffusion activation energy (J.mol^{-1})
h	heat transfer coefficient (J.m^{-2}.s^{-1}.K^{-1})
$[H_2]$	hydrogen concentration in the bed (mol.m^{-3})
$k_{\mathrm{c,p}}$	overall thermal diffusivity of the particle (J.m^{-1}.s^{-1}.K^{-1})
k_{d}^{k}	deactivation constant for k catalyst site type (s^{-1})
$k_{i\mathrm{H}}^{k}$	initiation of P_{H} rate constant for *k* catalyst site type (m^{3}·mol^{-1}.s^{-1})
k_{I}^{k}	initiation rate constant for *k* catalyst site type (m^{3}·mol^{-1}.s^{-1})
k_{p}^{k}	propagation rate constant for *k* catalyst site type (m^{3}·mol^{-1}.s^{-1})
k_{tH}^{k}	transfer to hydrogen constant for *k* catalyst site type (m^{3}·mol^{-1}.s^{-1})
k_{tM}^{k}	transfer to monomer constant for *k* catalyst site type (m^{3}·mol^{-1}.s^{-1})

k_{tsp}^{k}	spontaneous transfer constant for k catalyst site type (s^{-1})
K_{i1}	free volume parameters for the solvent
K_{i3}	free volume parameters for the polymer
$\dot{m}_{\mathrm{g,in}}$	inlet mass flow rates of the process gases ($kg.s^{-1}$)
P	pressure (bar)
P_{H}	concentration of polymer chains containing hydrogen ($mol.m^{-3}$)
P_r	concentration of "live" polymer chains of length *r* ($mol.m^{-3}$)
Q_{vap}	total enthalpy change due to evaporation of liquid in the reactor ($J.mol^{-1}$)
R	universal gas constant ($J.mol^{-1}.K^{-1}$)
R_{p}	polymerization rate ($mol.m^{-3}$ reactor $bed.s^{-1}$)
R_{v}	polymerization rate ($mol.m^{-3}cat.s^{-1}$)
S_i	solubility of component *i* (g/g.am.polymer)
$T_{\mathrm{g,in}}$	inlet gas stream temperature (K)
T_{r}	reduced temperature (K)
T_{w}	temperature of the exchanger (K)
T_{b}	bulk temperature of the reactor (K)
T	temperature (K)
U	overall heat transfer coefficient ($J.m^{-2}.s^{-1}.K^{-1}$)
$\hat{V}_i^*$	specific critical hole free volume required for the i^{th} component ($cm^3.g^{-1}$)
V_{R}	volume of reactor bed (m^3)
ω_i	mass fraction of the i^{th} component (-)

Greek letters

ξ_{13}	ratio of molar volumes for the solvent and polymer jumping units (-)
ρ_{ov}	overall particle density ($kg.m^{-3}$)
$-\Delta H_{\mathrm{p}}$	overall enthalpy of polymerization ($J.mol^{-1}$)
υ	molar volume ($m^3.mol^{-1}$)
ϕ_i	volume fraction of the i^{th} component (-)
χ	solvent-polymer interaction parameter (-)
w	acentric factor (-)

General Introduction

In 2020, polyolefins represent approximately 45% of the production of plastic materials worldwide, which makes them the most widely used family of polymers in the world. The worldwide market for polyethylene alone is expected to rise substantially to about 150 million tons by 2027, making it the most extensively produced polymer on the planet because of its broad range of properties and end-uses, low production cost, and relatively low environmental impact. PE products are used in many important fields, for example electrical and electronics, packaging, automotive, pharmaceuticals, building and construction.

Polyethylene can be made in solution, slurry and gas phase processes using ethylene, and very often an α-olefin comonomer. The polymerization of ethylene on supported catalysts in gas phase fluidized bed reactors (FBRs) continues to be the predominant process for production of approximately 75% of linear low density polyethylene (LLDPE) and 25% of high density polyethylene (HDPE) worldwide. However, due to the highly exothermic nature of the polymerization, the maximum rate of heat removal from the reactor is clearly a limiting step in the polymer production rate in gas phase reactors. Therefore, in order to optimize the productivity, condensed mode cooling is employed in order to increase the capacity of heat removal. In condensed mode operation, in addition to injecting ethylene, hydrogen, nitrogen, and eventually a comonomer, inert compounds, which are mainly alkanes as propane, isobutane, n-pentane or n-hexane, are used as induced condensing agents (ICAs). These alkanes can be partially liquefied in an external heat exchanger and then sprayed inside the reactor mainly to serve as a dispersing heat medium for removing the heat generated within the reactor. All of the species present in the gas phase, inert or not, will diffuse into the amorphous phase of the polymer. They will therefore change the physical, and possibly the chemical structure of the final polymer, which in turn can influence important parameters such as the reaction rate, through the change in the individual species solubility and diffusivity. In order to better control and understand the polymerization process, it is obviously important to know the solubility as well as the diffusivity of the individual species in gas mixtures in the amorphous phase of the polymer with precision.

Up to now, most of the experimental solubility studies were restricted to binary systems (penetrant – PE), with a limited number looking at ternary systems (penetrant 1 – penetrant 2 – PE). However, most of the ternary studies only measure the overall solubility of the gas mixture in the amorphous phase of the polymer, making thermodynamic models crucial when looking at the effect of the individual solubilities of the species inside the polymer. Obviously, this

means that if one wishes to develop models to quantify these effects, appropriate thermodynamic models are needed. It is clear that one cannot always use binary sorption models in order to predict the individual solubilities of penetrant molecules in multicomponent systems, and then estimate the overall solubility by simply adding the partial solubilities. It is necessary to account for the way that they interact with the polymer in a ternary (or quaternary) system. This is of course possible using equations of state (EoS), such as the Sanchez-Lacombe EoS.

The Sanchez-Lacombe EoS (SL EoS) is one of the most commonly used thermodynamic models in the field of polymer reaction engineering. However, the main drawback of this model is that it requires empirical, adjustable parameters that are specific to a given system. These adjustable interaction parameters in the SL EoS need to be estimated experimentally as there is no way to estimate them *à priori*. To do so, this equation of state has to be fitted to experimental solubility data, and such data is sorely lacking for multicomponent systems under conditions similar to those used in a polymerization process. Currently, gravimetry based on a magnetic suspension balance (MSB) is perhaps the most widely used technique for this type of solubility measurement because of its relative simplicity and high precision. A large number of studies have used this method to investigate the impact of partial pressures and temperatures on the solubility of (mostly) binary and (very occasionally) ternary systems (and as far as we have been able to determine, never quaternary systems). However, MSB experiments give only the total solubility of a given mixture in a polymer, and additional measurements or steps need to be taken to estimate the individual solubilities. Besides, the advantage of this method is that it can also give the global diffusivity of multicomponent systems, which is an important information.

In ***Chapter 2***, the gravimetric technique was used to measure the total solubility of ternary systems that are not available in the literature, such as ethylene/propane/LLDPE, ethylene/isobutane/LLDPE and ethylene/1-butene/LLDPE. Only global solubilities of the mixtures are measured with the magnetic suspension balance. In order to overcome the lack of individual solubility date in multicomponent systems, a novel approach for the estimation of the Sanchez-Lacombe interaction parameters, is proposed. This method is based on combining total solubility measurements with estimates for the compressibility factor of gas mixtures using the Peng-Robinson Equation of State (PR EoS). This novel approach makes it possible to calculate individual components solubilities for the two penetrants in non-ideal ternary systems where the third phase is polyethylene.

The important lack of solubility data in polyolefin systems, especially in ternary and quaternary systems at industrial conditions, inspired the work presented in ***Chapter 3.*** As an alternative of the gravimetric experiments, an accurate and reliable procedure based on pressure decay was developed. The advantage of this method is that it can give the overall solubility, as gravimetric technique, but also the partial solubilities of each component in the gas mixture. Ternary and quaternary individual and overall solubilities were measured using the pressure decay method and validated by the gravimetric technique. The effect of ICAs as well as comonomer on the solubility of ethylene in the amorphous phase of the polymer were studied in this chapter. The Sanchez-Lacombe EoS was expanded to include four components, therefore the pressure decay method was used to estimate the total and individual solubilities. Total solubilities were validated with experimental data through gravimetric method. This appears to be the first time that the application of the Sanchez-Lacombe EoS is extended from the ternary system to the quaternary system, including therefore three penetrants and a polymer.

A significant lack of data concerning the diffusivity of multicomponent systems is also observed in the literature. This information is crucial since it has been shown that accounting for the co-solubility as well as the co-diffusion effects have a noticeable impact on mass and heat transfer and therefore on the polymerization rate. The diffusivity of different penetrants in polyethylene will be studied in ***Chapter 4***. The diffusion in multicomponent polymeric systems is so far not completely understood, especially in ternary and more importantly in quaternary systems. It is therefore crucial to have more experimental and theoretical studies about the diffusion of mixtures of penetrants in the amorphous phase of the polymer since it has a great importance in ethylene polymerization reaction in gas phase. The overall diffusivity of binary, ternary and quaternary systems will therefore be measured through the gravimetric method, based on the magnetic suspension balance, and analyzed with Crank's solution to Fick's law using a two-level particle representation. This particle model assumes that the polymer particle is constituted of two sizes of compact polymer granules, with different fractions.

Knowledge of this thermodynamic data is key when describing ethylene polymerization in gas-phase since the physical and chemical properties of the produced polymer will change when varying the gas phase composition. During ethylene polymerization, the catalyst particle is first injected into the reactor. Monomer diffuses from the continuous phase of the reactor, and into the pores of the supported particle, where the active sites of the catalyst are found. When

monomer contacts the active sites of the catalyst particle, polymer formation takes place and as polymer accumulates at the active sites, the initial structure of the particle suffers a build-up of stress leading to the fragmentation process. The continuous formation of polymer, which will deposit on the catalyst surface and pores, causes the monomer to absorb and diffuse through this polymer layer to reach the active sites, where polymerization takes place. As the reaction proceeds, the particle continues to expand and the volume of polymer keep growing. This will result in gradients of temperature and concentration through the growing polymer particle leading to variations in local reaction rates and polymer properties. Thus, to describe the polymerization reaction, it is imperative to be able to predict the dynamics of mass and heat transfer in the growing particle.

In ***Chapter 5***, a comprehensive single particle growth model, accounting for mass and heat transfer limitations appearing during the early growth of a Ziegler-Natta catalyst in gas phase olefin polymerization, is developed. The Random-Pore Polymer Flow Model (RPPFM) will be adapted in order to estimate the overall particle polymerization rate as well as mass and energy balances, in order to predict the temporal-spatial evolution of concentration and temperature profiles in the polymer particle as well as molecular weight distributions. This chapter is based on the thermodynamic and diffusivity models developed in the first chapters, as the accurate determination of both the penetrants concentration inside the amorphous phase of the polymer and the effective penetrants diffusion coefficient is crucial in any particle growth modeling study. Therefore, the SL EoS will be used in order to describe the solubility of the different species inside the amorphous phase of the polymer at equilibrium (used as a boundary condition). And Vrentas and Duda diffusivity model is applied to calculate the diffusivity of penetrant molecules in the semicrystalline polymer. By incorporating an accurate thermodynamic model, the RPPFM is therefore able to predict the impact of the gas phase composition (i.e. ICA, hydrogen) on ethylene polymerization.

Finally, it should be recalled that gas phase processes are not the only ones used for PE production. The different species in a liquid phase cause the polymerizing particles to swell in a slurry process. The way they swell will depend on the used diluent, the reactor temperature and polymer properties. As in gas phase systems, very little information on the thermodynamic data of PE/liquid diluents related to slurry polymerization is available in the literature. Very few studies have investigated the solubility of liquid diluents in the amorphous phase of the polymer and the way the diluents swell the polymers. Knowledge of this thermodynamic data

is crucial if one needs to control the molecular weight of the produced polymer or optimize the degassing process. Besides, this is all the more important since these liquid diluents will change the physical properties of the produced polymer as they cause its swelling and softening due to their high solubility in the amorphous phase of the polymer. In ***Chapter 6***, an experimental study has been performed in order to measure the sorption and swelling of the amorphous phase of the polymer in presence of different liquid diluents under industrial conditions (i.e. diluents, temperatures) with different grades of polyethylene. The effect of temperature, diluent chain length, crystallinity and partial dissolution of the polymer have been studied.

All these thermodynamic data, both in gas and slurry phase, represent important tools for understanding the evolution of the growing polymer particle during ethylene polymerization reaction, and are necessary for accurate modeling of industrial reactors.

Chapter 1

Literature Review

1. Introduction to polyolefins

The term polyolefins is a general one that usually refers to polymers of ethylene (polyethylene, PE) or propylene (polypropylene, PP), and their copolymers with each other and other α-olefins such as 1-butene or 1-hexene. Polyolefins exhibit a huge range of properties despite their chemical simplicity (they are composed uniquely of carbon and hydrogen atoms, and nothing else!). Indeed, they range from rigid materials, which are used for car parts, to soft materials such as flexible fibres. Some are as clear as glass; others are completely opaque [1]. Some, such as microwave food containers, have high heat resistance while others melt easily. Indeed, the wide-spread use of polyolefins is due to their extensive range of properties and end-uses, low production cost and relatively low environmental impact.

1.1.Characteristics of polyolefins

In 2020, polyolefins represent approximately 45% of the production of plastic materials, which makes them the most significant family of polymers and the most widely used polymer in the world. The worldwide market for polyethylene is expected to rise substantially to about 2.6% over the next five years: from 108.3 million mt in 2016 to 150 million mt by 2027 [2].

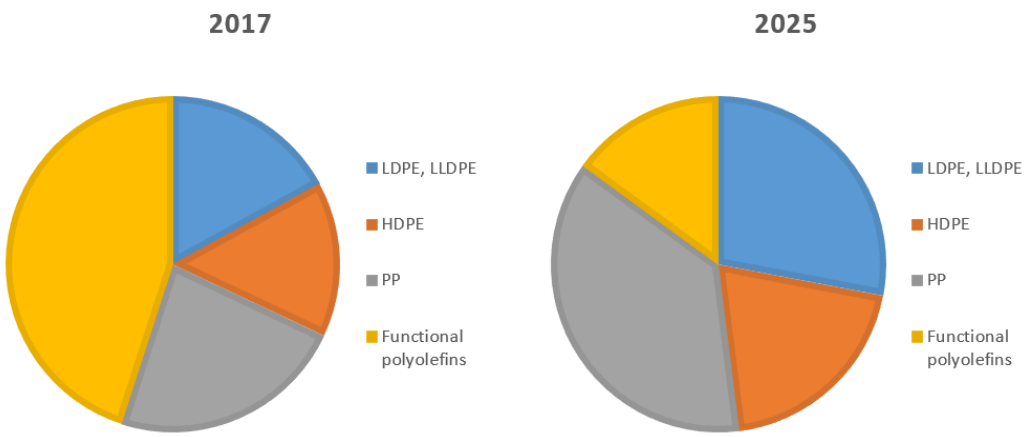

Figure 2. *Evolution of polyethylene worldwide market from 2017 to 2025*[3]

Polyethylene, the focus of the current thesis, is a macromolecule containing simple repeating units of monomers composed of covalently linked carbon atoms in which two hydrogen atoms are attached. **Figure 3** shows polyethylene molecular structure, where *n* is the number of ethylene monomer units in the α-olefin.

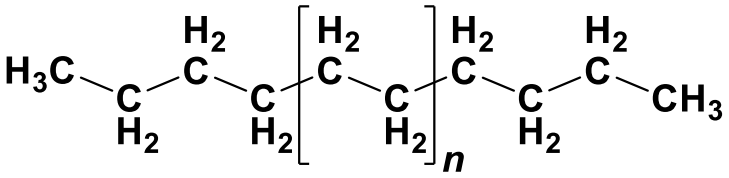

Figure 3. *Polyethylene molecular structure*

Polyethylene is used in the manufacture of a wide variety of consumer products, such as films, pressure pipes, insulation of wires and cables, and many other products [4]. These products are used in many important fields, as for example electrical & electronic, packaging, automotive, building & construction, and pharmaceuticals.

Polyethylene is divided into at least three main families, usually depending on its density: high-density polyethylene (HDPE), linear low-density polyethylene (LLDPE), and low-density polyethylene (LDPE).

Low-density polyethylene (LDPE) is made using free radical process and contains short chain branches (SCB) and long chain branches (LCB). These resins are produced under high pressures in autoclave or tubular reactors. High-density polyethylene (HDPE) and linear low-density polyethylene (LLDPE) are made with coordination catalysts and contain only SCBs. **Table 1** summarizes the main properties of the different types of polyethylene resins.

These resins can be obtained by slurry, solution or gas-phase processes, using different types of coordination catalysts. HDPE can be made with Ziegler-Natta, metallocene or chromium catalysts, but the latter cannot be used effectively for LLDPE as they do not incorporate comonomers very well. Special grades of LLDPE resins are made in solution processes, but most of this family of polymer is produced in gas-phase processes since the amorphous phase tends to be soluble in the diluents used in slurry reactors [5].

Table 1. *Density and crystallinity ranges for different commercial polyethylene resins*

Type of polyethylene	Density (g.cm-3)	Crystallinity (%)	Properties
HDPE	0.945 - 0.960	55 - 75	Linear homopolymer White opaque rigid solid MWD depends on catalyst
LDPE	0.915 – 0.940	30 - 55	Branched homopolymer Translucent flexible solid Broad MWD
LLDPE	< 0.920	30 - 45	Random copolymer Translucent flexible solid Narrow MWD

Polyethylene is often classified according to its melt flow index (MFI) and density. The overall density of the polymer is related to its crystallinity; more branches lead to lower density of the final polymer and therefore lower crystallinity. Indeed, this density can be controlled by adding a comonomer that will lead to higher branches inside the produced polymer. The MFI depends on the molecular weight distribution (MWD) and the LCB content of the polymer. It is a measure of the above molecular and structural chain characteristics which in turn affect the processability of the produced polymer; a lower polymer molecular weight leads to a higher MFI. These are part of the important properties of the polymer that have to be taken into account when producing special grades of polyethylene.

1.2.Catalysts for ethylene polymerization

As we just mentioned, there are three major types of catalyst used for the polymerization of olefins: Ziegler-Natta, Philips and metallocene catalysts.

Ziegler-Natta (ZN) catalyst are the most widely used catalyst due to their high activity and selectivity, and low cost. The fifth generation of Ziegler-Natta catalyst can lead to a productivity of 100-130 kg of polymer / gram of catalyst compared to 2-4 kg of polymer / gram of catalyst for the 1st generation of Z-N catalyst. These catalysts are composed of a transition metal salt of metals from group IV to VII, which is the (pre)catalyst itself, and a metal alkyl from group I to III; known as the co-catalyst or activator [6]. When the transition metal is exposed to the co-

catalyst, the polymerization active sites are created by alkylation then reduction of the transition metal centers. When Ziegler-Natta catalysts are used in supported form, they are usually found in the form of titanium tri- or tetrachloride, and are supported on magnesium dichloride ($MgCl_2$), or on silica (SiO_2) coated with $MgCl_2$. The presence of more than one type of active site in heterogeneous Ziegler-Natta catalyst can lead to a wide molecular weight distribution (MWD), with a polydispersity index (PI) between 4-10, and an inhomogeneous chemical composition distribution (CCD) [7]. Ziegler Natta catalysts can also be used in solution processes, most often for elastomers, but in this case, they are usually based on vanadium or vanadium oxide.

Phillips chromium catalysts are composed of a chromium oxide (CrOx) impregnated on a silica support. The particularity of this catalyst is that there is no need for a co-catalyst because it is activated *in situ* by the monomer (i.e. ethylene) during the polymerization. The exact mechanism by which the actives species are being created still remains unknown. However, several authors revealed that the metal forming the active site can exist simultaneously in different oxidation states [8]. This will lead to products having (very) broad molecular weight distribution with a PI that can be as high as 15 to 30 (as opposed to 4-10 for supported Ziegler-Natta catalysts). However, the high sensitivity of this catalyst to impurities can lead to some difficulties when using it. Phillips catalyst are only used in the supported form.

Finally, metallocenes, similarly to ZN catalysts, can be used in both molecular and supported form. Most metallocene catalysts require an activator like methylaluminoxane (MAO). However, recent studies revealed that it is possible to obtain commercially viable metallocene catalysts without MAO [9]. The main difference with the other catalysts is that only one degree of oxidation of the metal atom during the activation state is reached, leading to the formation of only one type of active site, even when supported. This is a very important property if one needs very fine control over comonomer incorporation or over MWD. However, metallocenes are much more expensive than Phillips or ZN catalysts. ***Table 2*** summarizes the main characteristics of coordination catalyst for olefin polymerization.

Table 2. *Main characteristics of coordination catalyst for olefin polymerization adapted from Asua [10].*

Type	Physical state	Polymer type
Ziegler-Natta	Heterogeneous	Non-uniform
	Homogeneous	Uniform
Phillips	Heterogeneous	Non-uniform
Metallocene	Heterogeneous	Uniform
	Homogeneous	Uniform

Ziegler–Natta and Phillips catalysts are considered to have multiple-site types, which explains why they make polymer with non-uniform properties: each site type produces polymer populations with different average microstructural properties. Ziegler–Natta catalysts can be homogeneous, meaning soluble in the reaction medium, or heterogeneous. When these catalysts are homogeneous, they have only one site type and synthesize polyolefins with uniform properties. Phillips catalysts, on the other hand, are always heterogeneous, meaning that short chains have higher comonomer content.

1.3.Processes for the production of polyolefins

Different industrial processes are used to produce polyolefins; high-pressure free radical and low-pressure catalyst polymerization.

Free radical polymerization (FRP) at high pressures is only used to produce LDPE homopolymer and copolymer (e.g. EVA grades). In the FRP process, the polymerization reaction is carried out in a pressure range of 1200–3500 bars and temperature range of 150–330 °C. These processes are inherently different from the gas phase and slurry processes that are the focus of the current thesis. In particular, they are run under supercritical conditions, and do not employ diluents or inert compounds to control heat transfer. This means that the thermodynamic aspects relevant to the solubility of small molecules in the polymer, and to the polymer swelling are unrelated to the thermodynamics of lower pressure processes.

As described above, olefins can be polymerized using a catalyst at lower pressures and temperatures. In this case, the catalytic polymerization of olefins is carried out in three main types of processes depending on the form of the catalyst (molecular or supported) and phase of the continuous medium in which the reaction takes place: solution, slurry, and gas phase.

In solution reactors, both the catalyst and the polymer are soluble in the reaction medium. The polymerization reaction is carried out in a temperature range of 100–250°C and a pressure from 40-100 bars, depending on the solvent used and on the desired polymer properties. These reactions are usually performed in a continuous stirred tank reactor (CSTR) or in a loop reactor. We will not consider this type of process in the current thesis.

Slurry processes can be classified into diluent and bulk. In diluent processes, used exclusively for PE, an inert diluent ($C_3 - C_6$ alkanes) is used to suspend the growing polymer particles. Bulk slurry processes are used only to make isotactic PP, and use liquefied monomer as the continuous medium. These processes can be run in autoclaves or loop reactors in a temperature between 80–110°C and a pressure from 5–65 bars.

Finally, in gas-phase polymerization processes, the polymer is formed on the supported catalyst and the growing particles are dispersed in a continuous gas phase. Gas-phase reactors are used to polymerize ethylene, propylene and higher α-olefins. Gas-phase processes can be used for both PE and PP. If PE is made in a gas phase process, one finds only fluidized bed reactors (FBRs) because they are the only type of reactor to provide sufficient heat removal capacity. PP can be made in both FBRs and stirred bed reactors because heat removal, while still an important challenge, is not quite as limiting in terms of production for PP[5]. In FBRs, the polymer particles are fluidized by a gaseous mixture of monomer, hydrogen and other compounds, while in stirred bed reactors, polymer particles are dispersed in the gas-phase due to a mechanical stirring. Gas phase processes typically operate at temperatures from 70–120°C and pressures of 5–30 bars.

In the present thesis we will focus our attention on ethylene polymerization processes, essentially in gas phase systems, but we will also look at certain aspects related to diluent slurry processes. For this reason, the rest of the discussion on the state-of-the-art and literature review will focus essentially on ethylene polymerization processes. Nevertheless, the reader should be aware that, from a fundamental point of view of thermodynamics and reactor operation, there are significant similarities between PP and PE processes.

2. Slurry Phase Ethylene Polymerization

As mentioned in the previous section, slurry processes for olefin polymerization can be divided into two main categories: diluent and bulk. Bulk slurry processes are used only to make isotactic PP, and use liquefied monomer as the continuous medium. Diluent processes use a chemically inert diluent (C_3 – C_6 alkanes) to suspend the growing polymer particles. In Phillips processes, isobutane is preferred over n-butane as it is a poorer solvent and swells the polymer less [5]. However, stirred tank slurry processes use mostly n-hexane as diluent [11].

Slurry processes utilize either stirred tank reactors or loop reactors. The first generation of slurry reactors for olefin polymerization were autoclave reactors, except for Phillips, which was the first company to introduce a loop reactor for olefin polymerization. Both configurations have residence time distributions that can be approximated as Continuous Stirred Tank Reactors (CSTRs).

Slurry loop reactors consist of 1 to 2 loop reactors in series. Typically, industrial slurry-phase loop reactors operate at temperatures of 70–120°C, pressures of 30–90 bar and a polymer-solids concentration of approximately 45% w/w [12–14]. The reaction mixture, consisting of monomer, diluent, catalyst, hydrogen and polymer, flows in the loop reactor by means of an axial centrifugal pump placed at the bottom of the reactor. Indeed, this pump is designated to maintain efficient suspension of the solid polymer particles in the liquid diluent [15] and therefore provides high flow velocities of the reaction mixture (i.e. 5-7 $m.s^{-1}$) that results in very well-defined mixing conditions and high heat transfer coefficients through the reactor wall [16]. Indeed, as the volume of the reactor and the solid concentration of the fluid slurry increase, the demands on the pump also increase [17]. Loop reactors are usually vertically installed (Borstar, Philips or Spheripol processes). The loop reactor is continuously fed with monomer and comonomer (i.e. ethylene and 1-hexene or 1-butene) and diluent (i.e. supercritical propane, isobutane, n-pentane, n-hexane) [18].

Table 3 shows the different industrial slurry reactors as well as the different diluents and comonomers used. With the exception of a small third phase region near the monomer injection part, two phases coexist in the major fraction of the volume of a slurry-loop reactor, namely, a liquid phase (i.e. diluent, monomer, comonomer and hydrogen) and a polymer phase (i.e. polymer and sorbed quantities of diluent, monomer, comonomer and hydrogen)[19]. During the polymerization reaction, polymer slurry is regularly discharged from the loop reactor by means

of the settling legs placed at the lower part of the loop reactor [15,20]. These settling legs periodically open to remove the highly concentrated slurry which consists of polymer solids and a fraction of the liquid dissolved in the latter [21]. Then, the product stream leaving the first reactor is either injected inside a second loop reactor with fresh monomer, diluent and hydrogen or removed from the reactor. If so, the highly concentrated slurry leaving the loop reactor is fed to a hot-flash separator where most of the diluent and unreacted monomers are flashed off and recycled, with high monomer conversion rates of 95–98%. The polymer is then dried and pelletized.

Table 3.Typical process condition for slurry polyethylene reactors

Process	Reactor type	Diluent	Comonomer
Mitsui	2 stirred autoclaves	Hexane	1-Hexene
Basell (Hostalen)	2-3 stirred autoclaves	Hexane	Butene
Equistar – Maruzen – Nissan	1-2 stirred autoclaves	Hexane	1-Hexene / 1-Butene
Chevron Phillips	Single loop	Isobutane	1-Hexene
Borealis - Borstar	2 loops / FBR	Supercritical Propane	1-Butene
Innovene S	1-2 loops	Isobutane	1-Hexene / 1-Butene
Total	1-2 loops	Isobutane	1-Hexene

The major advantages of a slurry process include mild operating conditions, high monomer conversion, ease of heat removal, and relative ease of processing. Indeed, slurry processes have better heat transfer capacity when the polymer particles are suspended in a liquid, with respect to the gas phase processes. Better heat transfer means higher space-time yield in slurry reactors, leading to higher volumes of produced polymer in shorter times. As a result, grade changes can be faster in slurry. However, slurry processes require the purchase, purification, removal and recycling of the solvent, which can impose extra costs and unit operations.

Control of temperature in slurry reactors is important since the operating temperature has a complex impact on the chemical and physical phenomena in PE slurry reactors. Indeed, increasing temperature can lead to higher catalyst productivity but also enhances the risk of

polymer swelling since the latter tends to become more soluble in the continuous phase at higher temperatures [21]. If the temperature reaches a critical point, particle swelling can occur and can lead to the production of more viscous or adhesive polymer slurry [14,22] causing the formation of relatively low densities (lower than 940 $kg.m^{-3}$). These issues of reactor fouling by polymer adhesion are consequently linked to the swelling of the amorphous phase of the polymer due to the sorption of these industrial liquid diluents.

Nevertheless, very few studies of phase equilibria for PE/liquid diluent systems can be found in the literature. Knowledge of this thermodynamic data is crucial if one needs to control the molecular weight of the produced polymer or to optimize the degassing process. Schnell et al.[23] experimentally and theoretically (Sanchez-Lacombe Equation of State) studied cloud point temperatures and pressures as a function of n-hexane/PE mixture at pressures up to 150 bar and temperatures up to 227°C. De Loos et al.[24] evaluated experimentally the lower solution temperature (LST) in n-hexane/LLDPE system as a function of pressure at temperatures of 127-327°C and pressures up to 130 bar. They showed that cyclohexane is a better solvent than n-heptane which is a better solvent than n-hexane. Pochivalov[25] also studied the LCST for LDPE in n-decane and n-tridecane in a wide temperature-concentration range at 290°C using gravimetric method. They concluded that n-decane is slightly a better solvent for LDPE than n-tridecane. Hamada et al.[26] determined the molecular weight dependence of the lower critical solution temperature (LCST) for linear PE fractions in n-pentane, n-hexane, n-heptane and n-octane. They found out that LCST increases with increasing the number of carbon atoms in the n-alkane. In the same manner, Strathmann et al.[27] studied n-hexane, n-octane, n-decane and n-hexadecane in polyethylene and found out that LCST increases as the chain length of the alkane increases. Besides, Nakajima et al.[28] showed that the amount of polyethylene dissolved in liquid solvents is function of the temperature and alkanes chain length. Aminabhavi et al.[29] showed the sorption of 14 organic liquids into HDPE geomembranes at 25, 50 and 70°C, as well as the swelling of the HDPE geomembrane. They showed that increasing the temperature increases the sorption and diffusion of the organic liquids through HDPE, hence increasing the swelling of HDPE. Finally, Krajakova et al.[30] studied the sorption and swelling of different PE films in presence of n-pentane, n-hexane and n-octane at temperatures in the range of 25-68°C. They showed that longer hydrocarbons diluents have a slightly higher solubility in all PE studied. Besides, they showed a significant increase of liquid n-alkanes solubility in function of PE crystallinity for crystallinities lower than 60 wt%, although almost constant solubility for sample crystallinity higher than 60 wt%.

To conclude, it has been shown that

- the heavier the liquid solvent, the higher its solubility in the polymer, and therefore the greater the swelling of the amorphous phase of the polymer
- the higher the temperature, the greater the solubility of liquid solvent in the amorphous phase of the polymer
- the lower the crystallinity, the higher the solubility of liquid solvents in the amorphous phase of the polymer.

Clearly, the thermodynamic data of PE/liquid diluents related to slurry polymerization is not enough available in the literature, contrarily to the thermodynamic of gas phase which was extensively studied and described in the literature. Indeed, gas phase polymerization reactors, such as FBRs, are the most commonly used reactors for the production of HDPE and LLDPE, but are limited by heat transfer issues due to the highly exothermic nature of ethylene polymerization.

3. Gas phase ethylene polymerization in fluidized bed reactors

3.1 Overview of FBRs

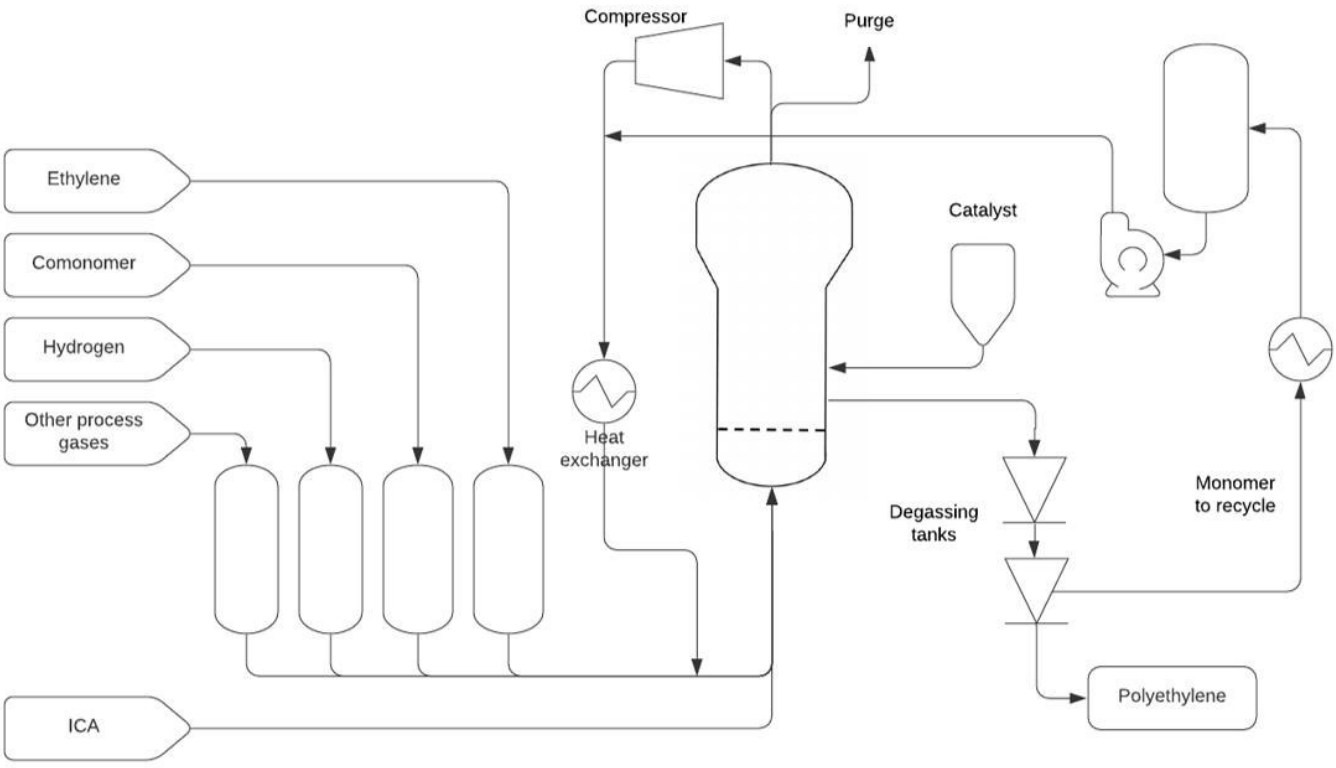

Figure 4. *Scheme of a gas phase process operating in a fluidized bed reactor*

This process was commercialized for the first time in the late 1970s. Ethylene polymerization is a highly exothermic reaction. Heat needs to be removed continuously in order to keep the temperature in the reactor at the desired level; the more heat one removes, the faster the polymerization can be allowed to go and the higher the productivity will be. Because of this, the only type of reactor currently used to polymerize ethylene in gas phase reactions is the FBR (except for the new Hyperzone technology which should come on line for the first time this year). An example of this FBR is shown in the scheme in **Figure 4**. Due to the solubility limitations inherent in LLDPE processes, this type of polymer must be made in the gas phase so it is in fact produced only in FBRs. It should be noted that plants making LLDPE can also make HDPE, and about a quarter of all HDPE is also made in a gas phase processes.

The reactor itself is simply a cylinder with an enlarged section at the top, and a distributor plate at the bottom. The role of the distributor plate is to ensure an even flow of the feed stream into the bottom of the reactor and to avoid growing polymer particles from falling into the feed zone. The diameter of the main section of the reactor is on the order of 2-6 meters, and the height of the main cylindrical section is about 10-20 meters, without taking into account the upper section of the reactor [31–33]. Industrial FBRs typically operate at temperatures of 75-110°C, and at pressures of 15-40 bar [34,35]. The feed stream contains a mixture of ethylene, hydrogen, nitrogen and various α-olefins (typically 1-butene or 1-hexene, and eventually 1-octene) that enter the reactor through the distributor plate. The catalyst particles (or occasionally pre-polymerized catalyst particles) are fed continuously to the reactor at a point above the gas distributor [36]. In addition to the reactive compounds injected to the reactor, inert compounds, usually alkanes such as propane, isobutane, isopentane or n-hexane, can be used as induced condensing agents (ICA) to enhance heat removal[37] and thus aid in increasing process productivity and safety [15–17].

As can be seen in **Figure 5**, an FBR is typically run with the gas (and eventually small amounts of liquid) flowing upwards, more or less in plug flow, and with the polymer particles flowing in a toroidal fashion, upwards through the middle of the bed, and downward along the reactor walls. Polymerization takes place as the catalyst and growing particles move through the bed, thus increasing in weight and size [38,39]. The unreacted gas mixture is recovered at the top of the bed, compressed in an external compressor and cooled in a heat exchanger before being fed back to the bottom of the reactor. The cooling of the feed stream helps to remove the heat of the reaction and compensate pressure drop [40–42]. The polymer product is removed near the

bottom of the FBR, and unreacted materials are separated from the product, cooled, liquefied and recycled.

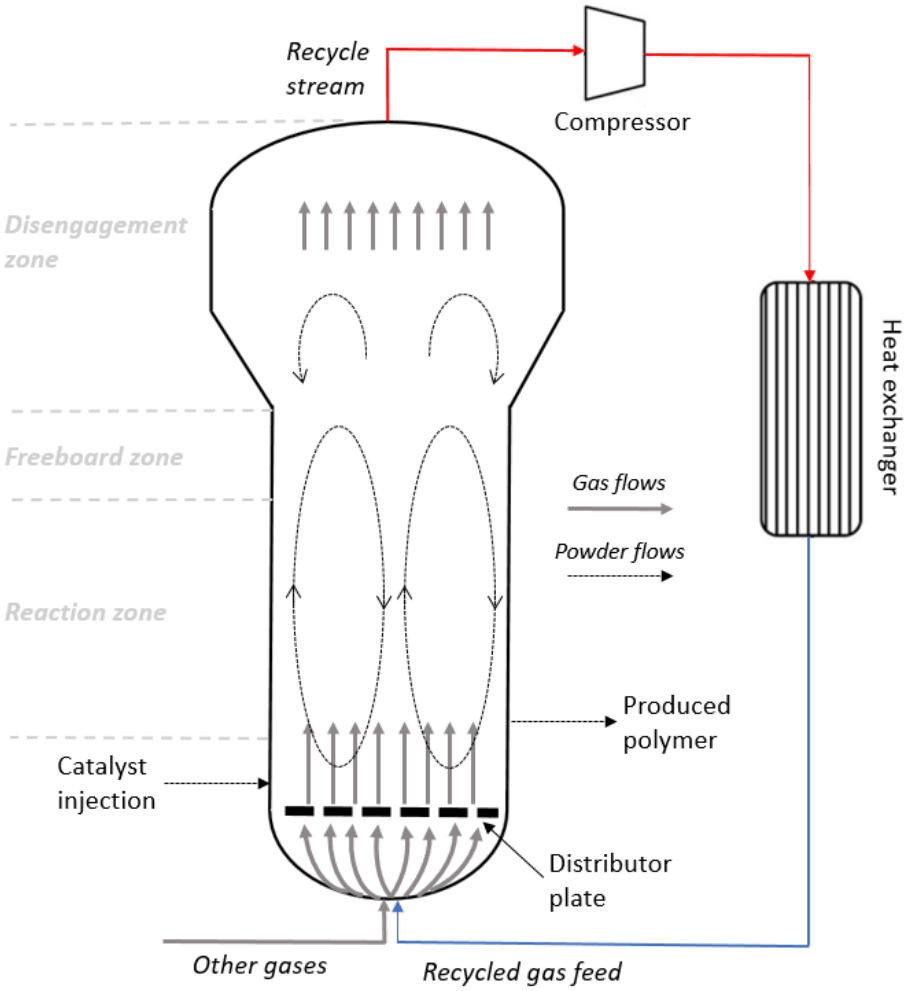

Figure 5. *Scheme of a fluidized bed reactor for olefin polymerization. Adapted from* [5]

The gas stream inside the reactor provides the fluidization of the growing polymer particles. Typically, the relative gas-particle velocity is on the order of 2-8 times the minimum fluidization rate; on the order of 0.5–1 m/s [43]. In order to get such high flow rates through the bed, low per pass ethylene conversions and high recycle ratios are common. Thus, even if the per pass conversion is between 5 and 20%, the overall conversion of this type of process can be quite high, on the order of 90-98% [44,45]. Furthermore, the particle size distribution (PSD) in the bed can be quite broad; going from several tens of microns up to several hundreds of microns for the final product. This shows the challenge of maintaining proper fluidization in order to avoid the presence of too many fines that could be moved out of the reactor to the compressor

while ensuring that the largest particles do not settle to the bottom and block the distributor plate. The disengagement zone of the FBR is designed to avoid the first problem. Here the diameter usually doubles, causing the linear velocity of the gas to drop by a factor of 4, leading to a decrease of the particle velocity below the value for minimum fluidization causing fines to fall back into the bed. This is why the minimum fluidization velocity of an FBR, which varies as the square of the particle diameter, has to be carefully estimated. Nevertheless, some particles are small enough so they do not fall and go to the disengagement zone. Therefore, the diameter of the reactor is enlarged by a factor of at least two, in order to minimize the fines from going out of the reactor by defluidizing them [46]. This disengagement zone allows not decreasing the gas flow through the bed, which would have important limitation on the maximum reaction rate because of heat transfer limitations.

Ethylene polymerization in gas-phase FBRs is highly exothermic, producing approximately 3600 $kJ.kg^{-1}$ of converted ethylene [44], which can pose significant problems of heat removal. One of the solutions to overcome these heat removal issues is the addition of induced condensing agents (ICAs) when injecting the gas phase mixture. This process is usually referred as condensed mode operation.

3.2. The use of alkanes to enhance heat removal – super dry and condensing mode operation

While space time yields in slurry processes might be higher than in gas phase, the latter remains the only way we have to make products like LLDPE or other polyolefins with a high amorphous content. The polymerization of ethylene in gas-phase fluidized bed reactors (FBRs) remains an important process for the production of polyethylene (i.e. LLDPE, HDPE). Nevertheless, the highly exothermic nature of ethylene polymerization and the poor heat transfer characteristics of the gas phase can pose significant problems of heat removal. It is therefore important to continuously remove heat generated by providing means to cool the bed since the maximum rate at which the heat of the reaction can be removed from the reactor is clearly a limiting step in the polymer production rate in gas phase reactors [5,22, 26,27, 28,51]. Indeed, increasing the polymer production rate without being able to remove the associated heat release would result in a drastic increase in the reactor temperature that can cause the polymer fusion and subsequently the reactor shut down [51].

As mentioned above, the temperature of the FBR is controlled to an isothermal level through continuously removing the heat of polymerization by circulating the gas from the fluidized bed

to a heat exchanger outside the reactor and recirculation of the cooled gas stream back into the reactor [36].

In order to understand better how heat transfer can be improved, let us look at a simplified steady-state state energy balance around a FBR, given by Equation (1):

$$\dot{m}_{\mathrm{g,in}} C_{pg,\mathrm{in}} \left(T_{\mathrm{g,in}} - T_{\mathrm{g}}\right) - UA\left(T_{\mathrm{g}} - T_{\mathrm{w}}\right) - Q_{\mathrm{vap}} + R_{\mathrm{p}} V_{\mathrm{R}} \left(-\Delta H_{\mathrm{p}}\right) = 0 \qquad (1)$$

where $\dot{m}_{\mathrm{g,in}}$ is the inlet gas mass flow rate, $T_{\mathrm{g,in}}$ is the inlet gas stream temperature and $C_{pg,\mathrm{in}}$ is the heat capacity of the inlet gas stream. *U* is the overall heat transfer coefficient, *A* is the surface area of contact between the exchanger and the gas, T_{g} is the temperature of the gas in the bed, T_{w} is the reactor wall temperature, Q_{vap} is the total enthalpy change due to evaporation of liquid in the reactor, R_{p} is the rate of the polymerization per unit of volume of reactor bed V_{R} and $-\Delta H_{\mathrm{p}}$ is the overall enthalpy of polymerization.

Equation (1) can then be rearranged as follow:

$$R_p V_R = \frac{\dot{m}_{\mathrm{g,in}} C_{pg,\mathrm{in}} \left(T_{\mathrm{R}} - T_{\mathrm{g,in}}\right) + UA\left(T_{\mathrm{g}} - T_{\mathrm{w}}\right) + Q_{\mathrm{vap}}}{\left(-\Delta H_{\mathrm{p}}\right)}$$

This equation shows that if one wishes to increase the productivity of the reactor ($R_p V_R$), this can be done by increasing the heat capacity of the inlet gas stream and/or increasing the enthalpy change due to the evaporation of liquid in the reactor. Increasing the value of the overall heat transfer coefficient is extremely difficult since it is a function of the gas flow rate but the minimum fluidization velocity has to be carefully respected if we want to avoid fines to be blown out of the reactor. Furthermore, it is also difficult to change the value of the bed temperature T_R significantly as this is linked to product quality, and can lead to major operability problems if it goes too high. In order to increase the productivity, alkanes can be added to the reactor, either in liquid or gas phase. If the inlet fluid temperature is greater than its dew point, Q_{vap} will be equal to zero, which will leave us the heat capacity of the inlet gas stream as only way to increase the productivity. The heat capacity of common process components in gas phase ethylene polymerization reactors is given in **Table 4**.

Looking at these values, and considering an inlet gas stream containing 9 bar of ethylene, 1 bar of hydrogen and 6 bar of nitrogen, this will lead to a heat capacity of 8.8 cal.K^{-1}.mol^{-1}. If we replace 6 bar of nitrogen by 1 bar of nitrogen + 5 bar of propane, the heat capacity will be increased about 38% higher. Consequently, replacing nitrogen by ICAs will increase the heat

capacity of the inlet gas stream, allowing us to generate and remove more heat, thereby leading to an increase of the productivity of the reactor.

Table 4. *Heat capacity of gaseous components used in the polymerization of ethylene in gas phase processes*

Gaseous component	**Heat Capacity** (25°C) ($cal.K^{-1}.mol^{-1}$)	**Reference**
Hydrogen	6.9	52
Nitrogen	7.0	52
Ethylene	10.4	53
Propylene	15.3	53
Propane	17.4	53
Iso-butane	23.1	53
Iso-pentane	28.4	53
n-hexane	34.0	53

Of course, if the feed stream is cooled to below its dew point, then the feed to the reactor will contain a certain amount of liquid (depending on its composition and temperature). This liquid will vaporize at a certain point in the reactor, allowing us to remove even more heat.

We will refer to running the process with a vapor only feed stream that contains ICA as "super dry mode" (as opposed to dry mode where no additional inert compounds are added and nitrogen is used to regulate partial pressures). A process with a partially liquefied feed is said to be running in condensed mode [54].

3.3. Beyond Heat Transfer – Further impact of ICA

A recent review [34] shows that using ICA, whether added in liquid form or only as vapors can have numerous effects beyond simply enhancing heat transfer. This is shown schematically in ***Figure 6***. Of course heat transfer is the initial reason for adding ICA, but (much like α-olefin comonomers) they will also influence many important aspects related to polymer thermodynamics (solubility, diffusion, etc.), the physical properties of the polymers, and certain aspects related to reactor operability (stickiness, pressure drop, etc.). Let us consider briefly each of these general points in turn.

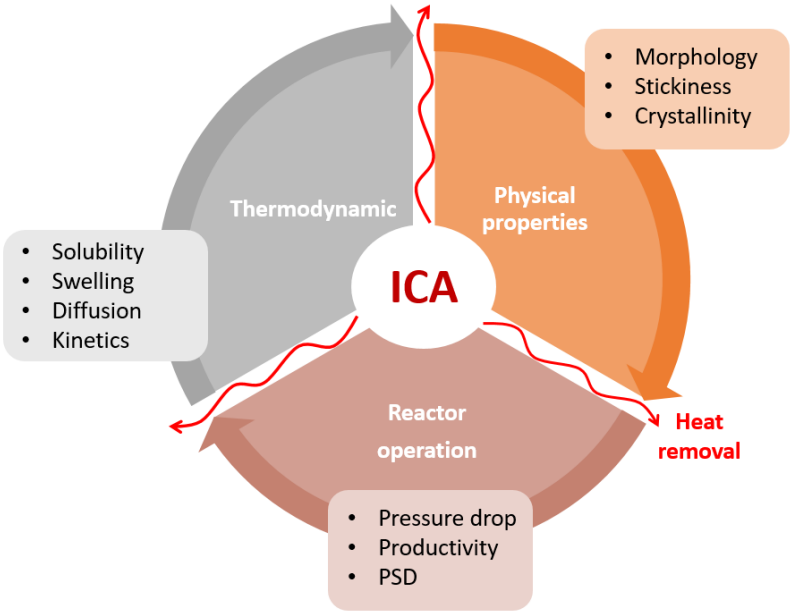

Figure 6. *Impact of ICA during condensed mode operation in gas-phase FBR.*

3.3.1. Solubility and diffusion: thermodynamically-related quantities

ICAs that are added to the reactor are chemically inert in the sense that they do not have any influence on the behavior of the active sites. However, the impact of ICAs is more complex than simply increasing the heat removal rate from the reaction. Indeed, they are able to change the chemical and physical properties of the polymer.

The amount and type of ICA injected in a FBR is one of the most important factors that affects the overall quantity of the dissolved species in the polymer. Indeed, these ICAs will dissolve inside the amorphous phase of the polymer, as well as the other gaseous species injected into the reactor (i.e. monomer, hydrogen, comonomer), and will therefore influence many properties of the polymer, and in particular, the concentration of the different species in the amorphous phase of the polymer. It turns out that the presence of a heavier component (i.e., ICA or comonomer) in the gas phase enhances the solubility of the lighter component (i.e., ethylene) in the amorphous phase of polymer, and vice-versa [36,55–62]. This phenomenon is often referred to as cosolubility effect, where heavy component acts as a co-solvent to ethylene and ethylene as an anti-solvent to the other.

This co-solubility effect will then enhance the local concentration of ethylene in the amorphous phase of the polymer causing an increase in the rate of polymerization, or decreases the

solubility of a comonomer leading to changes in the crystallinity of the polymer [63]. Alizadeh et al.[37,59] showed that adding 2.5 bars of n-pentane to 7 bars of ethylene leads to an increase in the initial polymerization rate by a factor 2.5 times with respect to that observed for 7 bars of ethylene alone. The same tendency is presented for n-hexane as ICA, where it has been shown that adding 0.8 bars of n-hexane leads to an increase of the initial activity of 1.8 times higher than with ethylene alone.

In addition to the impact of the different species on the solubility (i.e. at equilibrium) and the swelling of the amorphous phase of the polymer, changes in their diffusivity (i.e. before equilibrium) through the polymer to the active sites also occurs. For instance, Kanellopoulos et al.[64] showed that polymer swelling increases the diffusion rate for binary systems. Alves et al.[65] developed a diffusion model for ternary systems based on the free volume of penetrant/polymer systems that accounts for polymer swelling, as well as co-solubility effect. They showed that the presence of ICA increases the overall solubility of the mixture leading to higher degree of swelling of the polymer resulting in an increase of the diffusion coefficient.

Obviously, different ICAs and other penetrants will induce different changes in a given system. For instance, the swelling of the polymer particle by an ICA was studied in several papers [58,64,66,67] since this property is crucial when modeling fluidized bed reactors, and this will be discussed in detail in Section 3.3.3. Bashir et al.[58,66] used the Sanchez-Lacombe equation of state to model the swelling of the polymer in presence of different ICAs, and showed that heavier ICAs have higher solubility in the amorphous phase of the polymer and therefore leads to a higher degree of swelling of the polymer particle. Indeed, adding ICA increases the free volume of the amorphous phase of the polymer and promotes greater mobility of the chains, leading to the swelling of the particle. The ability to develop models to predict the contribution of these different phenomena is clearly very important if we wish to fine tune our control of polymer properties. This point will be discussed in more detail in Section 4.

3.3.2. Physical Properties

Since the sorption effects mentioned change the concentrations of reactive species in the polymer phase and thus at the active sites, they will have an impact on the polymerization rate and polymer properties. A series of recent articles from our research group studied theoretically and experimentally the solubility of ICAs in presence of ethylene inside the polymer [58,59,61,67–

[69]. They showed that the solubility of a given component in a polymer is function of the temperature, pressure, polymer crystallinity, and in the case of ternary systems, of the composition of the gas phase. Indeed, increasing the total pressure or decreasing the temperature leads to an increase in the solubility of the different species.

It has also been shown that the increase in ethylene concentration at the active sites due to the co-solvent effect of ICA, leads to an increase in the molecular weight of the produced polymer. Indeed, Namkajorn et al.[59] observed a significant increase in the molecular weight distribution when adding ICAs such as isopentane or n-hexane. Other authors also showed that the crystallinity of the particles in the reactor was substantially higher when ICA was present in the reactor than in the case of dry mode (i.e. no ICA). They attributed this to the impact of ICA on the kinetics of crystallization, which was validated in a separate study [70]. Furthermore, in the case of copolymerization, it has been shown that changing levels of ICA concentration for fixed monomer and comonomer pressures can also lead to changes in polymer crystallinity (i.e. incorporation of comonomer) by changing the monomer to comonomer ratio at the active sites [63].

As will be discussed in the Section 4, changing the rates of reaction, diffusivity, and polymer properties can all have an influence on how the polymer particles grow and how their morphology can change in the reactor; these are all critical issues from many points of view.

3.3.3 Reactor Operation

ICAs can have direct consequences on the basic operation of FBRs for PE. For instance, one can encounter different operational challenges caused by the addition of ICAs in the reactor. The introduction of liquid into a gas phase fluidized bed reactor could result in plugging of the distribution plate, non-uniformity of monomer concentrations inside the FBR and accumulation of liquid at the bottom of the reactor which can result in a complete reactor shut-down [42,43,71,72]. Other issues include a limit on the type and amount of ICA that can be introduced inside the reactor to avoid having the polymer becoming too sticky to discharge or to maintain a normal fluidization velocity [71]. While extremely important from an operational point of view, these and similar issues are outside of the scope of the current thesis. The reader is referred to references [34,43,71,72] for more detailed discussion of these points.

Adding ICA during ethylene polymerization in gas phase also changes the temperature inside the reactor. For instance, Andrade et al.[69] showed that in dry mode (i.e. without ICA), increasing the temperature in the reactor should increase the polymerization rate due to the activation energy of the exothermic reaction. Besides, the heat capacity of the gas phase is much lower in dry mode than in presence of ICAs, so the difference between the particle temperature and the gas phase will be lower in presence of ICA than in dry mode. This effect was also shown by Alizadeh et al.[37] by developing a single particle model in order to show the gradients of temperature and concentration within the growing polymer particle. The model demonstrated that the temperature of the particle rapidly increases at the beginning of the reaction and then gradually decreases as the reaction proceeds, to a steady-state value around the bulk temperature. This observation was explained by the fact that the temperature evolves in the same manner as the reaction rate during the polymerization reaction. This was also explained by the fact that the polymer particle size and thus its external surface area grow very rapidly during the initial steps of the polymerization which facilitates the exchange of generated heat and causes the particle temperature to decrease.

Furthermore, the importance of the cosolubility effect on the reactor operation was shown by Alves et al.[67], who developed a model demonstrating the impact of change in the polymer density and then in the polymer swelling on reactor modeling. Indeed, their model shows the impact of ICA on the production, reactor behavior and polymer PSD. They showed that the increase of ICA partial pressure increases the productivity, production, ethylene conversion and pressure drop. As an example, adding ICAs during ethylene polymerization in gas phase decreases the residence time inside the reactor of 22% in presence of propane and 42% in presence of isobutane with respect to the polymerization reaction in dry mode. This means that the catalyst needs a shorter time to produce polymer, leading therefore to an increase in the PE production rates.

4. Single particle modelling and kinetics

A growing polymer particle can be thought of as a microreactor, where heat and mass transport phenomena coupled to polymerization reactions and other processes take place [73]. Regardless of whether we are operating in a gas or slurry phase process, it can be said that the catalyst particle injected into a reactor will change rapidly, first by undergoing fragmentation, and then through the growth of the polymer particle. These processes, along with reactor operating conditions and the characteristics of the original catalyst support, are important steps in

determining the final properties of the produced polymer. The properties of the final polymer product depend on the molecular properties such as comonomer content, molecular weight distribution, degree of crystallinity, but also on the morphology of polymer particles such as the growth and the shape of particles and the intra-particle distribution of pore and polymer phases. It is therefore crucial to understand the different phenomena that occurs during ethylene polymerization in gas phase.

4.1.Particle morphology and structure

Before describing the particle growth during ethylene polymerization as well as writing the mathematical expressions to quantify these phenomena, we begin our discussion by looking at the initial morphology of the catalyst particles and their evolution during the polymerization.

Indeed, the role of a catalyst particle, and especially the role of the catalyst support, is mainly to transport the active sites into the reactor where they can be exposed to monomer to produce polymer. The advantage of starting and finishing with a particle is that it makes it simple to handle and to recover your final product. The knowledge of both the chemical nature of the support and its physical properties (i.e. high surface area, pore-size distribution) is essential in order to produce a catalyst and thus polymer particles with the desired properties.

Supported catalyst particles are highly porous and have diameters varying from 10 to 100 µm, depending on the type of polymerization process that will be performed [5]. These supported catalyst particles, often referred to as macrograin or macroparticle, are composed of an association of smaller structures, reported as micrograins or microparticles [74]. $MgCl_2$ and SiO_2 are the two most commonly used supports, and they have a high specific surface area so they maximize the number of accessible active sites per unit volume thereby allowing us to make as much product as possible with as little catalyst as possible. Most common catalyst supports have specific surface areas varying from 200 to 600 $m^2.g^{-1}$. Besides, these supports have to be friable enough so that they can be fragmented during the polymerization in order to allow monomer access to the active sites (more on this below). However, they have to be strong enough to allow the fragmentation to proceed in a controlled manner by avoiding the formation of fines [75]. Supports used for Ziegler-Natta catalysts are both silica and $MgCl_2$, whereas Phillips and metallocenes catalysts use mostly silica supports. $MgCl_2$ is a crystalline, ionic solid into which the Ziegler-Natta active sites are inserted via isomorphic lattice substitution [76,77]. Silica supports are amorphous solids, upon which either chromium oxide sites are fixed via calcination at high temperature, or metallocenes are adsorbed or immobilized on the silica surface [78–82].

These catalytic systems are fundamentally different from a chemical point of view but present however a number of common characteristics. For this reason, the following modeling section can be applied for both $MgCl_2$ and SiO_2 supported particles. This discussion is intended to help the reader understand the importance of the thermodynamic aspects being studied in the current thesis, so we will not go into great details. The interested reader is referred to references [74,75,81,83–85] for more details.

4.2.Particle growth during ethylene polymerization

During ethylene polymerization, the catalyst particle is first injected into the reactor. Monomer diffuses from the continuous phase of the reactor into the pores of the supported particle, where the active sites of the catalyst are found. When monomer contacts the active sites of the catalyst particle, polymer formation takes place and the fast-forming chains will be growing on the catalyst surface and pores. As polymer accumulates in the pores of the catalyst particle, the initial structure of the particle suffers a build-up of stress at different points, leading to the fragmentation process [74,83]. However, this fragmentation process lasts a very short period of time, on the order of 10^{-1} to 10^{-2} seconds, depending on the catalytic system [47]. During that time, the initial structure of the catalyst fragments into smaller fragments, but because of the polymer formed (if this occurs correctly) the particle itself remains intact.

The fragmentation process is important for the polymerization to progress reasonably quickly by conserving a satisfactorily fast access of the monomer to the active sites through creating or maintaining a sufficient pore space inside the polymer particle. As the fragmentation proceeds, the active sites located on the fragments of the initial catalyst particle are completely surrounded by the semi-crystalline polymer. Then, the reaction continues as monomer diffuses through the boundary layer around the catalyst particle and through its pores to reach the active sites. The continuous formation of polymer, which will deposit on the catalyst surface and pores, causes the monomer to sorb and diffuse through this polymer layer to reach the active sites, where polymerization takes place. Since the polymerization reaction is exothermic, the heat produced at the active sites needs to be transferred on the opposite direction of the monomer diffusion; through the polymer layer to the bulk phase [47]. As the reaction proceeds, the particle continues to expand and the volume of the polymer continues to grow [86,87]. This will result in gradients of temperature and concentration through the growing polymer particle as illustrated in **Figure 7**, leading to variations in local reaction rates and polymer properties. Thus, to describe the polymerization reaction, it is imperative to be able to predict the dynamics of mass and heat transfer in the growing particle.

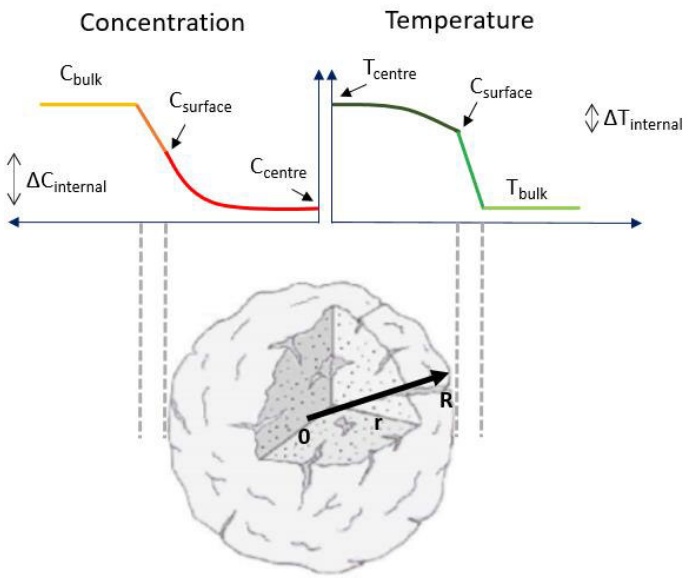

Figure 7. *Schematic representation of temperature and concentration gradient through the growing polymer particle. Adapted from* [47]

4.3.Particle modeling for the polymerization of olefins

When modeling polymerization reactors, quantifying heat and mass transfer inside a growing polymer particle is essential. Besides, knowledge of the intraparticle temperature profile is important since it impacts the polymerization kinetics, as well as the concentration profiles of the different species during polymerization reaction which in turn will influence the polymerization rate and the molecular weight evolution. Up to now, a number of particle models have been proposed in order to solve mass and energy balances around a growing polymer particle in order to obtain temperature and concentration profiles of reactants at every point inside the particle. So far, the Particle Flow Model (PFM) [88–90] and the multigrain model (MGM) [91,92] are considered the closest approximations to describe the phenomena at the mesoscale level during polymerization reasonably well. These models are illustrated in **Figure 8**.

In the case of the PFM, the growing polymer particle is assumed to be pseudo-homogeneous. Besides, the PFM assumes the polymerization reaction to be diffusion controlled, which makes this model able to predict the concentration and temperature gradients within the growing particle at each moment during the polymerization [37,93]. In the case of MGM, the growing polymer particle is assumed to be heterogeneous and is described as an agglomeration of identical spherical sub-particles. Each sub-particle consists of a fragment of the original catalyst particle with all actives sites on its external surface. The polymer particle is called macrograin

or secondary particle and the sub-particles are called micrograins or primary particles [89]. In brief, there are two ways of describing these two models [5]: the "structured" approach where the pores and the structure of the polymer particle are taken into account (MGM) and the "non-structured" approach where the porous particle is considered to be pseudo-homogeneous (PFM). However, both PFM and MGM assume that the active sites are homogeneously dispersed throughout the growing particle at the beginning of the reaction. Besides, it is usually assumed that the fragmentation step is instantaneous and complete at the beginning of the reaction [47].

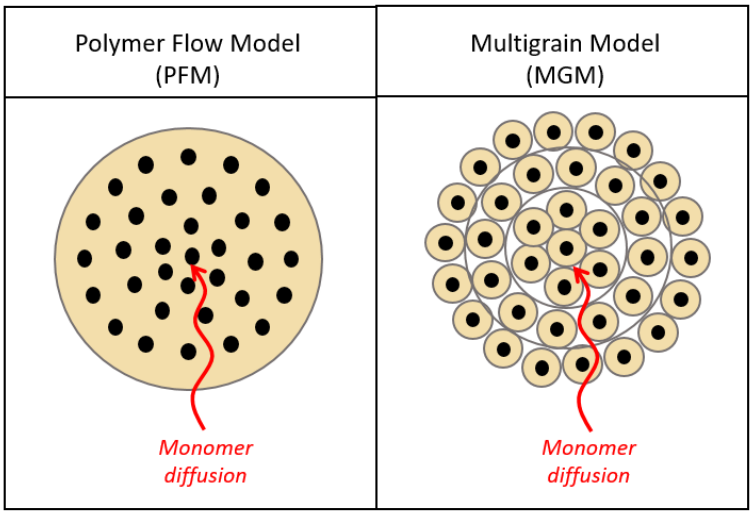

Figure 8. *Representation of the morphology of a growing catalyst/polymer particle using PFM and MGM. Active sites are the black circles and the polymer matrix the yellow ones. Adapted from* [37]

In these models, though they consider different morphology of the growing porous polymer particle, mass transport is described with Fick's diffusion law, where it is assumed at one level for the PFM and two levels for the MGM. Both models can provide a detailed description of the gradients of concentration and temperature profiles within the growing polymer particle, and the overall particle polymerization rate. The PFM offers the advantage of a relatively simpler mathematical description via the hypothesis that the particle constitute a pseudo-homogeneous medium that eases the numerical solution.

In the current study, a comprehensive mathematical particle growth model, accounting for mass and heat transfer limitations appearing during the early growth of a Ziegler-Natta or other supported catalysts in gas phase olefin polymerization is developed. PFM model will be adapted in order to estimate the overall particle polymerization rate as well as the spatial distribution of temperature, monomer, penetrant(s) and polymer molecular properties by solving a system of

partial differential equations describing the conservation of energy and molar species in a growing polymer particle. However, the accurate determination of both the monomer concentration at the catalyst active site and the effective monomer diffusion coefficient is crucial in any particle growth modeling study. This study will therefore show the importance of having an accurate thermodynamic model when developing a particle growth model.

The PFM was developed in the early 1980s and has been applied for almost all types of olefin polymerization catalysts. In all of the following balance equations, *t* and *r* represent the time and radial position inside the particle, respectively and R is the radius of the pseudohomogeneous particle at each moment during its growth.
The mass balance for the monomer *M* can be written as

$$\frac{\partial[C_{\mathrm{M}}]}{\partial t} = \frac{1}{r^2}\frac{\partial}{\partial r}\left(D_{\mathrm{M,ov}} r^2 \frac{\partial[C_{\mathrm{M}}]}{\partial r}\right) - R_{\mathrm{v}}$$

Where $[C_{\mathrm{M}}]$ is the ethylene molar concentration, $D_{\mathrm{M,ov}}$ is the overall (or effective) diffusivity of ethylene, and R_v is the rate of ethylene consumption.

The mass balance for inert compounds *ICA* can be written as

$$\frac{\partial[C_{\mathrm{ICA}}]}{\partial t} = \frac{1}{r^2}\frac{\partial}{\partial r}\left(D_{\mathrm{ICA,ov}} r^2 \frac{\partial[C_{\mathrm{ICA}}]}{\partial r}\right)$$

Where $[C_{\mathrm{ICA}}]$ and $D_{\mathrm{ICA,ov}}$ are the ICA molar concentration and overall diffusivity of the different ICAs, respectively.

Different initial and boundary conditions can be used for both mass balances but the most commonly used for monomer, comonomers or ICAs are

$$[C]_{(r,0)} = 0$$

$$[C]_{(R,t)} = [C]^{\mathrm{eq}}$$

$$\frac{\partial[C]_{(0,t)}}{\partial r} = 0$$

$[C_{\mathrm{M}}]^{\mathrm{eq}}$ is the overall equilibrium concentration of ethylene in the particle and $[C_{\mathrm{ICA}}]^{\mathrm{eq}}$ is the equilibrium concentration of the different reactants in the particle, both calculated with Sanchez-Lacombe EoS.

The energy balance equation can be written as

$$\rho_{\mathrm{ov}} C_{p,\mathrm{ov}} \frac{\partial T}{\partial t} = \frac{k_{\mathrm{c,p}}}{r^2} \frac{\partial}{\partial r}\left(r^2 \frac{\partial T}{\partial r}\right) + \left(-\Delta H_{\mathrm{p}}\right) R_{\mathrm{v}}$$

Where R_{v} is the rate of the reaction per unit of volume of catalyst. The initial and boundary conditions used for the energy balance are

$$T_{(r,0)} = T_{\mathrm{b}}$$

$$-k_{\mathrm{c,p}} \frac{\partial T_{(R,t)}}{\partial r} = h(T - T_{\mathrm{b}})$$

$$\frac{\partial T_{(0,t)}}{\partial r} = 0$$

Where T, ΔH_{p}, $k_{\mathrm{c,p}}$, ρ_{ov} and $C_{\mathrm{p,ov}}$ represent the temperature, the heat of polymerization, the overall thermal conductivity of the particle, the overall particle density, and the heat capacity of the particle, respectively. In the first boundary condition, h, and T_{b} are the heat transfer coefficient and the bulk temperature of the continuous gas phase in the reactor, respectively.

The set of coupled partial differential equations can be solved in a number of ways in order to have a better understanding of the heat and mass transfer resistance inside the growing polymer particle. The polymerization rate at the active sites can be obtained by two levels of models:

$$R_{\mathrm{v}} = k_{\mathrm{p}} C^* [C_{\mathrm{M}}] \qquad \text{or} \qquad R_{\mathrm{v}} = k_{\mathrm{p}} \mu_0 [C_{\mathrm{M}}]$$

Where k_{p} is the propagation rate constant described by Arrhenius law, C^* is the concentration of active sites per volume of catalyst and μ_0 is the concentration of activated catalyst sites. Indeed, the second model takes into account the kinetic model described in ***Table 5*** where living and dead polymer chains are described, whereas the first model using C^* is a big approximation. It is therefore more precise to use the second model.

4.4.Particle modeling studies for the polymerization of olefins

A great number of mathematical models can be found in the open literature to describe the growth of polymer particles during olefins polymerization, with different degrees of complexity.

Floyd and Ray[94] developed a multigrain particle model in order to investigate the effects of intraparticle mass and heat transfer for a range of catalyst activities. They introduced correlations for diffusion coefficients and sorption, and showed the importance of having a good thermodynamic description of the system. However, they used a correlation from Stern et al.[95] to estimate the Henry's law solubility coefficient, which is clearly deviating from realistic sorption data at higher pressures and from multicomponent systems. They also used a correlation given by Michaels and Bixler[96] to estimate the diffusion coefficients of vapors through semicrystalline polyethylene. Similar approaches (with perhaps different correlations) have been taken by most of the subsequent authors, but it is important to point out that they do not take into account mixture effects in multicomponent systems nor polymer swelling.

Floyd and Ray[97] used the multigrain particle model developed in their previous paper[94] to analyze heat and mass transfer resistances in the external boundary layer of the polymer particles. They showed that external mass transfer is negligible, even for the most active catalysts, also demonstrated by McKenna et al.[98] and Chiovetta et al.[87,99]. Nevertheless, they showed that external film temperature gradients can be large, especially for high-activity catalyst. Indeed, particle overheating due to external film resistance can result in gradients of 10s of K for large catalyst particles at the beginning of the polymerization. Besides, they also suggested that the heat transfer resistance in the external film is predicted to fall off rapidly during polymerization as polymer particles growth increases.

Hutchinson and Ray[100] refined the MGM of Floyd and Ray[94,97] and extended it to copolymerization systems. This model describes the effect of mass and heat transfer and predicts catalyst performance, polymerization rates and particle morphology. They showed the importance of mass transfer limitations inside the particle. They also demonstrated that the diffusion resistance could generally not explain the wide molecular weight distributions often observed in their studied systems, but did not account for compositional effects of the gas phase on the final results.

Kosek et al.[101] extended Hutchinson and Ray's work[100] to study polymer particle overheating during catalytic gas-phase olefin polymerization by using Fick's diffusion model. This model takes into account the heat and mass transfer resistance within both the particle boundary layer and inside the particle. They confirmed Floyd and Ray[94,97] results, which reports that intraparticle temperature gradients are negligible and that intraparticle mass transport resistance has an important effect on particle overheating, especially for high-activity catalyst in initial

stage. Besides, the overheating of polymer particles predicted by dynamic simulations is smaller in terms of maximum temperature rise than the overheating predicted by stationary models. They reported that dynamic simulations are better suited for the analysis of small polymer particles in the early stages of their growth, than steady-state modeling of polymer particle overheating [102,103].

Chiovetta and Estenoz[104] developed a geometrical model to reproduce the support structure in which they included diffusion and reaction phenomena to account for heat and mass transfer effects, and most importantly were the only authors to propose a model that allowed one to include the effect of particle fragmentation. This model was later extended by Chiovetta and Ferrero[105–108], and finaly by Chiovetta and Estenoz[87,99,104]. Indeed, they concentrated on the relationship between particle fragmentation and the development of concentration and temperature profiles in the growing polymer particle during the initial stages of polymerization. However, most common models assume the fragmentation to be instantaneous and complete at the beginning of the reaction [37,93,101,109]. The particle model developed in the current thesis will also include this assumption.

Parasu Veera et al.[110] developed a multigrain particle model in which monomer transport occurs not only by diffusion, but also by convection through the pores. The convection is then measured experimentally by the pressure gradient created by the monomer consumption within the particles. This will therefore lead to a significant higher monomer transport rates than thus predicted. Kittilsen et al.[111] showed the importance of the convective transport for big catalyst particles, highly active catalyst particle and high fraction of the reactive species in the fluid (i.e. comonomer).

Accurate estimation of the monomer concentration at the catalyst active site as well as the effective monomer diffusion coefficient are two issues that need to be carefully applied in particle modeling study. McKenna et al.[98] and Weickert et al.[112] have shown that the high activities observed with the modern catalysts cannot be explained by the Fickian diffusion of monomer, nor by Henry's law correlation for sorption data. This is an important aspect since these thermodynamic effects have a significant impact on the early growth of the catalyst particle as they cause the variation of catalyst morphology and porosity.

Yiagopoulos et al.[93] developed a particle growth model based on the PFM, accounting for both external and internal mass and heat transfer limitations. They included diffusional and convectional mass and heat fluxes. They introduced Sanchez-Lacombe thermodynamic model

to calculate the equilibrium monomer concentration in the amorphous polymer, but only for binary (one penetrant plus a polymer) systems. They investigated the effect of prepolymerization time and temperature on the overall polymerization rate and particle overheating. They showed that it is necessary to prepolymerize the highly active Ziegler-Natta catalyst before their injection into the reactor, which will reduce the internal and external mass and heat transfer resistance during the initial seconds of the polymerization. Wu et al.[113] presented similar results when investigating the effect of catalyst prepolymerization on the final polymer properties produced in gas phase ethylene/1-butene copolymerization

Kanellopoulos et al.[109] developed a new particle model called the random pore polymeric flow model (RPPFM) based on the modified polymeric flow model (MPFM) and the random pore diffusion model of Wakao and Smith[114]. Indeed, they analyzed the effects of initial catalyst size, catalyst morphology (i.e. porosity), growth and overheating of highly active Ziegler-Natta catalyst particles in a gas phase olefin polymerization. Indeed, they used the Sanchez-Lacombe equation of state to calculate the equilibrium concentration of monomer in the amorphous phase of the polymer. They also introduced a new diffusion model that takes into account the change in the particle porosity, the crystallinity of the polymer, the size of the penetrant molecules and the temperature. They showed that increasing the initial catalyst size decreases the initial polymerization rate due to mass transfer limitations and increases particle overheating due to heat transfer limitations. Furthermore, they showed that as the degree of crystallinity increases, the polymerization rate decreases due to the decrease of ethylene diffusion coefficient, and increases particle overheating due to a decrease in the rate of particle swelling.

Alizadeh et al.[37] developed a particle model based on the PFM in order to predict the transient behavior of concentration and temperature profiles within the growing polymer particle during gas-phase ethylene polymerization. They included an accurate thermodynamic description through Sanchez-Lacombe EoS as sorption model and Vrentas and Duda[115,116] as diffusion model. Indeed, they were the first to include multicomponent thermodynamic effects and showed that the gas phase composition (i.e. ethylene, n-hexane) had a noticeable impact on the mass and heat transfer, as well as on the polymerization rate.

Hoel et al.[92] also developed a Single Particle Model (SPM) to look at copolymer properties. One of their most interesting contributions (in the context of the current work) was the fact that they postulated that the lack of fundamental data or correlations relating diffusivity and monomer sorption to copolymer composition or crystallinity increase the difficulty of modeling particle growth process, especially for copolymerization.

The present thesis will then include a particle model based on the RPPFM developed by Kanellopoulos et al.[109] that will predict the concentration and temperature profiles within the growing polymer particle during gas-phase ethylene polymerization. This model is able to show the impact of different ICAs (i.e. n-hexane and n-pentane) on the mass and heat transfer, the polymerization rate but also on the molecular weight distribution of the produced polymer.

4.5.Kinetic modeling for the polymerization of olefins

Knowledge of the kinetics of polymerization is fundamental for the mathematical modeling of polyethylene particle growth. Understanding the kinetics on a microscale level is crucial in order to show the effects of multiple active sites on molecular weight distribution (MWD). Indeed, at this scale, multiple mechanisms occur such as site activation, polymer growth and catalyst deactivation. Several papers present a comprehensive detailed kinetic scheme for ethylene polymerization in gas-phase [93,117]. Yiannoulakis et al.[118] employed a kinetic model for homopolymerization to look at the effect of reaction operation on molecular weight. Then, Kiparissides et al.[117] implemented a kinetic scheme into a MGM to investigate the effect of reactor operation conditions on particle growth in a catalytic ethylene/1-butene copolymerization gas-phase FBR. Both used the method of moments to describe the chain length, and offered efficient ways for estimating kinetics parameters from experimental data. P

Population balances and the method of moments are the traditional ways of modeling the molecular weight distribution (MWD) for most polymerization reactions. Population balances are molar balances for the concentration of living and dead polymer chains of each length inside the reactor. Generally, only the zeroth, first and second moment equations are solved for both living and dead polymer chains. Besides, each active site type has generally a complete kinetic scheme involving activation, initiation, propagation, transfer and deactivation. The kinetic model in ***Table 5*** is developed to account for any number of active site types. The kinetic mechanism described in this study is similar to those outlined by [10,117,118].

The initiation of active sites consists of associating the active site to the monomer in order to form a living polymer chain of length 1. Then, the living polymer chains of length *r* grow by linking to monomer species, leading to a living polymer chain of length *r+1* with terminal monomer attached to the active center, corresponding to the propagation. Most dead polymer chains are produced by chain transfer reactions. These transfer reactions occur with monomer

(transfer to monomer) or with hydrogen (transfer to hydrogen), and both create living polymer chains of length one with different reactivities (i.e. P_{H}^{k} , P_{1}^{k}) and generate a dead polymer segment of length *r*. The spontaneous chain transfer reaction regenerates new active sites that can be initiated. And finally, active sites can deactivate spontaneously to form dead sites and dead polymeric segments.

Table 5. Kinetic scheme of ethylene homopolymerization over a Ziegler-Natta multiple site catalyst

Description	**Chemical reactions**	**Rate constants**
Initiation	$C_k^* + \mathrm{M} \longrightarrow P_1^k$	k_i^k
Propagation	$P_r^k + \mathrm{M} \longrightarrow P_{r+1}^k$	k_p^k
Transfer to H_2	$P_r^k + H_2 \longrightarrow P_{\mathrm{H}}^k + D_r^k$	k_{tH}^k
Initiation of P_H	$P_{\mathrm{H}}^k + \mathrm{M} \longrightarrow P_1^k$	k_{iH}^k
Transfer to monomer	$P_r^k + \mathrm{M} \longrightarrow P_1^k + D_r^k$	k_{tM}^k
Spontaneous chain transfer	$P_r^k \longrightarrow C_k^* + D_r^k$	k_{tsp}^k
Deactivation	$P_r^k \longrightarrow C_{\mathrm{d}}^k + D_r^k$	k_d^k

Where C^* is the concentration of vacant catalyst active sites, M is the monomer concentration, P_r is the concentration of "live" polymer chains, P_{H} is the concentration of polymer chains containing hydrogen, D_r is the concentration of dead polymer chains, H_2 denotes the hydrogen concentration, C_{d} is the concentration of deactivated catalyst site.

The single particle model can be numerically solved to calculate the temperature and concentration gradients inside the particle during ethylene polymerization in gas phase, but also to estimate the change in the reaction rate, the molecular weight distribution and the particle size when varying the gas phase composition inside the reactor. This model can be fitted to experimental data of both reaction rate and MWD in order to identify the kinetic parameters. Indeed, knowledge of the heat and mass transfer resistance inside the growing polymer particle as well as the variation of the MWD is a very important tool when modeling gas phase

polymerization reactors. MWD data can provide crucial details about polymer properties such as MFI which is related to the processability of the produced polymer.

Clearly, if we want to have confidence in model predictions, it is very important to know the exact values for the equilibrium concentrations of the different species present in the reactor in the amorphous phase of the polymer, as well as the diffusivity.

5. Penetrant sorption and diffusion in polyethylene

The discussion in the previous section demonstrates why it is so important to be able to model the sorption process, and to predict the impact of changing gas phase compositions on sorption, diffusion and related processes. In this section we will discuss the main models used for this purpose, show that in fact data for estimating model parameters is sorely lacking in the literature, and look at the different experimental studies that can help us to find useful data for process modelling.

5.1. Thermodynamic models describing sorption equilibrium

For the solubility studies of a single component in a polymer, the sorption of heavy components, especially at higher pressures, deviates considerably from the predictions of Henry's law. Moreover, Henry's law cannot be used for the calculation of solubilities of individual species in multicomponent systems in a polymer. It is therefore essential to use a more sophisticated thermodynamic model in order to be able to have a more realistic thermodynamic description of the system [119].

Advanced equilibrium thermodynamic models are classified into two main categories: activity coefficient models and equations of state (EoS). There are several drawbacks to the activity coefficient approach, including the fact that thermodynamic properties such as densities, enthalpies, entropies cannot be obtained from the same model because the excess Gibbs free energy is rarely known as a function of temperature and pressure [119]. This is why equations of state are favored for solvent-polymer systems, since they can capture the dependency of phase volume on pressure. This parameter is clearly crucial in the calculation of the solubility of solutes in the polymer phase and also the swelling degree of the polymer phase due to the sorption.

EoS are powerful tools for the investigation of thermodynamic properties and phase behavior of pure fluids and their mixtures. The most apparent progress in EoS for polymer systems has been made by applying statistical mechanics. Some models derived from statistical thermodynamics assumed molecules to have one or more segments, and the partition function of the system can be obtained by counting the possible configuration when these segments are arranged in hypothetical cells which are like the lattices in solid materials. Then the calculation of the thermodynamic quantities is made from the partition function on the basis of statistical mechanics. Although, many of the more recent theories describe molecules to be moving freely in continuous space [119].

The Sanchez-Lacombe equation of state (SL EoS) [120] based on lattice models and the Perturbated Chain Statistical Associating Fluid Theory (PC SAFT) [121] based on the perturbation theory are two such models that are widely used in the field of polymer reaction engineering. In this section, an overview of these two equations of state will be presented. **Figure 9** shows the sorption equilibrium of multicomponent systems in polyethylene with PC-SAFT and Sanchez-Lacombe EoS. The red circles are assumed to be the active solid catalyst site, the blue line the monomer particles, and the grey circles the formed polymer particles.

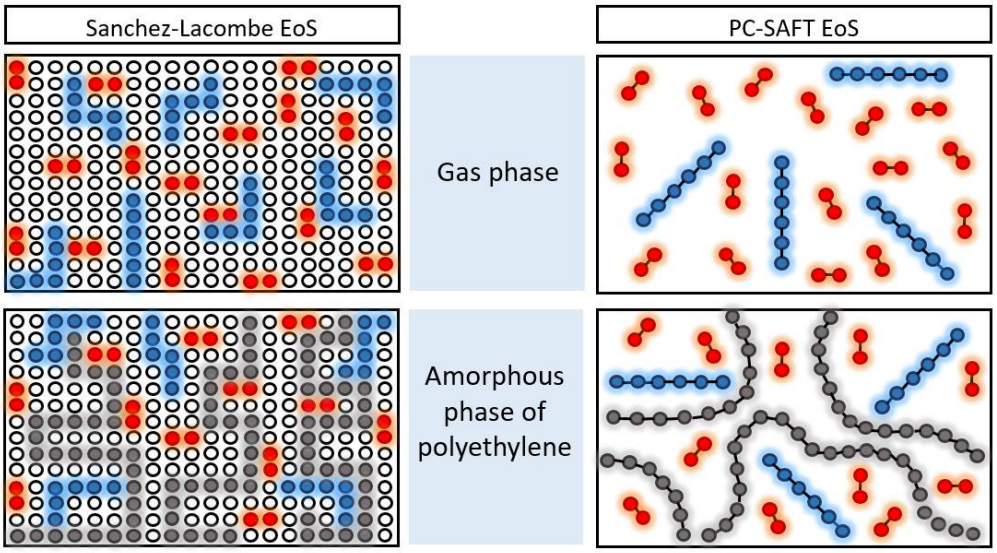

Figure 9. *Schematic representation of PC-SAFT EoS and Sanchez-Lacombe EoS describing sorption equilibrium of multicomponent species during gas-phase ethylene polymerization. Adapted from* [61]

5.1.1. Perturbated Chain Statistical Associating Fluid Theory (PC SAFT)

Statistical Associating Fluid Theory (SAFT) was one of the first models derived from the idea of the perturbation theory. Many modifications of the SAFT model were developed over the years, like the SAFT-LJ (SAFT Lennard-Jones) versions in which Lennard-Jones spheres served as a reference for the chain formation [122,123], and SAFT-VR (SAFT Variable Range) [124], in which the attractive potentials are allowed to show variable widths [125]. A detailed description of the different versions of the SAFT family can be found elsewhere[119]. Despite many theoretical improvements, one of the most successful modification remains the PC-SAFT model, which introduces a dispersion term to the SAFT model. It is the most widely used model of this family in the polymer industry since it provides excellent results when simulating polymer-solvent systems.

The PC-SAFT EoS is a continuum model where molecules, constituted of spherical segments of fixed diameter, are assumed to be moving freely in a continuous space [61]. This model is derived from the perturbation theory, where a reference system is considered to describe the repulsive interactions of the molecules. The perturbation terms are introduced as correction term that takes into account any deviation of real molecules from the reference system. In this model, the freely jointed molecules exhibit repulsive and attractive forces among them. The repulsive interactions are described by an expression of hard chain and the attractive interactions are divided into dispersion interactions (i.e. Van der Waals forces) and a contribution due to association (i.e. formation of hydrogen bonds). These contributions are assumed to be independent of each other and are then described by different perturbation terms. In PC-SAFT EoS, a pure substance is characterized by three parameters: the temperature-independent segment diameter σ, the number of segments per molecule *m*, and the energy corresponding to the interaction of two segments, ε/k. A detailed description of PC-SAFT development model can be found in elsewhere[121,126]. In order to solve this equation of state, k_{ij} interactions parameters between the penetrant molecules and the polymer need to be identified by fitting experimental solubility data to the model.

Xiong et al.[127] compared the performance of SAFT with SL to model cloud point curves in polyethylene systems with n-butane and n-pentane. For all temperature-pressure-composition ranges, the SAFT model predictions were found to be closer to the experimental data. Nevertheless, this comparison study has been reiterated in the past few years by the following authors.

Maity[128] used PC-SAFT to model the solubility of ethylene, carbon dioxide, nitrogen and methane in polyethylene below and above the melting point. He founds out that the adjustable solvent-solute binary interaction parameter k_{ij} is temperature-dependent, and developed a suitable correlation for all studied systems.

Kanellopoulos and Krallis[129] studied the solubility of ethylene, propane, 1-hexene, 1-butene in homo- and co-polyethylene. They showed that PC-SAFT provides an accurate description of the solubilities of olefins in solvents while SL enables good predictions of olefins solubilities in polyolefins. Besides, they showed that PC-SAFT is recommended for ethylene homopolymerization, while SL gives better predictions for ethylene copolymerization.

Banaszak et al.[62] used the molecular simulation method of united atom force field in order to parameterize the PC-SAFT EoS and then extended it to the ternary system of two solutes and a polymer. They predicted that introducing 1-hexene to the gas phase composition increases the solubility of ethylene in the amorphous phase of PE, whereas adding ethylene in the gas phase composition decreases 1-hexene solubility. This leads to a lower gas solubility compared to that predicted by summing the solubilities of the two binary systems. Their simulations were later experimentally validated by means of the gravimetric method conducted by Novak et al.[56].

More recently, Alizadeh et al.[61] studied the solubility of ethylene and n-hexane in polyethylene in a ternary system. They showed that SL EoS overestimates the solubility of both ethylene and n-hexane at all studied temperature, while PC-SAFT overestimates ethylene solubility and underestimates that of n-hexane for all measurement temperatures.

Chmelar et al.[130] used the PC-SAFT equation for the modeling of the sorption of propane and 1-hexene in polyethylene at different temperatures and different crystallinities of the polymer. They showed that the fitting error of the PC-SAFT model was about 5.7% in average with the experimental data.

Very recently, Greenhalgh et al.[131,132] have modeled the vapor solubility of ethylene, 1-butene, isobutane, isopentane, 1-hexene and n-hexane in a series of semicrystalline LLDPE as a function of temperature, pressure and vapor composition. They showed good agreement

between the experimental solubility measured with a magnetic suspension balance and the PC-SAFT model.

5.1.2. Sanchez-Lacombe Equation of State (SL EoS)

Sanchez-Lacombe is a model based on a lattice theory, meaning that pure components are assumed to be broken into parts and placed into a lattice structure [120,133,134]. The SL EoS is basically an extension of the classic Flory-Huggins theory. The main advantage of this model is that it introduces vacant lattice sites or holes, and varying the fraction of holes varies the density and the compressibility. SL assumes a random mixture of holes and "mers", where pure components can interact with intermolecular potential. The energies of hole-hole and mer-hole interactions are zero, whereas the mer-mer interaction has a non-zero interaction energy. In the SL EoS, the properties of a pure component is described by three lattice parameters: the mer-mer interaction energy ε, the closed-packed molar volume of a mer ν and the number of sites (mers) a molecule occupies in the lattice *r*. Moreover, the knowledge of three characteristic parameters for both penetrants and polymers is required: the characteristic pressure P^*, the characteristric temperature T^* and the characteristic density ρ^*. Bashir et al.[135] performed a sensitivity analysis to understand the effect of these three parameters on the predictive capability of SL EoS. It was found that SL EoS solubility predictions are more sensitive to the changes made in characteristic parameters of monomers (especially the monomer characteristic temperature) than those made in the characteristic parameters of the polymer. On a positive note, it is possible to know these parameters *a priori.*

However, the SL EoS includes interaction parameters between the penetrant molecules and the polymer. These are adjustable parameters that need to be estimated in order to obtain accurate thermodynamic predictions. To do so, this equation of state has to be fitted to experimental solubility data (this is also true of PC-SAFT). Here is where the major difficulty comes in: there is very little meaningful data available for multicomponent systems that allow us to obtain the interaction parameters for use in modelling gas phase PE systems.

Bashir et al. also used the SL EoS to estimate the partial molar volumes (PMV) of gases and polymers in binary [66] and ternary systems [58]. They showed that the PMV of gases in the ternary mixtures are greater than their PMV values in the corresponding binary mixture, due to the enhanced thermodynamic interactions. Moreover, the PMV of penetrating molecules can be affected by their concentration in the gas phase, leading to a high average PMV of penetrant at

low gas phase concentration of penetrant, and vice-versa. They attributed the cosolubility effect of a heavier component to its higher thermal expansion coefficient, which could create more free volume in the polymer phase required for the additional sorption of a lighter component. Furthermore, they extended the SL EoS to describe the solubility of ternary mixtures in gas-phase [68]. They demonstrated that SL EoS is in good agreement with the experimental values presented by Novak et al. [56]. This last group showed that the temperature, pressure and gas phase composition in the ethylene/1-hexene ternary mixture affect significantly the solubility behavior. In addition these same authors demonstrated that the co-solvent effect of 1-hexene dominates the anti-solvent effect of ethylene at high pressures and low temperatures, and vice-versa. Besides, they postulated that the predictive capabilities of SL EoS depend on binary interactions parameters which are temperature-dependent for their studied systems.

More recently, Bashir et al.[136] showed the solubility of ethylene, propane, isobutane and n-hexane and their mixtures in LLDPE at different temperatures and pressures, as well as the degree of polymer swelling due to the penetrant dissolution inside the polymer. They fitted SL EoS to binary experimental data in order to identify the interactions parameters k_{ij}, that they used for the ternary systems.

In the same direction, Alizadeh et al.[61] studied the solubility of ethylene and n-hexane in LLDPE and their mixture. They also used binary interaction parameters as input data to fit to ternary systems, and then rearranged k_{23} interaction parameter to have a better fitting of the ternary solubility.

Sun et al. [57] compared the SL EoS estimations with experimental data for ethylene, hydrogen and 1-hexene and their mixture in PE. They showed good agreement with the prediction data from SL EoS. Other authors have used the SL EoS in order to describe the solubility of different penetrants in binary and ternary systems [68,137–144] and show reasonable results compared to the experimental ones.

Both of the SL and PC-SAFT EoS have been used successfully [68,127], but the major drawback that they both share is the fact that they were developed for purely amorphous materials, so when applied to semi-crystalline materials, they cannot be used to predict the impact of the crystalline phase on penetrant solubility. Indeed, Andrade et al.[70] showed that when the crystalline fraction changes, part of the amorphous polymer may be affected by tie molecules that link crystalline lamella surrounding the amorphous region, causing the polymer to swell less. Nevertheless, we have chosen to use the SL EoS because of its mathematical simplicity,

which allows an extension to multicomponent systems and use in single particle and reactor models [7,37].

Table 6 contains a summary of most of the binary (one penetrant + PE) and ternary (two penetrants + PE) systems for which model parameters are available in the literature for the modelling of PE systems.

As we mentioned above, having a good estimation of the impact of the composition of the gas phase on the solubility of the monomer and the comonomer is important (in the very least; no information is available about the impact of heavy components on hydrogen) as this in turn will influence polymerization rates, polymer properties etc. In other words, if one wishes to model a realistic system, one cannot use binary sorption models to estimate the concentration of a single species in the polymer for multicomponent systems and simply add them to describe penetrant concentration in the system. It is necessary to account for the way that they interact with the polymer when mixed together. This means that interaction parameters between the different species and the polymer are needed in order to develop this kind of thermodynamic model. These interaction parameters are the only adjustable parameters in the SL EoS that need to be estimated in order to have a good thermodynamic representation. To do so, this equation of state has to be fitted to experimental solubility data, and such data is sorely lacking for multicomponent systems under conditions similar to those used in a polymerization process.

Table 6. Literature data for modeling methods of binary and ternary systems in polyolefins

Binary / Ternary systems	Modeling method	References
Methane / PE	SL EoS	65
Ethylene / PE	SL EoS PC SAFT	57,61,65,68,129,140,141 61,128–130,145–147
Ethylene / PP	SL EoS PC SAFT	65,68,129,140 129
Propane / PE	SL EoS PC SAFT	129 128–130,145,145,146,148
Propylene / PE	PC SAFT	130,146
Propylene / PP	SL EoS PC SAFT	65,68,129,140 129,145
1-butene / PE	SL EoS PC SAFT	68,129,140 128–130,145–147
n-butane / LDPE	SL EoS PC-SAFT	127,149,150 127,128,146,147
Isobutane / LDPE	SL EoS PC-SAFT	149,150 128
n-pentane / PE	SL EoS PC-SAFT	65,127 127,128,148
1-hexene / PE	SL EoS PC SAFT	57,68,140,149 128,130
n-hexane / PE	SL EoS PC SAFT	61,65,150 61,128
Ethylene / propylene / PE	SL EoS	65,140
Ethylene / 1-butene / PE	SL EoS	68,140
Ethylene / 1-hexene / PE	SL EoS PC SAFT	57,68,129,140 129
Ethylene / n-hexane / PE	SL EoS PC SAFT	61,65 61

5.1.3. Peng-Robinson equation (PR)

Contrarily to modeling the thermodynamics of polymer-penetrant systems, which, as we just saw are highly non-ideal, calculating the compressibility factor of non-ideal gases and their mixture under mild temperatures and pressures is more straightforward. This can be done in different ways, one of which is using cubic equations of state. Two of the most popular cubic EoS include the Soave-Redlich-Kwong (SRK) and the Peng-Robinson (PR) equations. Ting et al.[151] evaluated the Peng-Robinson EoS for its ability to correlate and predict vapor-liquid equilibrium for asymmetric mixtures of alkanes, and found that the PR EoS is accurate for fitting such mixtures.

We will therefore use the PR EoS when this type of calculation is needed, in particular to calculate the compressibility factor of the different species in gas mixtures. The Peng-Robinson [152] equation is given by:

$$P = \frac{R\,T}{\upsilon - b_{\mathrm{m}}} - \frac{a_{\mathrm{m}}(T)}{\upsilon(\upsilon + b_{\mathrm{m}}) + b_{\mathrm{m}}(\upsilon - b_{\mathrm{m}})} \qquad (2)$$

Where υ is molar volume. The parameter a_{m} is a measure of the attractive forces between molecules in the mixture and the parameter b_{m} is the van der Waals co-volume occupied by these molecules in the mixture. These parameters are defined as follow:

$$a_{\mathrm{m}} = \sum_{i=1}^{2}\sum_{j=1}^{2} x_i x_j \left(1 - k_{ij}\right)\sqrt{a_i a_j}$$

$$b_{\mathrm{m}} = \sum_{i=1}^{2} x_i b_i$$

a and b are the respective PR parameters for pure substances. x is the mole fraction of each component in the mixture and k_{ij} is the binary interaction parameter.

Applying the first equation at the critical point, we have:

$$a_i\left(T_{\mathrm{c},i}\right) = 0.45724\frac{R^2 {T_{\mathrm{c},i}}^2}{P_{\mathrm{c},i}}$$

$$b_i\left(T_{\mathrm{c},i}\right) = 0.07780\frac{R\,T_{\mathrm{c},i}}{P_{\mathrm{c},i}}$$

At temperatures other than the critical temperature, we have:

$$a_i(\mathrm{T}) = a_{ii}\left(T_{c,i}\right).\alpha_i\left(T_{\mathrm{r},i}, w_i\right)$$

$$b_i(\mathrm{T}) = b_i\left(T_{\mathrm{c},i}\right)$$

A relationship between α and the reduced temperature T_r can be made and linearized as follow

$$\alpha_i(T_{r,i}, w_i) = \left(1 + m_i\left(1 - {T_{r,i}}^{1/2}\right)\right)^2$$

The constant characteristic of each substance, m_i, is defined as follow:

$$m_i = 0.37464 + 1.54226\, w_i - 0.26992\, {w_i}^2$$

Equation (2) can be rewritten as:

$$A = \frac{a\, P}{R^2 T^2}$$

$$B = \frac{b\, P}{R\, T}$$

$$Z = \frac{P\, v}{R\, T}$$

Where Z is the compressibility factor.

5.2.Experimental methods for sorption measurement

As mentioned above, obtaining experimental data to fit the SL or PC-SAFT EoS is the key of being able to successfully model the impact of the composition of the gas phase, and in particular seemingly inert compounds on the polymerization and polymer properties.

Over the last decade, different experimental methods have been developed to measure the solubility and diffusivity of multicomponent systems in polymers. These experimental methods can be divided into four main classes:

- pressure decay methods in which the amount of the sorbed species is calculated from pressure-volume-temperature (PVT) continuous measurements in an equilibrium cell containing the polymer sample and a known amount of gas species;
- gravimetric methods in which the polymer sample is being saturated with a gas and the solubility is determined by continuously measuring the amount of gas that is sorbed or desorbed from the sample, until the sorption equilibrium is reached;
- oscillating methods in which the resonance characteristics of a vibrating support estimates the increase in mass that is due to the sorption of solute species;
- flow measurement methods like inverse gas chromatography, in which the gas phase composition is analyzed and from which the individual sorbed gases can be deduced.

5.2.1. Sorption studies for binary systems

Rogers et al.[153] (1959) were among the first investigators who measured using a quartz helix microbalance the equilibrium sorption of thirteen organic vapors in different polyethylene samples, having different crystallinities and densities at temperatures between 0-25°C. They revealed that the crystalline phase of polyethylene is physically impenetrable to the solute molecules, acting therefore like regions of cross-linkage. Another study from this research group showed that the solubility of these organic vapors follows Henry's law [154]. However, increasing the pressure of the solutes increases their solubility in the polymer, resulting in considerable plasticizing of polymer chains. The solubility of these vapors starts to increase exponentially and is then deviated from Henry's law.

Analogously, Michaels and Bixler[96] (1961) showed that the solubility of various gases like ethane, methane, ethylene and propylene in semicrystalline PE follows Henry's law throughout the range of their experimental investigation (5-55°C and low pressures < 1 atm). Besides, they confirmed that the crystalline phase of polyethylene does not sorb gas molecules, even small ones like Helium. These authors also found that the solubility coefficient was function of the Lennard-Jones force constant. This came from the fact that the more condensable the gas is, the higher is its solubility in the polymer.

Robeson and Smith[155] (1968) showed the solubility of ethane and butane in polyethylene in the temperature interval of 30-60°C. They also showed that increasing the pressure of the solute increases its solubility in the polymer, resulting in the plasticization of the polymer. They showed that the polymer film plasticizes ten times more with butane than with ethane in their temperature range of experiments.

Li and Long[156] (1969) investigated the solubility of ethylene, methane and nitrogen in polyethylene at 25°C using the quartz spring balance method. They showed that ethylene solubility increases exponentially with increasing the pressure, whereas those of methane and nitrogen increase asymptotically towards a saturation value. Besides, they found that the solubility of ethylene in polyethylene at high pressures (i.e. ethylene critical pressure) deviates from Henry's law.

Meyer and Blanks[157] (1983) measured the solubility of isobutane and propane in both HDPE and LLDPE at high temperatures (up to 260°C) and low pressures (< 3 bar) using a pseudo-gravimetric technique in a constant pressure system. They showed an increase of the solubility of both isobutane and propane when increasing their pressure and decreasing the temperature;

isobutane solubility being higher than propane, as expected. Moreover, they showed the importance of correcting the solubility data for polymer crystallinity as it increases the solubility of isobutane depending on the type of polymer.

Kulkarni and Stern[158] (1983) measured the equilibrium mass uptake of CO2, CH4, C2H4 and C3H8 by semicrystalline PE at gas pressures up to 40 atm and temperatures up to 35°C and found that the solubility coefficient of all penetrants was found to be independent of concentration, which indicates that the penetrant solubilities were within the limits of Henry's law limits.

Castro et al.[159] (1986) studied the solubility of n-butane, n-pentane, n-hexane and n-heptane in polyethylene membranes using gravimetric technique, at very low pressures (< 1 atm). They showed that the bigger the diluent, the higher is its solubility in the polymer. Moreover, they revealed a deviation of the experimental results with Henry's law, mostly at higher temperatures and pressures. This deviation pointed an important interaction between the solvent and the polymer.

Hutchinson and Ray[160] (1990) confirmed that Henry's law is not applicable for heavier hydrocarbon vapors that tend to swell and plasticize the polymer to a much greater extend. Besides, they showed that the crystallinity plays an important role in the sorption process since the crystallites tie the amorphous region together and limit the amount of polymer swelling, and thus the possible diffusion of species in the polymer.

Sato et al.[161] (1999) measured the solubility of CO_2 and N_2 in molten PP and HDPE at pressures up to 17 MPa by using a pressure decay method. They also showed a linear increase of the solubilities with pressure, which corresponds to Henry's law.

Yoon et al.[162,163] (1993) studied the effect of copolymer composition on the solubility of ethylene, propylene, 1-butene and 1-hexene in PE using a quartz spring balance. They showed that Henry's constant is almost independent of the copolymer composition for ethylene and propylene. However, they showed a strong dependency of the solubility of 1-butene and 1-hexene on copolymer composition.

Moore and Wanke[164] (2001) used the gravimetric method to show the solubility of ethylene, 1-butene and1-hexene in LLDPE having different crystallinities. They showed that the solubility of ethylene follows Henry's law for a wide range of temperatures and pressure. Moreover, they showed that Henry's law constant decreases with increasing the temperature and the

crystallinity of the polymer. Nevertheless, Henry's law is no longer followed for larger diluents, such as 1-butene or 1-hexene, since the bigger the diluent, the higher its solubility in the polymer, as also pointed out by Hutchinson and Ray[160].

Kiparissides et al.[141] (2003) used the magnetic suspension microbalance to show the solubility of ethylene in semicrystalline polyethylene at temperatures up to 80°C and pressures up to 66 atm. They also showed that the measured solubilities decrease with increasing temperature and increase with increasing ethylene pressure.

Chmelar et al.[130] (2004) showed the sorption of ethylene and 1-hexene in three polyethylene copolymers samples using the gravimetric method at temperatures up to 150°C and pressures up to 30 bar. Similarly to the studies done previously, they showed that the solubility of lighter components like ethylene follows Henry's law, and that the sorption isotherms of heavier components like 1-hexene are non-linear and increase exponentially at elevated pressures. The same research group measured after few years the solubility of propane and 1-hexene in polyethylene at temperatures and pressures relevant to industrial catalytic gas-phase polymerization of ethylene[165]. They showed that both propane and 1-hexene solubilities increased with decreasing temperature, as expected, and with decreasing PE crystallinity. Furthemore, the solubility of the heavier component, 1-hexene, is significantly larger than that of the lighter component, propane.

Reichert et al.[166] (2005) studied the sorption of propylene in PP particles formed by different polymerization processes, by means of a gravimetric method. They showed that the solubility of propylene in PP can be described by Henry's law at their experimental conditions.

Nagy et al.[167,168] (2007) showed the solubility of iso-hexane and n-hexane in LLDPE using the Cailletet apparatus, from which dew points and bubble points of mixture of known composition can be determined visually. They showed that iso-hexane is a poorer solvent than n-hexane for LLDPE, having a cloud point temperature of 25K less than for n-hexane/LLDPE mixture.

Yao et al.[137] (2011) measured the solubility of propylene in semicrystalline isotactic propylene (iPP) by means of a pressure-decay method. The results showed that the solubility of propylene in iPP increases at elevated pressure and decreases at elevated temperature. The same research group showed the solubility of propylene in HDPE, LDPE and LLDPE using the same pressure-decay approach [138]. They confirmed that the crystallinity has an important impact on propylene solubility. Besides, they showed that propylene solubility depends on the chain microstructure

of the polymer, since the solubility is higher in LDPE than in LLDPE, although these two samples have the same crystallinity.

Sun et al.[57] (2016) showed the solubility of hydrogen, ethylene and 1-hexene in semicrystalline polyethylene films using an intelligent gravimetric analyzer (IGA). It was found that the solubility of ethylene and 1-hexene decreases with the temperature, while that of hydrogen exhibits an opposite variation tendency in the experimental temperature range.

Greenhalgh et al.[131,132] (2018) presented the solubility of ethylene, 1-butene, isobutane, Isopentane, 1-hexene and n-hexane in a series of semicrystalline LLDPE using a magnetic suspension balance (MSB). They showed that the heavier the alkane is, the higher is its solubility in the amorphous phase of the polymer, meaning that ethylene solubility is the lowest and 1-hexene solubility is the highest for their experiments.

A summary of the data we found in the literature for binary systems is given in **Table 7**. A wide range of data is available, so it is possible to fit the interaction parameters for a wide range of compositions. However this is not enough because higher order systems show more complex interactions.

To conclude on the binary studies in the literature, it was shown that:

- Penetrants are soluble only in the amorphous phase of the polymer.
- Vapor solubility increases with pressure and decreases with temperature;
- Henry's law coefficient increases with temperature; Deviation from Henry's law is observed for heavy hydrocarbons at all temperatures and pressures.
- The solubility in the amorphous fraction of the polymer decreases if the overall crystallinity of the polymer increases (at constant temperature and pressure). Indeed, the crystallinity may affect diffusion and swelling of the amorphous phase of the polymer due to tie molecules that are crystalline lamellar that link the amorphous regions of the polymer;
- Heavier alkanes and alkenes are more soluble than their lighter counterparts for a given partial pressure and temperature;

Table 7. *Literature data of sorption of binary systems in polyolefins. P is the pressure in bar and T is the temperature in °C.*

Systems	Experimental techniques	Experimental conditions	References
Hydrogen / PE	IGA	T=[25-90] ; P=[0-10]	57
Methane / PE	Gravimetry	T=25 ; P= [13-90]	156
Ethylene/PE	IGA	T=[50-90] ; P=[0-10]	57
	Gravimetry	T=[25-150] ; P = [0-90]	130,131,141,156,158,162–164,169
Ethane / PE	Permeation	T=[30-60] ; P=[0-10]	155
Propane / PE	Pseudo-gravimetry	T=[150-260] ; P=[0-2.3]	157
	Gravimetry	T=[5,35] ; P=[0-40]	158
Propylene / PE	Gravimetry	T=[30-100] ; P=[1-3]	162,163
	Pressure decay	T=[75-110] ; P=[0-80]	166
n-butane / PE	Permeation	T=[30-60] ; P=[0-10]	155
	Gravimetry	T=[0-45] ; P=[0-9]	159
Isobutane / PE	Pseudo-gravimetry	T=[150-260] ; P=[0-2.3]	157
	Gravimetry	T=[50-85] ; P=[0-14]	131,132
1-butene / PE	Gravimetry	T=[30-100] ; P=[0-12]	131,141,162–164
n-pentane / PE	Gravimetry	T=[0-45] ; P=[0-7]	159
Isopentane / PE	Gravimetry	T=[50-85] ; P=[0-5]	131
n-hexane / PE	Gravimetry	T=[0-85] ; P=[0-2]	131,132,159
	Cailletet apparatus	T=[80-85] ; P=[0-1.6]	167,168
Iso-hexane / PE	Cailletet apparatus	T=[80-85] ; P=[0-1.6]	167,168
1-hexene / PE	IGA	T=[50-90] ; P=[0-0.25]	57
	Gravimetry	T=[50-150] ; P=[0-66]	131,141,162–164
n-heptane / PE	Gravimetry	T=[0-45] ; P=[0-0.5]	159
Propylene / PP	Gravimetry	T=[25-70] ; P=[0-10]	166
	Pressure decay	T=[75-110] ; P=[0-80]	137

5.2.2. Sorption studies for ternary systems

As we stated above, ternary data for PE systems is less common in the open literature, undoubtedly because it is more challenging to measure accurately. Also, usually only overall solubility is available.

Li and Long[156] (1969) determined the overall solubilities of ethylene-methane, ethylene-nitrogen and methane-nitrogen in polyethylene at 25°C using the quartz spring balance method. The data showed a very high plasticizing effect of the most permeating specie in the mixture at higher pressure. Indeed, they explain this effect by the co-solubility effect, where the solubility of the more soluble gas increases the solubility of the less soluble gas and therefore enhance the total solubility of the mixture.

Yoon et al.[162] (1993) studied the overall solubility of ethylene and propylene and their mixture in PE using a quartz spring balance. They found that the cosolubility effect is higher when increasing partial pressure of propylene while keeping the total pressure constant. They also showed that increasing the partial pressure of ethylene while keeping constant the partial pressure of propylene does not affect the solubility of propylene.

McKenna[170] (1997) showed the overall solubility of ethylene/butene in both HDPE and LDPE using a pressure-decay method at temperatures up to 94°C. No cosolubility effect was evident from the data, but it is possible that this is because of the very low partial pressures of butene (i.e. 0.65 bar) compared to the total pressure of 21 bar.

Moore and Wanke[164] (2001) showed the solubility of ethylene, 1-hexene, 1-butene and their mixtures in LLDPE using a gravimetric method at temperatures of 30-90°C and pressures up to 30 bar. They showed that there is a significant interaction between ethylene and 1-hexene during co-sorption since the amount of 1-hexene sorbed in the presence of ethylene is much lower than the amount sorbed by the polymer with pure 1-hexene. Besides, the solubility of these species, normalized with respect to the mass of the amorphous polyethylene, decreased with increasing polyethylene crystallinity.

Novak et al.[56] (2004) also studied the individual solubility of ethylene and 1-hexene mixture in LLDPE using the gravimetric technique at different temperatures up to 150°C and pressure conditions up to 30 bars. They showed that the solubility of the mixture of ethylene and 1-hexene is smaller than the sum of the solubilities of individual species at their respective partial pressures. They showed that adding 1-hexene enhances the solubility of ethylene, acting as a

co-solvent; this phenomenon is often referred to as the cosolubility effect. They also showed that increasing the ethylene pressure decreases the solubility of 1-hexene with respect to the binary 1-hexene/PE system. In this case the lighter component is an anti-solvent.

Chen et al.[139] (2004) estimated experimentally the individual solubility of ethylene and n-hexane mixture in LLDPE. They showed that the cloud point pressures are directly proportional to ethylene weight fraction. Moreover, supercritical ethylene increases the cloud point pressure of n-hexane/PE system.

Yao et al.[55] (2006) measured the individual solubility of ethylene with two types of ICAs (i.e. isopentane and n-hexane) in a semicrystalline polyethylene using a pressure decay method at several temperatures and a total pressure of 20 bars. They also showed the co-solubility effect, corresponding to an enhancement of ethylene solubility in polyethylene in presence of both ICAs, and a slight decrease of the solubility of ICAs in presence of ethylene.

Raharjo et al.[171] (2007) measured the solubility of pure and mixed CH_4 and n-C_4H_{10} on poly(dimethylsiloxane) using dilation-sorption experiments and densimetery. They showed that the solubility of CH_4 and n-C_4H_{10} increases in presence of high concentration of n-C_4H_{10} in PDMS. In contrast, the presence of CH_4 does not measurably affects n-C_4H_{10} solubility.

Sun et al.[57] (2016) showed the individual solubility of ethylene and 1-hexene mixture in semicrystalline polyethylene using an intelligent gravimetric analyser. They confirmed the co-solubility effect, where 1-hexene is acting as a co-solvent by increasing ethylene solubility, whereas ethylene is acting as an anti-solvent by decreasing 1-hexene solubility in the polymer. Moreover, it was found that the co-solubility of ethylene/1-hexene mixture is 10% smaller than the sum of the pure component solubilities.

Cancelas et al.[140] (2018) measured the overall solubility of ethylene, propylene and their mixture in isotactic polypropylene (iPP) with a high pressure sorption balance. They confirmed that the total solubility of the gas mixture is higher than the sum of gas solubilities of individual components. This is because the co-solvent effect of propylene on ethylene is higher that the anti-solvent effect of ethylene on propylene. The lower the temperature and the higher the pressure are, the higher is the solubility of ethylene and the lower is the solubility of propylene.

Finally, Greenhalgh et al.[131,132] (2018) presented the individual solubilities of mixed isobutane/isopentane, ethylene/isopentane and ethylene/n-hexane in a series of semicrystalline LLDPE using a magnetic suspension balance. They showed that increasing the weight fraction

of the most soluble component in the mixture increases the solubility of the less soluble component. Besides, for a constant partial pressure, the solubility of the more soluble pure component is higher than the solubility of the mixture, whereas the solubility of the less soluble pure component is smaller than in binary system. All these phenomenon confirm the presence of co-solubility effect during the sorption of a mixture of species in a polymer.

A summary of the data we found in the literature for ternary systems is given in **Table 8**. Less data is available for ternary systems than binary. To conclude on the ternary studies in the literature, it was shown that:

- Heavy components of a given family of compounds increase the solubility of lighter ones (co-solvent effect);
- Light components of a given family of compounds decrease the solubility of heavier ones (anti-solvent effect);
- Most studies used a gravimetric approach;
- The solubility of the mixture of species in ternary systems is smaller than the sum of the solubilities of individual species at their respective partial pressures in binary system
- Most studies only measure overall solubility, which makes the fitting to thermodynamic models more complicated

If we look at ***Table 7*** and ***Table 8*** showing the set of binary and ternary experimental systems we found, it can be seen that most studies employ some version of gravimetric experiments based on a magnetic suspension balance because of their relative simplicity and high precision. A large number of studies have used this method to investigate the impact of partial pressures and temperature on the solubility of (mostly) binary and (less occasionally) ternary systems. In terms of comonomer solubility, a large amount of data is available for 1-hexene and 1-butene solubility for different temperatures, pressures and PE crystallinity in mostly binary systems [130,131,141,162–164]. A more limited amount of data is available for 1-octene [142,162]. In the case of ICAs, the solubilities of n-hexane, isopentane have been studied for binary and ternary systems for a large range of temperature and polymer type [55,131,132,159,167,168], but very limited data can be found for the sorption of isobutane and propane in PE [131,132,157,158]; important diluents for a number of processes. Finally, it is not always an easy task to measure individual concentrations (and thus individual solubilities) in this type of apparatus, so very often it only provides total solubilities for a given mixture. The important lack of solubility data on polyolefin systems, especially ternary and quaternary systems at industrial conditions, has inspired this thesis.

Indeed, we will focus in the current thesis on building an experimental apparatus able to measure individual solubilities of multicomponent polyolefin systems at industrial conditions. These experimental data will therefore be crucial for thermodynamic modeling as well as for reactor modeling.

Table 8. *Literature data of sorption of ternary systems in polyolefins. P is the pressure in bar and T is the temperature in °C.*

Systems	Experimental techniques	Experimental conditions	Reference
Ethylene / Propylene / PE	Gravimetry	T=[30-100] ; P=[1-3]	162
Ethylene / Butene / PE	Pressure decay	T=[70-94] ; P=[1-21]	140
Ethylene / Isopentane / PE	Pressure decay	T=[70-90] ; P=[0-20]	55
	Gravimetry	T=80 ; P=[0-13]	131,132
Ethylene / n-hexane / PE	Pressure decay	T=[70-90] ; P=[0-10]	55
	Gravimetry	T=80 ; P=[0-13]	131,132
Ethylene / 1-hexene / PE	Gravimetry	T=69 ; P=[0-35]	56,164
	IGA	T=[50-90] ; P=[0-10]	57
Ethylene / Propylene / PP	Gravimetry	T=[50-85] ; P=[0-25]	140
Isobutane / Isopentane / PE	Gravimetry	T=80 ; P=[0-12]	131,132

5.3.Experimental and theoretical studies for diffusivity

The diffusion of gases and vapors in polymers has been the subject of a great number of studies, especially in binary systems[162,166,172–177]. However, most of these binary systems concern the diffusion of gases in polypropylene[140,166,172,177], and very few studies looked at the effect of the diffusion of gases in polyethylene. Furthermore, the diffusion of multicomponent mixtures of penetrants in polymeric system, e.g. in ternary and more importantly in quaternary systems, has not been considered to any great length.

Pino et al.[178] studied the diffusion of oxygen, carbon dioxide and nitrogen, and their mixture through polyethylene films with different degrees and types of chain branching, using a mass spectrometer technique at 22-25°C. They showed that mixing the different gases changes the solubility and diffusivity of each other.

Freeman et al.[171] investigated the diffusion of n-butane/methane mixture in poly(dimethylsiloxane) (PDMS) at temperatures up to 50°C and found that methane has a higher solubility and diffusivity in PDMS in presence of n-butane, with respect to the binary methane/PDMS.

Patzlaff et al.[166] compared the diffusivity of propylene in polypropylene polymerized in gas phase and liquid phase using the same Ziegler-Natta catalyst system, through gravimetric method at temperatures between 25-70°C. They showed that the effective diffusion coefficient increases with increasing the size of polymer particles, and that the effective diffusion coefficient is higher for particles produced in slurry phase polymerization, with respect to gas phase process.

Palamara et al.[177] extended the static sorption technique in order to study the diffusion of propylene and ethylene in atactic polypropylene (aPP) at temperatures of 25-70°C. The static sorption method is based on measuring the mass uptake of the polymer sample in a capsule in presence of different gases, as for the gravimetric method. The only exception is that the static sorption method uses several capsule experiments in parallel and stop them at different times before equilibrium in order to measure the fractional mass uptake as a function of time. It was found that the diffusivity of ethylene is higher than that of propylene in aPP at the same temperature and concentration, as one would expect for the smaller molecule. They validated their experimental diffusivity results by employing the Vrentas and Duda free-volume theory.

Cancelas et al.[140] studied the overall diffusivity of ternary ethylene/propylene/iPP using the same magnetic suspension balance (MSB) presented in Chapter 2 at temperature between 50-85°C. They showed that the diffusivity of the ternary mixture is higher than the diffusivity of the pure components.

In the same manner, Alves et al.[65] looked at the diffusion of ethylene/propylene/iPP, ethylene/n-hexane/PE and ethylene/n-pentane/PE by employing the free volume theory of Vrentas and Duda. They showed that, as expected, the ternary diffusivity of ethylene in presence of ICAs is higher than its binary diffusivity due to the co-solubility effect increasing ethylene concentration in the amorphous phase of the polymer. They also showed that the ternary

diffusivity of the different ICAs increases compared to the binary one, which is not an expected result due to the anti-solvent effect of ethylene on ICA, decreasing ICA concentration in the amorphous phase of the polymer. This might be due to a change in the free volume of the system, which will be discussed in more details in Chapter 4.

Clearly, it is desirable to be able to integrate such information into process models in order to help us better understand the impact of the process conditions on the final polymer product. It is therefore crucial to have more experimental and theoretical studies about the diffusion of mixtures of penetrants in the amorphous phase of the polymer since it has a great importance in ethylene polymerization reaction in gas phase. As explained previously, accounting for the co-solubility effect can help explain the increase in productivity[37,67]. The solubility of the different species will have an impact on the free volume of the amorphous phase of the polymer, which in turn can influence the diffusivities of the penetrants in the system. Taking into account the interaction between the different species when calculating diffusion coefficients improves the capacity of single particle models to explain high initial rates of polymerization in presence of ICAs[37].

The most widely used model that is able to take into account the interactions between the different penetrants when calculating the diffusivity of multicomponent system is the free volume theory. The free volume theory was developed by Fujita[179] and extensively modified by Vrentas and Duda[115,116,180–182]. The free volume is commonly referred to as the empty space between molecules in solution. Molecular transport is therefore governed by: (1) the existence of a hole (or free volume) of sufficient size adjacent to a penetrant molecule and (2) that same molecule possesses enough energy to overcome intermolecular interactions to jump into the hole. From this definition, Duda et al.[182,183] developed the well-known correlations for the binary self-diffusion coefficient, D_1, and the binary mutual coefficient, D, as follow:

$$D_1 = D_0 \exp\left(\frac{E_a}{R\,T}\right) \exp\left(\frac{-(\omega_1 \hat{V}_1^* + \omega_3 \hat{V}_3^* \xi_{13}}{\omega_1 \left(\frac{K_{11}}{\gamma}\right)\left(K_{21} + T - T_{g1}\right) + \omega_3 \left(\frac{K_{13}}{\gamma}\right)\left(K_{23} + T - T_{g3}\right)}\right)$$

$$D = D_1(1-\phi_1)^2(1-2\,\chi\,\phi_1)$$

In these equations, E_a is the diffusion activation energy, D_0 is a pre-exponential factor that is only function of the penetrant molecules, $\hat{V}_i^*$ is the specific critical hole free volume required for the ith component to make a jump, ω_i is the mass fraction of the i^{th} component, ξ_{13} is the ratio of molar volumes for the solvent and polymer jumping units, γ is an overlap factor

(between 0.5 and 1) which is introduced because the same free volume is available to more than one molecule[183]. K_{11} and K_{21} are the free volume parameters for the solvent, while K_{13} and K_{23} are for the polymer. ϕ_1 is the volume fraction of component 1 and χ is the solvent-polymer interaction parameter.

It is clear that this equation requires a great number of parameters, that are not always available in the literature for all polyolefins systems, such as the pre-exponential factor D_0 as well as K_{1i}/γ and K_{2i}. Furthermore, these parameters will be even more numerous for ternary systems, and higher orders systems. More details about the development procedure of Vrentas and Duda equation for ternary systems will be found in Chapters 4 and 5. In order to overcome these issues, Alves et al.[65] replaced the denominator of Vrentas and Duda's equation which represents the hole free volume by $V \times f_{\mathrm{FV}}$ where V is the specific volume (m^3 kg^{-1}) and f_{FV} is the free volume fraction measured by SL EoS. The detailed procedure on implementing the SL EoS into Vrentas and Duda free volume equation can be found elsewhere[65]. It is highlighted here that experimental and theoretical studies about solubility of multicomponent systems are also needed for diffusivity calculation, and are therefore crucial tools.

6. Conclusion

In the current chapter, an introduction to polyolefins, and in particular polyethylene which is the focus of the current thesis, is provided in ***Section 1***. The different commonly used catalysts for ethylene polymerization were briefly reviewed, as well as the different industrial processes for the production of polyethylene (i.e. gas phase, slurry and solution).

Gas phase ethylene polymerization processes have been presented in detail in **Section 3.1**, as this will be the focus of a large part of the thesis. The process of ethylene polymerization in gas phase FBRs has been described to better understand the phenomena occurring in an industrial point of view. Indeed, this process offers a wide range of advantages in terms of high overall conversion as well as broad particle morphology. However, the highly exothermic nature of ethylene polymerization in gas phase poses significant problems of heat removal. The rate of the polymer production in these reactors is limited by the rate at which the heat is removed from the reactor. In order to optimize the productivity, condensed mode cooling is employed in order to increase the capacity of heat removal. Condensed mode operation is described in **Section 3.2**, and its importance in gas phase FBRs is highlighted. This operation mode uses alkanes that are partially liquefied in an external heat exchanger and then sprayed inside the reactor mainly to serve as a dispersing heat medium. These alkanes are usually called induced condensing agents (ICAs) and will change the thermodynamic and physical properties as well as reactor operation of ethylene polymerization in gas phase.

However, the thermodynamics of ethylene polymerization in gas phase is yet not completely understood, and more experimental and theoretical studies are needed. The lack of experimental and theoretical studies on the solubility and the diffusivity of multicomponent systems in polyolefins is highlighted in Section 5.

It was revealed in ***Section 5.2.*** that most of the experimental solubility studies were restricted to binary systems (penetrant – PE), with a limited number looking at ternary systems (penetrant 1 – penetrant 2 – PE). These experimental studies demonstrate that the interactions between the different components in a gas phase mixture exist and must be taken into account. Thus, when modeling ternary (or higher orders systems), it is necessary to account for the way the different penetrants interact with the polymer. This can be achieved by using equations of state (EoS). The Sanchez-Lacombe equation of state (SL EoS) based on lattice models and the Perturbated Chain Statistical Associating Fluid Theory (PC SAFT) based on the perturbation theory, which are the two widely used models in the field of polymer reaction engineering, were described in

details in ***Section 5.1***. The Sanchez-Lacombe EoS will be used in the current thesis. These experimental and theoretical studies demonstrated the importance of the co-solvent effect that leads to an increase of ethylene solubility in presence of heavier penetrant, and the anti-solvent effect decreasing the penetrant solubility in presence of lighter penetrants like ethylene. It would therefore be interesting to look at higher orders systems (i.e. quaternary) in order to analyze the interactions between the different penetrants with the polymer. Would the co-solvent and anti-solvent effect remain the same? Would the interactions between the small molecules remain negligible? Can we assume ternary systems when describing quaternary systems? All these questions will be explained through experimental data using the gravimetric and pressure decay method and then validated with an extension of the SL EoS for quaternary systems.

A significant lack of data concerning diffusivity of multicomponent gas phase mixtures is also observed in the literature and was discussed in ***Section 5.3***. Most experimental diffusivity studies are related to binary systems in polyolefins. Diffusion of multicomponent mixtures in polymeric systems is not extensively studied, especially in ternary and more importantly in quaternary systems. Some of the few ternary studied systems revealed a co-diffusion effect, where the ternary diffusivity of ethylene in presence of ICA is higher than its binary diffusivity. This was explained by the co-solvent effect increasing ethylene concentration in the amorphous phase of the polymer. However, studies about a possible anti-diffusion effect of the penetrants are not completely discerned and must be studied in more details. *We can therefore ask if the co-diffusion effect is higher than the co-solvent effect? Does the anti-solvent effect affect the diffusion in the amorphous phase of the polymer? Would these anti and co-diffusion effects remain the same for higher order systems?* All these questions will be investigated through experimental data using the gravimetric technique and validated with Vrentas and Duda diffusion model.

Knowledge of this thermodynamic data is key when describing ethylene polymerization in gas-phase since it will change the physical and possible the chemical properties of the produced polymer. The evolution of the particle morphology and growth during the polymerization is described in ***Section 4.1.*** and ***Section 4.2***. A number of models are able to quantitatively describe these phenomena, and the Particle Flow Model (PFM) [88–90] and the multigrain model (MGM) [91,92] are considered the closest approximations to describe this phenomena at the mesoscale level during polymerization reasonably well. These models are described and analyzed in ***Section 4.3.*** The Random-Pore PFM (RPPFM) will be used in the current thesis.

We could therefore ask what is the effect of using an accurate thermodynamic model in the particle model? Is it important to have both solubility and diffusivity data for ternary systems when describing homopolymerization? Will the gas phase composition have a great impact on the productivity as well as on the morphology of the produced polymer? All these questions will be solved through a particle model including a kinetic and thermodynamic models.

Gas phase processes are clearly not the only ones used for polyethylene production. The slurry phase processes discussed in ***Section 2*** will be the focus of Chapter 6. The different phenomenon occurring in slurry phase have been highlighted, as well as process issues such as the control of temperature, the high amount of swelling of the amorphous phase of the polymer, the risk of reactor fouling due to plasticization of polymer slurry. Although slurry processes have better heat transfer capacity with respect to gas phase processes, the thermodynamics of slurry processes has to be carefully taken into account such as the solubility of liquid diluents in the amorphous phase of the polymer and the swelling of the later. However, very few experimental or theoretical studies related to slurry polymerization are available in the literature. A number of questions remain open in the field of slurry processes. *How will the solubility and swelling vary with respect to the temperature, the type of diluent and the density of the polymer? What are the limits of temperatures for each solvent before the plasticization of the polymer? Are these properties important to take into account when modeling slurry reactors?* All of these questions will be examined through experimental studies of the solubility, swelling and dissolution of the amorphous phase of the polymer in function of temperature and type of solvent.

7. References

1. The Freedonia Group, 'Word Polyethylene', pp 1-495. *The Freedonia Group* https://www.freedoniagroup.com/industry-study/world-polyethylene-3210.htm (2014).

2. S&P Global Plantts, 'Petrochemicals infographic: What's in store for global polyethylene and polypropylene out to 2027?' - The barrel Blog [Accessed 15 March 2020]. https://blogs.platts.com/2017/09/07/infographic-whats-store-global-polyethylene-polypropylene-2027/ (2017).

3. Plastics Market Size, Share & Trends Report, 2020-2027 [Accessed 09 June 2020]. https://www.grandviewresearch.com/industry-analysis/global-plastics-market.

4. Hassan, A., Bagherzadeh, E., Anthony, R. G., Borsinger, G. & Hassan, A. System and process for production of polyethylene and polypropylene. (2011).

5. Polyolefin Microstructural Modeling. in 187–269 (Wiley-VCH Verlag GmbH & Co. KGaA, 2012). doi:10.1002/9783527646944.ch6.

6. Albizzati, E. & Galimberti, M. Catalysts for olefins polymerization. *Catalysis Today* **41**, 159–168 (1998).

7. Alizadeh, A. Study of sorption, heat and mass transfer during condensed mode operation of gas phase ethylene polymerization on supported catalyst. (Departement of Chemical Engineering, Queen's University, 2014).

8. McDaniel, M. P. Supported Chromium Catalysts for Ethylene Polymerization. in *Advances in Catalysis* (eds. Eley, D. D., Pines, H. & Weisz, P. B.) vol. 33 47–98 (Academic Press, 1985).

9. Heterogeneous Single-Site Catalysts for Olefin Polymerization | Chemical Reviews. https://pubs.acs.org/doi/10.1021/cr9902401.

10. Asua, J. M. Introduction to Polymerization Processes. in *Polymer Reaction Engineering* 1–28 (John Wiley & Sons, Ltd, 2008). doi:10.1002/9780470692134.ch1.

11. Polyethylene by Slurry-Phase Polymerization. 6.

12. Khare, N. P. *et al.* Steady-State and Dynamic Modeling of Commercial Slurry High-Density Polyethylene (HDPE) Processes. *Ind. Eng. Chem. Res.* **41**, 5601–5618 (2002).

13. Meng, W., Li, J., Chen, B. & Li, H. Modeling and Simulation of Ethylene Polymerization in Industrial Slurry Reactor Series. *Chinese Journal of Chemical Engineering* **21**, 850–859 (2013).

14. Fouarge, L., Lewalle, A., Auwera, M. V. D. & Brande, F. V. D. Swell control in slurry loop reactor. (2005).

15. Giguere, R., Mignon, D., Tanguy, P. & Fradette, L. Process for preparing a polyethylene product in a polymerization loop reactor. (2016).

16. Zacca, J. J. & Ray, W. H. Modelling of the liquid phase polymerization of olefins in loop reactors. *Chemical Engineering Science* **48**, 3743–3765 (1993).

17. Hottovy, J. D., Zellers, D. A. & Franklin, R. K. Pumping apparatus for slurry polymerization in loop reactors. (2006).

18. Marechal, P. Process for producing bimodal polyethylene resins. (2006).

19. Kufeld, S. E. *et al.* Slurry polymerization reactor having large length/diameter ratio. (2006).

20. III, R. K. F. *et al.* High polymer solids slurry polymerization employing 1-olefin comonomer. (2004).

21. McGrath, P. J., Morris, R. J. & Kreitz, R. W. Cascaded boiling pool slurry reactors for producing bimodal low to medium density polyethylene polymers. (2004).

22. Siraux, D. Optimisation of the ethylene polymerisation process. (2010).

23. Schnell, M., Stryuk, S. & Wolf, B. A. Liquid/Liquid Demixing in the System n-Hexane/Narrowly Distributed Linear Polyethylene. *Ind. Eng. Chem. Res.* **43**, 2852–2859 (2004).

24. de Loos, Th. W., de Graaf, L. J. & de Swaan Arons, J. Liquid - liquid phase separation in linear low density polyethylene - solvent systems. *Fluid Phase Equilibria* **117**, 40–47 (1996).

25. Pochivalov, K. V., Lebedeva, T. N., Ilyasova, A. N., Basko, A. V. & Kudryavtsev, Y. V. A new look at the semicrystalline polymer – liquid systems: Phase diagrams low-density polyethylene – n-alkanes. *Fluid Phase Equilibria* **471**, 1–7 (2018).

26. Hamada, F., Fujisawa, K. & Nakajima, A. Lower Critical Solution Temperature in Linear Polyethylene–n-Alkane Systems. *Polym J* **4**, 316–322 (1973).

27. Luettmer-Strathmann, J., Schoenhard, J. A. & Lipson, J. E. G. Thermodynamics of n-Alkane Mixtures and Polyethylene-n-Alkane Solutions: Comparison of Theory and Experiment. *Macromolecules* **31**, 9231–9237 (1998).

28. Nakajima, A. & Hamada, F. Estimation of thermodynamic interactions between polyethylene and n-alkanes by means of melting point measurements. *Kolloid-Z.u.Z.Polymere* **205**, 55–61 (1965).

29. Aminabhavi, T. M. & Naik, H. G. Sorptionrdesorption, diffusion, permeation and swelling of high density polyethylene geomembrane in the presence of hazardous organic liquids. 12 (1999).

30. Krajakova, L., Laskova, M., Chmelar, J., Jindrova, K. & Kosek, J. Sorption of Liquid Diluents in Polyethylene: Comprehensive Experimental Data for Slurry Polymerization. *Ind. Eng. Chem. Res.* **58**, 7037–7043 (2019).

31. Dumain, A. Polymerization of olefins in a fluidized bed reactor. 10.

32. Mirzaei, A., Kiashemshaki, A. & Emami, M. Fluidized Bed Polyethylene Reactor Modeling in Condensed Mode Operation. *Macromol. Symp.* **259**, 135–144 (2007).

33. Farag, H., Ossman, M., Mansour, M. & Farid, Y. Modeling of fluidized bed reactor for ethylene polymerization: effect of parameters on the single-pass ethylene conversion. *Int J Ind Chem* **4**, 20 (2013).

34. Chinh, J.-C., Filippelli, M. C. H., Newton, D. & Power, M. B. Polymerization process. (1996).

35. Xie, T., McAuley, K. B., Hsu, J. C. C. & Bacon, D. W. Gas Phase Ethylene Polymerization: Production Processes, Polymer Properties, and Reactor Modeling. *Ind. Eng. Chem. Res.* **33**, 449–479 (1994).

36. Banat, Y., Al-Obaidi, F. & Malek, A. K. Olefin gas phase polymerisation. (2011).

37. Alizadeh, A., Sharif, F., Ebrahimi, M. & McKenna, T. F. L. Modeling Condensed Mode Operation for Ethylene Polymerization: Part III. Mass and Heat Transfer. *Ind. Eng. Chem. Res.* **57**, 6097–6114 (2018).

38. Fischbuch, D. B. *et al.* Low molecular weight induced condensing agents. (2010).

39. Fernandes, F. A. N. & Lona, L. M. F. Fluidized bed reactor for polyethylene production. The influence of polyethylene prepolymerization. *Braz. J. Chem. Eng.* **17**, 163–170 (2000).

40. Mirzaei, A., Kiashemshaki, A. & Emami, M. Fluidized Bed Polyethylene Reactor Modeling in Condensed Mode Operation. *Macromol. Symp.* **259**, 135–144 (2007).

41. Bernier, R. J. N., Boysen, R. L., Brown, R. C., Scarola, L. S. & Williams, G. H. Gas phase polymerization process. (1995).

42. III, J. M. J., Jones, R. L. & Jones, T. M. Fluidized bed reaction systems. (1985).

43. Dumain, A. & Raufast, C. Process for gas phase polymerization of olefins in a fluidized bed reactor. (1989).

44. McKenna, T. F. L. Condensed Mode Cooling of Ethylene Polymerization in Fluidized Bed Reactors. *Macromol. React. Eng.* **13**, 1800026 (2019).

45. McAuley, K. B., Talbot, J. P. & Harris, T. J. A comparison of two-phase and well-mixed models for fluidized-bed polyethylene reactors. *Chemical Engineering Science* **49**, 2035–2045 (1994).

46. Di, D. G. Apparatus for improved fluidized beds and reactors containing same. (1967).

47. Polyolefin Reaction Engineering | Wiley. *Wiley.com* https://www.wiley.com/en-us/Polyolefin+Reaction+Engineering-p-9783527317103.

48. Griffin, J. R. & DeChellis, M. L. Process for polymerizing monomers in fluidized beds. (1995).

49. Penzo, G., Mei, G. & Meier, G. Gas-phase olefin polymerization process. (2004).

50. Wonders, A. G., Edmund, M. A., Messina, A. D., Bellner, S. P. & Ford, R. R. Method for improving cooling of fluid bed polymer reactor. (2000).

51. Herzog, M., Isnard, J.-P., Lalanne-Magne, C. V. & Shin, M. J. Process for the continuous gas-phase (co-) polymerisation of olefins in a fluidized bed reactor. (2003).

52. Chase, M. W. NIST-JANAF Themochemical Tables, Fourth Edition [Accessed 25 May 2020]. *J. Phys. Chem. Ref. Data, Monograph 9* 1–1951 (1998).

53. Lide, D. R. *et al.* CRC Handbook of Chemistry and Physics. 2661.

54. Wu, W. Introducing a condensing agent into a fluidized bed polymerization reactor operated in the condensing mode. (2001).

55. Yao, W., Hu, X. & Yang, Y. Modeling the solubility of ternary mixtures of ethylene,iso-pentane,n-hexane in semicrystalline polyethylene. *J. Appl. Polym. Sci.* **104**, 3654–3662 (2007).

56. Novak, A. *et al.* Ethylene and 1-hexene sorption in LLDPE under typical gas-phase reactor conditions: Experiments. *J. Appl. Polym. Sci.* **100**, 1124–1136 (2006).

57. Sun, J. *et al.* Solubility measurement of hydrogen, ethylene, and 1-hexene in polyethylene films through an intelligent gravimetric analyzer. *J. Appl. Polym. Sci.* **134**, (2017).

58. Bashir, M. A., Monteil, V., Kanellopoulos, V., Ali, M. A.-H. & McKenna, T. Partial Molar Volumes and Thermal Expansion Coefficients as an Explanation for Co-Solvent Effect of Penetrants in Multicomponent Polymer Mixtures. *Macromol. Chem. Phys.* **216**, 2129–2140 (2015).

59. Namkajorn, M., Alizadeh, A., Somsook, E. & McKenna, T. F. L. Condensed-Mode Cooling for Ethylene Polymerization: The Influence of Inert Condensing Agent on the Polymerization Rate. *Macromol. Chem. Phys.* **215**, 873–878 (2014).

60. McKenna, T. F. L. *et al.* Improved understanding of the impact of alkanes when using condensed mode cooling for PE production. 4.

61. Alizadeh, A. *et al.* Modeling Condensed Mode Operation for Ethylene Polymerization: Part I. Thermodynamics of Sorption. *Ind. Eng. Chem. Res.* **56**, 1168–1185 (2017).

62. Banaszak, B. J. *et al.* Ethylene and 1-Hexene Sorption in LLDPE under Typical Gas Phase Reactor Conditions: A Priori Simulation and Modeling for Prediction of Experimental Observations. *Macromolecules* **37**, 9139–9150 (2004).

63. Ishola, N., Andrade, F. N., Machado, R. & McKenna, T. F. L. Condensed Mode Cooling for Ethylene Polymerization: Part VI. Impact of Induced Condensing Agents on Comonomer Incorporation.

64. Kanellopoulos, V., Mouratides, D., Tsiliopoulou, E. & Kiparissides, C. An Experimental and Theoretical Investigation into the Diffusion of Olefins in Semi-Crystalline Polymers: The Influence of Swelling in Polymer-Penetrant Systems. *Macromolecular Reaction Engineering* **1**, 106–118 (2007).

65. Alves, R. F. & McKenna, T. F. L. Estimation of diffusion coefficients for multiple penetrant/polyolefin systems based on sorption data. *Chemical Engineering Journal* **383**, 123114 (2020).

66. Bashir, M. A., Monteil, V., Kanellopoulos, V., Al-haj Ali, M. & McKenna, T. F. L. An Equation of State-Based Modeling Approach for Estimating the Partial Molar Volume of Penetrants and Polymers in Binary Mixtures. *Ind. Eng. Chem. Res.* **52**, 16491–16505 (2013).

67. Alves, R., Bashir, M. A. & McKenna, T. F. L. Modeling Condensed Mode Cooling for Ethylene Polymerization: Part II. Impact of Induced Condensing Agents on Ethylene Polymerization in an FBR Operating in Super-Dry Mode. *Ind. Eng. Chem. Res.* **56**, 13582–13593 (2017).

68. Bashir, M. A., Al-haj Ali, M., Kanellopoulos, V. & Seppälä, J. Modelling of multicomponent olefins solubility in polyolefins using Sanchez–Lacombe equation of state. *Fluid Phase Equilibria* **358**, 83–90 (2013).

69. Andrade, F. N. & McKenna, T. F. L. Condensed Mode Cooling for Ethylene Polymerization: Part IV. The Effect of Temperature in the Presence of Induced Condensing Agents. *Macromol. Chem. Phys.* **218**, 1700248 (2017).

70. Andrade, F. N., Fulchiron, R., Collas, F. & McKenna, T. F. L. Condensed Mode Cooling for Ethylene Polymerization: Part V—Reduction of the Crystallization Rate of HDPE in the Presence of Induced Condensing Agents. *Macromolecular Chemistry and Physics* **220**, 1800563 (2019).

71. Cai, P. *et al.* Condensing mode operation of gas-phase polymerization reactor. (2005).

72. III, J. M. J., Jones, R. L., Jones, T. M. & Beret, S. Method for fluidized bed polymerization. (1986).

73. Grof, Z., Kosek, J. & Marek, M. Modelling of Morphogenesis of Growing Polyolefin Particles. *AIChE Journal* **51**, 2048–2067 (2005).

74. McKenna, T. F. L., Di Martino, A., Weickert, G. & Soares, J. B. P. Particle Growth During the Polymerisation of Olefins on Supported Catalysts, 1 - Nascent Polymer Structures. *Macromol. React. Eng.* **4**, 40–64 (2010).

75. Alizadeh, A. & McKenna, T. F. L. Particle Growth during the Polymerization of Olefins on Supported Catalysts. Part 2: Current Experimental Understanding and Modeling Progresses on Particle Fragmentation, Growth, and Morphology Development. *Macromol. React. Eng.* **12**, 1700027 (2018).

76. Soga, K. & Shiono, T. Ziegler-Natta catalysts for olefin polymerizations. *Progress in Polymer Science* **22**, 1503–1546 (1997).

77. McKenna, T. F. & Soares, J. B. P. Single particle modelling for oleÿn polymerization on supported catalysts: A review and proposals for future developments. *Chemical Engineering Science* 19 (2001).

78. Fisch, A. G. *et al.* Investigation of silica particle structure containing metallocene immobilized by a sol–gel method. *Journal of Non-Crystalline Solids* **354**, 3973–3979 (2008).

79. PULLUKAT, T. J. & HOFF, R. E. Silica-Based Ziegler–Natta Catalysts: A Patent Review. *Catalysis Reviews* **41**, 389–428 (1999).

80. McDaniel, M. P. Fracturing silica-based catalysts during ethylene polymerization. *J. Polym. Sci. Polym. Chem. Ed.* **19**, 1967–1976 (1981).

81. Hamielec, A. E. & Soares, J. B. P. Polymerization reaction engineering — Metallocene catalysts. *Progress in Polymer Science* **21**, 651–706 (1996).

82. Kaminsky, W. New polymers by metallocene catalysis. *Macromolecular Chemistry and Physics* **197**, 3907–3945 (1996).

83. McKenna, T. F. L. Growth and Evolution of Particle Morphology: An Experimental & Modelling Study. *Macromol. Symp.* **260**, 65–73 (2007).

84. Grof, Z., Kosek, J. & Marek, M. Modeling of morphogenesis of growing polyolefin particles. *AIChE J.* **51**, 2048–2067 (2005).

85. Grof, Z., Kosek, J., Marek, M. & Adler, P. M. Modeling of morphogenesis of polyolefin particles: Catalyst fragmentation. *AIChE J.* **49**, 1002–1013 (2003).

86. van Grieken, R., Carrero, A., Suarez, I. & Paredes, B. Effect of 1-Hexene Comonomer on Polyethylene Particle Growth and Kinetic Profiles. *Macromol. Symp.* **259**, 243–252 (2007).

87. Estenoz, D. A. & Chiovetta, M. G. A structural model for the catalytic polymerization of ethylene using chromium catalysts. Part II: Thermal effects. *Polym. Eng. Sci.* **36**, 2229–2240 (1996).

88. Debling, J. A. & Ray, W. H. Heat and Mass Transfer Effects in Multistage Polymerization Processes: Impact Polypropylene. *Ind. Eng. Chem. Res.* **34**, 3466–3480 (1995).

89. Hutchinson, R. A., Chen, C. M. & Ray, W. H. Polymerization of olefins through heterogeneous catalysis X: Modeling of particle growth and morphology. *J. Appl. Polym. Sci.* **44**, 1389–1414 (1992).

90. Hatzantonis, H., Yiannoulakis, H., Yiagopoulos, A. & Kiparissides, C. Recent developments in modeling gas-phase catalyzed olefin polymerization fluidized-bed reactors: The effect of bubble size variation on the reactor's performance. *Chemical Engineering Science* 23 (2000).

91. Galvan, R. & Tirrell, M. Molecular weight distribution predictions for heterogeneous Ziegler-Natta polymerization using a two-site model. *Chemical Engineering Science* **41**, 2385–2393 (1986).

92. Hoel, E. L., Cozewith, C. & Byrne, G. D. Effect of diffusion on heterogeneous ethylene propylene copolymerization. *AIChE Journal* **40**, 1669–1684 (1994).

93. Yiagopoulos, A., Yiannoulakis, H., Dimos, V. & Kiparissides, C. Heat and mass transfer phenomena during the early growth of a catalyst particle in gas-phase olefin polymerization : the effect of prepolymerization temperature and time. *Chemical Engineering Science* **56**, 3979–3995 (2001).

94. Floyd, S., Choi, K. Y., Taylor, T. W. & Ray, W. H. Polymerization of olefins through heterogeneous catalysis. III. Polymer particle modelling with an analysis of intraparticle heat and mass transfer effects. *J. Appl. Polym. Sci.* **32**, 2935–2960 (1986).

95. Stern, S. A., Mullhaupt, J. T. & Gareis, P. J. The effect of pressure on the permeation of gases and vapors through polyethylene. Usefulness of the corresponding states principle. *AIChE J.* **15**, 64–73 (1969).

96. Michaels, A. S. & Bixler, H. J. Solubility of gases in polyethylene. *J. Polym. Sci.* **50**, 393–412 (1961).

97. Floyd, S., Choi, K. Y., Taylor, T. W. & Ray, W. H. Polymerization of olefines through heterogeneous catalysis IV. Modeling of heat and mass transfer resistance in the polymer particle boundary layer. *J. Appl. Polym. Sci.* **31**, 2231–2265 (1986).

98. McKenna, T. F., Dupuy, J. & Spitz, R. Modeling of transfer phenomena on heterogeneous Ziegler catalysts: Differences between theory and experiment in olefin polymerization (an introduction). *J. Appl. Polym. Sci.* **57**, 371–384 (1995).

99. Estenoz, D. A. & Chiovetta, M. G. A structural model for the catalytic polymerization of ethylene using chromium catalysts. Part I: Description and solution. *Polym. Eng. Sci.* **36**, 2208–2228 (1996).

100. Hutchinson, R. A., Chen, C. M. & Ray, W. H. Polymerization of olefins through heterogeneous catalysis X: Modeling of particle growth and morphology. *J. Appl. Polym. Sci.* **44**, 1389–1414 (1992).

101. Kosek, J., Grof, Z., ák, A., Štěpánek, F. & Marek, M. Dynamics of particle growth and overheating in gas-phase polymerization reactors. *Chemical Engineering Science* **56**, 3951–3977 (2001).

102. McKenna, T. F., Cokljat, D. & Wild, P. CFD Modelling of heat transfer during gas phase olefin polymerisation. *Computers & Chemical Engineering* **22**, S285–S292 (1998).

103. Hutchinson, R. A. & Ray, W. H. Polymerization of olefins through heterogeneous catalysis. VII. Particle ignition and extinction phenomena. *J. Appl. Polym. Sci.* **34**, 657–676 (1987).

104. Estenoz, D. A. & Chiovetta, M. G. Olefin polymerization using supported metallocene catalysts: Process representation scheme and mathematical model. *J. Appl. Polym. Sci.* **81**, 285–311 (2001).

105. Ferrero, M. A. & Chiovetta, M. G. Catalyst fragmentation during propylene polymerization: Part I. The effects of grain size and structure. *Polym. Eng. Sci.* **27**, 1436–1447 (1987).

106. Ferrero, M. A. & Chiovetta, M. G. Catalyst fragmentation during propylene polymerization: Part II. Microparticle diffusion and reaction effects. *Polym. Eng. Sci.* **27**, 1448–1460 (1987).

107. Ferrero, M. A. & Chiovetta, M. G. Catalyst fragmentation during propylene polymerization. III: Bulk polymerization process simulation. *Polym. Eng. Sci.* **31**, 886–903 (1991).

108. Ferrero, M. A. & Chiovetta, M. G. Effects of catalyst fragmentation during propylene polymerization. IV: Comparison between gas phase and bulk polymerization processes. *Polym. Eng. Sci.* **31**, 904–911 (1991).

109. Kanellopoulos, V., Dompazis, G., Gustafsson, B. & Kiparissides, C. Comprehensive Analysis of Single-Particle Growth in Heterogeneous Olefin Polymerization: The Random-Pore Polymeric Flow Model. 4 (2004).

110. Veera, U. P., Weickert, G. & Agarwal, U. S. Modeling monomer transport by convection during olefin polymerization. *AIChE Journal* **48**, 1062–1070 (2002).

111. Kittilsen, P., Svendsen, H. & McKenna, T. F. Modeling of transfer phenomena on heterogeneous Ziegler catalysts. IV. Convection e ects in gas phase processes. *Chemical Engineering Science* 9 (2001).

112. Weickert, G., Meier, G. B., Pater, J. T. M. & Westerterp, K. R. The particle as microreactor: catalytic propylene polymerizations with supported metallocenes and Ziegler–Natta catalysts. *Chemical Engineering Science* **54**, 3291–3296 (1999).

113. Wu, Q., Wang, H. & Lin, S. Gas-phase versus slurry copolymerization of ethylene with 1-butene over MgCl2-supported titanium catalysts after prepolymerization. *Macromolecular Chemistry and Physics* **197**, 155–163 (1996).

114. Wakao, N. & Smith, J. M. Diffusion and Reaction in Porous Catalysts. https://pubs.acs.org/doi/pdf/10.1021/i160010a007 (2002) doi:10.1021/i160010a007.

115. Vrentas, J. S., Duda, J. L. & Ling, H. C. Free-volume equations for polymer-penetrant diffusion. *Journal of Membrane Science* **40**, 101–107 (1989).

116. Vrentas, J. S., Duda, J. L. & Ling, H.-C. Self-diffusion in polymer-solvent-solvent systems. *J. Polym. Sci. Polym. Phys. Ed.* **22**, 459–469 (1984).

117. Yiannoulakis, H., Yiagopoulos, A., Pladis, P. & Kiparissides, C. Comprehensive Dynamic Model for the Calculation of the Molecular Weight and Long Chain Branching Distributions in Metallocene-Catalyzed Ethylene Polymerization Reactors. *Macromolecules* **33**, 2757–2766 (2000).

118. Chatzidoukas, C., Kiparissides, C., Perkins, J. D. & Pistikopoulos, E. N. Optimal grade transition campaign scheduling in a gas-phase polyolefin FBR using mixed integer dynamic optimization. in *Computer Aided Chemical Engineering* (eds. Kraslawski, A. & Turunen, I.) vol. 14 71–76 (Elsevier, 2003).

119. Guerrieri, Y., Valverde, K., Costa, G. & Embiruu, M. A Survey of Equations of State for Polymers, Chap.16. in (2012). doi:10.5772/48391.

120. Sanchez, I. C. & Lacombe, R. H. An elementary equation of state for polymer liquids. *J. Polym. Sci. B Polym. Lett. Ed.* **15**, 71–75 (1977).

121. Gross, J. & Sadowski, G. Perturbed-Chain SAFT: An Equation of State Based on a Perturbation Theory for Chain Molecules. *Ind. Eng. Chem. Res.* **40**, 1244–1260 (2001).

122. Banaszak, M., Chiew, Y. C., O'Lenick, R. & Radosz, M. Thermodynamic perturbation theory: Lennard-Jones chains. *J. Chem. Phys.* **100**, 3803–3807 (1994).

123. Johnson, J. K., Mueller, E. A. & Gubbins, K. E. Equation of State for Lennard-Jones Chains. *J. Phys. Chem.* **98**, 6413–6419 (1994).

124. Paricaud, P., Galindo, A. & Jackson, G. Modeling the Cloud Curves and the Solubility of Gases in Amorphous and Semicrystalline Polyethylene with the SAFT-VR Approach and Flory Theory of Crystallization. *Ind. Eng. Chem. Res.* **43**, 6871–6889 (2004).

125. Gil-Villegas, A. *et al.* Statistical Associating Fluid Theory for Chain Molecules with Attractive Potentials of Variable Range. *The Journal of Chemical Physics* **106**, 4168–4186 (1997).

126. Wei, Y. S. & Sadus, R. J. Equations of state for the calculation of fluid-phase equilibria. *AIChE Journal* **46**, 169–196 (2000).

127. Xiong, Y. & Kiran, E. Comparison of Sanchez–Lacombe and SAFT model in predicting solubility of polyethylene in high-pressure fluids. *J. Appl. Polym. Sci.* **55**, 1805–1818 (1995).

128. Maity, S. K. Correlation of solubility of single gases/hydrocarbons in polyethylene using PC-SAFT. *Asia-Pac. J. Chem. Eng.* **7**, 406–417 (2012).

129. Krallis, A. & Kanellopoulos, V. Application of Sanchez–Lacombe and Perturbed-Chain Statistical Associating Fluid Theory Equation of State Models in Catalytic Olefins (Co)polymerization Industrial Applications. *Ind. Eng. Chem. Res.* **52**, 9060–9068 (2013).

130. Chmelař, J. *et al.* Equilibrium sorption of ethylene in polyethylene: Experimental study and PC-SAFT simulations. *Polymer* **59**, 270–277 (2015).

131. Moebus, J. A. & Greenhalgh, B. R. Modeling Vapor Solubility in Semicrystalline Polyethylene. *Macromol. React. Eng.* **12**, 1700072 (2018).

132. Savatsky, B. J., Moebus, J. A. & Greenhalgh, Brian. R. Parameterization of Models for Vapor Solubility in Semicrystalline Polyethylene. *Macromol. React. Eng.* **13**, 1900003 (2019).

133. Lacombe, R. H. & Sanchez, I. C. Statistical thermodynamics of fluid mixtures. *J. Phys. Chem.* **80**, 2568–2580 (1976).

134. Sanchez, I. C. & Lacombe, R. H. Statistical Thermodynamics of Polymer Solutions. *Macromolecules* **11**, 12 (1978).

135. Bashir, M. A. *et al.* The Effect of Pure Component Characteristic Parameters on Sanchez-Lacombe Equation-of-State Predictive Capabilities. *Macromolecular Reaction Engineering* **7**, 193–204 (2013).

136. Bashir, M. A., Kanellopoulos, V., Al-haj Ali, M. & McKenna, T. F. L. Applied Thermodynamics for Process Modeling in Catalytic Gas Phase Olefin Polymerization Reactors. *Macromol. React. Eng.* **14**, 1900029 (2020).

137. Yao, Z., Zhu, F., Chen, Z., Zeng, C. & Cao, K. Solubility of Subcritical and Supercritical Propylene in Semicrystalline Polypropylene. *Journal of Chemical & Engineering Data* **56**, 1174–1177 (2011).

138. Yao, Z. *et al.* Solubility of Subcritical and Supercritical Propylene in the Semicrystalline Polyethylenes. *J. Chem. Eng. Data* **60**, 3033–3038 (2015).

139. Chen, X., Yasuda, K., Sato, Y., Takishima, S. & Masuoka, H. Measurement and correlation of phase equilibria of ethylene + n-hexane + metallocene polyethylene at temperatures between 373 and 473K and at pressures up to 20MPa. *Fluid Phase Equilibria* **215**, 105–115 (2004).

140. Cancelas, A. J. *et al.* Solubility and Diffusivity of Propylene, Ethylene, and Propylene-Ethylene Mixtures in Polypropylene. *Macromol. Chem. Phys.* **219**, 1700565 (2018).

141. Kiparissides, C., Dimos, V., Boultouka, T., Anastasiadis, A. & Chasiotis, A. Experimental and theoretical investigation of solubility and diffusion of ethylene in semicrystalline PE at elevated pressures and temperatures. *J. Appl. Polym. Sci.* **87**, 953–966 (2003).

142. Kanellopoulos, V., Mouratides, D., Pladis, P. & Kiparissides, C. Prediction of Solubility of α-Olefins in Polyolefins Using a Combined Equation of State Molecular Dynamics Approach. *Ind. Eng. Chem. Res.* **45**, 5870–5878 (2006).

143. Haruki, M., Mano, S., Koga, Y., Kihara, S. & Takishima, S. Phase behaviors for the supercritical ethylene+1-hexene+hexane+polyethylene systems at elevated temperatures and pressures. *Fluid Phase Equilibria* **295**, 137–147 (2010).

144. Haruki, M., Sato, K., Kihara, S. & Takishima, S. High pressure phase behavior for the supercritical ethylene+cyclohexane+hexane+polyethylene systems. *The Journal of Supercritical Fluids* **49**, 125–134 (2009).

145. Haslam, A. J. *et al.* Predicting enhanced absorption of light gases in polyethylene using simplified PC-SAFT and SAFT-VR. *Fluid Phase Equilibria* **243**, 74–91 (2006).

146. Tumakaka, F., Gross, J. & Sadowski, G. Modeling of polymer phase equilibria using Perturbed-Chain SAFT. *Fluid Phase Equilibria* **194–197**, 541–551 (2002).

147. Gross, J., Spuhl, O., Tumakaka, F. & Sadowski, G. Modeling Copolymer Systems Using the Perturbed-Chain SAFT Equation of State. *Ind. Eng. Chem. Res.* **42**, 1266–1274 (2003).

148. von Solms, N., Michelsen, M. L. & Kontogeorgis, G. M. Prediction and Correlation of High-Pressure Gas Solubility in Polymers with Simplified PC-SAFT. *Ind. Eng. Chem. Res.* **44**, 3330–3335 (2005).

149. Minelli, M. & De Angelis, M. G. An equation of state (EoS) based model for the fluid solubility in semicrystalline polymers. *Fluid Phase Equilibria* **367**, 173–181 (2014).

150. Jomekian, A. & Poormohammadian, S. J. Improved prediction of solubility of gases in polymers using an innovative non-equilibrium lattice fluid/Flory-Huggins model. *Fluid Phase Equilibria* **500**, 112261 (2019).

151. Ting, P. D., Joyce, P. C., Jog, P. K., Chapman, W. G. & Thies, M. C. Phase equilibrium modeling of mixtures of long-chain and short-chain alkanes using Peng–Robinson and SAFT. *Fluid Phase Equilibria* **206**, 267–286 (2003).

152. Peng, D.-Y. & Robinson, D. B. A New Two-Constant Equation of State. *Ind. Eng. Chem. Fund.* **15**, 59–64 (1976).

153. Rogers, C. E., Stannett, V. & Szwarc, M. The Sorption of Organic Vapors by Polyethylene. *J. Phys. Chem.* **63**, 1406–1413 (1959).

154. Rogers, C. E., Stannett, V. & Szwarc, M. The sorption, diffusion, and permeation of organic vapors in polyethylene. *J. Polym. Sci.* **45**, 61–82 (1960).

155. Robeson, L. M. & Smith, T. G. Permeation of ethane–butane mixtures through polyethylene. *J. Appl. Polym. Sci.* **12**, 2083–2095 (1968).

156. Li, N. N. & Long, R. B. Permeation through plastic films. *AIChE J.* **15**, 73–80 (1969).

157. Meyer, J. A. & Blanks, R. F. Solubility of isobutane and propane in polyethylene at high temperatures and low pressures. *J. Appl. Polym. Sci.* **28**, 725–741 (1983).

158. Kulkarni, S. S. & Stern, S. A. The diffusion of CO2, CH4, C2H4, and C3H8 in polyethylene at elevated pressures. *J. Polym. Sci. Polym. Phys. Ed.* **21**, 441–465 (1983).

159. Castro, E. F., Gonzo, E. E. & Gottifredi, J. C. Thermodynamics of the absorption of hydrocarbon vapors in polyethylene films. *Journal of Membrane Science* **31**, 235–248 (1987).

160. Hutchinson, R. A. & Ray, W. H. Polymerization of olefins through heterogeneous catalysis. VIII. Monomer sorption effects. *J. Appl. Polym. Sci.* **41**, 51–81 (1990).

161. Sato, Y. *et al.* Solubilities and diffusion coefficients of carbon dioxide and nitrogen in polypropylene, high-density polyethylene, and polystyrene under high pressures and temperatures. *Fluid Phase Equilibria* **162**, 261–276 (1999).

162. Yoon, J.-S. & Chung, C.-Y. Solubility and diffusion coefficient of gaseous ethylene and α-olefin in ethylene/α-olefin random copolymers. 6.

163. Yoon, J.-S., Yoo, H.-S. & Kang, K.-S. Solubility of α-olefins in linear low density polyethylenes. *European Polymer Journal* **32**, 1333–1336 (1996).

164. Moore, S. J. & Wanke, S. E. Solubility of ethylene, 1-butene and 1-hexene in polyethylenes. *Chemical Engineering Science* **56**, 4121–4129 (2001).

165. Chmelar, J., Haškovcová, K., Podivinská, M. & Kosek, J. Equilibrium sorption of propane and 1-hexene in polyethylene: experiments and PC-SAFT simulations. *Industrial & Engineering Chemistry Research* **56**, (2017).

166. Patzlaff, M., Wittebrock, A. & Reichert, K.-H. Sorption studies of propylene in polypropylene. Diffusivity in polymer particles formed by different polymerization processes. *J. Appl. Polym. Sci.* **100**, 2642–2648 (2006).

167. De Loos, T. W., Van der Kooi, H. J. & Ott, P. L. Vapor-liquid critical curve of the system ethane + 2-methylpropane. *J. Chem. Eng. Data* **31**, 166–168 (1986).

168. Nagy, I., Krenz, R. A., Heidemann, R. A. & de Loos, T. W. High-pressure phase equilibria in the system linear low density polyethylene+isohexane: Experimental results and modelling. *The Journal of Supercritical Fluids* **40**, 125–133 (2007).

169. Hutchinson, R. A. & Ray, W. H. Polymerization of olefins through heterogeneous catalysis—the effect of condensation cooling on particle ignition. *J. Appl. Polym. Sci.* **43**, 1387–1390 (1991).

170. McKenna, T. F. Solubility and crystallinity data for ethylene/polyethylene systems. *European Polymer Journal* **34**, 1255–1260 (1998).

171. Raharjo, R. D., Freeman, B. D., Paul, D. R., Sarti, G. C. & Sanders, E. S. Pure and mixed gas CH4 and n-C4H10 permeability and diffusivity in poly(dimethylsiloxane). *Journal of Membrane Science* **306**, 75–92 (2007).

172. Kröner, T. & Bartke, M. Sorption of Olefins in High Impact Polypropylene – Experimental Determination and Mass Transport Modeling. *Macromolecular Reaction Engineering* **7**, 453–462 (2013).

173. Sato, Y. *et al.* Solubility and Diffusion Coefficient of Carbon Dioxide in Biodegradable Polymers. *Ind. Eng. Chem. Res.* **39**, 4813–4819 (2000).

174. Dimos, V. & Kanellopoulos, N. Hybrid model for the diffusion of simple and complex penetrants in polymers. *J. Appl. Polym. Sci.* **104**, 2877–2885 (2007).

175. Kiparissides, C., Dimos, V., Boultouka, T., Anastasiadis, A. & Chasiotis, A. Experimental and theoretical investigation of solubility and diffusion of ethylene in semicrystalline PE at elevated pressures and temperatures. *Journal of Applied Polymer Science* **87**, 953–966 (2003).

176. Chen, M., Wang, J., Jiang, B. & Yang, Y. Diffusion measurements of isopentane, 1-hexene, cyclohexane in polyethylene particles by the intelligent gravimetric analyzer. *Journal of Applied Polymer Science* **127**, 1098–1104 (2013).

177. Palamara, J. E., Mulcahy, K. A., Jones, A. T., Danner, R. P. & Duda, J. L. Solubility and Diffusivity of Propylene and Ethylene in Atactic Polypropylene by the Static Sorption Technique. *Ind. Eng. Chem. Res.* **44**, 9943–9950 (2005).

178. Pino, M., Duckett, R. A. & Ward, I. M. Single and mixed gas diffusion through polyethylene films. *Polymer* **46**, 4882–4890 (2005).

179. Fujita, H. Diffusion in polymer-diluent systems. in *Fortschritte Der Hochpolymeren-Forschung* 1–47 (Springer, 1961). doi:10.1007/BFb0050514.

180. Vrentas, J. S. & Duda, J. L. Diffusion in polymer—solvent systems. I. Reexamination of the free-volume theory. *J. Polym. Sci. Polym. Phys. Ed.* **15**, 403–416 (1977).

181. Vrentas, J. S. & Duda, J. L. Diffusion in polymer–solvent systems. II. A predictive theory for the dependence of diffusion coefficients on temperature, concentration, and molecular weight. *J. Polym. Sci. Polym. Phys. Ed.* **15**, 417–439 (1977).

182. Duda, J. L., Vrentas, J. S., Ju, S. T. & Liu, H. T. Prediction of diffusion coefficients for polymer-solvent systems. *AIChE J.* **28**, 279–285 (1982).

183. Zielinski, J. M. & Duda, J. L. Predicting polymer/solvent diffusion coefficients using free-volume theory. *AIChE J.* **38**, 405–415 (1992).

Chapter 2

A Novel Approach for the Estimation of the Sanchez-Lacombe Interaction Parameters for Ternary Polyolefins Systems

1. Introduction

As discussed in Chapter 1, the sorption of ethylene, comonomers and alkanes (used as induced condensing agents, ICA, for instance) is non-ideal[1–3]. In other words the solubility of a mixture of gases in the amorphous phase of a polymer is not the same as the sum of the solubilities of the pure species. Over the last decade, different experimental methods have been developed to measure the solubility of gases in polymers. However, most of these experimental solubility studies are restricted to binary systems (penetrant - PE), with a limited number looking at ternary systems (penetrant 1 – penetrant 2 - PE)[4–13]. These studies showed that the solubility of a given component in a polymer is function of the structure of the penetrant, the temperature, the pressure and the polymer density and crystallinity. In the case of ternary systems, the composition of the gas-phase has been shown to be very important[14]. For instance, Yao et al.[4] measured ethylene-alkane-PE systems by varying the partial pressure of n-hexane and iso-pentane. They showed that the solubility of ethylene in ternary systems is higher than its solubility in binary system. Other authors showed the same effect in the presence of co-monomers in ternary systems[6,15,16]. Chmelar et al.[7] showed that the sorption of 1-hexene increases ethylene solubility in the amorphous PE. This phenomenon is often referred to as the cosolubility effect. These same authors also demonstrated that increasing ethylene pressures can lead to a decrease in the solubility of 1-hexene at constant 1-hexene pressure, considered as the anti-solvent effect.

All these studies show the importance of accounting for the overall composition of the gas phase, since the solubility of monomer and comonomer will be directly impacted by the relative amounts of the different species present in the mixture. It is therefore necessary to account for the way that the different species present in the gas phase mixture interact with the polymer in a ternary system. Obviously, this means that if one needs to develop models to quantify these effects, appropriate thermodynamic models that can account for these phenomena are needed.

This is of course possible using equations of state. The Sanchez-Lacombe equation of state (SL EoS) is one of the most widely used thermodynamic model in the field of polymer reaction engineering. The only adjustable parameters in the SL EoS are the interaction parameters between the penetrant molecules and the polymer (if we assume negligible interactions between the small molecule penetrants), that need to be estimated experimentally. To do so, this equation

of state has to be fitted to experimental solubility data, and such data is sorely lacking for multicomponent systems under conditions similar to those used in a polymerization process.

Currently, gravimetric experiments based on a magnetic suspension balance (MSB) are perhaps the most widely used technique for this type of solubility measurement because of their relative simplicity and high precision. A large number of studies have used this method to investigate the impact of partial pressures and temperatures on the solubility of (mostly) binary[6,7,9–13,] and (very occasionally) ternary systems[11,7,17,20]. However, it is not straightforward to measure individual concentrations (and thus individual solubilities) in this type of apparatus, so MSB experiments often give only the total solubilities for a given mixture. The advantage of these experiments is that they are rapid once the device is calibrated, and one can also have access to overall diffusivity data.

In the present Chapter, the gravimetric technique was used to measure the total solubility of ternary systems that are not available in the literature, such as ethylene/propane/LLDPE-B, ethylene/isobutane/LLDPE-B and ethylene/1-butene/LLDPE-B. These systems were measured at 70°C and total pressures up to 5 bars. Since individual solubilities cannot be measured experimentally with the suspension balance, we used the compressibility factor of the gas mixture calculated with the Peng-Robinson EoS (PR EoS) as second data source to estimate the two necessary interaction parameters for the SL EoS. The measured overall solubilities and the compressibility factors from PR EoS were then used to fit the interaction parameters of the SL EoS. The observed trends were theoretically interpreted because no available data can be found in the literature for these studied systems.

2. Experimental section

2.1.Materials

Ethylene and argon with minimum purities of 99.5%, and propylene, butene, butane, and propane with minimum of purities of 99% were obtained from Air Liquide Germany. Argon was used as blank gas. Linear low-density polyethylene (LLDPE-B) powders were graciously supplied by Borealis.

2.2.Polymer characterization

The crystallinity of the polymer samples was measured using differential scanning calorimetry (DSC 3+ by Mettler Toledo). Polyethylene samples were weighed (i.e. around 5-7 mg) and placed in an aluminium capsule with a volume of 40 µL. The sample was first cooled to -20°C

and then heated from −20 to 180 °C at a heating rate of 10°C min^{-1}, held for 5 minutes at that temperature and then cooled from 180 to −20 °C at a rate of 10°C min^{-1}. This temperature was maintained for 5 minutes, and the sample was reheated to 180°C at a rate of 10°C min^{-1}. The melting behavior of the samples was studied in the second heating cycle in order to detect the melting point and the melting enthalpy of the samples. The ratio of the heat of fusion of the sample to that of the completely crystallized polyethylene was used to calculate the degree of crystallization. A heat of fusion of 293 J g^{-1} for completely crystallized polyethylene was used for the calculation. The STARe software was used for data acquisition and data analysis. The crystallinity of the LLDPE-B samples used during this study was measured at 48.3%.

2.3.Gravimetric method

The gravimetric apparatus used to measure the equilibrium solubility data is a magnetic suspension balance (Rubotherm GmbH), connected to a pressure cell that contains the polymer sample. The weighing mechanism of the balance is separated from the pressure cell, so it is not exposed to high temperatures and pressures. The detailed experimental apparatus is shown in ***Figure 10***.

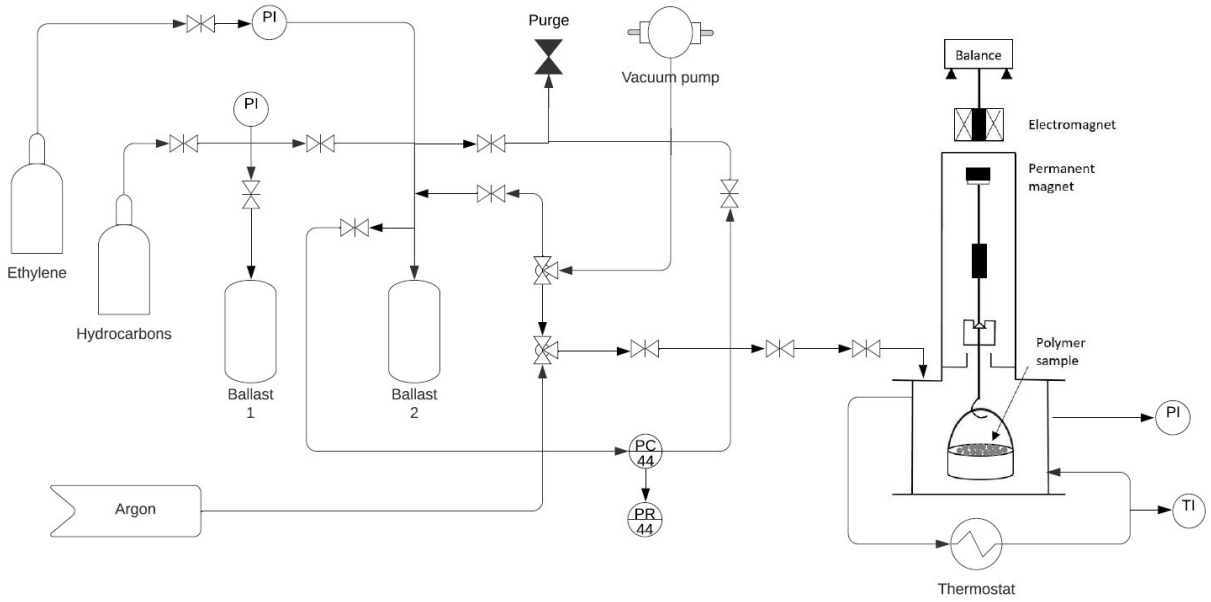

Figure 10. *P&ID of the sorption reactor based on gravimetric method*

The apparatus is equipped with temperature and pressure sensors, vacuum pump, heating gas bottles, and recording computer. The data acquired from the gravimetric experiment are pressure, temperature, time and sample mass. The magnetic coupling between the balance and

the sample in the pressure chamber allows an accuracy of 0.1 mg for weight measurements. The setup is described in more details in references[17–19], but we will briefly describe the measuring procedure and the corrections that have to be done.

1-2 grams of polymer particles (powder withdrawn directly from the reactor) are used for each sorption experiment (m_{sample}). The polymer sample is first degassed under 40 mbar of vacuum for at least 45 minutes at the desired temperature. The process gas mixture is then injected into the pressure cell at the desired pressure and temperature. Pressure steps are then performed in the chamber, and as this pressure is increased, the gas density increases which results in higher buoyancy force acting on the container and the sample. The reading of the balance must be corrected for this buoyancy force. First, a blank run using nitrogen and without polymer sample determines the buoyancy of the sample container. Then, a second run with the polymer sample is performed to estimate the volume of the measured sample required for the buoyancy correction of the sample mass.

$$m_{\text{corrected}} = m_{\text{balance}} + V_{\text{container+sample}}\,\rho_{\text{gas}} \qquad (1)$$

Where the volume of the container with the sample has been calculated during the second run. Gas densities of propane, isobutane and 1-butene and their mixture at the temperature and pressure of interest were calculated for each set of experimental condition using the ideal gas law corrected for compressibility calculated with Peng-Robinson EoS.

The mass of the sample with the adsorbed gas is given by the following expression:

$$m = m_{\text{corrected}} - m_{\text{container}}$$

Since PE is semicrystalline, it is necessary to evaluate the solubility by taking into account the crystalline phase where the solubility of the penetrants is zero. Thus, the solubility in the amorphous phase of the polymer is expressed as specific mass change of the sample due to the sorption.

$$S_{\text{am}} = \frac{m - m_{\text{sample}}}{m_{\text{sample}}\,(1-\chi)}$$

Where χ is the crystallinity fraction. Kosek et al.[17] demonstrated that taking into account the impact of temperature on the crystallinity of the polymer sample is an essential step for the solubility measurement. Therefore, the mass fraction of crystalline material in the polymer at the temperature of interest (i.e. T=70°C) has been estimated at 47.6% using differential scanning calorimetry (DSC 3+ by Mettler Toledo).

3. Thermodynamic modeling

3.1. Model development

3.1.1. Sanchez-Lacombe EoS

The Sanchez-Lacombe EoS is a lattice-fluid model in which pure components are assumed to be broken into parts and placed into a lattice structure. The SL EoS is basically an extension of the classic Flory-Huggins theory. The main advance is that this model introduces vacant lattice sites to account for the compressibility and the density changes. Thus, the system volume or density can vary by changing the fraction of holes in the lattice structure[20]. The main equation of state is given by:

$$\bar{\rho}^2 + \bar{P} + \bar{T}\left[\ln(1-\bar{\rho}) + \left(1-\frac{1}{r}\right)\bar{\rho}\right] = 0 \qquad (2)$$

where $\bar{T}$, $\bar{P}$, $\bar{\rho}$ are the reduced temperature, pressure, volume and density, respectively. r is the number of sites (mers) a molecule occupies in the lattice. These reduced parameters, depending on the characteristic properties, are defined as follows:

$$\bar{T} = {}^{T}/_{T^*} \qquad \bar{P} = {}^{P}/_{P^*} \qquad \bar{\rho} = {}^{\rho}/_{\rho^*} = {}^{1}/_{\bar{V}} \qquad (3)$$

where T^*, P^*, and ρ^* are the scale factors known as the characteristic temperature, pressure, and density respectively, which are used to characterize each pure component in the mixture. The parameters of SL EoS for each pure component are given in ***Table 9***.

Table 9. *Pure component parameters used in SL EoS*

Component	T^* (K)	P^* (bar)	ρ^* (kg/m^3)	Ref
Ethylene	283	3395	680	[21]
Propane	371	3090	690	[20]
Isobutane	398	2840	720	[20]
1-butene	410	3350	770	[22]
1-hexene	450	3252	814	[23]
Propylene	345.4	3788	755	[18]
LLDPE	667	4370	900	[21]
Polypropylene	690.6	3007	885.6	[18]

$\bar{P}$, $\bar{T}$, $\bar{\rho}$ and $\bar{V}$ are the reduced pressure, temperature, density and volume, respectively. These characteristic parameters depend on three lattice parameters, describing the thermodynamic

properties of a pure components: ε^*, v^* and r, where ε^* is the mer-mer interaction energy (J mol^{-1}) and v^* the closed-packed molar volume of a mer (m^3 mol^{-1}).

$$T^* = {\varepsilon^*}/{R} \qquad P^* = {\varepsilon^*}/{v^*} \qquad \rho^* = {MW}/{(rv^*)} \qquad V^* = N(rv^*) \tag{4}$$

Where MW is the molecular weight of the component and R is the universal gas constant (J K^{-1} mol^{-1}).

When the SL EoS is used for a mixture of components, it is necessary to define combining rules based on the Van der Waals mixing rule for the estimation of mixture properties (i.e. $\varepsilon^*_{\text{mix}}$, v^*_{mix}, r_{mix}) based on the respective values of the pure component values.

The characteristic closed-packed molar volume of a "mer" of the mixture, v^*_{mix} is defined as follows:

$$v^*_{\text{mix}} = \sum_{i=1}^{N_c} \sum_{j=1}^{N_c} \phi_i \phi_j v^*_{ij} \tag{5}$$

With

$$v^*_{ij} = \frac{v^*_{ii} + v^*_{jj}}{2} \left(1 - n_{ij}\right) \tag{6}$$

Where ϕ is the volume fraction of the i^{th} and j^{th} component in the mixture, N_c is the number of component in the mixture and n_{ij} corrects the possible deviation of v^*_{ij} from the arithmetic mean value of v^*_{ii} and v^*_{jj} of the pure component. In the present study, the value of the interaction parameter n_{ij} is assumed to be equal to zero.

The closed-packed volume fraction of the i$^{\text{th}}$ component at the limit of zero temperature or incompressible state, ϕ_i^{gas} is defined as:

$$\phi_i^{\text{gas}} = \frac{\omega_i^{\text{gas}}}{\rho_i^* v_i^*} \Big/ \sum_{j=1}^{N_c} \left(\frac{\omega_j^{\text{gas}}}{\rho_j^* v_j^*} \right) \tag{7}$$

where ω_i^{gas} is the mass fraction of the component i in the gas phase.

The mixing rule for the characteristic interaction energy for the mixture $\varepsilon^*_{\text{mix}}$ is defined as:

$$\varepsilon^*_{\text{mix}} = \frac{1}{v^*_{\text{mix}}} \sum_{i=1}^{N_c} \sum_{j=1}^{N_c} \phi_i \phi_j \varepsilon^*_{ij} v^*_{ij} \tag{8}$$

The cross-energy parameter between mers of component (i) and component (j), ε^*_{ij} is introduced in order to take into account the interactions between components in mixtures.

$$\varepsilon^*_{ij} = \left(\varepsilon^*_{ii} \varepsilon^*_{jj}\right)^{0.5} \left(1 - k_{ij}\right) \tag{9}$$

in which ε_{ii}^* and ε_{jj}^* are the interation energy between mers of the i^{th} and j^{th} component respectively. k_{ij} is a binary interaction parameter between the different components of the mixture, which is employed as adjustable parameter to fit the model to experimental solubility data.

The mixing rule for the number of sites (mers) occupied by a molecule of the mixture, r_{mix}, is given by:

$$\frac{1}{r_{\text{mix}}} = \sum_{j=1}^{N_c} \frac{\phi_j}{r_j} \tag{10}$$

where r_j is the number of sites occupied by molecule *j* in the lattice.

For the calculation of sorption equilibrium for polymer-penetrant system, the chemical potential of the i^{th} component in a multicomponent system can be expressed as

$$\mu_i^{\text{gas}} = R_g T \left[ln\phi_i^{\text{gas}} + 1 - \frac{r_i}{r_{\text{mix}}^{\text{gas}}} \right] \tag{11}$$

$$+ r_i \left\{ \begin{array}{l} -\bar{\rho}^{\text{gas}} \left[\frac{2}{v^{*\text{gas}}_{\text{mix}}} \left(\left(\phi_1^{\text{gas}} v_i^* \varepsilon_i^* + \phi_j^{\text{gas}} v_{ij}^* \varepsilon_{ij}^* \right) - \varepsilon^{*\text{gas}}_{\text{mix}} \left(\phi_1^{\text{gas}} v_i^* + \phi_j^{\text{gas}} v_{ij}^* \right) \right) + \varepsilon^{*\text{gas}}_{\text{mix}} \right] + \\ \frac{R_g T}{\bar{\rho}^{\text{gas}}} \left[(1 - \bar{\rho}^{\text{gas}}) \ln(1 - \bar{\rho}^{\text{gas}}) + \frac{\bar{\rho}^{\text{gas}}}{r_i} ln\bar{\rho}^{\text{gas}} \right] + \frac{P}{\bar{\rho}^{\text{gas}}} \left[2 \left(\phi_i^{\text{gas}} v_i^* + \phi_j^{\text{gas}} v_{ij}^* \right) - v^{*\text{gas}}_{\text{mix}} \right] \end{array} \right\}$$

Where

$$v^{*\text{gas}}_{\text{mix}} = (v_1^* - v_2^*)\phi_1^{gas} + v_2^* \tag{12}$$

$$\varepsilon^{*\text{gas}}_{\text{mix}} = \frac{(\varepsilon_1^* v_1^* + \varepsilon_2^* v_2^* - \varepsilon_{12}^* (v_1^* + v_2^*))\phi_1^{gas^2} + (\varepsilon_{12}^* (v_1^* + v_2^*) - 2\varepsilon_2^* v_2^*)\phi_1^{gas} + \varepsilon_2^* v_2^*}{(v_1^* - v_2^*)\phi_1^{gas} + v_2^*} \tag{13}$$

We consider that the chemical potential of each component at equilibrium is equal to the chemical potential of the polymer as follows:

$$\mu_i^{\text{pol}} = \mu_i^{\text{gas}} \qquad i=1,2... \tag{14}$$

In which μ_i^{gas} can be the chemical potential of the monomer, the comonomer, or the ICA.

By solving equations (2) and (11) using a nonlinear algebraic equation solver (e.g. in Matlab), for each component in the ternary system, the mass fraction of each sorbed component in the amorphous polymer (where *1* refers to the monomer, *2* to the penetrant molecule (i.e. comonomer or ICA) and *3* to the polymer, and the superscript *pol* means in the polymer phase) can be calculated as follows

$$\omega_1^{\mathrm{am}} = \frac{\rho_1^* v_1^* \phi_1^{\mathrm{pol}}}{\rho_1^* v_1^* \phi_1^{\mathrm{pol}} + \rho_2^* v_2^* \phi_2^{\mathrm{pol}} + \rho_3^* v_3^* \phi_3^{\mathrm{pol}}} \quad (15)$$

$$\omega_2^{\mathrm{am}} = \left(\frac{\rho_2^* v_2^* \phi_2^{\mathrm{pol}}}{\rho_1^* v_1^* \phi_1^{\mathrm{pol}}}\right) \omega_1^{\mathrm{am}} \quad (16)$$

$$\omega_{\mathrm{pol}}^{\mathrm{am}} = 1 - \omega_1^{\mathrm{am}} - \omega_2^{\mathrm{am}} \quad (17)$$

Finally, the solubility of each component at equilibrium, in gram of component per gram of polymer, S, can be calculated as follows

$$S_i^{\mathrm{am}} = \frac{\omega_i^{\mathrm{am}}}{\omega_{\mathrm{pol}}^{\mathrm{am}}}(1-\chi) \qquad i,j = 1,2$$

where χ is the crystallinity of the polymer.

For more details on the development and the application of SL EoS to ternary systems, readers may refer to Alizadeh et al.[24].

3.1.2. Peng-Robinson EoS

The Peng-Robinson (PR) equation of state[25] for gas mixture is defined as

$$P = \frac{R\,T}{v - b_{\mathrm{m}}} - \frac{a_{\mathrm{m}}(T)}{v(v+b_{\mathrm{m}}) + b_{\mathrm{m}}(v-b_{\mathrm{m}})} \quad (18)$$

Where v is molar volume. The parameter a_{m} is a measure of the attractive forces between molecules in the mixture and the parameter b_{m} is the van der Waals co-volume occupied by these molecules in the mixture. These parameters are defined as follow:

$$a_{\mathrm{m}} = \sum_{i=1}^{2}\sum_{j=1}^{2} x_i x_j (1 - l_{ij})\sqrt{a_i a_j} \quad (19)$$

$$b_{\mathrm{m}} = \sum_{i=1}^{2} x_i b_i \quad (20)$$

a and b are the respective PR parameters for pure substances. x is the mole fraction of each component in the mixture and l_{ij} is the binary interaction parameter. This interaction parameter is identified using the experimental compressibility data, but very few experiments are available in the literature. The measure of the compressibility factor when using identified l_{ij} compared to that assuming $l_{ij} = 0$ shows a difference of less than 0.4% for ethylene/propane mixture, at the same conditions than the gravimetric experiments[31]. Therefore, as for SL model, we will consider for this study that there is no interaction between small molecules, meaning that $l_{ij} = 0$.

Applying the first equation at the critical point, we have:

$$a_i(T_{\mathrm{c},i}) = 0.45724\frac{R^2 {T_{\mathrm{c},i}}^2}{P_{\mathrm{c},i}} \quad (21)$$

$$b_i(T_{c,i}) = 0.07780 \frac{R\,T_{c,i}}{P_{c,i}} \quad (22)$$

At temperatures other than the critical temperature, we have:

$$a_i(\mathrm{T}) = a_{ii}(T_{c,i})\,.\,\alpha_i(T_{r,i}, w_i) \quad (23)$$

$$b_i(\mathrm{T}) = b_i(T_{c,i}) \quad (24)$$

A relationship between α and the reduced temperature T_r can be made and linearized by Peng and Robinson[25] as follow

$$\alpha_i(T_{r,i}, w_i) = \left(1 + m_i\left(1 - {T_{r,i}}^{1/2}\right)\right)^2 \quad (25)$$

Since the acentric factors of all studied species are $w \leq 0.49$, m_i, which is a constant characteristic of each substance, is defined as follow:

$$m_i = 0.37464 + 1.54226\,w_i - 0.26992\,{w_i}^2 \quad (26)$$

Equation (16) can be rewritten as:

$$Z^3 - (1-B)Z^2 + (A - 3B^2 - 2B)Z - (AB - B^2 - B^3) = 0 \quad (27)$$

Where Z is the compressibility factor.

$A = \frac{a\,P}{R^2T^2}$ $\qquad B = \frac{b\,P}{R\,T}$ $\qquad Z = \frac{P\,v}{R\,T}$

Table 10 indicates the required properties to implement the PR equation of the components studied in this chapter.

Table 10. *Critical temperature and pressure, acentric factors and molecular weight for selected fluids.*

	Ethylene	**Propane**	**Isobutane**	**1-butene[a]**	**1-hexene**	**Propylene**	**Ref**
***w* (-)**	0.089	0.153	0.183	0.191	0.28	0.144	[26]
T_c (K)	282.36	369.83	407.82	419.95	504.03	364.76	[27]
P_c (bar)	50.318	42.471	36.4	40.4	31.4	46.126	[27]
***MW* (g.mol^{-1})**	28.054	44.1	58.12	56.108	84.16	42.08	[26]

[a] The properties of 1-butene were taken from reference[28]

The roots function of Matlab is used to solve this polynomial equation. This equation yields one or three roots depending upon the number of phases in the system. In the two-phase region, the largest root is for the compressibility factor of the vapor while the smallest positive root corresponds to that of the liquid.

3.2.Model solution procedure

We will define our ternary system as one containing ethylene (1), a penetrant (2) which can be a comonomer or an ICA, and a polymer (3). The corresponding interaction parameters in order to solve SL EoS are k_{12}, k_{13}, k_{23} which are the interactions between the monomer and the penetrant, the monomer and the polymer and the penetrant and the polymer, respectively. k_{12} is assumed equal to zero due to low chemical affinity between like molecules. The interaction parameters are used to define the cross interaction energy $\varepsilon_{ij}^{*} = \left(\varepsilon_i^{*}\varepsilon_j^{*}\right)^{0.5}\left(1 - k_{ij}\right)$; when k_{ij}=0, the cross potential follows Lorentz-Berthelot combining rules[32] (i.e. $\varepsilon_{ij}^{*} = \left(\varepsilon_i^{*}\varepsilon_j^{*}\right)^{0.5}$) while if the value is far from 1, then there is a deviation from these rules. Therefore, the heavier the penetrant, the more the interaction with the polymer deviates from Lorentz-Berthelot combining rules. This leaves us two interaction parameters that need to be estimated to solve the Sanchez-Lacombe EoS. In order to do that, one needs to fit this model to experimental solubility data that have been measured for this study using a magnetic suspension balance. However, as we have only global solubilities from this apparatus, this measurement leaves us with only one experimental data to identify two interactions parameters. The calculation of the compressibility factor of the different gaseous species in the mixture represents therefore a crucial input data as it can be compared to the compressibility factor calculated through SL EoS.

From equations (3) and (4), we can calculate the compressibility factor as follows:

$$Z = \frac{P\,v}{R\,T} = \frac{\bar{P}\,\bar{v}}{\bar{T}}r \tag{14}$$

We can then extend Equation (2) from SL EoS to calculate the compressibility factor[29] as follows:

$$Z = -r\left[\frac{1}{\bar{\rho}}\ln(1-\bar{\rho}) + \left(1 - \frac{1}{r}\right) + \frac{\bar{\rho}}{\bar{T}}\right] \tag{15}$$

The identification of the two interaction parameters is now possible by fitting three "experimental" data (one overall solubility, two compressibility factors) to the Sanchez-Lacombe model. Since, no available experimental data can be found for the compressibility factor, it was calculated with another equation of state, for instance the Peng-Robinson EoS[25]. This will be acceptable as input to the estimation procedure as the compressibility factor for the vapor phase does not have interactions with the polymer and we can therefore have confidence that the value is correct. The detailed procedure of the development of SL EoS associated with PR EoS for the identification of k_{ij} interaction parameters is presented in ***Figure 11***. The identification of the two interaction parameters in the SL EoS for ternary systems is achieved by minimizing the average relative deviation, ARD, between the experimental overall solubility and the one calculated with SL EoS, as well as between the compressibility factors of each specie in the mixture calculated with PR EoS with the ones calculated with SL EoS, as follows:

$$ARD = \sum_{i=1}^{t} \frac{|S_{\text{tot}}^{\text{SL}} - S_{\text{tot}}^{\text{exp}}|}{S_{\text{tot}}^{\text{exp}}} + \sum_{i=1}^{t} \frac{|Z_1^{\text{SL}} - Z_1^{\text{PR}}|}{Z_1^{\text{PR}}} + \sum_{i=1}^{t} \frac{|Z_2^{\text{SL}} - Z_2^{\text{PR}}|}{Z_2^{\text{PR}}}$$

Once the available experimental overall solubility as well as the calculated compressibility factors from PR EoS are fitted to SL EoS, we can therefore identify the k_{ij} interaction parameters, that will next lead to the calculation of the partial solubilities and the concentrations of the different species in the mixture, as well as the polymer swelling due to the dissolution of these species in the amorphous phase of the polymer.

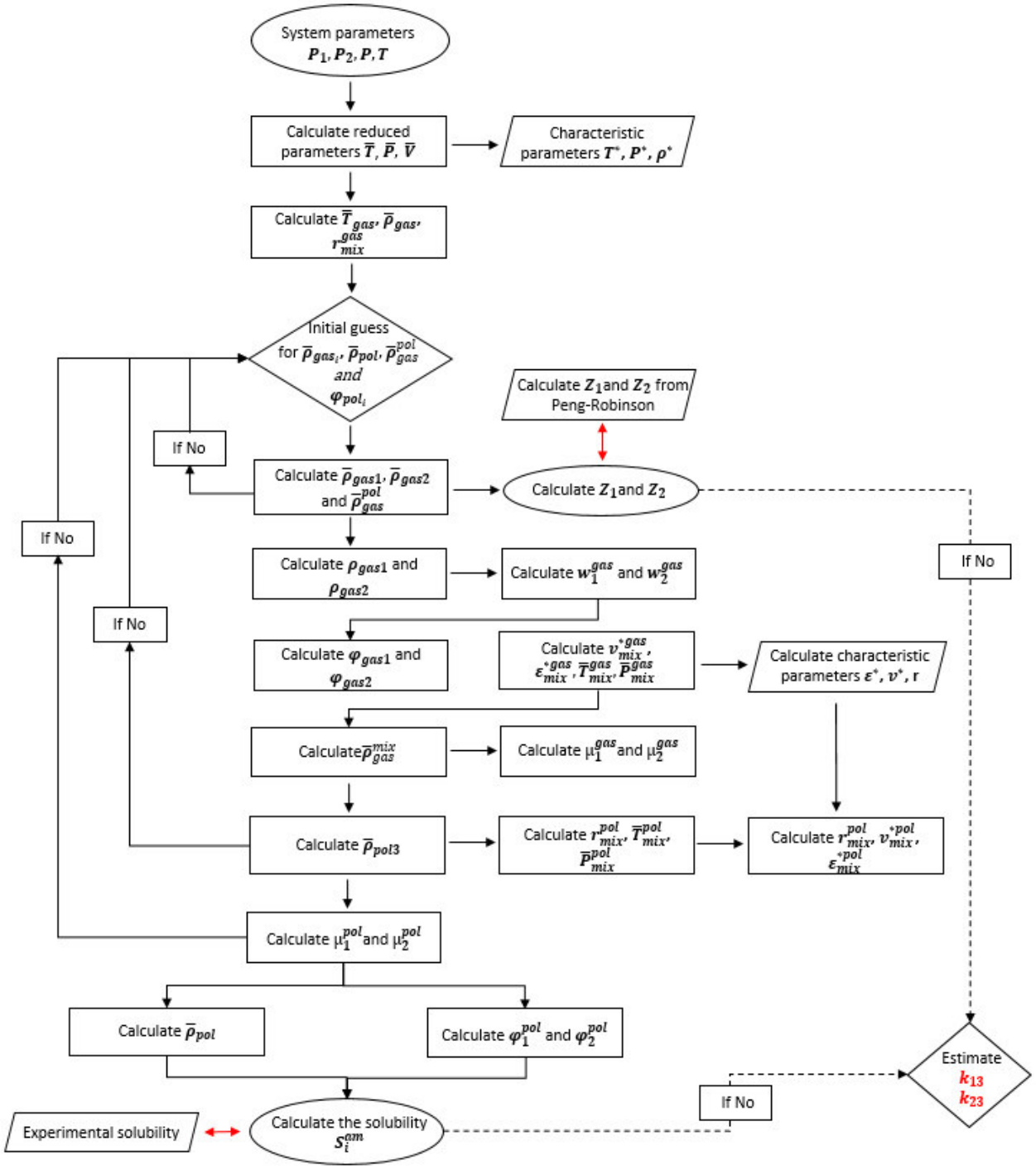

Figure 11. *Flowchart for the modeling of ternary systems with SL EoS*

4. Results and discussion

In this Chapter, a novel approach consisting of combining the compressibility factor calculated with Peng-Robinson plus experimental global solubility results has been used to predict the interactions parameters needed for SL EoS. We will first validate this new approach using previously published experimental data for ternary systems, and then use it to predict the partial

solubility of species in ternary systems from the new experimental measurements of the overall solubility using the magnetic suspension balance.

4.1.Model validation on literature data

Cancelas et al.[18] measured the overall solubility of an equimolar ethylene/propylene mixture in iPP at temperatures above 70°C and pressures up to 25 bar, using the same magnetic suspension balance. They used the interaction parameters from the two binary systems and readjusted k_{23} at low temperatures to fit the ternary data. In the current study, their experimental overall solubility data for ternary system of ethylene/propylene/iPP coupled with the Peng-Robinson EoS were used in order to identify the ternary interaction parameters, without using binary interactions parameters. ***Figure 12*** shows the experimental overall solubilities measured by Cancelas et al.[18] and the corresponding model predictions obtained from SL EoS employing the interaction parameters estimated from overall solubility plus the Peng-Robinson EoS (this approach will henceforth be referred to as SL-PR). In ***Figure 12***, ***Figure 13*** and ***Figure 14***, the symbols represent experimental values of the total solubility, and the lines represent the theoretical solubilities calculated with SL-PR method.

Table 11. *Comparison of ternary interaction parameters of ethylene/propylene mixture in iPP identified with the novel approach SL-PR by fitting experimental solubilities of Cancelas et al.[18]*

	T = 50 °C	**T = 70 °C**	**T = 85 °C**
k_{13} from [18]	-0.01	-0.015	-0.02
k_{13} SL-PR	-0.0095	-0.0157	-0.0192
k_{23} from [18]	0.01	0.005	-0.005
k_{23} SL-PR	0.0137	-0.00026	-0.00043

A comparison of the ternary interaction parameters of ethylene/propylene mixture in iPP identified in this study and those identified by Cancelas et al.[18] is given in ***Table 11***. Note that the interaction parameters are temperature-dependent. Indeed, they identified binary k_{ij} interaction parameters for both binary systems of ethylene/iPP and propylene/iPP by fitting their experimental solubilities as well as solubility data from literature to binary SL EoS. These k_{ij} were then used for ternary system of ethylene/propylene/iPP, but k_{23} had to be readjusted for lower temperatures in order to fit better their experimental ternary global solubility. As can be seen, we find an excellent agreement between the ternary interactions parameters determined

with the novel approach SL-PR and the ones determined by Cancelas et al.[18]. However, in the SL-PR method, no re-adjustment of the parameters is required, which makes this novel methodology more robust. Partial solubilities of each component in the mixture can then be calculated using SL EoS, as can be seen in ***Figure 13*** and ***Figure 14***. These figures show the solubility of ethylene and propylene in ethylene/propylene/iPP mixture, respectively, at 50, 70 and 85°C.

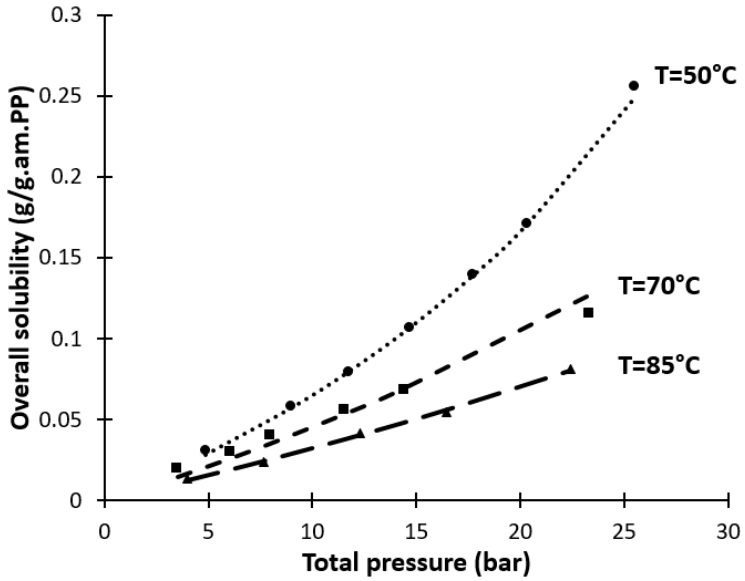

Figure 12. *Overall solubilities of an equimolar ethylene/propylene mixture in iPP at 50, 70 and 85°C. The points are desorption measurements from [18] and the curves are SL-PR predictions.*

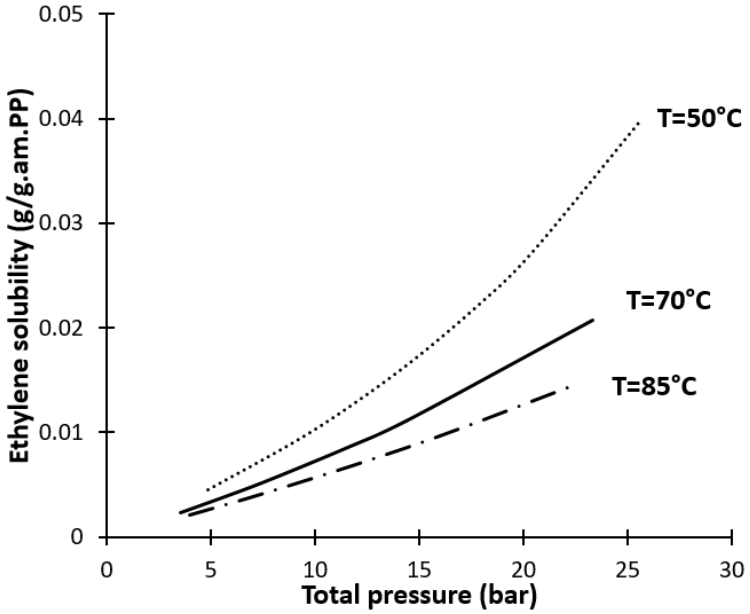

Figure 13. *Ethylene partial solubility in an equimolar ethylene/propylene mixture in iPP at 50, 70 and 85°C from SL. k_{ij} were taken from* ***Table 11***

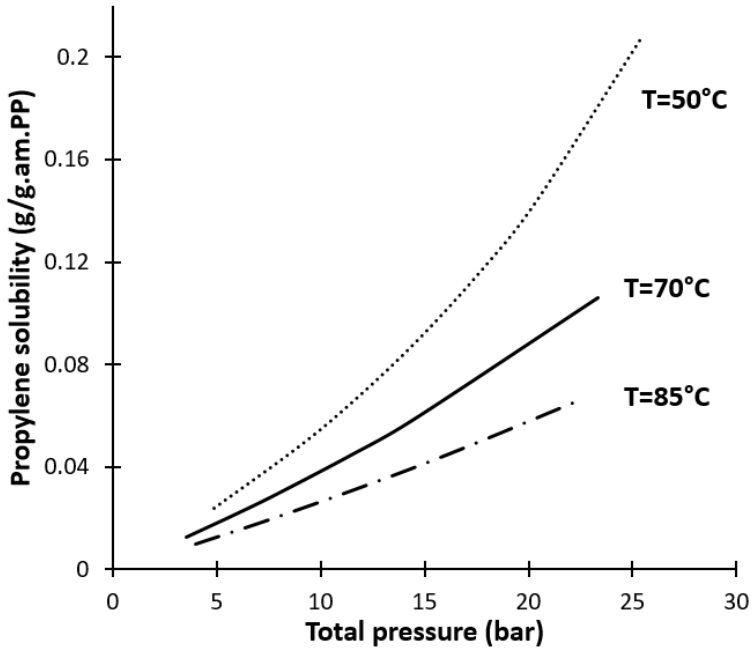

Figure 14. *Propylene partial solubility in an equimolar ethylene/propylene mixture in iPP at 50, 70 and 85°C from SL. k_{ij} were taken from* ***Table 11***

The second system used to validate this approach is ethylene/1-hexene/LLDPE. Novak et al.[6] measured ethylene/1-hexene mixture overall solubility in LLDPE-1-hexene copolymer with a constant composition of 4.3 mol% 1-hexene and 95.7 mol% ethylene at 70, 90 and 150°C. In ***Figure 15***, the overall experimental solubility of ethylene/1-hexene mixture in LLDPE is compared with the corresponding model predictions obtained from SL EoS using the SL-PR method at the different temperatures. In ***Figure 15*** the symbols represent experimental values of the total solubility, and the lines represent the theoretical solubilities calculated with SL-PR method. Ternary interaction parameters were then obtained by fitting SL EoS to the experiments by Novak et al.[6] at 70, 90 and 150°C in ***Table 12*** compared to the interaction parameters obtained by Bashir et al.[14]. These last authors fitted the experimental values of the total solubility found by Novak et al.[13] with the SL EoS in a manner similar to how Cancelas et al.[31] did for the ethylene-propylene-iPP system, i.e. they started from the binary interaction parameters identified in binary systems by Novak et al. [13] and re-adjusted these parameters. Partial solubilities of each component in the mixture are then predicted using SL EoS, as can be seen in ***Figure 16*** and ***Figure 17***. These figures show the solubility of ethylene and 1-hexene in ethylene/1-hexene/LLDPE mixture, respectively, at 70, 90 and 150°C.

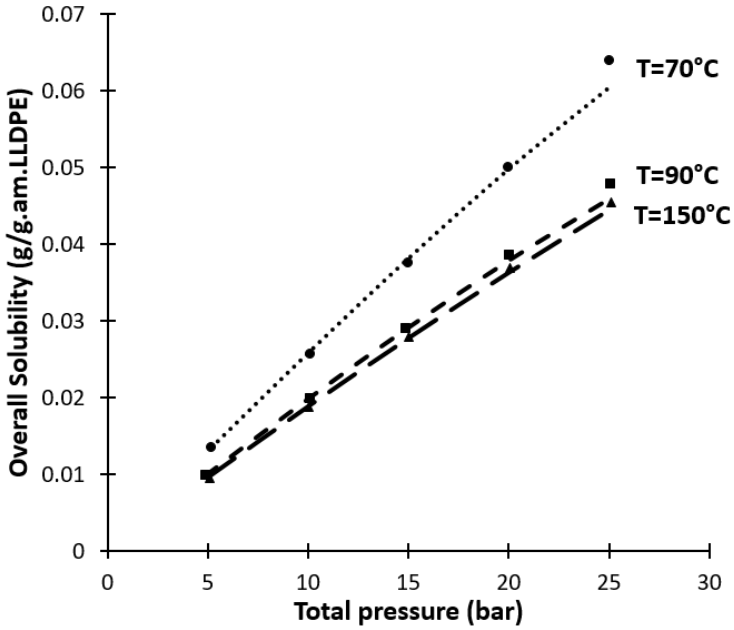

Figure 15. *Overall solubilities of an ethylene/1-hexene mixture in LLDPE with 4.3 mol% 1-hexene and 95.7 mol% ethylene at 70, 90 and 150°C. The points are sorption measurements from [6] and the curves are SL-PR predictions.*

Table 12. Comparison of ternary interaction parameters of ethylene/1-hexene mixture in LLDPE identified with the novel approach SL-PR by fitting experimental solubilities of Novak et al.[6] with the interaction parameters found by Bashir et al.[14]

	T = 70 °C	**T = 90 °C**	**T = 150 °C**
k_{13} **from [14]**	0.038	0.038	-0.05
k_{13} **SL-PR**	0.04188	0.0313	-0.01393
k_{23} **from [14]**	0.027	0.016	-0.03
k_{23} **SL-PR**	0.04894	0.0403	-0.03258

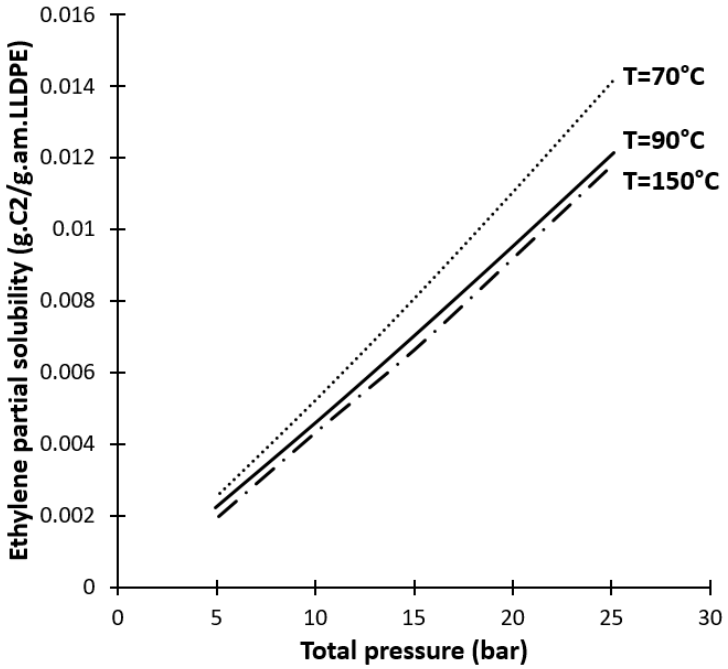

Figure 16. Ethylene partial solubility in ethylene/1-hexene/LLDPE ternary mixture at 70, 90 and 150°C calculated from SL EoS. k_{ij} were taken from ***Table 12***

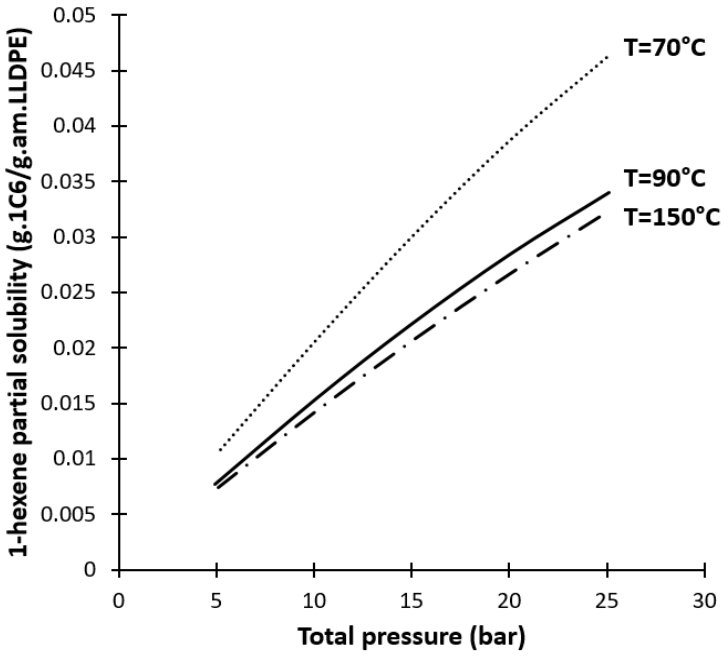

Figure 17. 1-hexene partial solubility in ethylene/1-hexene/LLDPE ternary mixture at 70, 90 and 150°C calculated from SL EoS. k_{ij} were taken from ***Table 12***

We can use these results to study the co- and anti-solvent effects of 1-hexene and ethylene in this system. Binary data for ethylene/LLDPE and 1-hexene/LLDPE were taken from Novak et

al.[6] data and then fitted to the binary SL EoS. The correlations of binary k_{ij} for ethylene/LLDPE and 1-hexene/LLDPE, with respect to temperature are listed in ***Table 5***. ***Figure 18*** and ***Figure 19*** show the solubility of ethylene and 1-hexene in binary (ethylene/PE and 1-hexene/PE) and ternary (ethylene/1-hexene/PE) systems under the same composition as Novak et al.[6] (4.3 mol% 1-hexene and 95.7 mol% ethylene) for the ternary simulations. The solubilities calculated assuming a binary and/or a ternary system are compared in ***Figure 18*** and ***Figure 19*** for 70 and 90°C, and the simulations indicate a co-solubility effect which is enhanced at higher temperature. It is shown that the partial solubility of ethylene in the ternary system is higher than its binary solubility, meaning that ethylene solubility is enhanced by the addition of 1-hexene to the gas phase (co-solubility effect). On the other hand, it is shown that the ternary partial solubility of 1-hexene is lower than its binary solubility, meaning that ethylene acts as an anti-solvent to 1-hexene. It is also shown that the anti-solvent effect of ethylene is higher than the co-solvent effect of 1-hexene.

Table 13. *Temperature dependence of k_{ij} for ethylene/LLDPE and 1-hexene/LLDPE binary systems. T is in °C*

System	k_{ij}
Ethylene/LLDPE	$-2.93 \times 10^{-4}T + 5.87 \times 10^{-2}$
1-hexene/LLDPE	$-8.23 \times 10^{-4}T + 8.89 \times 10^{-2}$

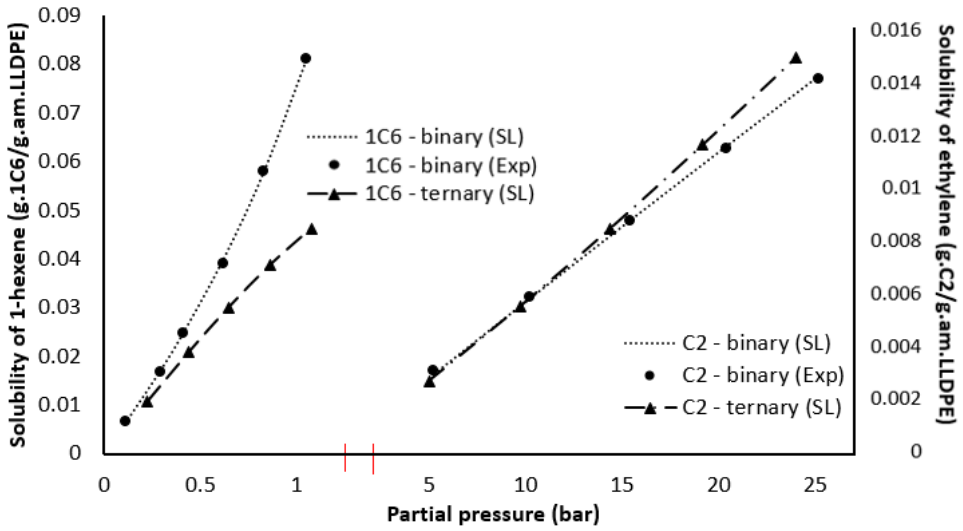

Figure 18. *Ethylene and 1-hexene partial solubility in ternary system at 70°C with 5 mol% 1-hexene and 95 mol% ethylene and their corresponding partial pressures for each pure component for binary simulations. k_{ij} for ternary system were taken from **Table 12** and k_{ij} for binary systems were taken from **Table 5**.*

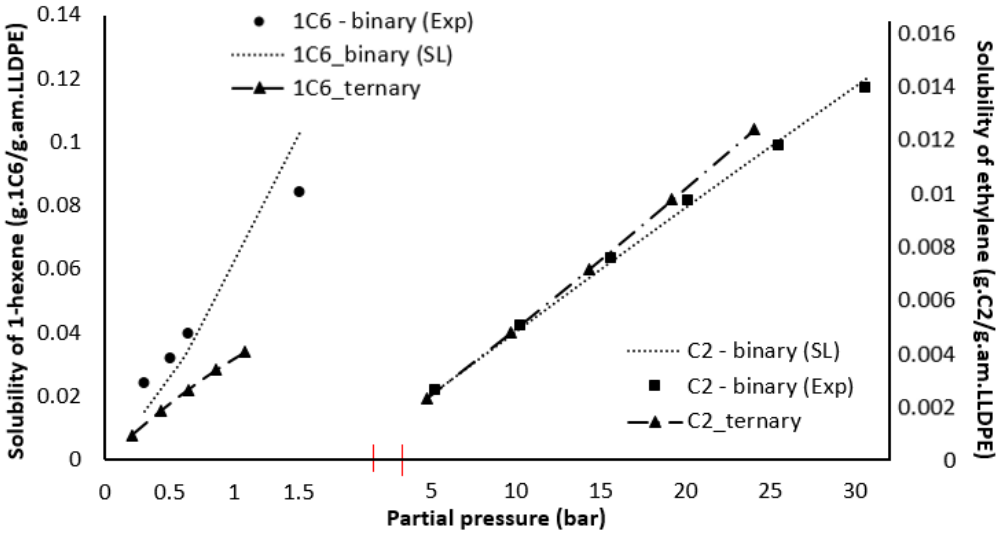

***Figure 19**. Ethylene and 1-hexene partial solubility in ternary system at 90°C with 5 mol% 1-hexene and 95 mol% ethylene and their corresponding partial pressures for each pure component for binary simulations. k_{ij} for ternary system were taken from **Table 12** and k_{ij} for binary systems were taken from **Table 5**.*

The novel approach of SL combined with Peng-Robinson has been validated with the available experimental data for different conditions (i.e. temperature, composition, pressure, polymer type) and show reasonable results. This technique can then be used for the different studied overall solubilities measured with a magnetic suspension balance.

4.2.Model application to new experimental data

In general, the solubility of penetrants in the amorphous phase of the polymer depends on the pressure, the temperature, the type of penetrant and PE properties. For the following solubility studies, we kept the temperature, PE type and gas phase composition constant; while increasing the total pressure of the injected mixture.

Table 14 shows the total pressure and the composition of the gas phase mixtures studied here. The overall solubility of these three systems will be measured for a pressure up to 5 bars and a constant temperature of 70°C. These solubility data will then be correlated using Sanchez-Lacombe combined to Peng-Robinson (i.e. SL-PR) to predict the individual solubility data and the interaction parameters.

Table 14. Gas-phase molar composition of the different studied ternary mixtures

System	Composition
Ethylene / Propane / LLDPE-B	$0 < P_{tot} < 5$ bar $x_{C2} = 0.509$ / $x_{C3} = 0.491$
Ethylene / Isobutane / LLDPE-B	$0 < P_{tot} < 4$ bar $x_{C2} = 0.485$ / $x_{iC4} = 0.515$
Ethylene / 1-Butene / LLDPE-B	$0 < P_{tot} < 4$ bar $x_{C2} = 0.617$ / $x_{1C4} = 0.383$

The results of this approach are shown in Figure **20** through Figure **23**. The symbols represent experimental values of the total solubility in Figure **20**, and the different compressibility factors for the vapor mixtures calculated with Peng-Robinson EoS in ***Figure 21-Figure 23***. It can be seen from **Figure 20** that, as expected, the total solubility increases as the total pressure of the system increases. It is also important to note that the more condensable the penetrant is, the higher the total solubility of the mixture is at a given pressure. Indeed, for a fixed total pressure, the total solubility of the mixture in presence of 1-butene is higher than the solubility in presence of isobutane, which is higher than the solubility in presence of propane.

These data points are used to fit the k_{ij} from SL EoS for the different mixtures, the values of which are shown in *Table 15*. Indeed, when one has only global solubilities, identifying these interaction parameters is crucial in order to have the partial solubilities of each component in the mixture. These parameters are also useful to predict the solubility at different pressures. In order to do so, the approach discussed above was used to fit both global solubility from SL EoS to experiments and compressibility factor from SL EoS to Peng-Robinson EoS. Note that the model fits the data well, with the difference between the model and the experiments in ***Figure 20*** being on the order of 1 – 4%, indicating that we can have confidence in these values for the pressures and temperature used in the experiments. ***Figure 21-Figure 23*** show that the calculated compressibility factors from SL EoS are in good agreement with the ones calculated with Peng-Robinson EoS, with a maximum difference of 0.8%. It should be pointed that this set of interaction parameters are only valid at temperature equal to 70°C.

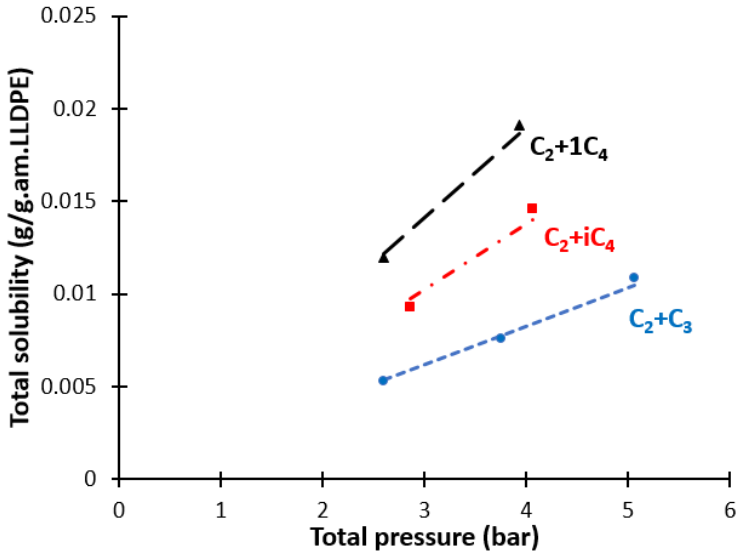

Figure 20. *Total solubility of ethylene/penetrant mixture in LLDPE-B in presence of different penetrants at 70°C. Points represent experimental values (average of 2 or 3 runs) and the lines represent the predictions of the SL EoS with the fitted parameters. k_{ij} are defined in* ***Table*** **15**

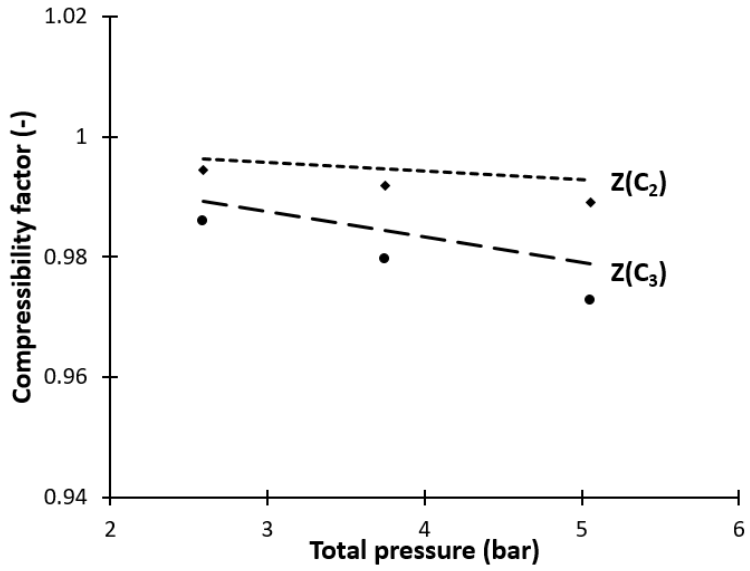

Figure 21. *Compressibility factor of ethylene (C_2) and propane (C_3) in C_2/C_3/LLDPE-B mixture. Points represent compressibility values calculated with Peng-Robinson and the lines represent the predictions of the compressibility factor from the ternary SL EoS*

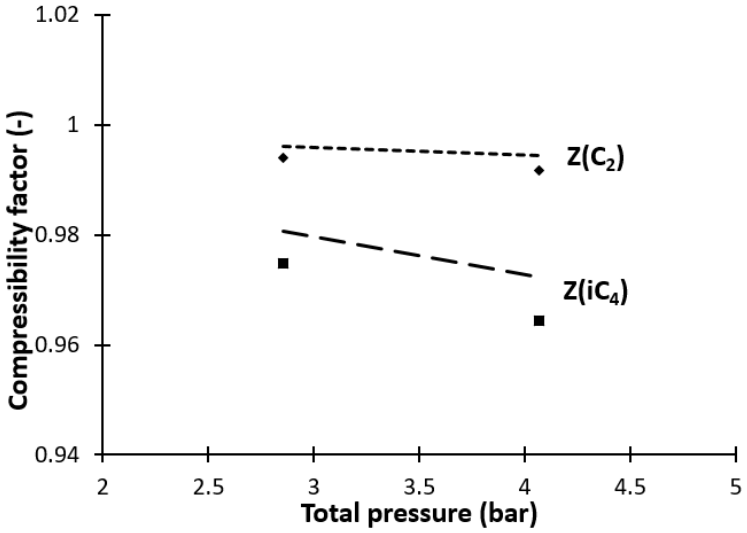

Figure 22. *Compressibility factor of ethylene (C_2) and isobutane (iC_4) in C_2/iC_4/LLDPE-B mixture. Points represent compressibility values calculated with Peng-Robinson and the lines represent the predictions of the compressibility factor from the ternary SL EoS*

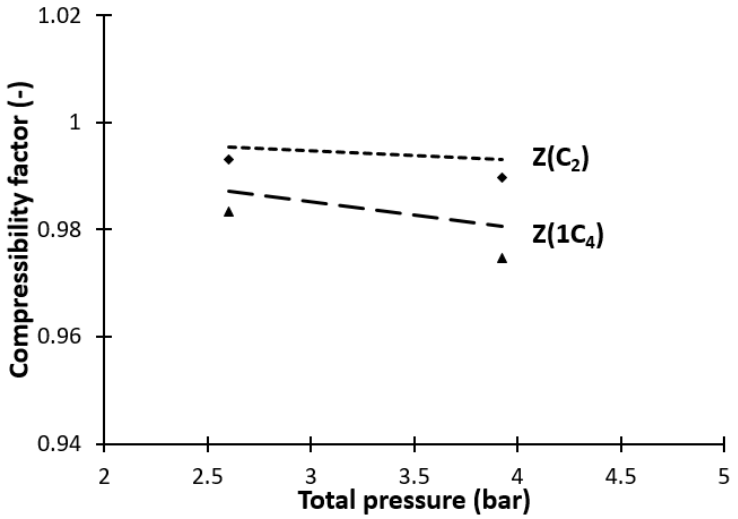

Figure 23. *Compressibility factor of ethylene (C_2) and 1-butene ($1C_4$) in C_2/$1C_4$/LLDPE-B mixture. Points represent compressibility values calculated with Peng-Robinson and the lines represent the predictions of the compressibility factor from the ternary SL EoS*

Once the k_{ij} identified by this new approach, we can calculate the partial solubility of each component in the mixture. ***Figure 24***, ***Figure 25*** and ***Figure 26*** show the global and partial solubility of each component of the mixture in the amorphous phase of LLDPE-B, in presence of different penetrants; propane, isobutane and 1-butene, respectively. It is shown, as expected

for the considered molar fraction, that the partial solubility of ethylene is lower than the partial solubility of the heavier components (i.e. propane, isobutane, 1-butene).

Table 15. *Identified ternary interaction parameters by fitting experimental solubility data to SL EoS for different systems at 70°C*

Systems	**k_{ij} at 70°C**
Ethylene / Propane / LLDPE-B	k_{13}= -0.03329, k_{23}= 0.03905
Ethylene / Isobutane / LLDPE-B	k_{13}= -0.06856, k_{23}= 0.04839
Ethylene / 1-Butene / LLDPE-B	k_{13}= -0.09495, k_{23}= 0.04618

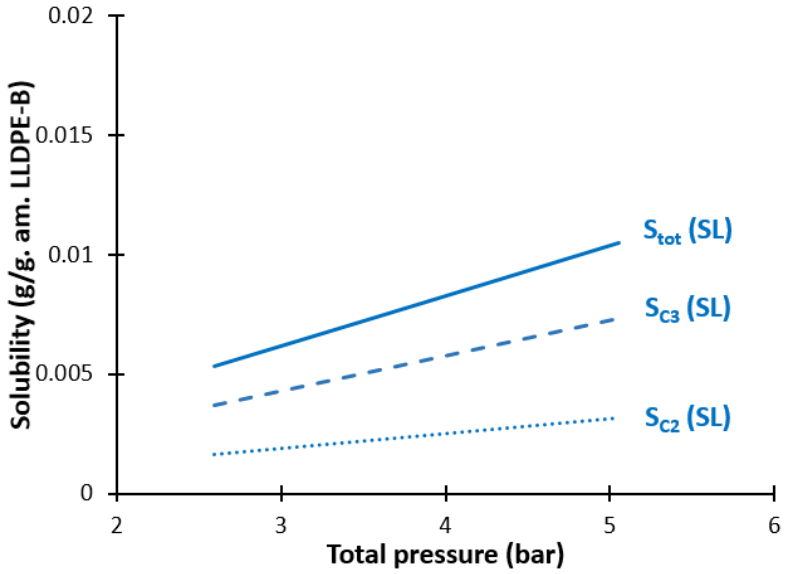

Figure 24. *Total solubility S_{tot} (SL), partial solubility of ethylene S_{C2} (SL) and partial solubility of propane S_{C3} (SL) in LLDPE-B at 70°C from SL-PR method (ternary system C_2/C_3/LLDPE-B). k_{ij} are defined in* ***Table*** **15**

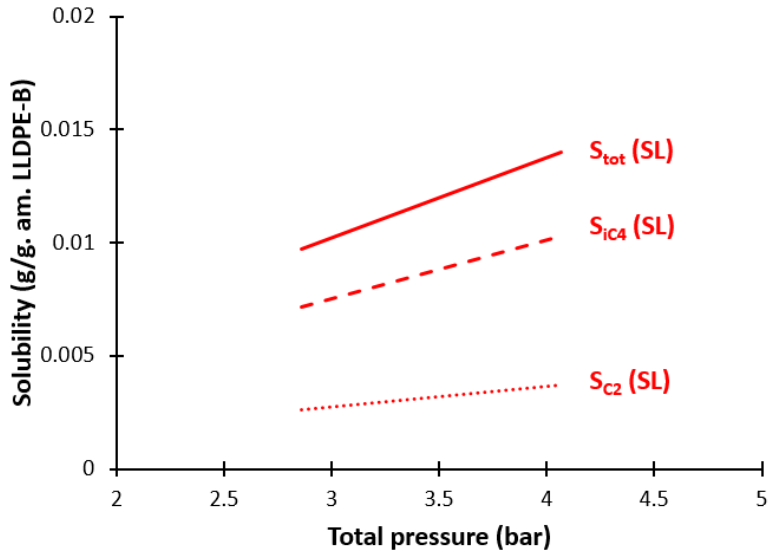

Figure 25. *Total solubility S_{tot} (SL), partial solubility of ethylene S_{C2} (SL) and partial solubility of isobutane S_{iC4} (SL) in LLDPE-B at 70°C from SL EoS (ternary system C_2/iC_4/LLDPE-B). k_{ij} are defined in* ***Table*** **15**

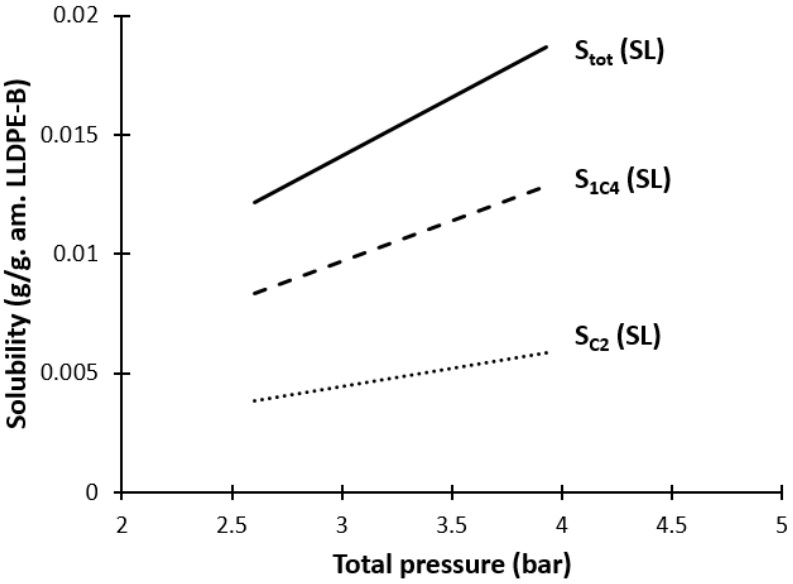

Figure 26. *Total solubility S_{tot} (SL), partial solubility of ethylene S_{C2} (SL) and partial solubility of 1-butene S_{1C4} (SL) in LLDPE-B at 70°C from SL EoS (ternary system C_2/$1C_4$/LLDPE-B). k_{ij} are defined in* ***Table*** **15**

The degree of polymer swelling caused by the sorption of the different ethylene/penetrants mixture in the amorphous phase of the polymer was calculated using SL EoS and is shown in **Figure 27.** This figure illustrates the degree of LLDPE swelling in presence of propane, isobutane and 1-butene at 70°C at the same experimental conditions (c.f.

Table 14). The evolution of polymer swelling as a function of the total pressure follows the same trends as that observed for the solubility. Heavier alkanes cause higher LLDPE swelling compared to lighter ones. At a total pressure of 4 bars, the swelling in presence of propane is about 1.2%, 1.9% for isobutane and 2.55% for 1-butene. It can be concluded that the degree of polymer swelling is insignificant over the range of pressures used in these experiments.

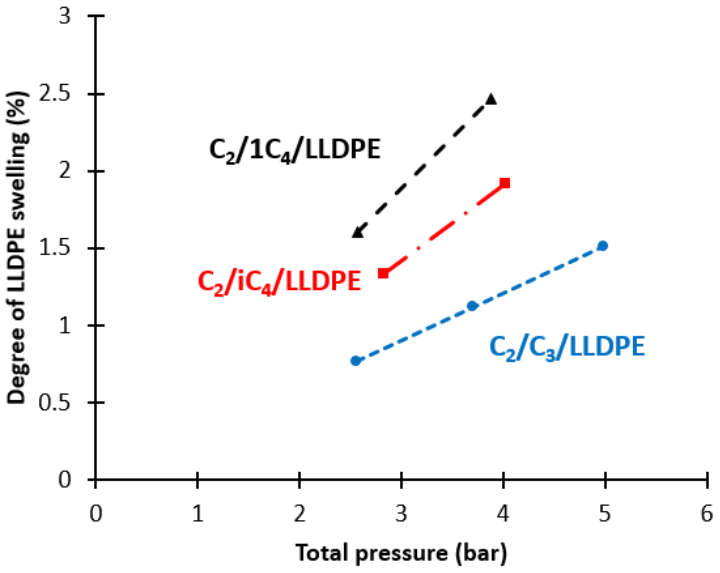

Figure 27.*Degree of LLDPE swelling caused by the sorption of different penetrants; propane (C3), isobutane (iC4) and 1-butene (1C4) at 70°C. Gas phase composition is given in* ***Table 14*** *and kij are defined in* ***Table 15***

Figure **28** shows the experimental solubility of ethylene in the binary system of ethylene/LLDPE and the ternary solubility of ethylene in presence of propane, isobutane and 1-butene in LLDPE. It shows that the ternary solubility of ethylene is higher than its corresponding binary solubility due to the co-solubility effect. Indeed, adding heavier components will increase the solubility of ethylene and vice-versa. Besides, it shows that the heavier the penetrant, the higher the partial solubility of ethylene in the amorphous phase of LLDPE-B. Note that the molar fractions were not exactly the same for all the components (c.f. ***Table 14)***. However, if we consider 1-butene for instance, its molar fraction was lower than isobutane and propane (x_{1C4}=0.383, x_{iC4}=0.515 and x_{C3}=0.491). Even with a lower fraction of 1-butene, the co-solubility effect was higher than in presence of isobutane or propane.

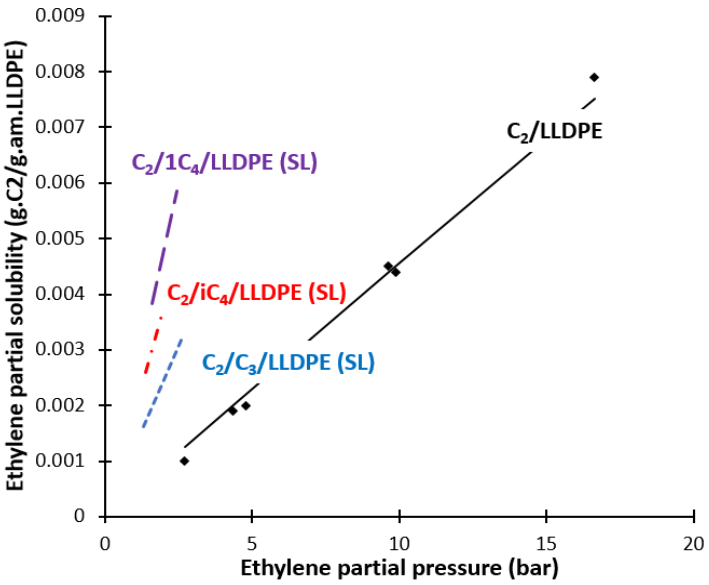

Figure 28. *Partial ternary solubility of ethylene from SL EoS in presence of C_3, iC_4 and $1C_4$ with the molar fractions: x_{1C4}=0.383, x_{iC4}=0.515, x_{C3}=0.491; k_{ij} for ternary systems are defined in* ***Table*** **15.** *Comparison to binary solubility of C_2/LLDPE, where points represent the experimental solubility and the line represents the solubility fitted to SL EoS, with k_{ij} defined in* ***Table 8***

Figure 29 shows the solubility of propane, isobutane and 1-butene in binary (diluent/PE) and ternary (ethylene/diluent/PE) systems. The same compositions as in ***Table 14*** were used for the ternary simulations and their corresponding partial pressures for each pure component were used for the binary simulation. This figure shows the anti-solvent behavior of ethylene. Indeed, adding ethylene to the gas phase composition decreases the solubility of ICAs, with respect to the binary solubility. Ethylene acts therefore as an anti-solvent to ICA by decreasing its partial solubility in the amorphous LLDPE-B. Besides, we can see that ethylene anti-solvent effect is higher (about 20%) for isobutane than for propane (note that they were added at almost the same fraction x_{iC4}=0.515 and x_{C3}=0.491).

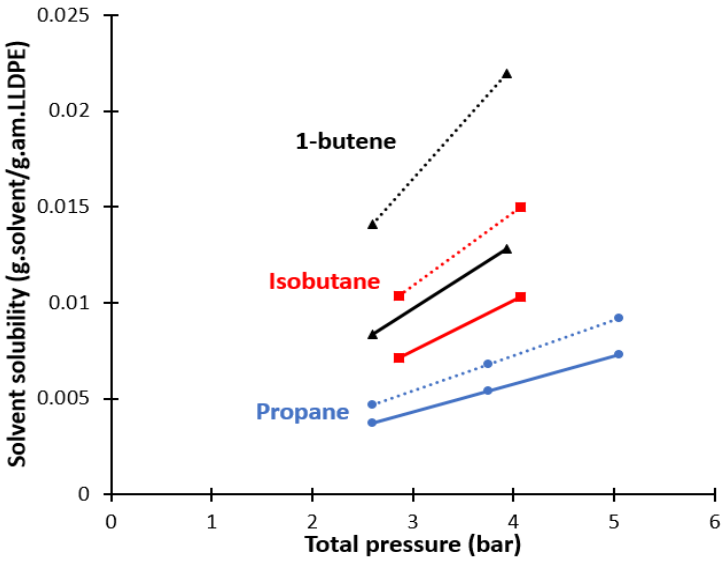

Figure 29. *Solubility of propane, isobutane and 1-butene in binary (diluent/LLDPE) and ternary (ethylene/diluent/LLDPE) systems using SL EoS.k_{ij} for ternary systems are defined in* ***Table 15****. k_{ij} for binary systems are defined in* ***Table 8****. The lines represent diluent partial solubility in ternary systems and the dotted lines represent diluent solubility in binary systems.*

Table 16. *Binary interaction parameters at T=70°C used in this work*

System	Binary k_{ij}	Ref
Ethylene/LLDPE	0.0546	Our work
Propane/LLDPE	0.023	[3]
Isobutane/LLDPE	0.0265	[3]
1-Butene/LLDPE	0.0418	Fitting to [30]

5. Conclusion

The overall equilibrium solubility of ethylene/propane/LLDPE-B, ethylene/isobutane/LLDPE-B and ethylene/1-butene/LLDPE-B were determined gravimetrically at 70°C in the pressure range of 0-5 bar. The measured solubilities were evaluated in gram of the mixture per gram of amorphous PE. The observed trends were theoretically interpreted because no available data can be found in the literature for these studied systems. The results showed, as expected, an anti-solvent behavior of ethylene and a co-solvent behavior of the penetrant. Adding heavy components to the binary ethylene/PE system increases the solubility of ethylene in the amorphous phase of the polymer, whereas ethylene decreases the solubility of heavier components in the amorphous polymer. Besides, the more condensable the penetrant, the higher will be these effects.

The measured solubilities were fitted to the Sanchez-Lacombe equation of state, in order to identify the interactions parameters, k_{ij}, between the different components and the polymer. In this Chapter, a novel approach consisting of implementing Peng-Robinson EoS to SL EoS (i.e. SL-PR) has been used in order to predict the interactions parameters needed for SL EoS. Introducing the compressibility factor as input data is crucial when having only overall solubilities since we can therefore have an additional data for the fitting of SL EoS. This approach was first validated with the experimental available data and showed reasonable results, leading to its application to the experimental measured overall solubilities through the gravimetric method. Good agreement was observed between experimental overall solubility and SL EoS combined to Peng-Robinson, with a difference of 1-4% for overall solubilities and a maximum of 0.8% for the compressibility factor.

Capturing partial solubilities of the different penetrants in the polymer in multicomponent systems leads to a better understanding of the thermodynamic occurring during ethylene polymerization in gas phase. Furthermore, this will be a crucial tool when extending SL EoS to quaternary systems, since we will have three interaction parameters that needs to be identified from the SL EoS.

6. References

1. McKenna, T. F. L. Condensed Mode Cooling of Ethylene Polymerization in Fluidized Bed Reactors. *Macromol. React. Eng.* **13**, 1800026 (2019).

2. Banaszak, B. J. *et al.* Ethylene and 1-Hexene Sorption in LLDPE under Typical Gas Phase Reactor Conditions: A Priori Simulation and Modeling for Prediction of Experimental Observations. *Macromolecules* **37**, 9139–9150 (2004).

3. Alves, R., Bashir, M. A. & McKenna, T. F. L. Modeling Condensed Mode Cooling for Ethylene Polymerization: Part II. Impact of Induced Condensing Agents on Ethylene Polymerization in an FBR Operating in Super-Dry Mode. *Ind. Eng. Chem. Res.* **56**, 13582–13593 (2017).

4. Yao, W., Hu, X. & Yang, Y. Modeling the solubility of ternary mixtures of ethylene,iso-pentane,n-hexane in semicrystalline polyethylene. *J. Appl. Polym. Sci.* **104**, 3654–3662 (2007).

5. McKenna, T. F. Solubility and crystallinity data for ethylene/polyethylene systems. *European Polymer Journal* **34**, 1255–1260 (1998).

6. Novak, A. *et al.* Ethylene and 1-hexene sorption in LLDPE under typical gas-phase reactor conditions: Experiments. *J. Appl. Polym. Sci.* **100**, 1124–1136 (2006).

7. Chmelař, J., Haškovcová, K., Podivinská, M. & Kosek, J. Equilibrium Sorption of Propane and 1-Hexene in Polyethylene: Experiments and Perturbed-Chain Statistical Associating Fluid Theory Simulations. *Ind. Eng. Chem. Res.* **56**, 6820–6826 (2017).

8. Yao, W., Hu, X. & Yang, Y. Modeling solubility of gases in semicrystalline polyethylene. *J. Appl. Polym. Sci.* **103**, 1737–1744 (2007).

9. Moore, S. J. & Wanke, S. E. Solubility of ethylene, 1-butene and 1-hexene in polyethylenes. *Chemical Engineering Science* **56**, 4121–4129 (2001).

10. Savatsky, B. J., Moebus, J. A. & Greenhalgh, Brian. R. Parameterization of Models for Vapor Solubility in Semicrystalline Polyethylene. *Macromol. React. Eng.* **13**, 1900003 (2019).

11. Kanellopoulos, V., Mouratides, D., Pladis, P. & Kiparissides, C. Prediction of Solubility of α-Olefins in Polyolefins Using a Combined Equation of State Molecular Dynamics Approach. *Ind. Eng. Chem. Res.* **45**, 5870–5878 (2006).

12. Yoon, J.-S., Yoo, H.-S. & Kang, K.-S. Solubility of α-olefins in linear low density polyethylenes. *European Polymer Journal* **32**, 1333–1336 (1996).

13. Moebus, J. A. & Greenhalgh, B. R. Modeling Vapor Solubility in Semicrystalline Polyethylene. *Macromol. React. Eng.* **12**, 1700072 (2018).

14. Bashir, M. A., Al-haj Ali, M., Kanellopoulos, V. & Seppälä, J. Modelling of multicomponent olefins solubility in polyolefins using Sanchez–Lacombe equation of state. *Fluid Phase Equilibria* **358**, 83–90 (2013).

15. Nath, S. K., Banaszak, B. J. & de Pablo, J. J. Simulation of Ternary Mixtures of Ethylene, 1-Hexene, and Polyethylene. *Macromolecules* **34**, 7841–7848 (2001).

16. Sun, J. *et al.* Solubility measurement of hydrogen, ethylene, and 1-hexene in polyethylene films through an intelligent gravimetric analyzer. *J. Appl. Polym. Sci.* **134**, (2017).

17. Chmelař, J. *et al.* Equilibrium sorption of ethylene in polyethylene: Experimental study and PC-SAFT simulations. *Polymer* **59**, 270–277 (2015).

18. Cancelas, A. J. *et al.* Solubility and Diffusivity of Propylene, Ethylene, and Propylene-Ethylene Mixtures in Polypropylene. *Macromol. Chem. Phys.* **219**, 1700565 (2018).

19. Kröner, T. & Bartke, M. Sorption of Olefins in High Impact Polypropylene – Experimental Determination and Mass Transport Modeling. *Macromolecular Reaction Engineering* **7**, 453–462 (2013).

20. Sanchez, I. C. & Lacombe, R. H. An elementary molecular theory of classical fluids. Pure fluids. *J. Phys. Chem.* **80**, 2352–2362 (1976).

21. Alizadeh, A. *et al.* Modeling Condensed Mode Operation for Ethylene Polymerization: Part I. Thermodynamics of Sorption. *Ind. Eng. Chem. Res.* **56**, 1168–1185 (2017).

22. Bashir, M. A., Ali, M. A., Kanellopoulos, V. & Seppälä, J. Combined EoS and elastic constraints models to predict thermodynamic properties for systems involving semi-crystalline polyolefins. *Fluid Phase Equilibria* **388**, 107–117 (2015).

23. Bashir, M. A., Monteil, V., Kanellopoulos, V., Ali, M. A.-H. & McKenna, T. Partial Molar Volumes and Thermal Expansion Coefficients as an Explanation for Co-Solvent Effect of Penetrants in Multicomponent Polymer Mixtures. *Macromol. Chem. Phys.* **216**, 2129–2140 (2015).

24. Alizadeh, A. Study of sorption, heat and mass transfer during condensed mode operation of gas phase ethylene polymerization on supported catalyst. (Departement of Chemical Engineering, Queen's University, 2014).

25. Peng, D.-Y. & Robinson, D. B. A New Two-Constant Equation of State. *Ind. Eng. Chem. Fund.* **15**, 59–64 (1976).

26. Poling, B., Prausnitz, J. & O'Connell, J. *The Properties of Gases and Liquids*. (2000).

27. Lin, H. & Duan, Y.-Y. Empirical correction to the Peng–Robinson equation of state for the saturated region. *Fluid Phase Equilibria* **233**, 194–203 (2005).

28. Ambrose, D. *Vapour-Liquid Critical Properties*. (1979).

29. Mirzaei, A., Kiashemshaki, A. & Emami, M. Fluidized Bed Polyethylene Reactor Modeling in Condensed Mode Operation. *Macromol. Symp.* **259**, 135–144 (2007).

30. Chmelar, J. *et al.* Softening of polyethylene powders at reactor conditions. *Chemical Engineering Journal* **228**, 907–916 (2013).

31. Fateen, S.-E. K., Khalil, M. M. & Elnabawy, A. O. Semi-empirical correlation for binary interaction parameters of the Peng–Robinson equation of state with the van der Waals mixing rules for the prediction of high-pressure vapor–liquid equilibrium. Journal of Advanced Research 4, 137–145 (2013)

32. Pedrosa, N., Vega, L. F., Coutinho, J. A. P. & Marrucho, I. M. Phase Equilibria Calculations of Polyethylene Solutions from SAFT-Type Equations of State. Macromolecules 39, 4240–4246 (2006)

Chapter 3

Experimental and Theoretical Solubility for Multicomponent Systems

1. Introduction

As was discussed in Chapter 2, there is a significant lack of solubility data for multicomponent gas/liquid/solid mixtures in polyolefin systems. Very few solubility studies are related to ternary systems (penetrant 1 – penetrant 2 - PE)[1–10], and as far as we have been able to determine, never for quaternary systems (penetrant 1 – penetrant 2 - penetrant 3 - PE). The knowledge of the solubility in quaternary systems represents an important contribution to the modelling of olefin polymerizations since these systems are more realistic, approaching the conditions found in industry.

In the previous chapter, we began by looking at the solubility in ternary systems using gravimetry (i.e. a magnetic suspension balance) to measure the overall solubility. The total solubility data could be combined with an estimate of the compressibility factor of the gas mixture from an external source (i.e. Peng-Robinson EoS) to successfully calculate the Sanchez-Lacombe interaction parameters for the 2 penetrants. However, it is necessary to add a third data source if we wish to measure individual solubilities from SL EoS and estimate the k_{ij} for quaternary and higher order systems.

In the current chapter, we will discuss an experimental set-up based on the pressure decay method that uses rapid micro gas-chromatography measurements to calculate individual solubilities of multicomponent gas mixtures in different polyethylene samples at industrial conditions. The advantage of this method is that it gives the overall solubility, as gravimetric technique, but also the partial solubilities of each component in the gas mixture. Ternary and quaternary individual and overall solubilities will be measured using the pressure decay method, and the overall experimental solubility will be validated with the sorption experiments performed on the magnetic suspension balance (MSB). The ternary studied systems are ethylene/propane/PE, ethylene/isobutane/PE and ethylene/1-butene/PE at temperatures between 70-90°C. Then, quaternary experiments of ethylene/propane/1-butene/PE and ethylene/isobutane/1-butene/PE will be performed at 70 and 85°C. All this experimental data will be key for thermodynamic modeling, and will be fitted to SL EoS model for ternary and quaternary systems in order to identify the interactions parameters for these specific studied systems. To the best of our knowledge, this is the first time that the solubility is measured experimentally and theoretically in quaternary polyolefin systems.

2. Materials and methods

2.1.Materials

Ethylene (C2) with a minimum purity of 99.5%, and propane (C3a), propylene (C3e), 1-butene (1C4), isobutane (iC4) and n-butane (nC4), all with a minimum of purity of 99% were obtained from Air Liquide France. Argon with a minimum purity of 99.5% was also obtained from Air Liquide France and used as blank gas. Polyethylene and polypropylene powders were graciously supplied by Borealis, such as HDPE-B, LLDPE-B and by Ineos, such as HDPE-I, LLDPE-I and HiPP.

2.2.Polymer characterization

The crystallinity of the polymer samples was measured using differential scanning calorimetry (DSC 3+ by Mettler Toledo). Polyethylene samples were weighed (i.e. around 5-7 mg) and placed in an aluminium capsule with a volume of 40 µL. The sample was first cooled to -20°C and then heated from −20 to 180 °C at a heating rate of 10°C min^{-1}, held for 5 minutes at that temperature and then cooled from 180 to −20 °C at a rate of 10°C min^{-1}. This temperature was maintained for 5 minutes, and the sample was reheated to 180°C at a rate of 10°C min^{-1}. The melting behavior of the samples was studied in the second heating cycle in order to detect the melting point and the melting enthalpy of the samples. The ratio of the heat of fusion of the sample to that of the completely crystallized polyethylene was used to calculate the degree of crystallization. A heat of fusion of 293 J g^{-1} for completely crystallized polyethylene was used for the calculation. The STARe software was used for data acquisition and data analysis.

Molar mass measurements of polyethylene (PE) were performed using a Viscotek High-Temperature Triple Detection GPC (HT-GPC) system (Malvern Instruments) that incorporates a differential refractive index, a viscometer, and a light scattering detector. The Omnisec software was used for data acquisition and data analysis. The molecular weight distributions (MWD) were calculated by means of a conventional calibration curve based on linear polyethylene standards from 300 to 130 000 g mol^{-1} (Polymer Standards Service).

Sample densities, ambient temperature crystallinities and polydispersities are summarized in ***Table 17***, and the thermograms of these same polymers are presented in ***Figure 30***. It can be seen from this last figure that while the crystallinity of the 2 HDPE powders remains virtually constant at temperatures up to 90°, that of the LLDPE samples is temperature dependent over

the range used in the solubility experiments (up to 90°C). For that reason, the fraction of amorphous polymer in the LLDPE samples was calculated at the temperature of the experiment.

Table 17. *Characteristics of the polymer powders used for sorption measurements*

	Density (kg.m^{-3})	Crystallinity (%)	PI
HDPE-B	945	65.7	10.9
LLDPE-B	923	48.3	8.8
HiPP	880	60	-
HDPE-I	954	69.5	2.97
LLDPE-I	926	$\chi = -0.378 \times T + 75.85$	2.03

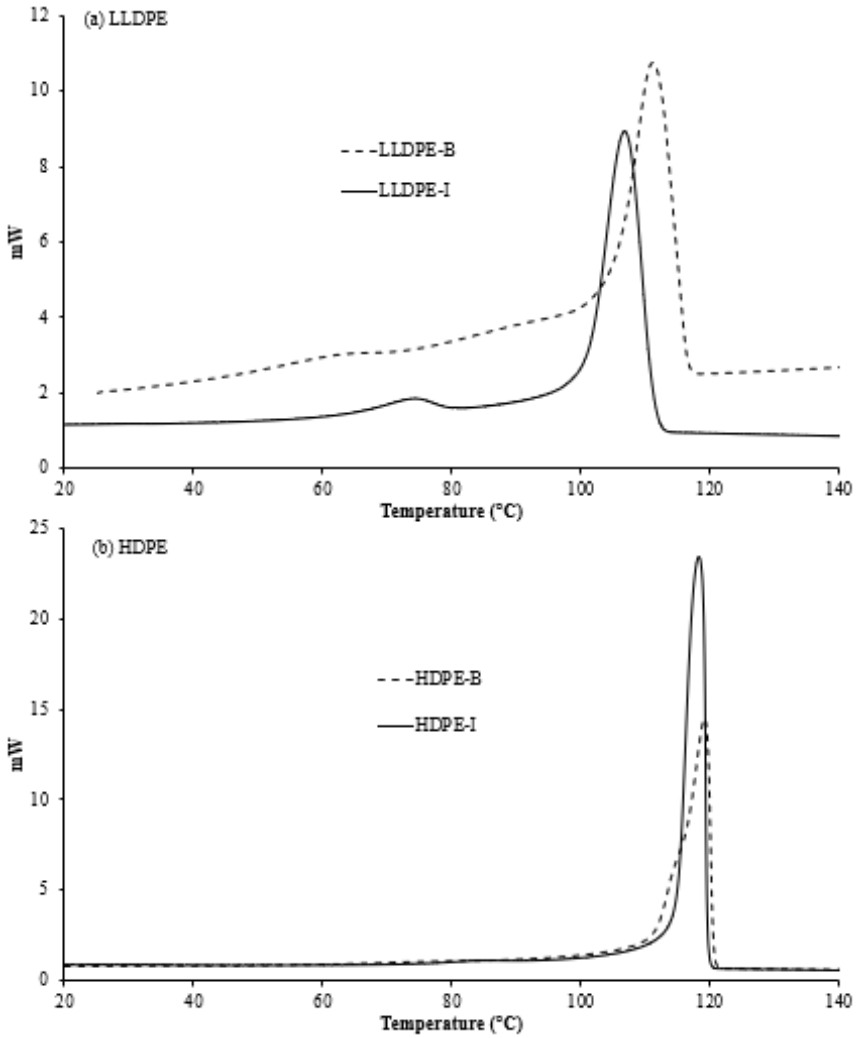

Figure 30. *DSC thermograms of the 4 PE shown in Table 17. (a) LLDPE and (b) HDPE.*

2.3.Pressure decay method

2.3.1. Reactor set-up

A 2-liter stirred vessel is used to measure the gas phase solubility of pure components and their mixtures under standard gas phase polymerization conditions in order to generate data for thermodynamic models. The set-up is based on the pressure decay method[1,10].

The experimental set-up describing the pressure decay method for sorption measurements is shown in ***Figure 31***, and a schema of the concept is given in ***Figure 32***. The reactor is heated by an oil circulating through an external jacket, and is equipped with temperature and pressure sensors, a vacuum pump, and a recording computer. The gaseous components fed to the reactor can be preheated to avoid liquefaction. The composition of the gas phase mixture injected into the reactor is measured with a microGC (Agilent 490 – Mobile Micro GC, SRA Instruments) located at the outlet of the reactor. The microGC has first been calibrated with the different studied gases at different composition. Each calibration curve includes a minimum of 8 points, in order to have confidence in the obtained results. The microGC is connected to the reactor through a pressure regulating valve. The gas phase composition is measured by injecting the gas mixture through a column during 10-20 seconds. These injections are performed at the beginning of each experiment, as well as at the end of each pressure step. SOPRANE II software was used for data acquisition and data analysis.

Figure 31. *Experimental set-up of the pressure decay method for sorption measurements*

The volume of the reactor, and any ends of lines between the reactor and nearest valves is calculated by injecting a known quantity of argon into the empty reactor. Then, a known amount of polymer powder of known crystallinity is introduced inside the reactor to around 2/3rd of the reactor volume. The reactor is then closed and put under vacuum for 30 minutes for degassing. A known quantity of argon is then injected into the reactor containing the polymer powder in order to calculate exactly the volume of void space inside the reactor excluded by the polymer powder.

$$V_{\text{void}} = \frac{Z_{\text{Ar}}\, n_{\text{Ar}} R\, T}{P_{\text{Ar}}}$$

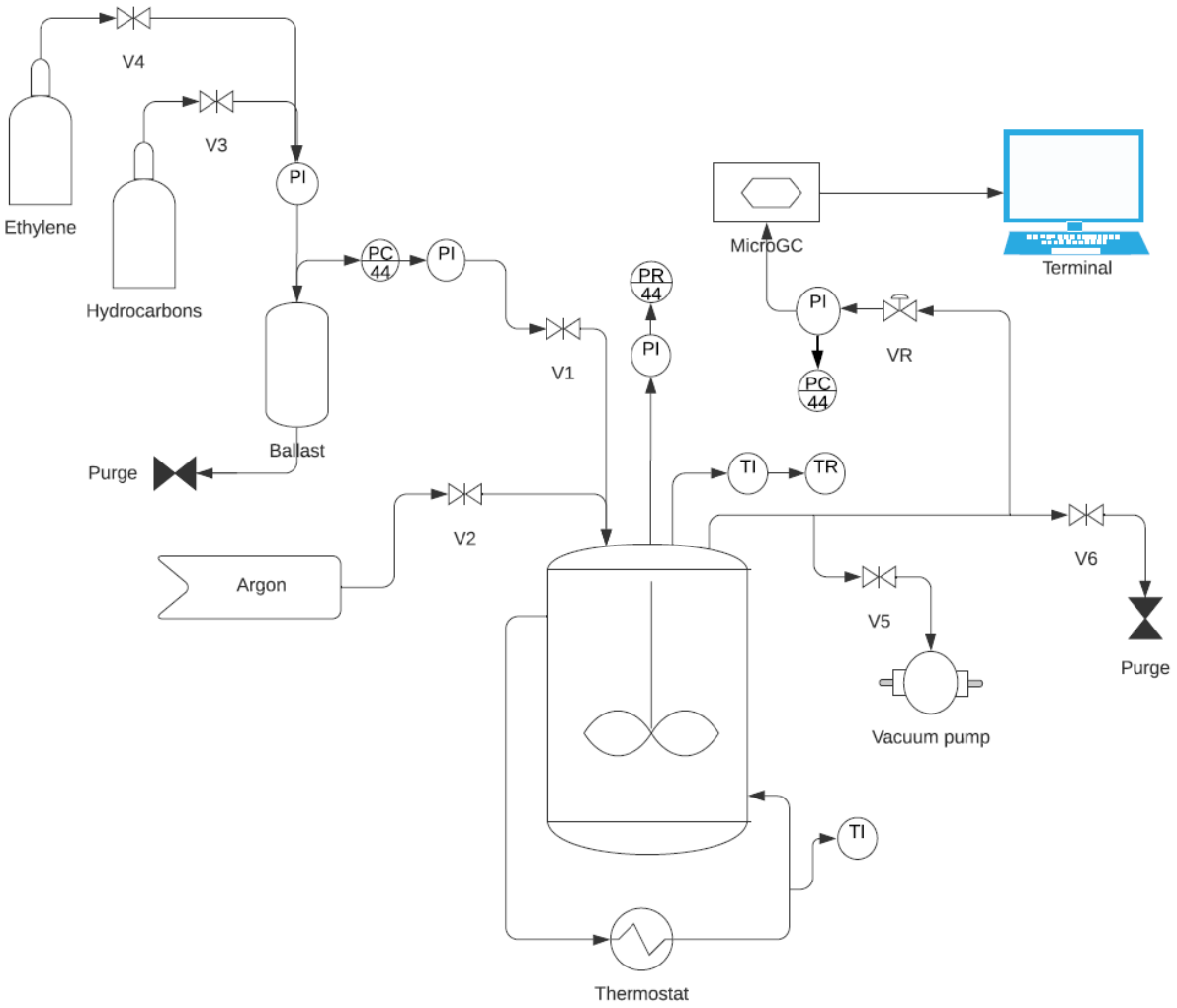

Figure 32. *P&ID of the sorption reactor based on pressure decay method*

The reactor is then degassed and put under vacuum again. A known amount of process gas (or mixture of process gases) is then injected from the mixture ballast to the reactor. This process gas (or mixture) will occupy the volume of void space inside the reactor but will also absorb inside the polymer. The number of moles of the process gas in the mixture that occupies the void space of the reactor (i.e. V_{void}) is calculated as follows:

$$n_i^{\text{gas}} = \frac{x_i \, P_{\text{gas}}^{\text{tot}} \, V_{\text{void}}}{Z_i^{\text{gas}} \, R \, T}$$

Where $P_{\text{gas}}^{\text{tot}}$, Z_i^{gas} and x_i are the total pressure, the compressibility factor of component i, and the gas phase composition of component i given by the microGC. T is the temperature of the reactor and R is the ideal gas constant.

The pressure drop inside the mixture ballast indicates the amount of gas that is fed into the vessel, n_i^{feed}. The difference between the number of moles of gas fed into the reactor and the one that occupies the void space of the reactor gives the solubility of these gases inside the amorphous phase of the polymer.

$$n_i^{\text{pol}} = n_i^{\text{feed}} - n_i^{\text{gas}}$$

Where n_i^{pol} is the number of moles of component *i* inside the polymer.

The partial solubility of component *i* inside the amorphous phase of the polymer, S_i^{am} (g of solvent/ g of amorphous polymer), is given by:

$$S_i^{\text{am}} = n_i^{\text{pol}} \frac{MW_i}{m_{\text{PE}}(1-\chi)}$$

Where MW_i is the molecular weight of component *i*, m_{PE} is the mass of polymer used for the experiment, and χ is the degree of crystallinity of the polymer.

The overall solubility of the mixture of gases inside the amorphous phase of the polymer, $S_{\text{mix}}^{\text{am}}$, is therefore:

$$S_{\text{mix}}^{\text{am}} = \sum_{i=1}^{N_c} S_i^{\text{am}}$$

Where N_c is the number of components in the gas mixture injected into the reactor.

Note that this treatment neglects the change in the polymer volume due to swelling upon sorption of the penetrants. Bashir et al.[11] showed that the degree of polymer swelling at 70°C is about 3% for ethylene/propane/LLDPE system and 8% for ethylene/isobutane/LLDPE system, at a total pressure of 6 bars. Consequently, the swelling of polyethylene by the different penetrants will be neglected in the evaluation of the experimental solubility, as it is below the accuracy of the pressure decay measurments. We will see from the validation steps below that this simplification has no measurement impact on the solubility measurements.

2.3.2. Validation in binary systems

Binary solubilities of ethylene and propylene in different polymer powders (i.e. HDPE-B and HiPP) were first measured in order to validate our approach, as data for the solubility of binary systems is available in the literature.

The first studied system is ethylene in HiPP. The first measurement point is taken at *T*=52.5°C and then temperature steps were performed until 91.9°C. The experiment is then repeated at different ethylene pressures and at the same temperature steps. Each experiment was repeated twice at the same conditions and ***Figure 33*** shows the average of both experiments. Sato et al.[12] measured the solubility of ethylene and propylene in HiPP of crystallinity of 58.1 wt.% with a magnetic suspension balance, and their data was compared to our experiments, since the crystallinity of the used HiPP in this study is about 60 wt.% (c.f. ***Table 17***). ***Figure 33*** shows that the experimental solubility of ethylene in HiPP agrees well with the data of Sato et al.[12], with an average difference of 5.7%.

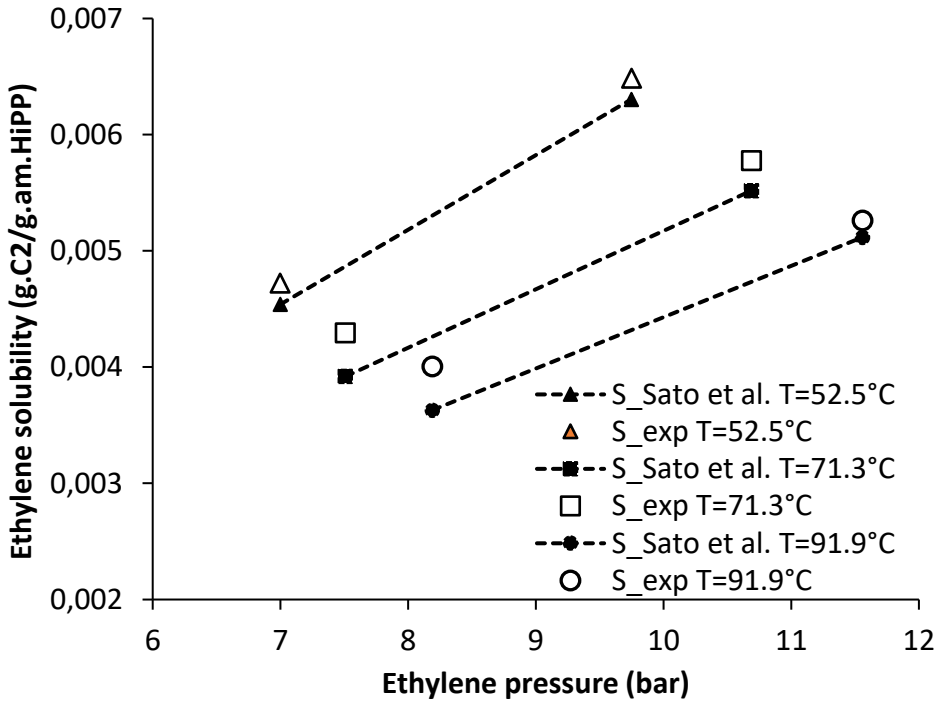

Figure 33. *Ethylene solubility in the amorphous phase of HiPP at different temperatures and ethylene pressures. The lines represent the solubility from Sato et al.[12] and the points represent the experimental solubility measured with the pressure decay method.*

The solubility of propylene in HiPP and ethylene in HDPE-B were then measured following the same procedure as previously, and are shown in ***Figure 34*** and ***Figure 35***, respectively. Propylene solubility is first measured at 51.9°C and 4.40 bar and then temperature steps were performed until *T*=91.8°C. ***Figure 34*** shows that the experimental solubility of propylene in HiPP follows nicely Sato et al.[12] data with an average difference of 6.7%. Ethylene solubility is first measured at 55°C and 9.5 bar and then temperature steps were performed until *T*=74°C. ***Figure 35*** shows that the experimental points are in good agreement with the literature data

from Moore and Wanke[6] with an average difference of 5.8%. Indeed, Moore and Wanke[6] measured by gravimetry the solubility of ethylene in HDPE of crystallinity of 70%, which is close to that of HDPE-B (c.f. ***Table 17***).

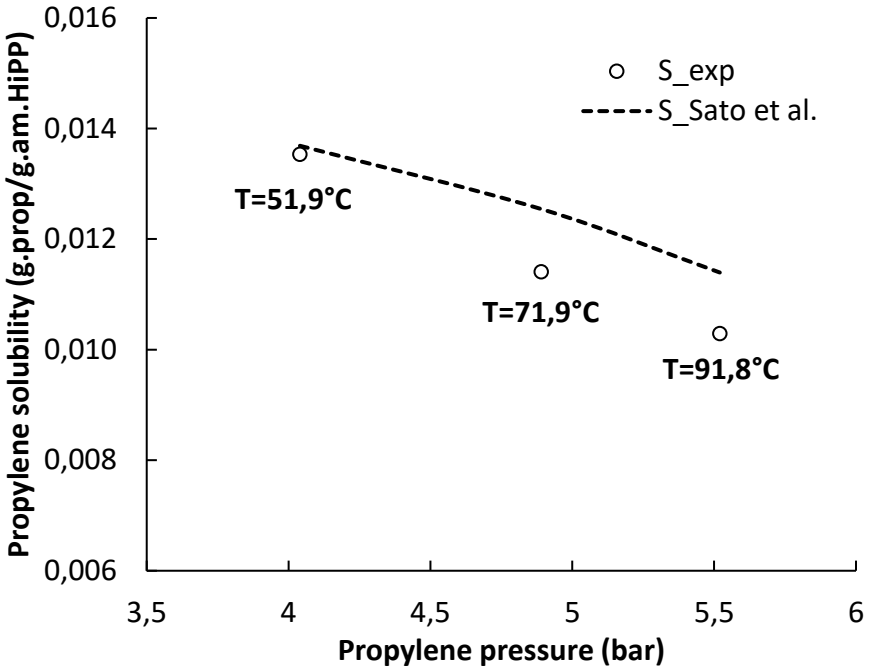

Figure 34. *Propylene solubility in the amorphous phase of HiPP at different temperatures and propylene pressures. The lines represent the solubility from Sato et al.[12] and the points represent the experimental solubility measured with the pressure decay method.*

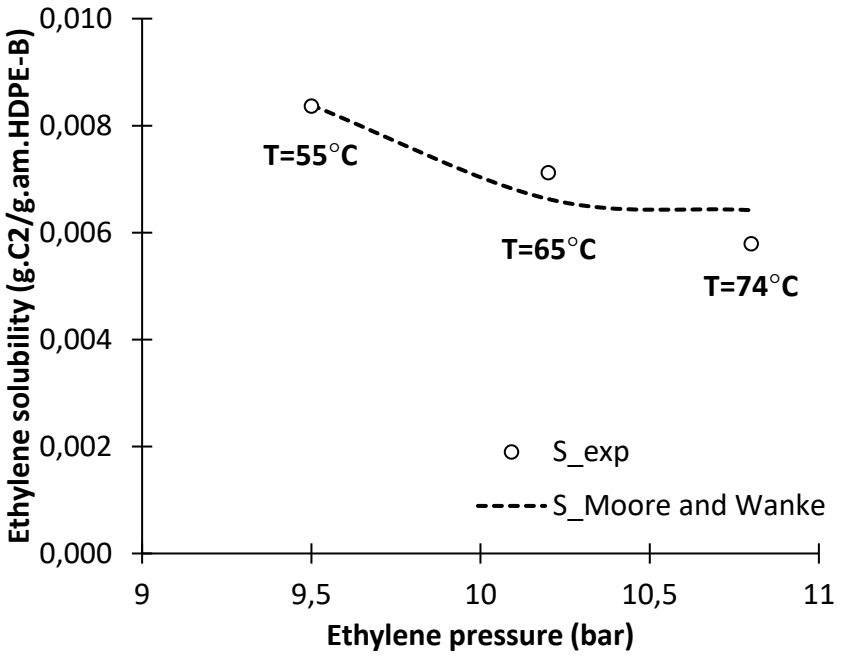

Figure 35. *Ethylene solubility in the amorphous phase of HDPE-B at different temperatures and ethylene pressures. The lines represent the solubility from Moore and Wanke[6] and the points represent the experimental solubility measured with the pressure decay method.*

Once our experimental approach validated for the binary systems, the solubility of mixtures of gases in polyethylene powders can be performed with confidence. Ternary and quaternary systems will therefore be studied in Section 3 since those systems are lacking in the literature, and they are very important in order to have a more realistic description of ethylene polymerization in gas-phase.

2.4.Gravimetric method

Solubility measurements were achieved using a high-pressure magnetic suspension balance (Rubotherm GmbH), connected to a pressure cell that contains the polymer sample. The detailed experimental apparatus and measuring procedure are shown in Chapter 2 and in references[3,4,13–15].

The total solubility of ternary and quaternary systems will therefore be measured with the magnetic suspension balance to confirm the results of the pressure decay method. However, the experimental set-up with the magnetic suspension balance can only be used to measure the overall solubility of mixture of gases in the amorphous phase of the polymer.

3. Sanchez-Lacombe EoS for quaternary systems

The Sanchez-Lacombe equation of state has been used in order to determine the thermodynamic properties that are important in gas-phase ethylene polymerization, including the solubility of the different species in the amorphous phase of the polymer as well as the swelling of the polymer phase due to the sorption of these species, for a number of systems. However, this equation of state has not been extended to more than 2 penetrants and a polymer in the literature, mostly because experimental data does not exist for validation. Therefore, we will need to extend SL EoS to describe the thermodynamic properties of quaternary systems including a monomer, a comonomer, an ICA and a polymer.

3.1.Model development

The Sanchez-Lacombe EoS (SL EoS) is a lattice-fluid model in which pure components are assumed to be broken into parts and placed into a lattice structure. The SL EoS is basically an extension of the classic Flory-Huggins theory. The main advance is that this model introduces vacant lattice sites or holes to account for the compressibility and the density changes. Thus,

the system volume or density can vary by changing the fraction of holes in the lattice structure. The main equation of state is given by:

$$\bar{\rho}^2 + \bar{P} + \bar{T}\left[\ln(1-\bar{\rho}) + \left(1 - \frac{1}{r}\right)\bar{\rho}\right] = 0 \qquad (1)$$

where $\bar{T}$, $\bar{P}$, $\bar{\rho}$ are the reduced temperature, pressure, and density respectively, given by:

$$\bar{T} = {}^{T}/_{T^*} \qquad \bar{P} = {}^{P}/_{P^*} \qquad \bar{\rho} = {}^{\rho}/_{\rho^*}$$

where T^*, P^*, and ρ^* are the scale factors known as the characteristic temperature, pressure, and density respectively, which are used to characterize each pure component in the mixture. Three lattice parameters describe the thermodynamic properties of a pure components: ε^*, v^* and r which are the mer-mer interaction energy, the closed-packed molar volume of a mer and the number of mers a molecule occupies in the lattice, respectively. The scale factors are defined from these lattice parameters as follows:

$$T^* = {}^{\varepsilon^*}/_{R} \qquad P^* = {}^{\varepsilon^*}/_{v^*} \qquad \rho^* = {}^{MW}/_{(rv^*)}$$

Where R is the universal gas constant.

These parameters of SL EoS for each pure component are given in Table 2.

Table 18. Pure component parameters used in SL EoS

Component	T^* (K)	P^* (bar)	ρ^* (kg m^{-3})	Ref
Ethylene	283	3395	680	[16]
Propane	371	3090	690	[17]
Isobutane	398	2840	720	[17]
1-butene	410	3350	770	[18]
Propylene	345.4	3788	755	[14]
HDPE	650	4250	905	[11]
LLDPE	667	4370	900	[16]

For a mixture of components, it is necessary to define combining rules based on the Van der Waals mixing rule for the estimation of $\varepsilon^*_{\text{mix}}$, v^*_{mix}, and r_{mix}, to be able to use the equation of state to calculate the properties of the mixture.

The characteristic closed-packed molar volume of a "mer" of the mixture, v^*_{mix} is defined as

$$v^*_{\text{mix}} = \sum_{i=1}^{N_c}\sum_{j=1}^{N_c} \phi_i \phi_j v^*_{ij}$$

With

$$v^*_{ij} = \frac{v^*_{ii} + v^*_{jj}}{2}\left(1 - n_{ij}\right)$$

Where ϕ is the volume fraction of the i^{th} and j^{th} component in the mixture, N_c is the number of component in the mixture and n_{ij} corrects the possible deviation of v^*_{ij} from the arithmetic mean value of v^*_{ii} and v^*_{jj} of the pure component. In the present study, the value of the interaction parameter n_{ij} is assumed to be equal to zero.

For quaternary systems, the characteristic closed-packed molar volume of the gas and polymer phase, respectively, are defined as follows:

$$v^{*\text{gas}}_{\text{mix}} = v^*_{11}\phi_1^{\text{gas}} + v^*_{22}\phi_2^{\text{gas}} + v^*_{33}\phi_3^{\text{gas}}$$

$$v^{*\text{pol}}_{\text{mix}} = v^*_{11}\phi_1^{\text{pol}} + v^*_{22}\phi_2^{\text{pol}} + v^*_{33}\phi_3^{\text{pol}} + v^*_{44}\phi_4^{\text{pol}}$$

The closed-packed volume fraction of the i^{th} component at the limit of zero temperature or incompressible state, ϕ_i^{gas} is defined as

$$\phi_i^{\text{gas}} = \frac{\omega_i^{\text{gas}}}{\rho_i^* v_i^*} \Bigg/ \sum_{j=1}^{N_c}\left(\frac{\omega_j^{\text{gas}}}{\rho_j^* v_j^*}\right)$$

where ω_i^{gas} is the mass fraction of the component *i* in the gas phase.

In quaternary system, the mass fraction of component 1 is defined as follows:

$$\phi_1^{\text{gas}} = \frac{\dfrac{\omega_1^{\text{gas}}}{\rho_1^* v_1^*}}{\dfrac{\omega_1^{\text{gas}}}{\rho_1^* v_1^*} + \dfrac{\omega_2^{\text{gas}}}{\rho_2^* v_2^*} + \dfrac{\omega_3^{\text{gas}}}{\rho_3^* v_3^*}}$$

Where

$$\omega_i^{\text{gas}} = \frac{\rho_i^{\text{gas}}}{\sum_{i=1}^{N_c} \rho_i^{\text{gas}}}$$

The mixing rule for the characteristic interaction energy for the mixture $\varepsilon^*_{\text{mix}}$ is defined as

$$\varepsilon^*_{\text{mix}} = \frac{1}{v^*_{\text{mix}}} \sum_{i=1}^{N_c} \sum_{j=1}^{N_c} \phi_i \phi_j \varepsilon^*_{ij} v^*_{ij}$$

For quaternary systems, the characteristic interaction energy for the gas mixture is defined as follows:

$$\begin{aligned} \varepsilon^{*\text{gas}}_{\text{mix}} = \frac{1}{v^{*\text{gas}}_{\text{mix}}} \Big(& \varepsilon^*_1 v^*_1 \phi_1^{\text{gas}2} + \varepsilon^*_2 v^*_2 \phi_2^{\text{gas}2} + \varepsilon^*_1 v^*_3 \phi_3^{\text{gas}2} + \varepsilon^*_4 v^*_4 \phi_4^{\text{gas}2} + 2\varepsilon^*_{12} v^*_{12} \phi_1^{\text{gas}} \phi_2^{\text{gas}} \\ & + 2\varepsilon^*_{13} v^*_{13} \phi_1^{\text{gas}} \phi_3^{\text{gas}} + 2\varepsilon^*_{14} v^*_{14} \phi_1^{\text{gas}} \phi_4^{\text{gas}} + 2\varepsilon^*_{23} v^*_{23} \phi_2^{\text{gas}} \phi_3^{\text{gas}} + 2\varepsilon^*_{24} v^*_{24} \phi_2^{\text{gas}} \phi_4^{\text{gas}} \\ & + 2\varepsilon^*_{34} v^*_{34} \phi_3^{\text{gas}} \phi_4^{\text{gas}} \Big) \end{aligned}$$

For the sake of brevity, the characteristic interaction energy for the polymer phase mixture, $\varepsilon^{*\text{gas}}_{\text{mix}}$, is detailed in Appendix A.

The cross-energy parameter between mers of component *i* and component *j*, ε^*_{ij}, is introduced in order to take into account the interactions between the different components in the mixture, as defined by Lorentz-Berthelot combining rules[19].

$$\varepsilon^*_{ij} = \left(\varepsilon^*_{ii} \varepsilon^*_{jj}\right)^{0.5} \left(1 - k_{ij}\right)$$

in which ε^*_{ii} and ε^*_{jj} are the interation energy between mers of the i^{th} and j^{th} component respectively. k_{ij} is a binary interaction parameter between the different components of the mixture, which is employed as adjustable parameter to fit the model to experimental solubility data.

Finally, the mixing rule for the number of sites (mers) occupied by a molecule of the mixture, r_{mix}, is given by:

$$\frac{1}{r_{\text{mix}}} = \sum_{j=1}^{N_c} \frac{\phi_j}{r_j}$$

where r_j is the number of sites occupied by molecule *j* in the lattice.

For quaternary systems, the number of sites occupied in the lattice by a molecule of gas phase mixture is defined as follows:

$$\frac{1}{r_{\text{mix}}^{\text{gas}}} = \frac{\phi_1^{\text{gas}}}{r_1} + \frac{\phi_2^{\text{gas}}}{r_2} + \frac{\phi_3^{\text{gas}}}{r_3}$$

Assuming that the number of site occupied by the gaseous species are negligible compared to that of the polymer, $r_4 >> r_1, r_2, r_3$, the number of sites occupied in the lattice by a molecule of polymer phase mixture is defined as follows:

$$\frac{1}{r_{\text{mix}}^{\text{pol}}} = \frac{\phi_1^{\text{pol}}}{r_1} + \frac{\phi_2^{\text{pol}}}{r_2} + \frac{\phi_3^{\text{pol}}}{r_3}$$

For the calculation of sorption equilibrium for polymer-solvent system, the chemical potential of the i^{th} component in each phase of the mixture of multicomponent species can be expressed as:

$$\mu_i^{\text{gas}} = \text{R}\,T\left[\ln\phi_i^{\text{gas}} + \left(1 - \frac{\text{r}_\text{i}}{r_{\text{mix}}^{\text{gas}}}\right)\right] \qquad (2)$$

$$+ r_i\left\{-\bar{\rho}_{\text{gas}}\left[\frac{2}{\upsilon^{*\text{gas}}_{\text{mix}}}\left(\sum_{j=1}^{Nc}\phi_j^{\text{gas}}\upsilon_{\text{ij}}^{*}\varepsilon_{\text{ij}}^{*} - \varepsilon^{*\text{gas}}_{\text{mix}}\sum_{j=1}^{Nc}\phi_j^{\text{gas}}\upsilon_{\text{ij}}^{*}\right) + \varepsilon^{*\text{gas}}_{\text{mix}}\right]\right.$$

$$+\frac{\text{R}\,T}{\bar{\rho}_{\text{gas}}}\left[\left(1-\bar{\rho}_{\text{gas}}\right)\ln\left(1-\bar{\rho}_{\text{gas}}\right) + \frac{\bar{\rho}_{\text{gas}}}{r_i}ln\bar{\rho}_{\text{gas}}\right]$$

$$\left.+\frac{P}{\bar{\rho}_{\text{gas}}}\left(2\sum_{j=1}^{Nc}\phi_j^{\text{gas}}\upsilon_{\text{ij}}^{*} - \upsilon^{*\text{gas}}_{\text{mix}}\right)\right\}$$

We consider that the chemical potential of each solute component at equilibrium is equal to the chemical potential of the polymer as follows:

$$\mu_i^{\text{pol}} = \mu_i^{\text{gas}} \quad i=1,2,3,4$$

The same expression of the chemical potential in the gas phase (2) can be rewritten for the polymer phase, with all the characteristic parameters calculated for the polymer. This equation will lead to the identification of the closed-packed volume fractions of solute components in the polymer phase, ϕ_1^{pol}, ϕ_2^{pol} and ϕ_3^{pol}.

By solving simultaneously the three non-linear equations based on equation (2) for solute species 1, 2 and 3 and the equation of state (1) of SL for the polymer phase; the reduced polymer

phase density, $\bar{\rho}_{\text{pol}}$, as well as the closed-packed volume fractions of solute components in the polymer phase ϕ_1^{pol}, ϕ_2^{pol}, ϕ_3^{pol}, can be identified.

All the properties of interest can be deduced from these parameters. The volume fraction of each sorbed component in the amorphous polymer can therefore be calculated as

$$\omega_i^{\text{am}} = \frac{\rho_i^* v_i^* \phi_i^{\text{pol}}}{\rho_1^* v_1^* \phi_1^{\text{pol}} + \rho_2^* v_2^* \phi_2^{\text{pol}} + \rho_3^* v_3^* \phi_3^{\text{pol}} + \rho_4^* v_4^* \phi_4^{\text{pol}}}$$

$$\omega_i^{\text{am}} = \frac{\rho_i^* v_i^*}{\rho_1^* v_1^*} \frac{\phi_i^{\text{pol}}}{\phi_1^{\text{pol}}} \omega_1^{\text{am}} \qquad i = 2,3$$

$$\omega_4^{\text{am}} = 1 - \omega_1^{\text{am}} - \omega_2^{\text{am}} - \omega_3^{\text{am}}$$

Finally, the solubility of each component at equilibrium, in gram of component per gram of amorphous polymer can be calculated as follows

$$S_i^{\text{am}} = \frac{\omega_i^{\text{am}}}{\omega_{\text{pol}}^{\text{am}}} (1 - \chi) \qquad i = 1,2,3$$

where χ is the crystallinity of the polymer.

3.2.Modelling algorithm

For quaternary systems, the interaction parameters between the penetrating molecules and the polymer are required and cannot be taken from ternary systems *a priori*. We consider here a system containing a monomer (1), an ICA (2), a comonomer (3) and a polymer (4). The corresponding interaction parameters in order to solve the SL EoS are : k_{12}, k_{13}, k_{14}, k_{23}, k_{24}, k_{34} which are the interaction parameters between the monomer and the ICA, the monomer and the comonomer, the monomer and the polymer, the ICA and the comonomer, the ICA and the polymer and the comonomer and the polymer, respectively. Only k_{14}, k_{24}, k_{34} parameters are estimated by fitting SL EoS to experimental data, while k_{12}, k_{13} and k_{24} are equal to zero because we assume that the interaction between small olefin molecules does not deviate from Lorentz-Berthelot combining rules (used to calculate the potential)[20].

The novel approach used in Chapter 2 where SL EoS is combined to Peng-Robinson EoS (i.e. PR EoS) cannot be used for quaternary systems when only overall solubility data is available because three interaction parameters need to be identified from only two input data. This makes the pressure decay method, from which partial solubilities are measured, crucial to model the

solubility of quaternary systems with SL EoS. The procedure allowing to identify SL interaction parameters through overall and partial solubility in the amorphous phase of the polymer is shown in ***Figure 36***.

Partial solubilities of the different components in the mixture are calculated with SL EoS and are then fitted to the experimental data in order to identify the three interaction parameters, k_{14}, k_{24}, k_{34}. The fitting procedure minimizes the percent average relative deviation, *ARD*, between the experimental and calculated partial and total solubilities, as follows:

$$ARD = \left(\frac{|S_{\text{tot}}^{\text{SL EoS}} - S_{\text{tot}}^{\text{exp}}|}{S_{\text{tot}}^{\text{exp}}} + \sum_{j=1}^{N_c} \frac{|S_j^{\text{SL EoS}} - S_j^{\text{exp}}|}{S_j^{\text{exp}}} \right) \times 100$$

Where $S_{\text{tot}}^{\text{SL EoS}}$ and $S_{\text{tot}}^{\text{exp}}$ are respectively the overall solubility of the mixture calculated with SL EoS and the one measured experimentally. $S_j^{\text{SL EoS}}$ and S_j^{exp} are respectively the partial solubility of component j calculated with SL EoS and that measured experimentally. N_c is the number of component j in the mixture.

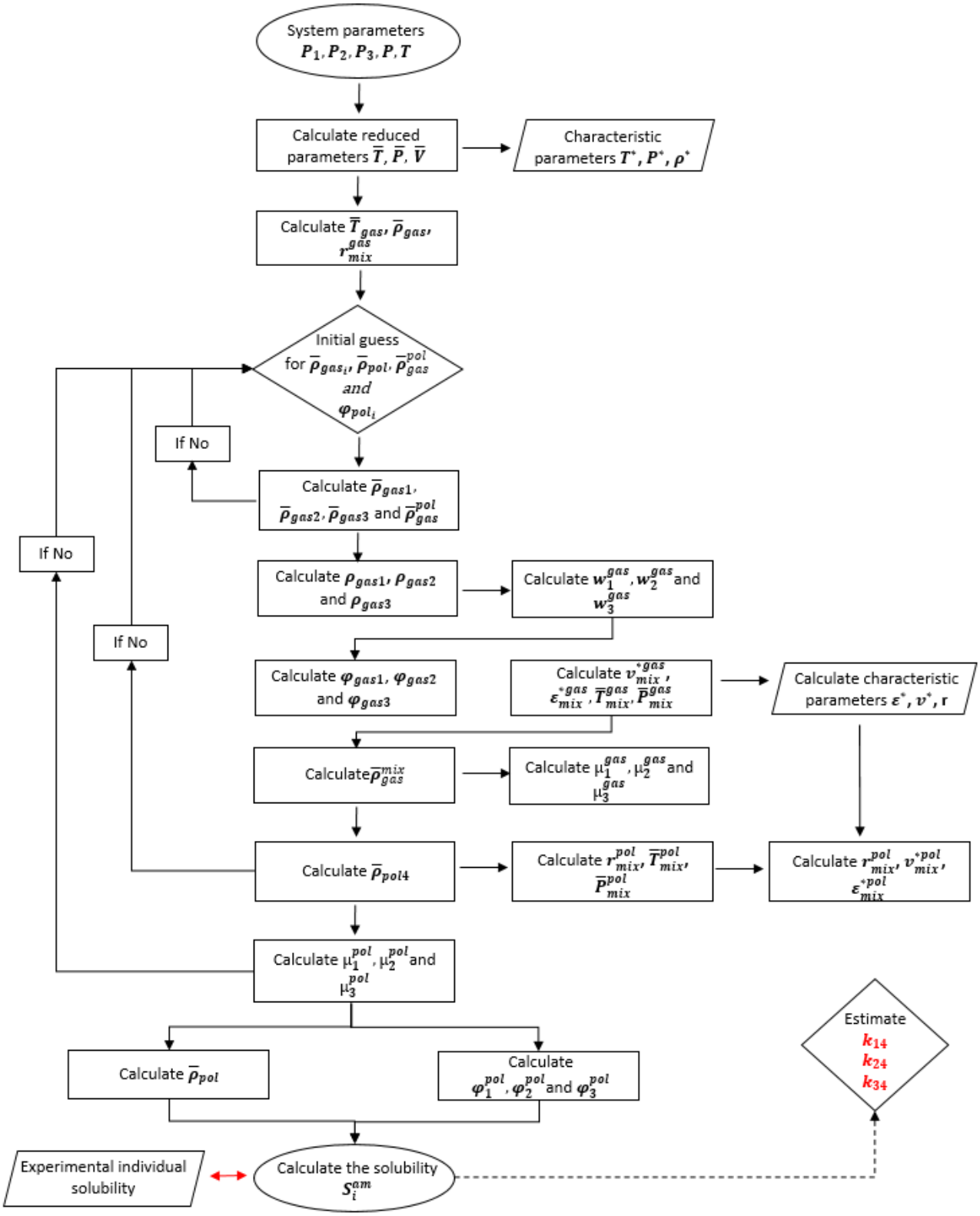

Figure 36. *Flowchart for the modeling of quaternary systems with Sanchez-Lacombe Equation of State*

4. Results and discussion

4.1.Ternary systems

Different ternary systems containing (1) ethylene, (2) penetrant and (3) polyethylene were experimentally studied using the pressure decay method. The same polymer was used in order to compare these ternary systems, and therefore to quantify the impact of adding different penetrants to ethylene/PE system. The overall solubility of the gas mixture as well as their partial solubility in the amorphous phase of the polymer were measured. ***Table 19*** shows the range of pressure and temperature and the composition of the gas mixtures for the ternary systems considered here.

Table 19. *Gas phase molar composition of the different ternary studied system using pressure decay method*

System	Temperature (°C)	Composition
Ethylene/Propane/LLDPE-I	T=[80, 90]	P_{tot} = [5, 7.9] bar x_{C_2} = 0.497 $x_{C_{3a}}$ = 0.503
Ethylene/Propylene/LLDPE-I	T=[68, 78]	P_{tot} = [2.2, 5.2] bar x_{C_2}= [0.475, 0.395] $x_{C_{3e}}$= [0.525, 0.605]
Ethylene/1-Butene/LLDPE-I	T=[68, 84]	P_{tot} = [3.2, 4] bar x_{C_2}= [0.834, 0.496] x_{1C_4}= [0.166, 0.504]

Figure 37 compares the overall solubility of the three studied ternary systems: ethylene/propane/LLDPE-I, ethylene/propylene/LLDPE-I and ethylene/1-butene/LLDPE-I, at a total pressure up to 8 bars and temperature up to 90°C. ***Figure 37*** shows that, as expected, the total solubility increases as the total pressure of the system increases and as the temperature of the system decreases. It is important to note that the heavier the penetrant is, the higher is the total solubility of a mixture at a given total pressure. Indeed, at the same total pressure of the system and the same temperature, the overall solubility in presence of 1-butene is higher than in presence of propylene, which is higher than in presence of propane.

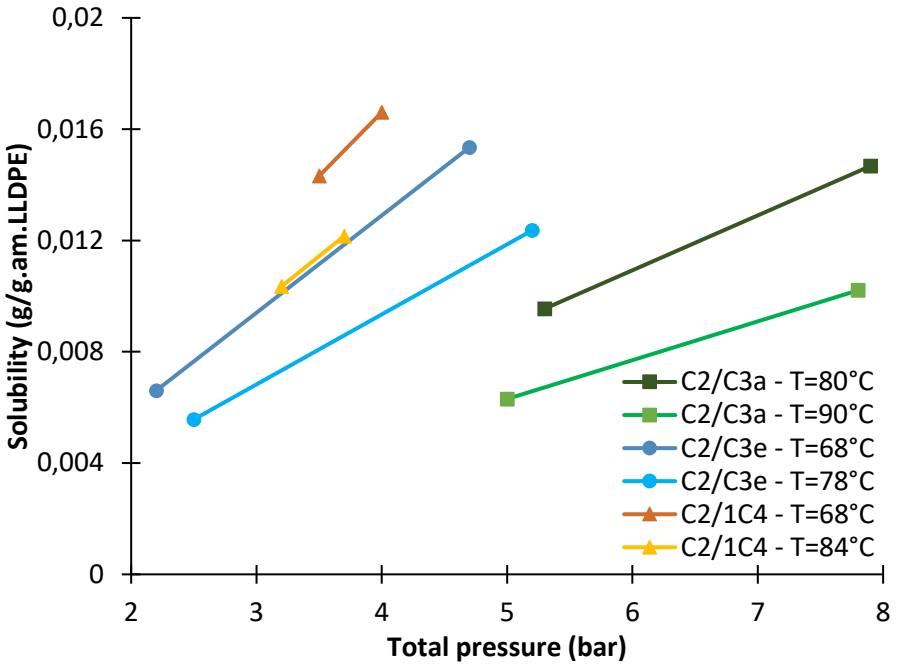

Figure 37. *Total solubility of ethylene/propane, ethylene/propylene and ethylene/1-butene in LLDPE-I at temperatures between 68-90°C. Gas compositions of the different systems is given in* ***Table 19***

Figure 38 through ***Figure 43*** show the overall and partial solubilities of the different penetrants in the amorphous phase of the polymer at different temperatures, for each studied systems. The experimental solubility is then correlated to SL EoS in order to estimate the interaction parameters, k_{ij}, for each system at each temperature. The k_{ij} correlations thus obtained are shown in ***Table 20.*** The figures show that SL EoS is in good agreement with the experimental solubility data performed with the pressure decay method. The maximum difference between the experiments and SL EoS is 1% for ethylene/propane/LLDPE-I system, 5% for both ethylene/propylene/LLDPE-I and ethylene/1-butene/LLDPE-I systems. It can also be seen that in general, when the overall solubility increases with pressure, also the individual solubility of ethylene and the other penetrant increases, except for 1-butene (c.f. ***Figure 43*** and ***Figure 44***). For this later system, at 68°C, increasing the total pressure leads to an increase of ethylene solubility and to a decrease of that of 1-butene while the inverse occurs at 84°C. Note however that the composition for ethylene/1-butene/LLDPE-I at the two studied temperatures are different (i.e. x_{C_2}=0.834 and x_{1C_4}=0.166 at 68°C compared to x_{C_2}=0.496 and x_{1C_4}=0.504 at 84°C, c.f. ***Table 19***), so we should expect a different behavior of the gas phase between both temperatures.

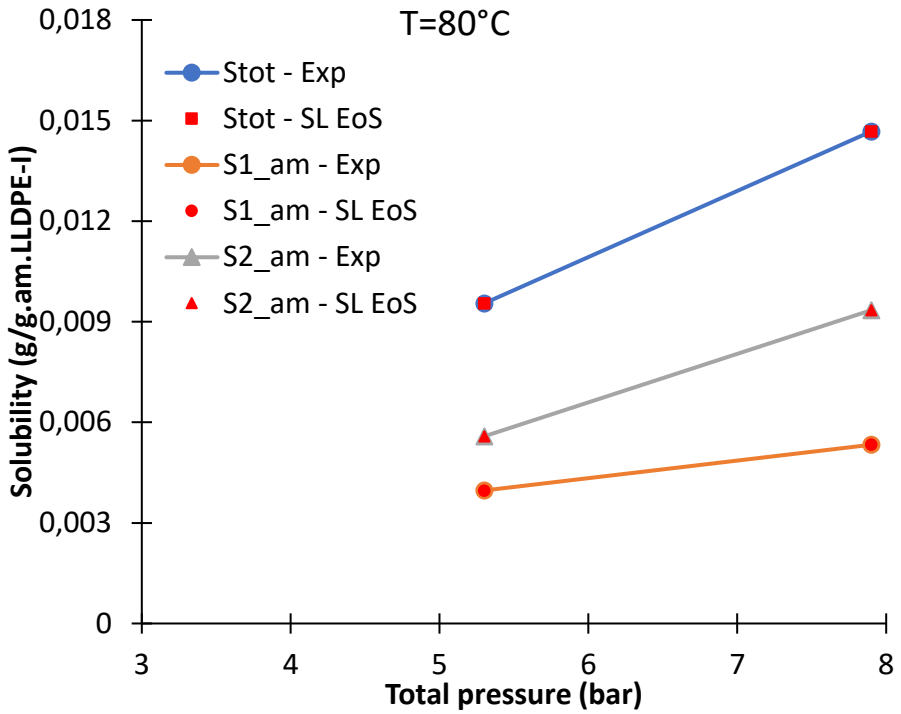

Figure 38. *Total (S_tot) and partial solubility of ethylene (S1_am) and propane (S2_am) in ethylene/propane/LLDPE-I system at 80°C. The lines represent the experimental solubility and the red points represent the solubility calculated with SL EoS. Gas phase composition is x_{C2}=0.497 and x_{C3a}=0.503 at 80°C. k_{ij} correlations are given in* ***Table 20***

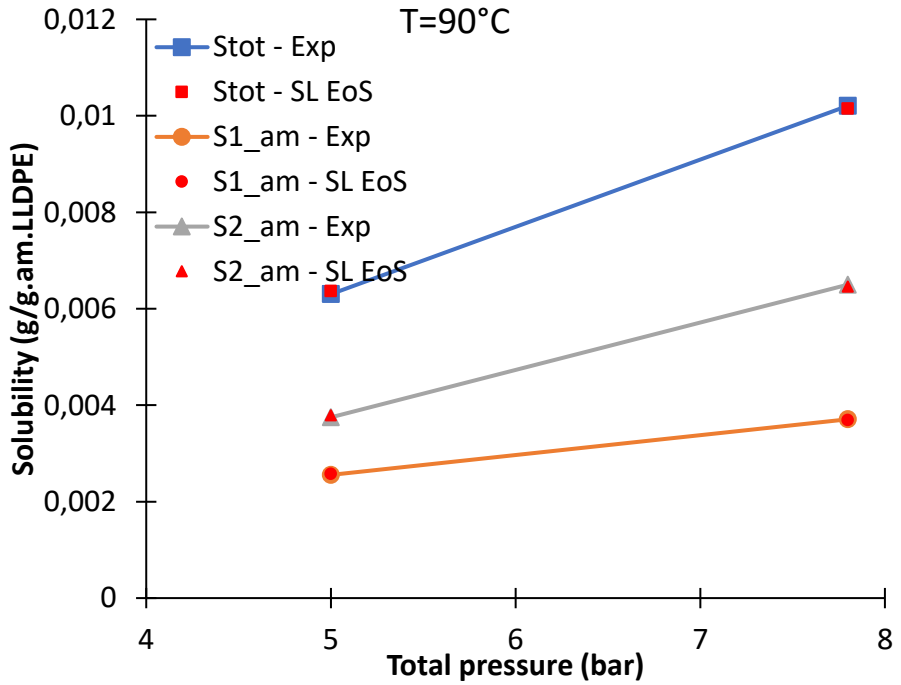

Figure 39. *Total (S_tot) and partial solubility of ethylene (S1_am) and propane (S2_am) in ethylene/propane/LLDPE-I system at 90°C. The lines represent the experimental solubility and the red points represent the solubility calculated with SL EoS. Gas phase composition is x_{C2}=0.497 and x_{C3a}=0.503 at 90°C. k_{ij} correlations are given in* ***Table 20***

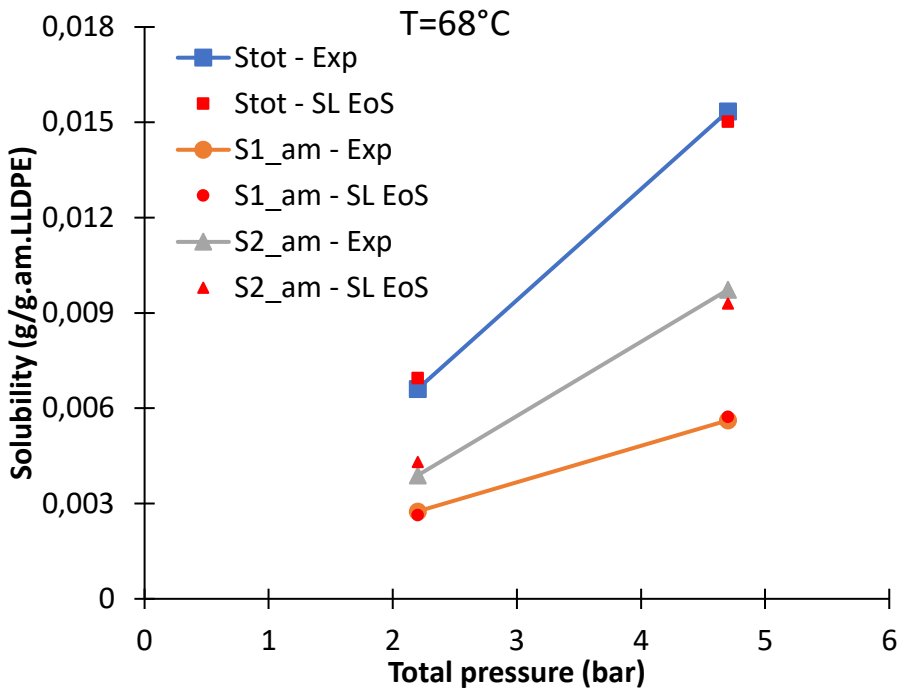

Figure 40. *Total (S_tot) and partial solubility of ethylene (S1_am) and propylene (S2_am) in ethylene/propylene/LLDPE-I system at 68°C. The lines represent the experimental solubility and the red points represent the solubility calculated with SL EoS. Gas phase composition is x_{C2}=0.475 and x_{C3e}=0.525 at 68°C. k_{ij} correlations are given in* ***Table 20***

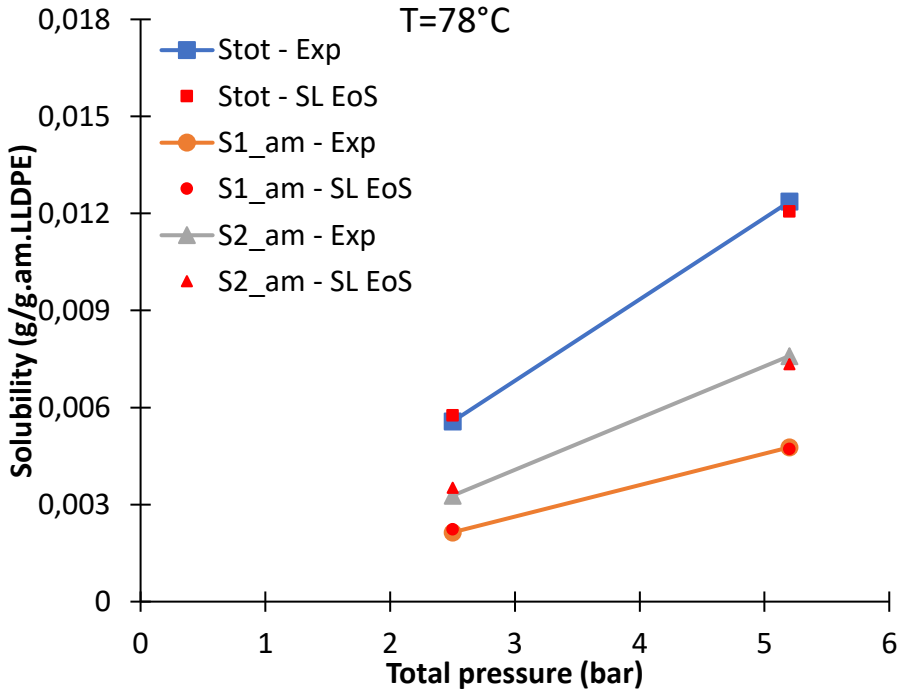

Figure 41. *Total (S_tot) and partial solubility of ethylene (S1_am) and propylene (S2_am) in ethylene/propylene/LLDPE-I system at 68°C. The lines represent the experimental solubility and the red points represent the solubility calculated with SL EoS. Gas phase composition is x_{C2}=0.395 and x_{C3e}=0.605 at 68°C. k_{ij} correlations are given in* ***Table 20***

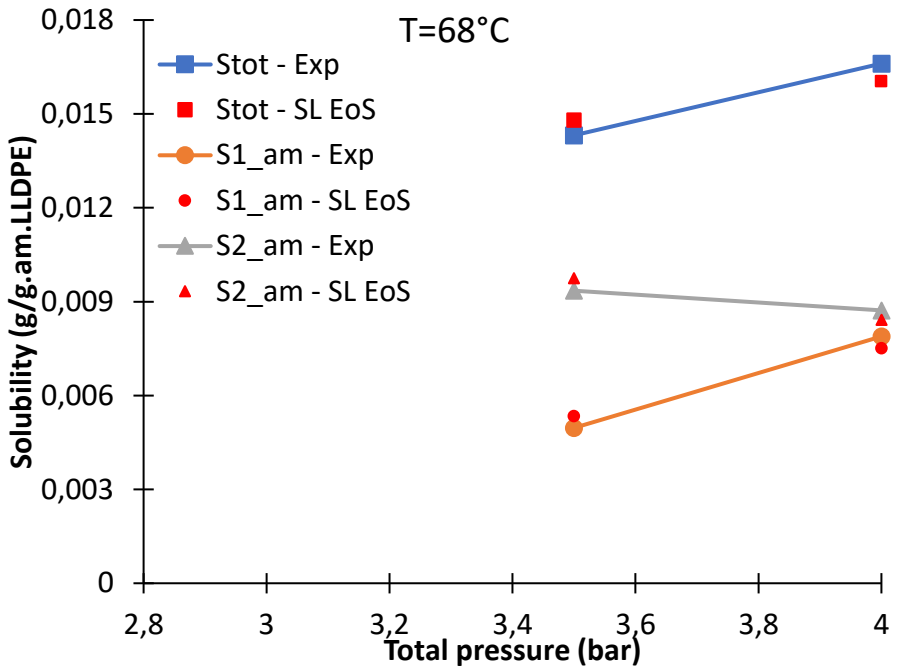

Figure 42. *Total (S_tot) and partial solubility of ethylene (S1_am) and 1-butene (S2_am) in ethylene/1-butene/LLDPE-I system at 68°C. The lines represent the experimental solubility and the red points represent the solubility calculated with SL EoS. Gas phase composition is* x_{C2}*=0.834 and* x_{1C4}*=0.166 at 68°C.* k_{ij} *correlations are given in* ***Table 20***

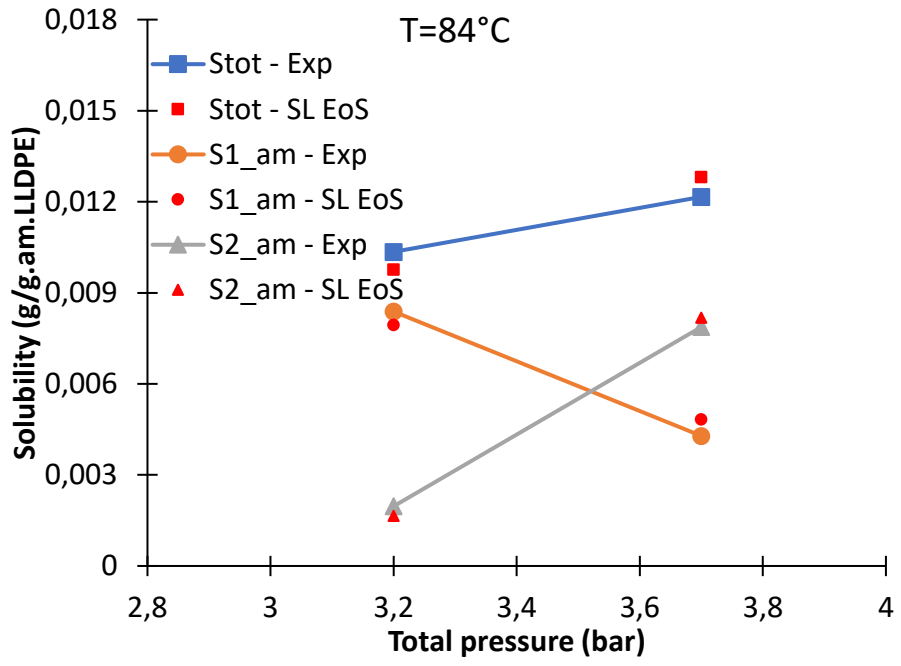

Figure 43. *Total (S_tot) and partial solubility of ethylene (S1_am) and 1-butene (S2_am) in ethylene/1-butene/LLDPE-I system at 84°C. The lines represent the experimental solubility and the red points represent the solubility calculated with SL EoS. Gas phase composition is* x_{C2}*=0.496 and* x_{1C4}*=0.504 at 84°C.* k_{ij} *correlations are given in* ***Table 20***

Table 20. *k_{ij} correlation with respect to temperature (°C) for ethylene/propane/LLDPE-I, ethylene/propylene/LLDPE-I and ethylene/1-butene/LLDPE-I systems*

	Correlation
Ethylene/Propane/LLDPE-I	$k_{13} = 0.0021 \times T - 0.23$ $k_{23} = 0.001 \times T - 0.069$
Ethylene/Propylene/LLDPE-I	$k_{13} = 0.0016 \times T - 0.2138$ $k_{23} = 0.0007 \times T - 0.0265$
Ethylene/1-Butene/LLDPE-I	$k_{13} = -0.0011 \times T - 0.0336$ $k_{23} = -0.0002 \times T + 0.0854$

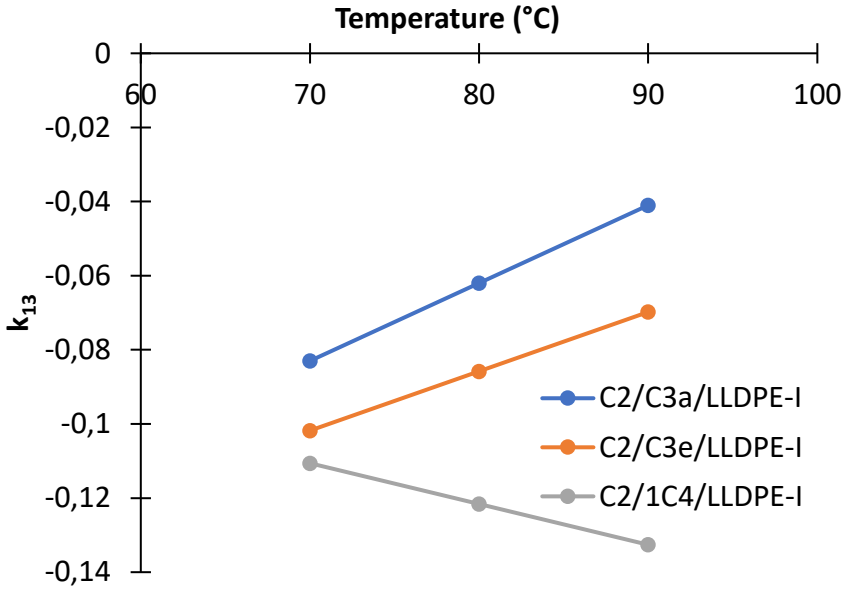

Figure 44. *Temperature dependent correlation of k_{13} for the different studied systems of ethylene/propane/LLDPE-I (C_2/C_{3a}/LLDPE-I), ethylene/propylene/LLDPE-I (C_2/C_{3e}/LLDPE-I) and ethylene/1-butene/LLDPE-I ($C_2/1C_4$/LLDPE-I).*

It is known that the interaction parameters are function of the components composing the gaseous mixture, the polymer type and the temperature. ***Table 20*** shows the temperature dependent correlations of the interaction parameter, k_{ij}, for the different studied systems. It can be seen that the interaction parameter between ethylene and the polymer, k_{13}, is dependent on the nature of the second penetrant. For the temperatures of interest, heavier penetrants lead to lower k_{13}, but higher in the absolute value, as can be seen in ***Figure 44***. Remember that the

interaction parameters are used to define the cross interaction energy $\varepsilon_{ij}^{*} = \left(\varepsilon_i^{*}\varepsilon_j^{*}\right)^{0.5}\left(1 - k_{ij}\right)$; When k_{ij}=0, the cross-potential follows Lorentz-Berthelot combining rules[19] (i.e. $\varepsilon_{ij}^{*} = \left(\varepsilon_i^{*}\varepsilon_j^{*}\right)^{0.5}$) while if the value is far from 1, then there is a deviation from these rules. So, there is a higher deviation of the interaction between the polymer and $1C_4$, than C_{3e}, than C_{3a}. This was also observed for the ternary experiments performed on the magnetic suspension balance in Chapter 2. A similar study was also considered by Chmelar et al.[21], and they found that the interaction parameter between 1-hexene and PE was lower than the one between propane and PE. They explained that the purpose of k_{ij} is to correct the energy interactions of unlike chain segments of the penetrant and the polymer. Therefore, the heavier the penetrant, the more the interaction with the polymer deviates from Lorentz-Berthelot combining rules. Furthermore, Bashir et al.[23] noted that unlike ethylene, propylene and hexene at 90°C, only 1-butene showed a negative k_{ij} in a binary system. Thus, while perhaps not immediately expected, this result is not attributable to experimental error. This negative value of the interaction parameter suggests that 1-butene has a higher interaction energy with polyethylene than do the other compounds studied here.

4.1.1. Validation with the SL-PR method

The advantage of the pressure decay method is that it leads to the measure of both the overall and partial solubility of each component in the gaseous mixture (so three data points) in order to estimate the interaction parameters, k_{ij}. As a further validation of the experimental set-up presented in this work, the overall solubilities measured using the pressure decay method are treated using the Sanchez-Lacombe – Peng-Robinson (SL-PR) approach used in Chapter 2. This method will therefore validate our experimental approach by comparing the k_{ij} interaction parameters identified when fitting SL EoS to the overall and partial solubilities of the ternary systems above with those estimated using the SL-PR. ***Figure 45*** and ***Figure 47*** show the SL-PR fitting of the overall solubility of ethylene/propane/LLDPE-I at 80°C and ethylene/propylene/LLDPE-I at 68°C, respectively. ***Figure 46*** and ***Figure 48*** show the compressibility factor calculated with Peng-Robinson EoS to that calculated from SL EoS, for ethylene/propane/LLDPE-I mixture at 80°C and ethylene/propylene/LLDPE-I mixture at 68°C, respectively. The calculated compressibility factors from SL EoS are in good agreement with the ones calculated with Peng-Robinson EoS, with a maximum difference of less than 1%. It is also shown that the SL-PR model fits the overall solubility data well, with a difference between the model and the experiments of 2% for ethylene/propane/LLDPE-I and 12% for ethylene/propylene/LLDPE-I.

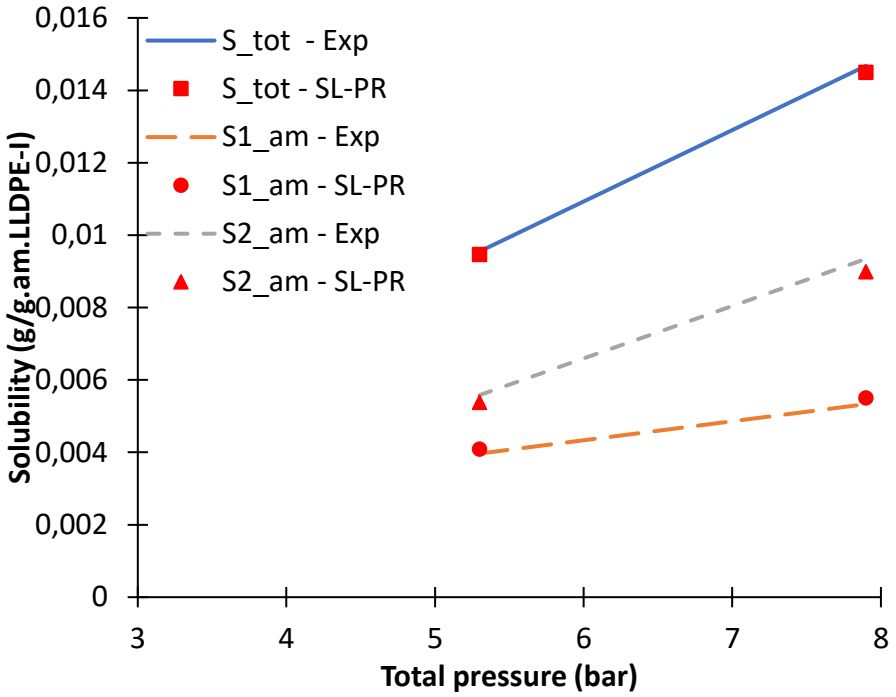

Figure 45. *Overall and partial solubility of ethylene/propane/LLDPE-I ternary system at 80°C. The estimation of the partial solubility is achieved by using the SL-PR method. Molar composition of the system is given in* ***Table 19*** *and* k_{ij} *used for this study is given in* ***Table 20***

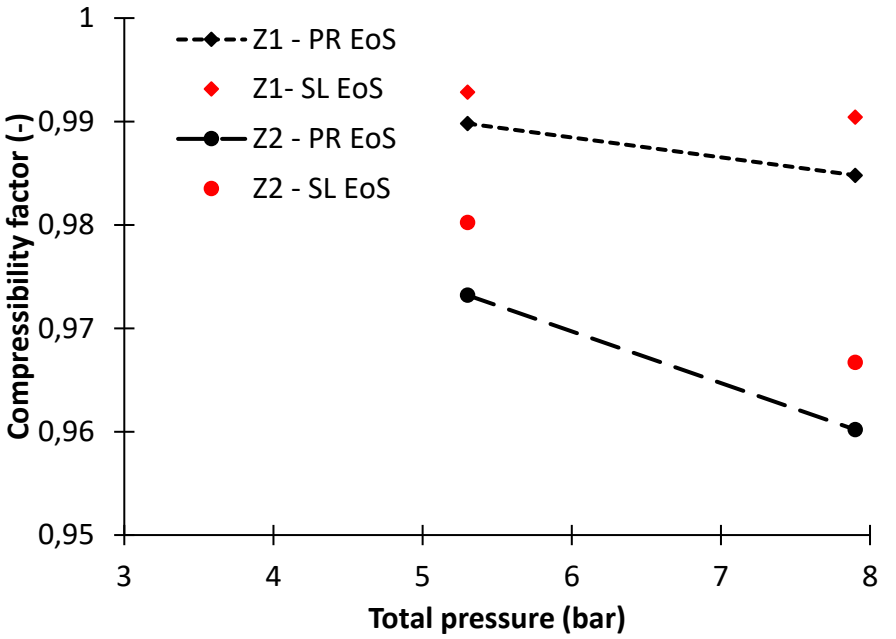

Figure 46. *Compressibility factor of ethylene (Z_1) and propane (Z_2) in ethylene/propane/LLDPE-I system at 80°C. The lines represent compressibility values calculated with Peng-Robinson and points represent the predictions of the compressibility factor from the ternary SL EoS.*

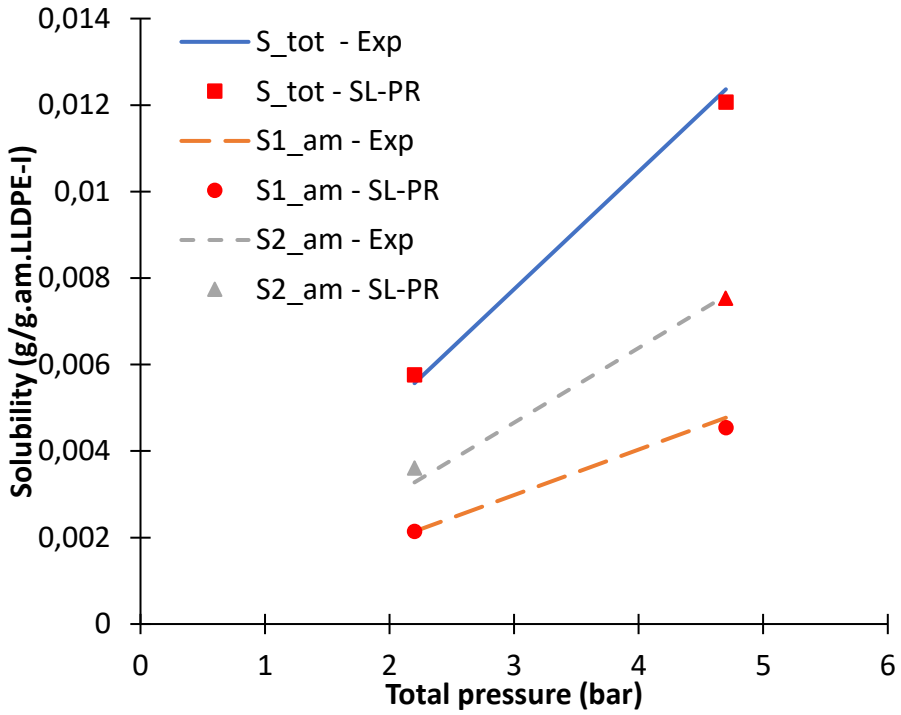

Figure 47. *Overall and partial solubility of ethylene/propylene/LLDPE-I ternary system at 68°C. The estimation of the partial solubility is achieved by using the SL-PR method. Molar composition of the system is given in* ***Table 19*** *and* k_{ij} *used for this study is given in* ***Table 20***

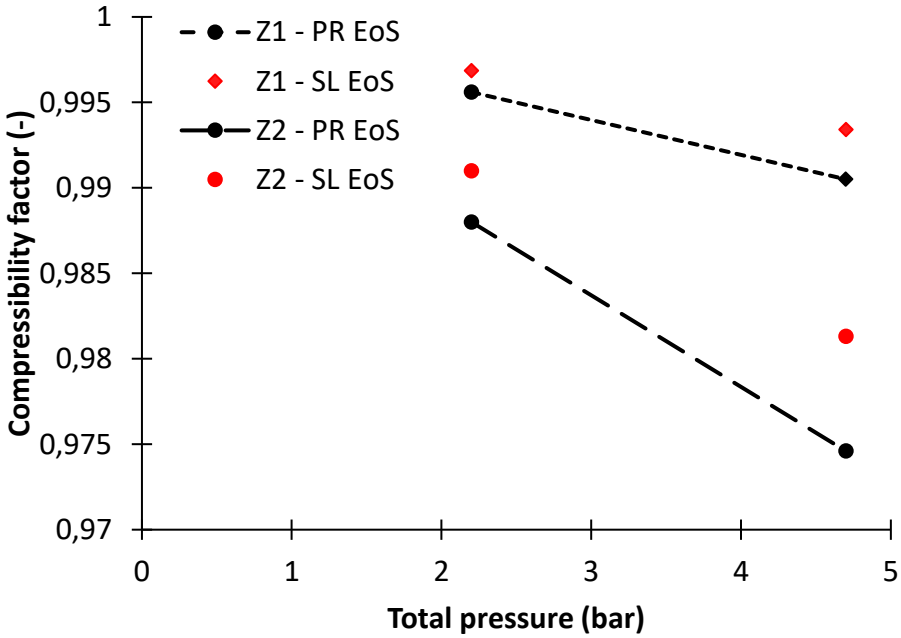

Figure 48. *Compressibility factor of ethylene (Z_1) and propylene (Z_2) in ethylene/propylene/LLDPE-I system at 68°C. The lines represent compressibility values calculated with Peng-Robinson and points represent the predictions of the compressibility factor from the ternary SL EoS.*

Table 21 compares the k_{ij} interaction parameters identified when fitting SL EoS to the overall and partial solubilities of the ternary systems and when only overall solubility of the ternary system is available and is therefore combined to the calculation of the compressibility factor of each component in the system through Peng-Robinson EoS (i.e. SL-PR). It is shown that the interaction parameters are quite similar, giving therefore confidence in the pressure decay experiments for the estimation of the individual solubilities.

Table 21. *Comparison of the predicted k_{ij} for ethylene/propane/LLDPE-I and ethylene/propylene/LLDPE-I with the SL EoS and with SL EoS combined to PR EoS (SL-PR)*

	SL EoS with overall and partial solubilities	**SL-PR with only overall solubility**
Ethylene/Propane/LLDPE-I	$k_{13} = -0.062$ $k_{23} = 0.011$	$k_{13} = -0.0628$ $k_{23} = 0.0121$
Ethylene/Propylene/LLDPE-I	$k_{13} = -0.089$ $k_{23} = 0.0281$	$k_{13} = -0.081$ $k_{23} = 0.0281$

4.1.2. Comparison between binary and ternary systems

A comparison between binary and ternary systems will be achieved in this section in order to show the impact of ethylene as well as the different penetrants on the overall solubility of the gas mixture in the amorphous phase of the polymer. In order to do so, the binary solubilities of ethylene, propane, propylene and 1-butene in LLDPE will be compared to the ternary solubility of ethylene/penetrant/LLDPE-I at 80°C. The binary solubilities in LLDPE were estimated from Chmelar et al.[21] since they used an LLDPE with a density of 923 kg m^{-3} and a crystallinity of 50.3 wt%, that are close to the characteristic of the LLDPE-I sample used for the pressure decay experiments (c.f. ***Table 17***). The different binary interaction parameters are given in ***Table 22*** at 80°C.

Table 22. Binary interaction parameters at 80°C for ethylene, propane, propylene and 1-butene in LLDPE.

System	Binary k_{ij}	Ref
Ethylene/LLDPE	0.00387	Fitting to [21]
Propane/LLDPE	-0.0068	Fitting to [21]
Propylene/LLDPE	-0.00812	Fitting to [21]
1-Butene/LLDPE	0.0155	Fitting to [21]

Figure 49-Figure 51 show the predicted (i.e. SL EoS) binary solubilities of ethylene and the different penetrants, estimated from Chmelar et al.[21], and the predicted total solubilities of mixtures of ethylene and the same penetrants for different fractions each in ternary systems at 80°C. k_{ij} interaction parameters at 80°C were taken from ***Table 22*** for all binary systems and from ***Table 20*** for the ternary studied systems. It is shown that the overall solubility of ternary systems of ethylene/penetrant in LLDPE is between the binary solubility of ethylene and that of the penetrant, at each gas phase composition.

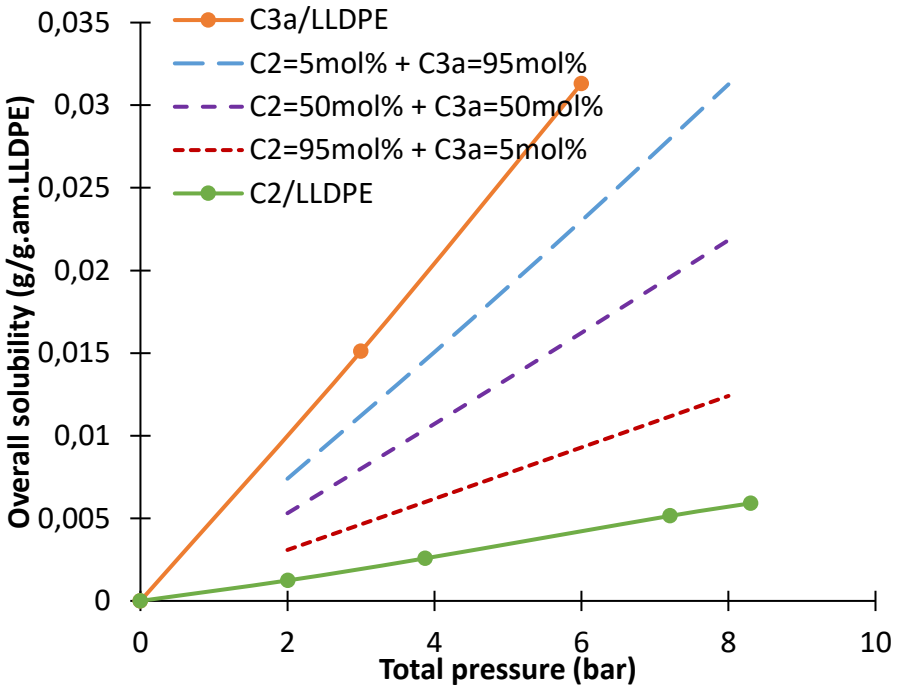

*Figure 49. Solubility of binary ethylene/LLDPE (C2) and propane/LLDPE (C3a) systems and overall solubility of their mixture in ternary system of ethylene/propane/LLDPE at 80°C, calculated with SL EoS. Different composition of the gaseous mixture in the ternary system is shown. k_{ij} for binary systems are defined in **Table 22** and for ternary systems in **Table 20***

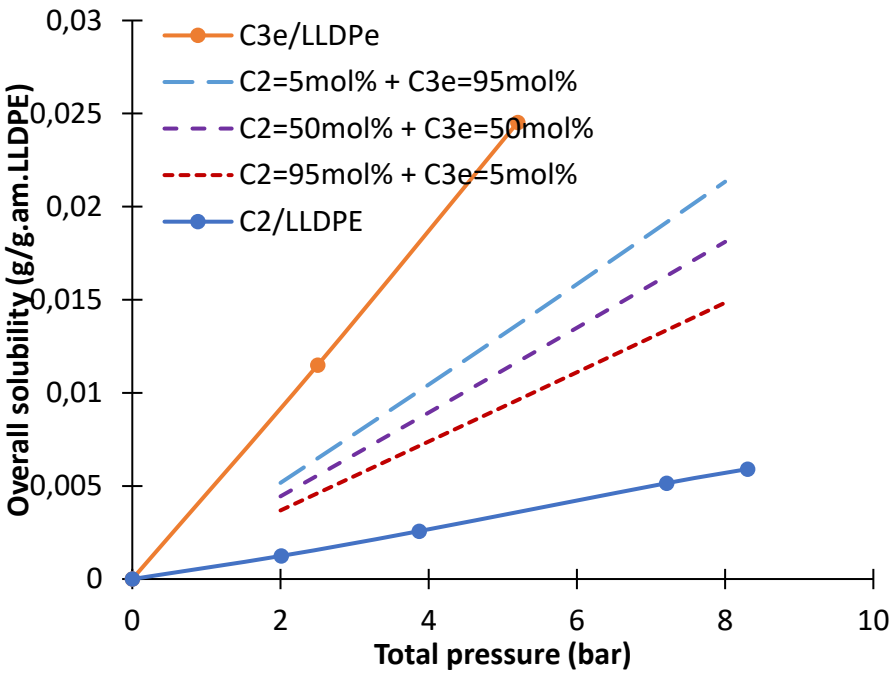

Figure 50. *Solubility of binary ethylene/LLDPE (C2) and propylene/LLDPE (C3e) systems and overall solubility of their mixture in ternary system of ethylene/propylene/LLDPE at 80°C, calculated with SL EoS. Different composition of the gaseous mixture in the ternary system is shown.* k_{ij} *for binary systems are defined in* ***Table 22*** *and for ternary systems in* ***Table 20***

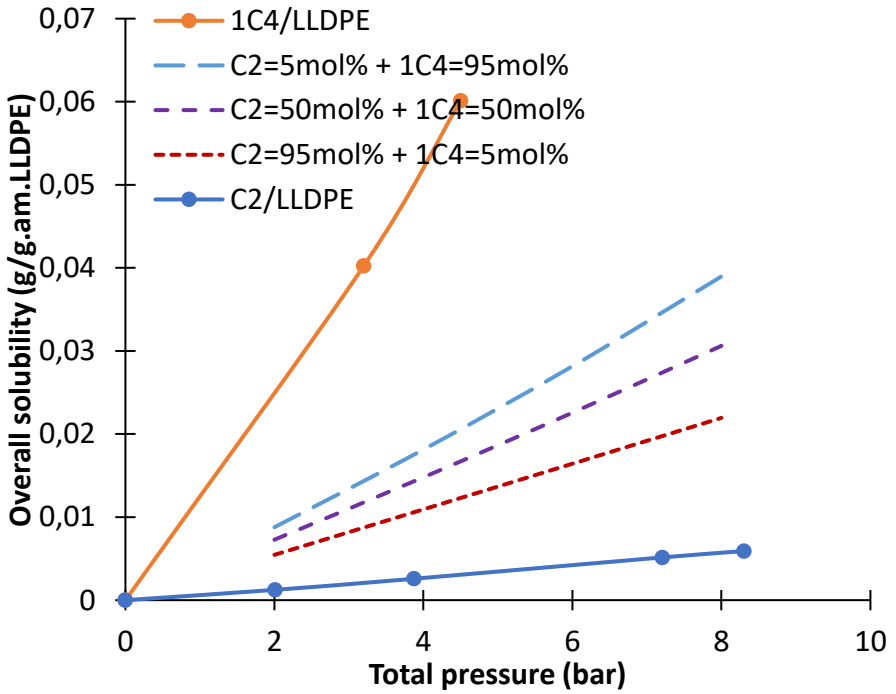

Figure 51. *Solubility of binary ethylene/LLDPE (C2) and 1-butene/LLDPE (1C4) systems and overall solubility of their mixture in ternary system of ethylene/1-butene/LLDPE at 80°C, calculated with SL EoS. Different composition of the gaseous mixture in the ternary system is shown.* k_{ij} *for binary systems are defined in* ***Table 22*** *and for ternary systems in* ***Table 20***

4.1.3. Co-solvent effect in ternary systems

As mentioned above, the co-solvent effect refers to the observed increase in the concentration of a given species due to the presence of another species in the mixture. This can have important implications in terms of polymerization rate and polymer properties. ***Figure 52*** and ***Figure 53*** show ethylene solubility in the binary system and its individual solubility in the ternary mixtures with 5 and 30 mol% of propane, propylene and 1-butene at 80°C, respectively. It is clear that adding even 5 mol% of the different studied penetrants leads to an important increase of the partial solubility of ethylene in the ternary system. For instance, it can be seen in ***Figure 52*** that at a total pressure of 4 bars, the partial solubility of ethylene is increased by a factor of 1.3 in presence of propane, 1.8 in presence of propylene and 3.3 in presence of 1-butene. It can be concluded that a co-solvent effect of the different penetrants on the solubility of ethylene in the amorphous phase of the polymer is preponderant in the ternary systems. Besides, it is clearly shown that the heavier the penetrant added in the ternary system is, the higher is the co-solvent effect of the different penetrants on ethylene concentration in the amorphous phase of the polymer.

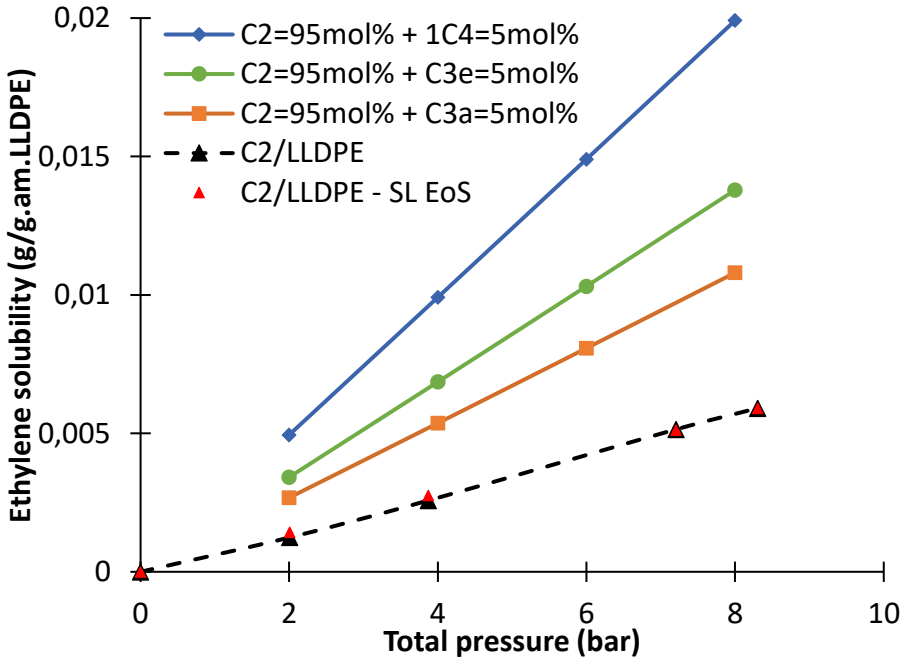

Figure 52. *Binary solubility of ethylene in LLDPE taken from[21] (dotted lines) and from SL EoS (points) and the partial ternary solubility of ethylene in presence of 5 mol% of propane, propylene and 1-butene in LLDPE-I at 80°C. k_{ij} for the studied ternary systems at the temperature of interest are defined in* ***Table 20*** *and for the ethylene/LLDPE binary system in* ***Table 22****.*

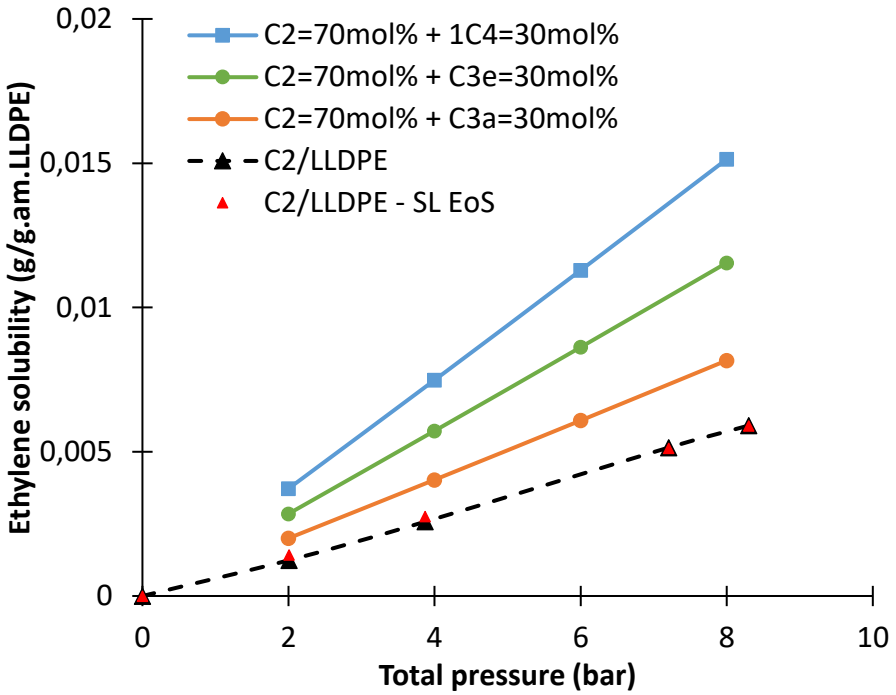

Figure 53. *Binary solubility of ethylene in LLDPE taken from[21] (dotted lines) and from SL EoS (points) and the partial ternary solubility of ethylene in presence of 30 mol% of propane, propylene and 1-butene in LLDPE-I at 80°C. k_{ij} for the studied ternary systems at the temperature of interest are defined in* ***Table 20*** *and for the ethylene/LLDPE binary system in* ***Table 22****.*

4.1.4. Anti-solvent effect in ternary systems

The co-solvent effect of heavier components on ethylene is accompanied by an opposite anti-solvent effect of ethylene on the other species. ***Figure 54*** and ***Figure 55*** show the solubility of pure propane, propylene and 1-butene and their individual solubilities in the ternary mixtures with 5 and 30 mol% of ethylene in LLDPE. It can be observed that adding ethylene to binary penetrant/LLDPE system leads to a decrease of the penetrant partial solubility in the ternary system, due to the anti-solvent effect. As an example, ***Figure 54*** shows that adding 5 mol% of ethylene decrease the partial solubility of propane by a factor of 0.46, 0.58 for propylene, and 0.38 for 1-butene at a total pressure of 4 bar. It is clear that the heavier the penetrant is, the higher is the anti-solvent effect of ethylene on the penetrants concentration in the amorphous phase of the polymer. Furthermore, we can see that at an equivalent concentration, the co-solvent effect of the heavier molecules is more pronounced than the anti-solvent effect of ethylene.

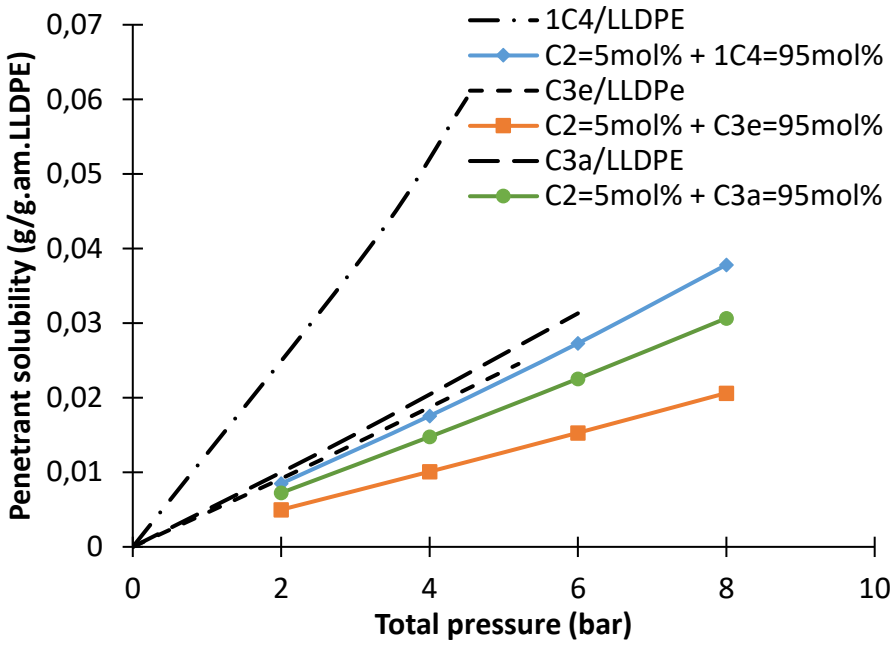

Figure 54. *Binary solubility of 1-butene (1C4), propylene (C3e) and propane (C3a) and the partial ternary solubility of these penetrants with 5 mol% of ethylene in LLDPE at 80°C, calculated with SL EoS. k_{ij} for the studied ternary systems at the temperature of interest are defined in* ***Table 20*** *and for the ethylene/LLDPE binary system in* ***Table 22****.*

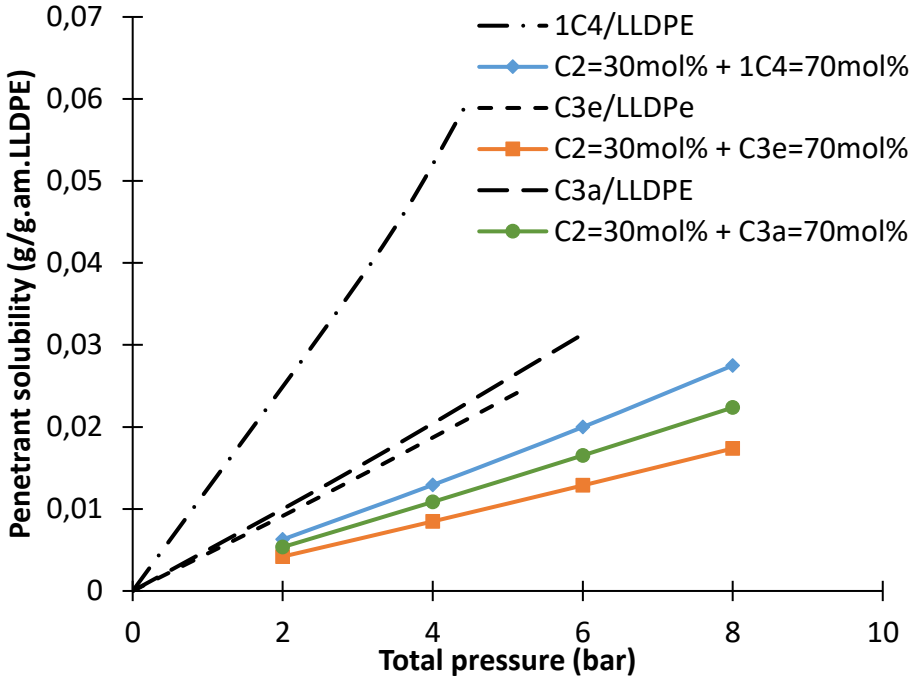

Figure 55. *Binary solubility of 1-butene (1C4), propylene (C3e) and propane (C3a) and the partial ternary solubility of these penetrants with 30 mol% of ethylene in LLDPE at 80°C, calculated with SL EoS. k_{ij} for the studied ternary systems at the temperature of interest are defined in* ***Table 20*** *and for the ethylene/LLDPE binary system in* ***Table 22****.*

4.2. Quaternary systems

4.2.1. Pressure decay experiments

There is no reason to believe that co- and anti-solvent effects would not be present in quaternary systems; rather one would expect the complexity of the interactions to increase. For instance, when the vapour phase contains only 2 components it is relatively straight forward to envisage how changing the fraction of one or the other would have on overall and partial solubilities. In quaternary systems this is less obvious. Furthermore, as mentioned above, it is known that the degree of crystallinity of a PE can influence the solubility of penetrants even if one considers only the amorphous fraction of the material. This means that if one wishes to have thermodynamic data for different mixtures and different polymer grades, it would be necessary to perform a large number of experiments.

To show the importance of performing these higher order experiments, and to better discern the impact of polymer properties on the equilibrium solubility, quaternary experiments were performed with both the pressure decay method and the magnetic suspension balance (gravimetric method). These quaternary systems contain (1) ethylene, (2) ICA, (3) comonomer and (4) polyethylene Some of these experiments were performed using polyethylenes with different crystallinities and molecular weight distributions in order to show the impact of changing the polymer type on the solubility modeling since k_{ij} are function of the polymer type and crystallinity. The characteristics of the different polymer samples are shown in ***Table 1.*** The studied system is ethylene/propane/1-butene/PE at different temperatures and a total pressure up to 5 bars. The studied temperatures, pressures and the gas phase molar composition of the different quaternary studied system are shown in **Table 23**.

Table 23. Gas-phase molar composition of the different studied quaternary systems using pressure decay method

System	Polymer Type	Temperature (°C)	Composition
Ethylene / Propane / 1-Butene	LLDPE-I	T=[69 ; 84]	P_{tot} = [2.5, 5] bar x_{C_3} = 0.54, x_{1C_4} = 0.18
	HDPE-I	T=73	P_{tot} = [2.5, 5] bar x_{C_3} = 0.43, x_{1C_4} = 0.17
	HDPE-B	T=75	P_{tot} = [2.7, 5] bar x_{C_3} = 0.46, x_{1C_4} = 0.19

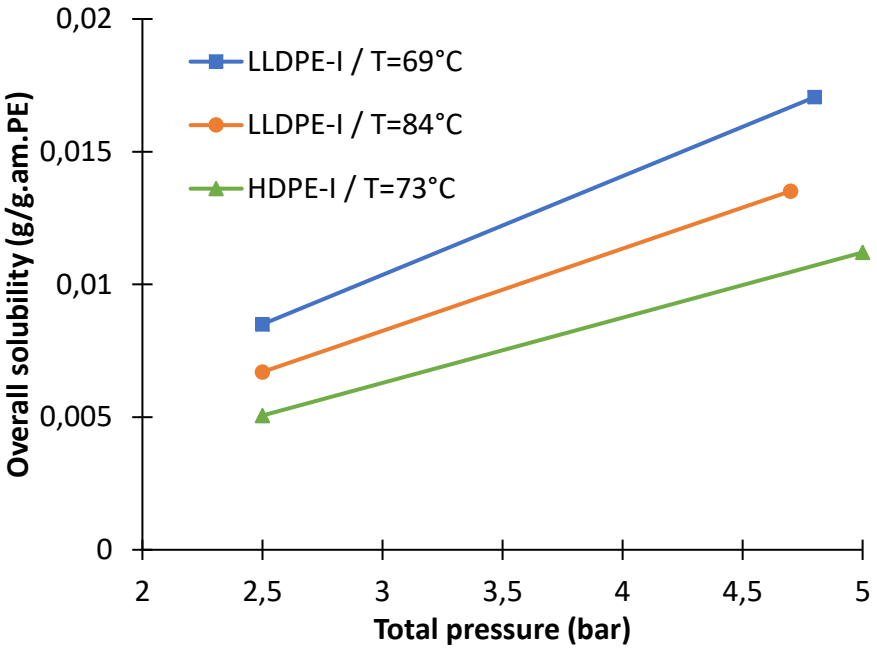

Figure 56. Overall solubility of ethylene/propane/1-butene in different PE types (HDPE-I and LLDPE-I) and at different temperatures, using pressure decay method. Gas phase composition is shown in **Table 23**. PE characteristics are shown in ***Table 1.***

Figure 56 shows the overall solubility of ethylene/propane/1-butene in HDPE-I and LLDPE-I, at different temperatures up to 84°C and different molar composition of the gas phase. It is shown that as for ternary systems, the solubility increases with increasing total pressure and with decreasing the temperature. Furthermore, it can be seen that the solubility is higher in the amorphous phase of LLDPE-I than in the amorphous HDPE-I, as expected. This observation has been attributed to the elastic effects due to the presence of more tie molecules in HDPE than in LLDPE[22]. It is proposed that these tie molecules stop the amorphous phase of the polymer from swelling, thereby reducing gas sorption in the amorphous phase of the polymer.

Figure 57 and ***Figure 58*** show the overall and partial solubilities of ethylene/propane/1-butene mixture in LLDPE-I at 69 and 84°C and total pressure up to 5 bars. It is shown that increasing the temperature decreases the overall solubility of the quaternary system in the amorphous phase of LLDPE-I, as expected. Furthermore, the partial solubility of ethylene, propane and 1-butene are also decreased when increasing the temperature. It is important to note that ethylene partial solubility decreases when increasing the total pressure of the system since its fraction in the gas phase in the second pressure step is lower compared to the first pressure step, which is not the case for propane and 1-butene.

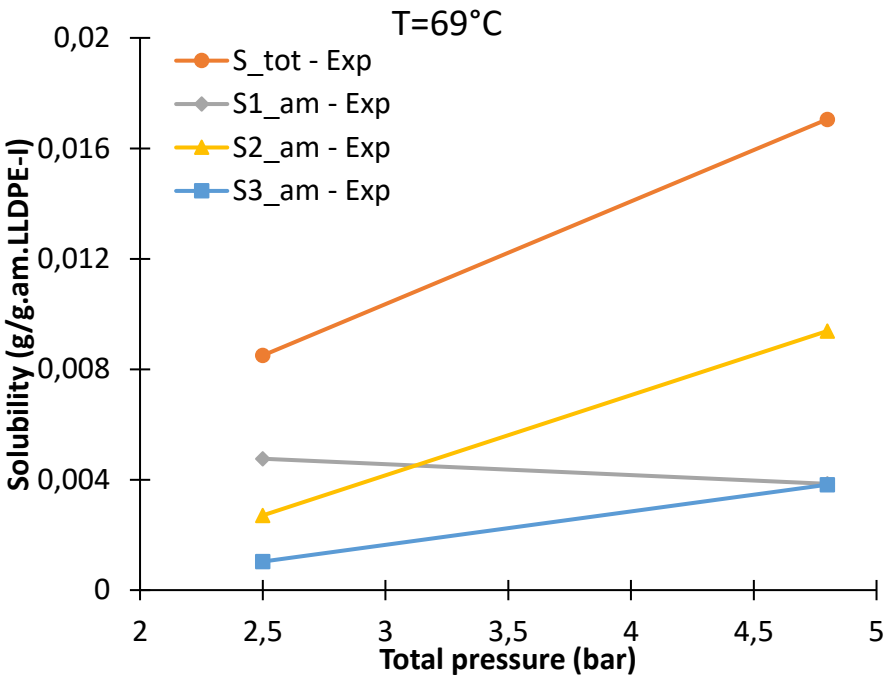

Figure 57. *Total and partial solubility of ethylene/propane/1-butene/LLDPE-I system at 69°C. S_tot, S1_am, S2_am and S3_am are the total solubility of the mixture and the overall solubility of ethylene, propane and 1-butene in the amorphous phase of the polymer, respectively. Gas phase composition of the mixture is given in* ***Table 23***

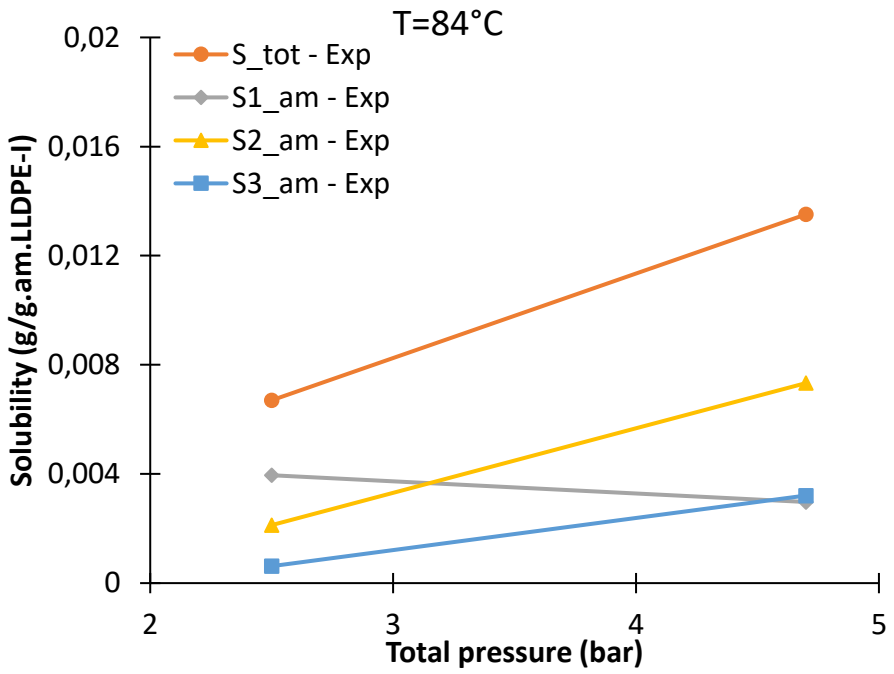

Figure 58. *Total and partial solubility of ethylene/propane/1-butene/LLDPE-I system at 84°C. S_tot, S1_am, S2_am and S3_am are the total solubility of the mixture and the overall solubility of ethylene, propane and 1-butene in the amorphous phase of the polymer, respectively. Gas phase composition of the mixture is given in* ***Table 23***

Figure 59 and ***Figure 60*** show the solubility of ethylene/propane/1-butene mixture in different HDPE grades, HDPE-I and HDPE-B, respectively. As with LLDPE, increasing the total pressure increases the overall solubility. Note that a lower fraction of propane and a higher fraction of ethylene have been used for HDPE-I and HDPE-B than was the case with the LLDPE-I, as can be seen in *Table 14*.

This explains the fact that partial solubility of ethylene increases slightly with respect to the LLDPE experiments, and propane partial solubility is less increased. Furthermore, as explained above, the overall and partial solubility are lower in the amorphous phase of HDPE compared to LLDPE. It can be seen in **Figure 56** that there is a significant difference in the solubility of the quaternary system in the amorphous phase of LLDPE-I compared to HDPE-I. Indeed, the difference in the overall solubility in HDPE-I is about 60% at a total pressure of 2.5 bars compared to LLDPE-I at almost the same temperature. This can also be explained by the difference that can be seen in the crystallinity of these PE in **Table 17**; 56.2% for LLDPE-I compared to 69.5% for HDPE-I.

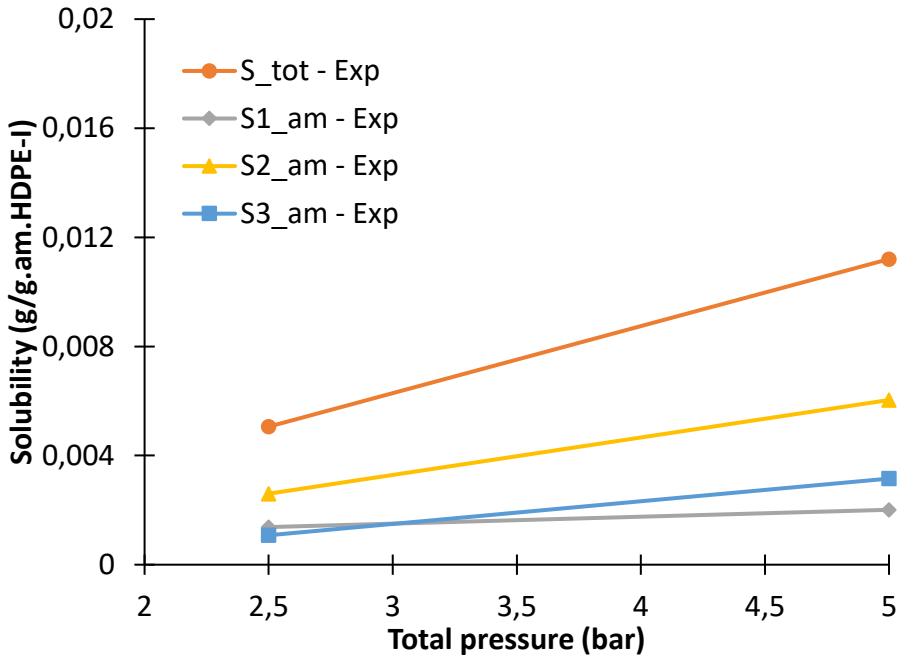

Figure 59. *Total and partial solubility of ethylene/propane/1-butene/HDPE-I system at 73°C. S_tot, S1_am, S2_am and S3_am are the total solubility of the mixture and the overall solubility of ethylene, propane and 1-butene in the amorphous phase of the polymer, respectively. Gas phase composition of the mixture is given in* ***Table 23***

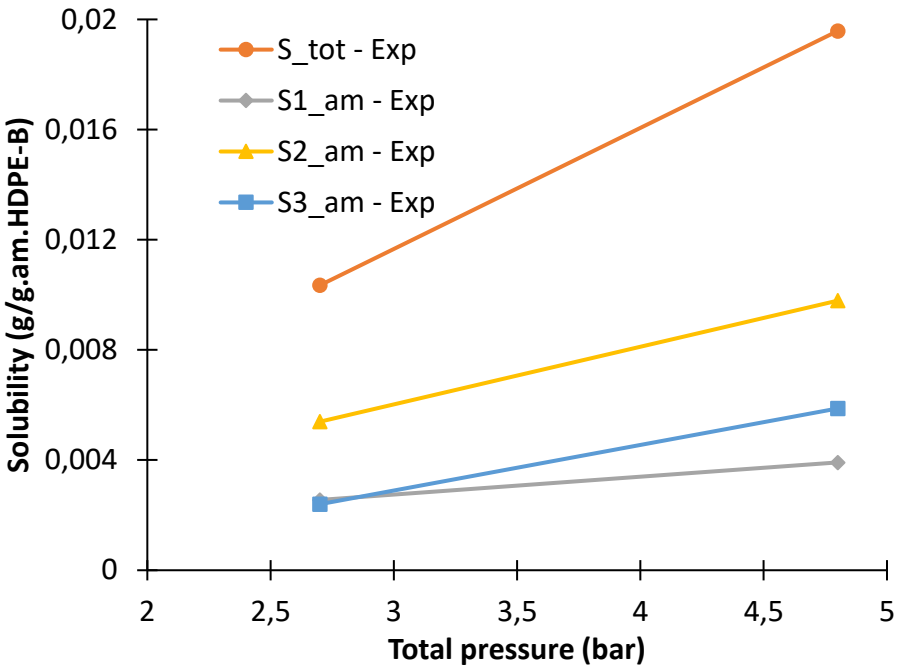

Figure 60. *Total and partial solubility of ethylene/propane/1-butene/HDPE-B system at 75°C. S_tot, S1_am, S2_am and S3_am are the total solubility of the mixture and the overall solubility of ethylene, propane and 1-butene in the amorphous phase of the polymer, respectively. Gas phase composition of the mixture is given in* ***Table 23***

4.2.2. Gravimetric experiments

Similar sorption experiments for quaternary systems were also performed using the gravimetric method to validate our approach using the pressure decay method combined to the µGC. Note that the gravimetric method gives only the overall solubility, whereas the pressure decay method gives both overall and partial solubility of the gaseous mixture in the amorphous phase of the polymer.

For each solubility experiment, we kept the temperature, PE type and gas phase composition constant; while increasing the total pressure of the injected mixture. Two quaternary systems were studied: ethylene/propane/1-butene/LLDPE-B and ethylene/isobutane/1-butene/LLDPE-B**.** ***Table 8*** shows the total pressure and the composition of the gas phase for each studied quaternary system. The overall solubility of these two systems will be measured for a pressure up to 6.2 bars and a constant temperature of 70°C. Each experiment was repeated 2-3 times to verify its repeatability. However, the gas phase composition varies slightly between each repeated experiment.

Table 24. *Gas-phase molar composition of the different studied quaternary systems with the magnetic suspension balance, at 70°C*

System	Composition
Ethylene / Propane / 1-butene / LLDPE-B	P_{tot} = [2.5 - 6.2] bar 0.39 < x_{C_3} < 0.42 0.17 < x_{1C_4} < 0.23
Ethylene / Isobutane / 1-butene / LLDPE-B	P_{tot} = [2.5 - 6.5] bar 0.4 < x_{iC_4} < 0.43 0.17 < x_{1C_4} < 0.23

Figure 61 and ***Figure 62*** show the overall solubility of ethylene/propane/1-butene/LLDPE-B and ethylene/isobutane/1-butene/LLDPE-B, respectively, measured with the magnetic suspension balance at 70°C. It is first shown that, as expected, increasing the total pressure increases the overall solubility of both quaternary systems. Furthermore, it is interesting to see that the overall solubility of the quaternary mixture with propane as ICA is higher than the one with isobutane for the same composition of the gas-phase. These results cannot be explained yet since only overall solubilities are available. The partial solubilities of each component in these quaternary systems are needed in order to better understand the different interactions that occur between the gaseous species in the mixture.

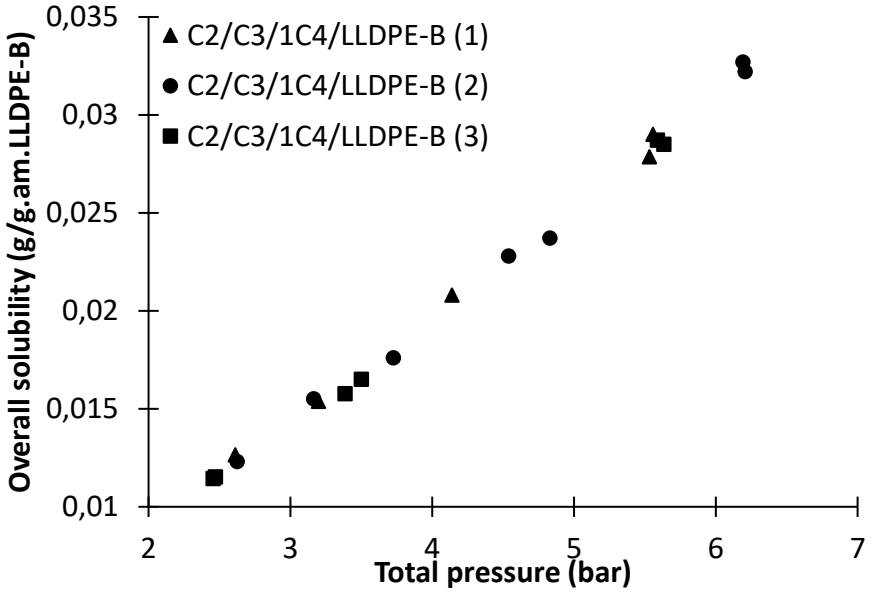

Figure 61. *Overall solubility of quaternary system of ethylene/propane/1-butene/LLDPE-B at 70°C with different composition of the gas-phase. Gas-phase composition for each experiment is* x_{C_3}*=0.42 and* x_{1C_4}*=0.17 for (1),* x_{C_3}*=0.39 and* x_{1C_4}*=0.23 for (2) and* x_{C_3}*=0.34 and* x_{1C_4}*=0.25 for (3)*

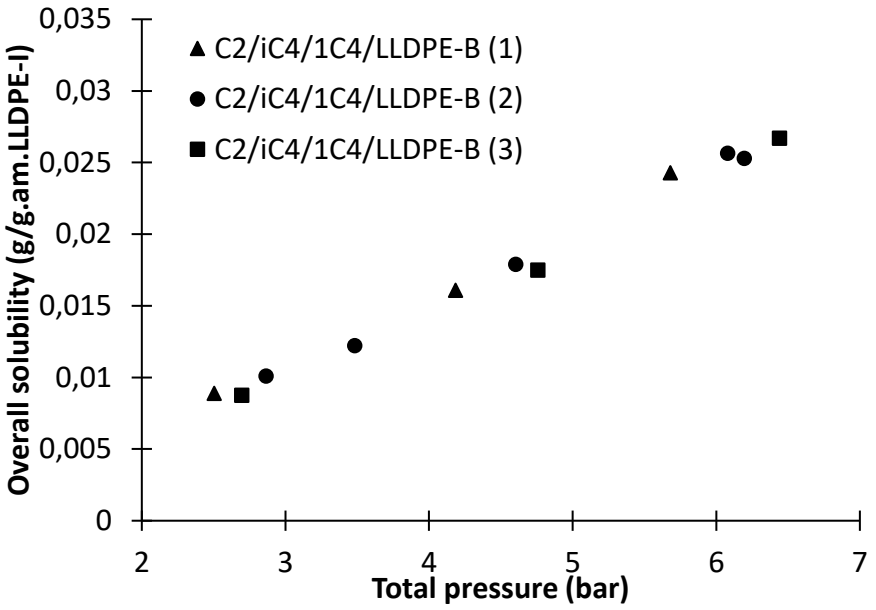

Figure 62. *Overall solubility of quaternary system of ethylene/isobutane/1-butene/LLDPE-B at 70°C with different composition of the gas-phase. Gas-phase composition for each experiment is x_{iC_4}=0.43 and x_{1C_4}=0.17 for (1), x_{iC_4}=0.4 and x_{1C_4}=0.23 for (2) and x_{iC_4}=0.44 and x_{1C_4}=0.21 for (3)*

4.2.3. Validation with SL EoS for quaternary systems

The experimental solubility data achieved using the pressure decay method will be fitted to the SL EoS for quaternary systems in order to identify the interaction parameters needed for SL modeling. Having four experimental data (i.e. overall solubility and partial solubility of the three penetrants) makes it possible to identify the three SL interaction parameters, k_{14}, k_{24}, k_{34}. Note that these k_{ij} are temperature dependent and function of the polymer type. It is therefore interesting to have different PE grades and different temperatures, to see their impact on the identified k_{ij}.

Table 25 shows the identified k_{ij} (representing the interactions between the different penetrants and the polymer) for the studied quaternary systems using pressure decay method. It is shown that these interaction parameters are temperature dependent but are also a function of the type of polymer. ***Figure 63*** shows that the k_{ij} parameters for ethylene/propane/1-butene/LLDPE-I decreases with increasing the temperature. Furthermore, it is shown that the interaction parameter between the lighter component and the polymer is the lowest one, and the interaction parameter between the heavier component and the polymer is the highest one. The same trend was also observed for the ternary systems where the interaction between ethylene and the polymer, k_{13}, was lower than the one between the penetrant and the polymer, k_{23}, for all studied ternary systems.

Table 25. k_{ij} *identified by fitting SL EoS to experimental data through pressure decay method*

System	Temperature (°C)	k_{ij}
Ethylene/Propane/1-Butene/LLDPE-I	69	k_{14} = -0.099 k_{24} = 0.022 k_{34} = 0.081
	84	k_{14} = -0.104 k_{24} = 0.016 k_{34} = 0.074
Ethylene/Propane/1-Butene/HDPE-I	73	k_{14} = -0.048 k_{24} = 0.055 k_{34} = 0.102
Ethylene/Propane/1-Butene/LLDPE-B	70	k_{14} = -0.091 k_{24} = -0.0205 k_{34} = 0.657
Ethylene/Propane/1-Butene/HDPE-B	75	k_{14} = -0.117 k_{24} = 0.019 k_{34} = 0.064

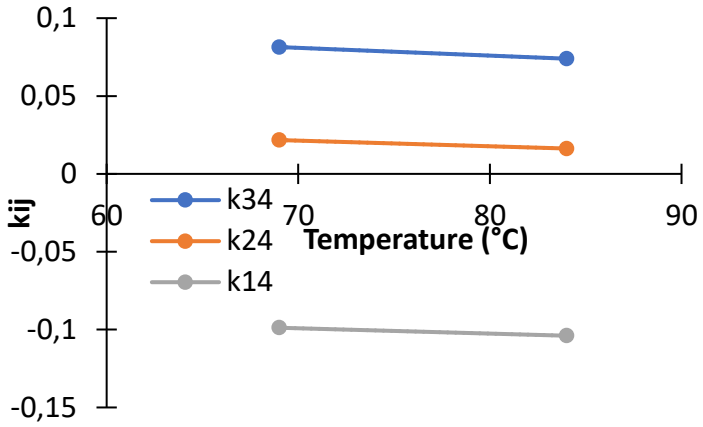

Figure 63. Temperature dependent kij interaction parameters between ethylene (k_{14}), propane (k_{24}), 1-butene (k_{34}) and the polymer for ethylene/propane/1-butene/LLDPE-I quaternary system.

Figure 64-Figure 67 compares the overall and partial solubility measured from the pressure decay experimental method and SL model for quaternary systems using k_{ij} shown in ***Table 9.*** The Sanchez-Lacombe model was extended in order to describe quaternary systems (c.f. Section 3) and the detailed procedure of the model calculation is shown in the Appendix A.

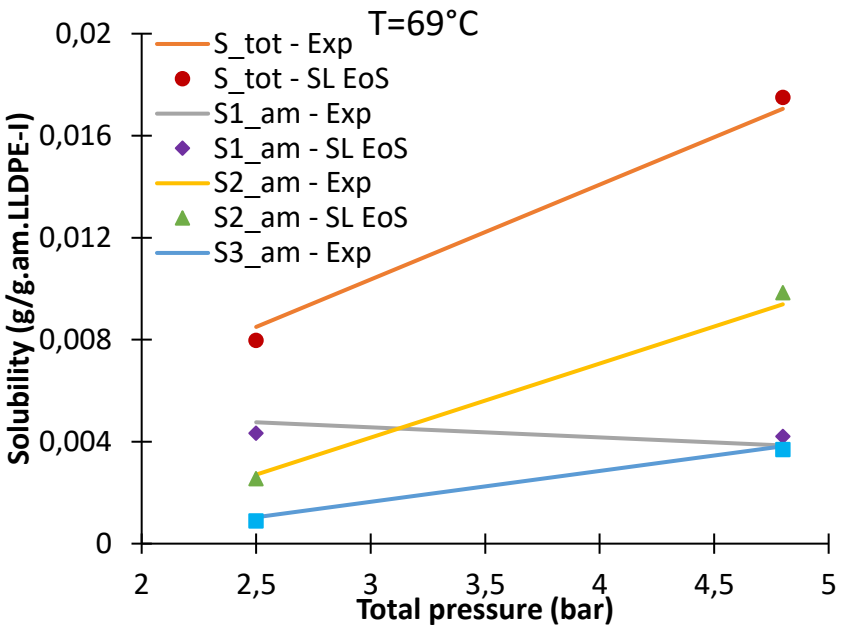

Figure 64. *Experimental and SL modeling of overall and partial solubility of each component in ethylene/propane/1-butene/LLDPE-I at 69°C. Gas phase composition of the mixture is given in* ***Table 23****.* k_{ij} *are given in* **Table 25**

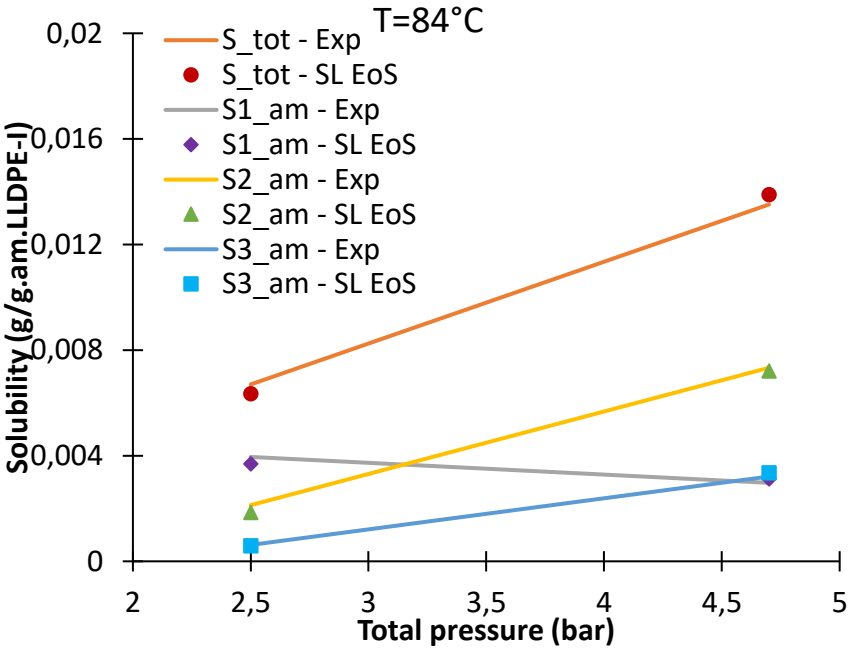

Figure 65. *Experimental and SL modeling of overall and partial solubility of each component in ethylene/propane/1-butene/LLDPE-I at 84°C. Gas phase composition of the mixture is given* ***Table 23****.* k_{ij} *are given in* **Table 25**

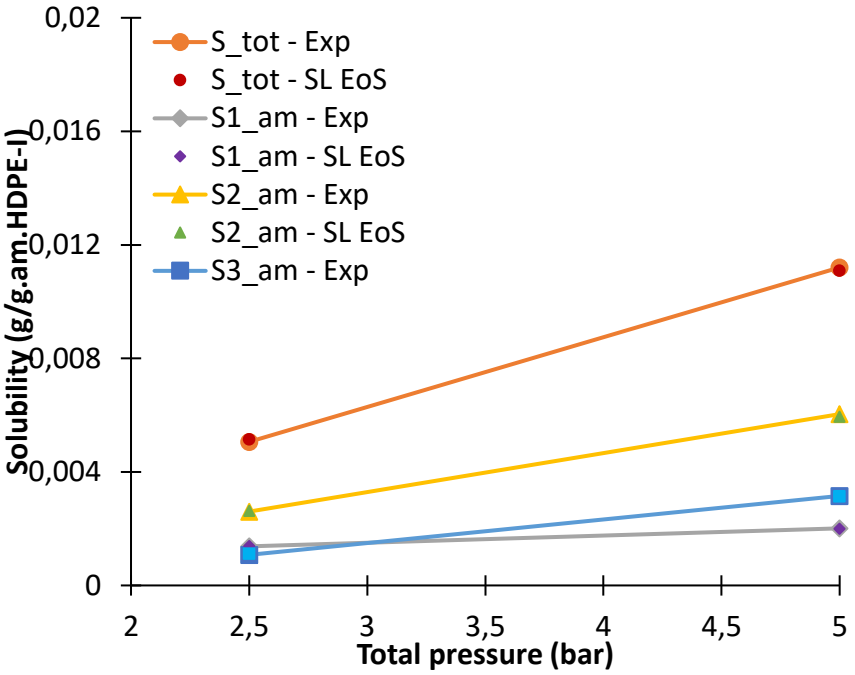

Figure 66. Experimental and SL modeling of overall and partial solubility of each component in ethylene/propane/1-butene/HDPE-I at 73°C. Gas phase composition of the mixture is given in ***Table 23****. k_{ij} are given in* **Table 25**

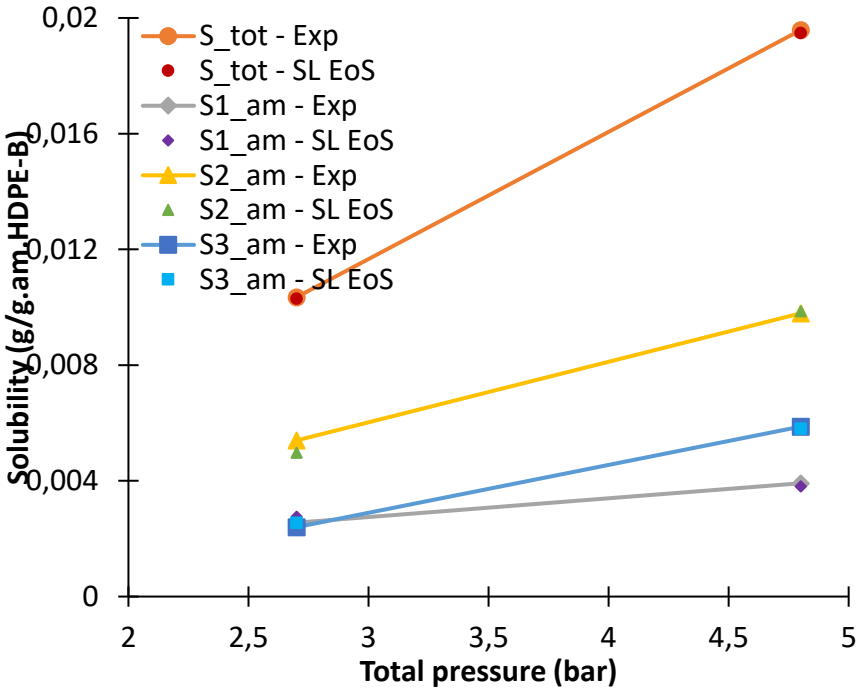

Figure 67. Experimental and SL modeling of overall and partial solubility of each component in ethylene/propane/1-butene/HDPE-B at 75°C. Gas phase composition of the mixture is given in ***Table 23****. k_{ij} are given in* **Table 25**

Concerning the quaternary system of ethylene/propane/1-butene/LLDPE-B performed with the magnetic suspension balance, the overall quaternary solubility is the only measured data. This

information alone could not give the partial solubilities of each component in the gas mixture from SL EoS, even with the combined SL-PR method developed in Chapter 2.

Figure 68 shows the overall solubility of ethylene/propane/1-butene/PE quaternary system normalized by the partial solubility of each component in HDPE-I and LLDPE-I at 73°C, from SL EoS, using the k_{ij} identified in ***Table 9***. Note that both systems with HDPE-I and LLDPE-I have been simulated with the same gas phase composition of the mixture (x_{C_2}=0.66, $x_{C_{3a}}$=0.16 and x_{1C_4}=0.16). The purpose of this simulation is to compare the changes in the partial solubility of the different components in the gas phase mixture in different polyethylene samples (i.e. HDPE-I and LLDPE-I). If the solubility of a component changes in the same relative manner from HDPE-I to LLDPE-I, it is not unreasonable to suppose that the relative solubilities of the same 3 components for a similar gas mixture will be the same in another polymer. It can be seen from ***Figure 68*** that the solubility of the different species in the mixture in both HDPE-I and LLDPE-I follows the same tendency. This means that the same changes in the partial solubility occur, with a difference of 2% for the partial solubility of propane up to 9% for the partial solubility of 1-butene when comparing HDPE-I to LLDPE-I.

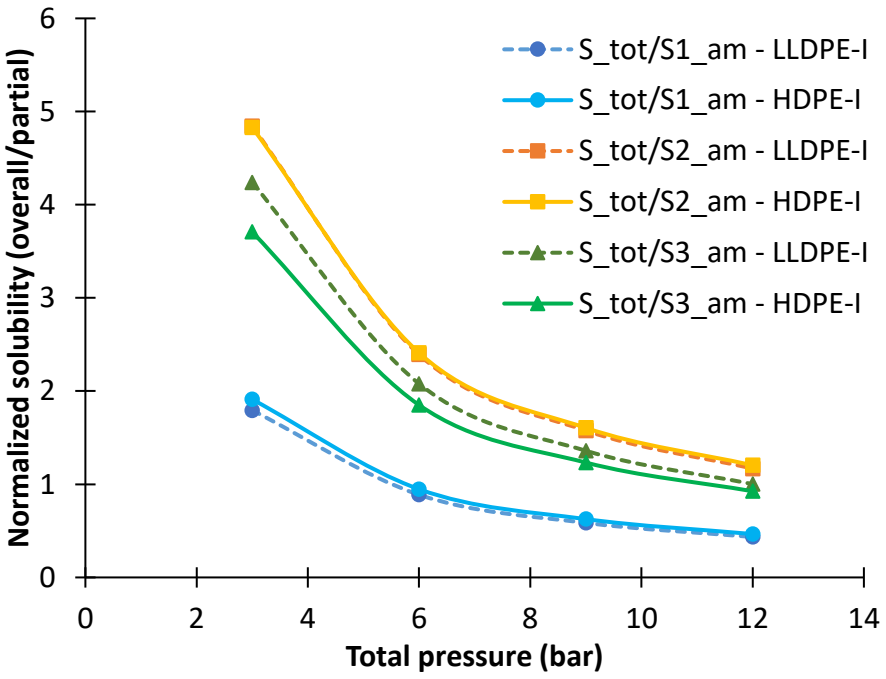

Figure 68. *Overall solubility of ethylene/propane/1-butene/PE quaternary system normalized by the partial solubility of each component in HDPE-I (lines) and LLDPE-I (dotted lines) at 73°C. Gas phase composition for both system is x_{C_2}=0.66, $x_{C_{3a}}$=0.16 and x_{1C_4}=0.16. k_{ij} are given in* **Table 25**

In order to overcome the issues of measuring only the overall solubility when using the gravimetric method, the SL-PR method will be used and combined to the measure of the overall solubility normalized by the partial solubility of the different penetrants in HDPE-B quaternary system. This will permit the calculation of the partial solubilities of the different species in ethylene/propane/1-butene/LLDPE-B system. Gas phase composition of the quaternary system in both HDPE-B and LLDPE-B is given in **Table 23** and ***Table 24*** and it can be seen that almost the same composition have been used for both PE grades. Therefore, we would expect to see the same tendency of the partial solubilities of the different components for both polymers, as can be seen for HDPE-I and LLDPE-I in ***Figure 68***.

The application for the quaternary systems of the SL-PR method combined to the measure of the normalized solubility is shown in ***Figure 69*** where it can be seen that the model fits the data well, with an average difference between the model and the experiments being on the order of 2%. ***Figure 70-Figure 72*** show that the calculated compressibility factors from SL EoS are in good agreement with the ones calculated with Peng-Robinson EoS, with an average difference of 0.24% for ethylene, 0.42% for propane and 0.37% for 1-butene.

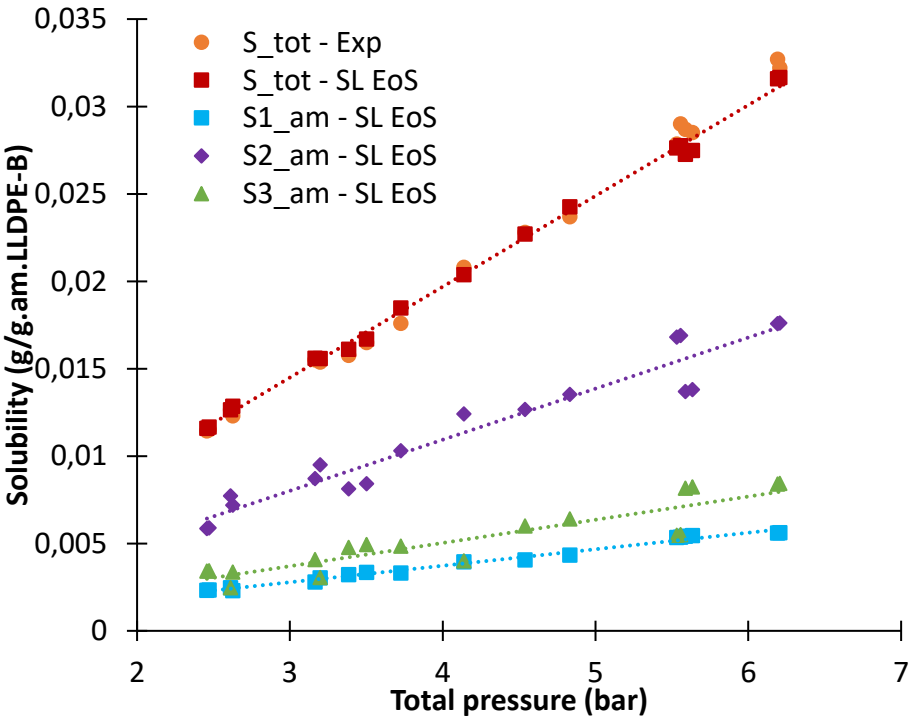

Figure 69. *Experimental and SL modeling of overall and partial solubility of each component in ethylene/propane/1-butene/LLDPE-B at 70°C. Gas phase composition of the mixture is given in* **Table 24.** *k_{ij} are given in* **Table 25**

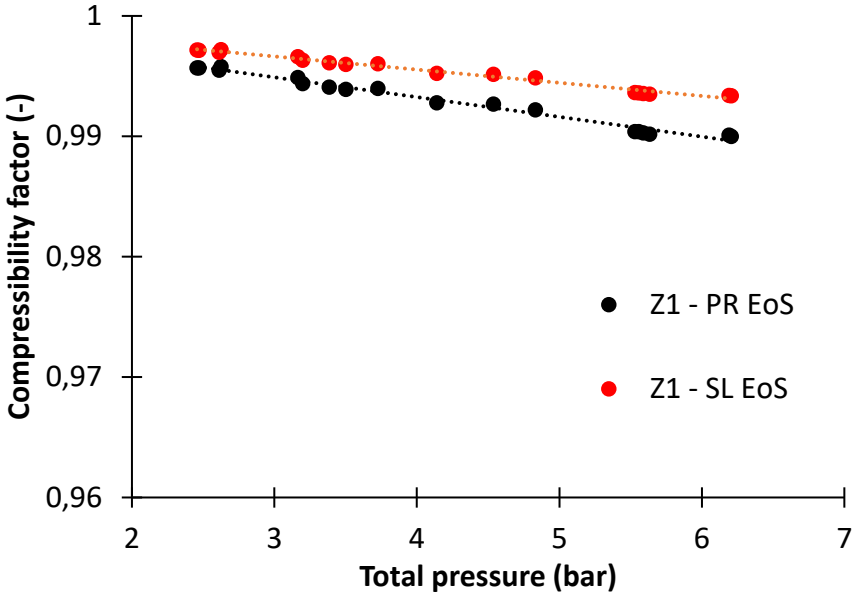

Figure 70. *Compressibility factor of ethylene in $C_2/C_3/1C_4$/LLDPE-B quaternary system at 70°C. The red points represent the compressibility values calculated with Peng-Robinson (Z_1 – PR EoS) and the black points represent the predictions of the compressibility factor from the ternary SL EoS (Z_1 – SL EoS). The dashed lines are simply trend lines to guide the eye.*

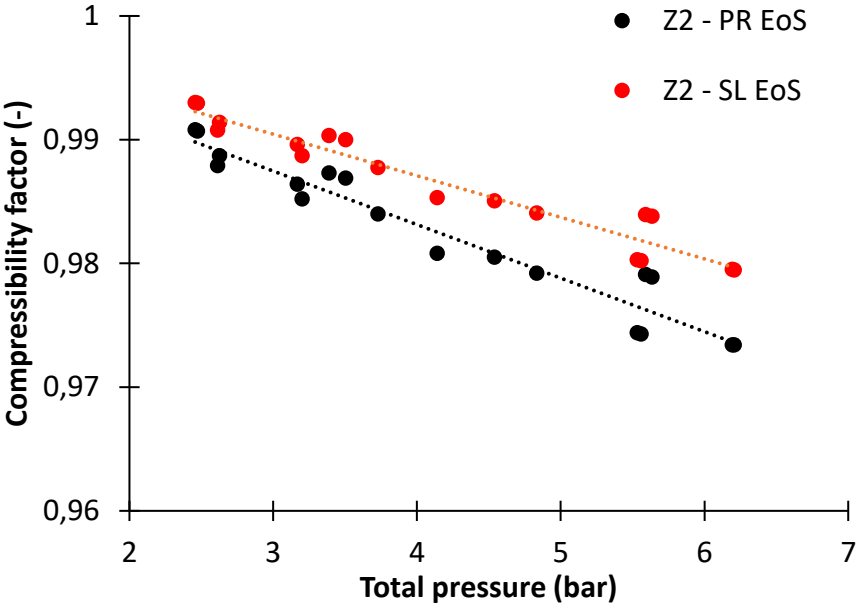

Figure 71. *Compressibility factor of propane in $C_2/C_3/1C_4$/LLDPE-B quaternary system at 70°C. The red points represent the compressibility values calculated with Peng-Robinson (Z_1 – PR EoS) and the black points represent the predictions of the compressibility factor from the ternary SL EoS (Z_1 – SL EoS). The dashed lines are simply trend lines to guide the eye.*

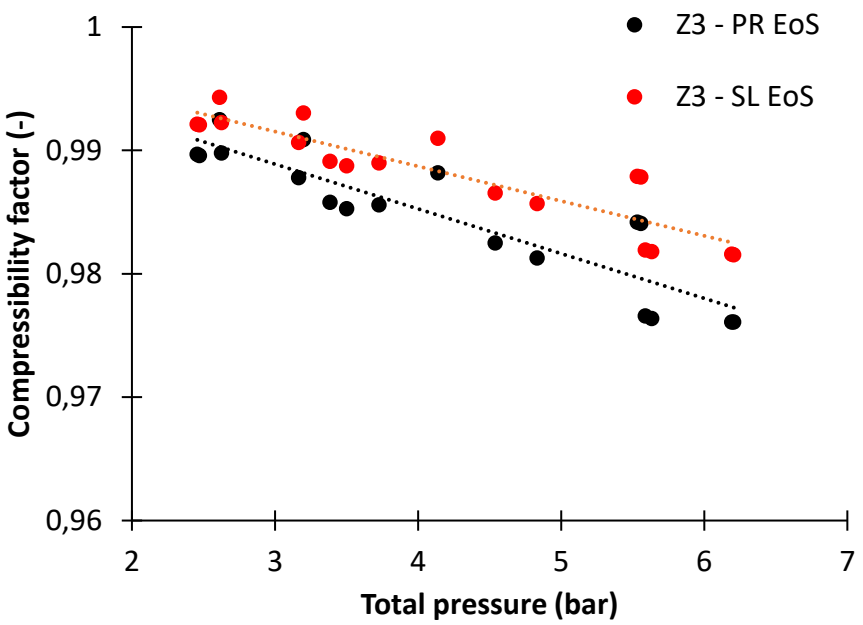

Figure 72. *Compressibility factor of 1-butene in $C_2/C_3/1C_4$/LLDPE-B quaternary system at 70°C. The red points represent the compressibility values calculated with Peng-Robinson (Z_1 – PR EoS) and the black points represent the predictions of the compressibility factor from the ternary SL EoS (Z_1 – SL EoS). The dashed lines are simply trend lines to guide the eye.*

Once the k_{ij} identified, we can therefore model these systems for different gas phase composition in order to better understand the effect of gas phase composition in quaternary systems.

4.2.4. The effect of polymer properties

Let us look briefly at the impact of the polymer properties on the overall solubility of vapors in different types of PE. As discussed above, the more crystalline the polymer is, the lower the solubility of a given penetrant in the amorphous phase is expected to be. This is evident from the graphs in ***Figure 73***. While the temperatures are not identical for all of the experiments in this figure, the difference between the solubility of ethylene/propane/1-butene mixture in LLDPE-B and in HDPE-I cannot be explained by 3°C difference in the temperatures of the two experiments.

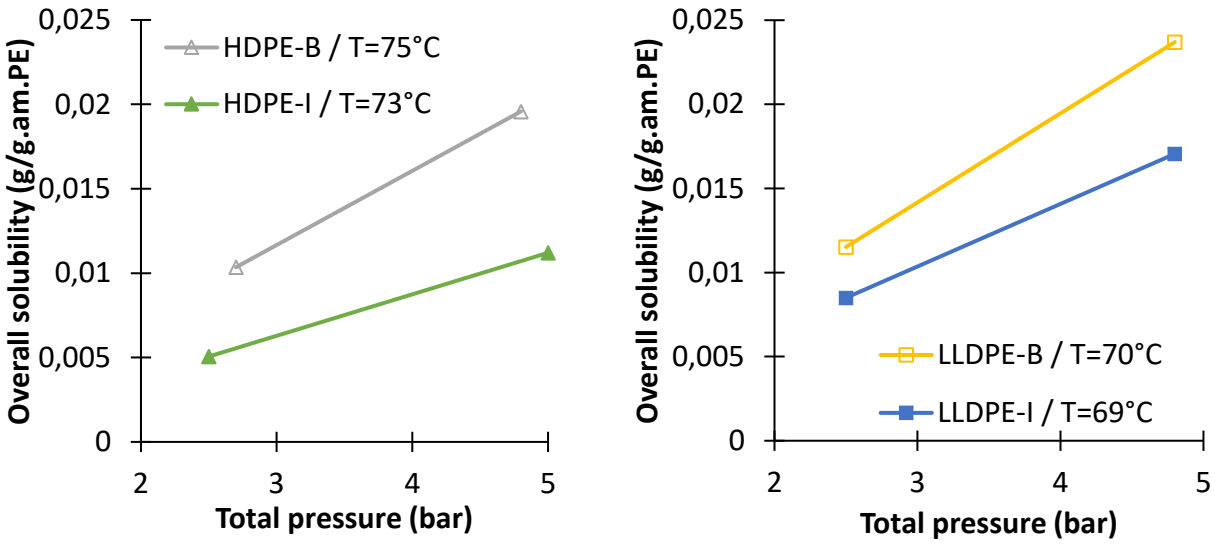

Figure 73. *Overall solubility of ethylene/propane/1-butene in HDPE on the left and LLDPE on the right at different temperatures, using gravimetry for HDPE-B, HDPE-I and LLDPE-I and pressure decay method for LLDPE-B. Gas phase composition is shown in* ***Table 23*** *and* **Table 24**. *PE characteristics are shown in* ***Table 1***

However, differences in the overall crystallinity of a sample, especially measured at room temperature are not enough to explain the differences observed in ***Figure 73***. For instance, both of the LLDPE have almost the same global crystallinity, as do the two HDPE powders. Note that the thermograms of the LLDPE-B and LLDPE-I in ***Figure 30*** have different shapes, indicating that there are clearly going to be differences in the macromolecular architectures of the different polymers. However, if one considers the HDPE products, the differences in the thermograms are not particularly striking, yet there is at least as much difference in the total solubility of the gaseous mixture in the two HDPE products as in the two LLDPE products. It is therefore unlikely that the degree of crystallinity alone can be responsible for the observed differences in the solubility. Where one can see a difference between the two LLDPE and the two HDPE is in the molecular weight distributions, shown in ***Figure 74***. HDPE-B and LLDPE-B have broader molecular weight distribution compared to HDPE-I and LLDPE-I. It is possible that the broader molecular weight distribution has a different molecular structure (less homogeneous) that favors the sorption of penetrants. Note that we are not proposing that a difference in chain length is directly responsible for the solubility differences, but rather something linked to the organization of the chains in the matrix that is correlated with the solubility. The polydispersity of the "I" polymers is very low, going from just over 2 for the LLDPE-I to 3 for the HDPE-I. While no information is available on the type of catalyst used to make these products, one would suspect from these polydispersity values that a metallocene

catalyst was used to make them. It is well known that one characteristic of polymers made with metallocenes is that this type of catalyst is a uniform incorporator of comonomer – in other words all polymer chains have the same chemical composition. On the other hand, it is reasonable to propose that the "B" polymers, with polydispersities on the order of 8.8 for the LLDPE-B and 10.9 for the HDPE-B, are made with a Ziegler-type catalyst. Ziegler catalysts are known to have a non-uniform incorporation of comonomers, with the shorter chains containing more comonomer than the longer ones. Is it possible that the difference in terms of the homogeneity of chain structure can lead to a different organization of the amorphous phase, where higher degrees of inhomogeneity favor the swelling of the amorphous phase more than is the case in homogeneously organized polymers? Obviously, the observations shown here do not permit us to interpret the results to this degree, but a future study linking different facets of macromolecular architecture to the swelling of the amorphous phase might be interesting and useful.

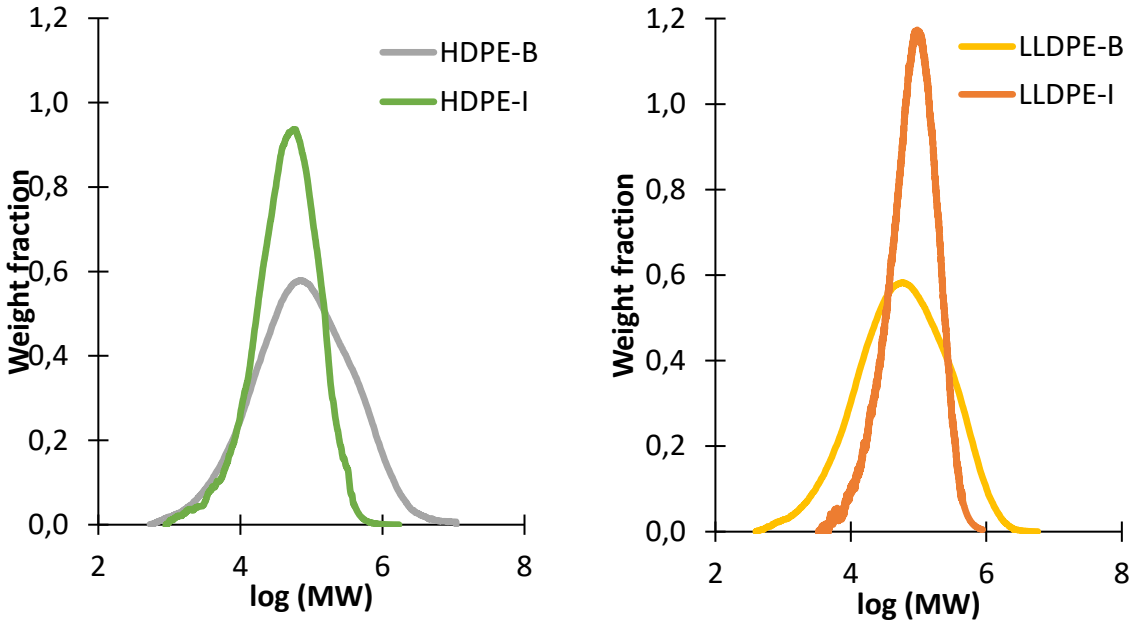

Figure 74. Molecular weight distribution of the different used PE samples performed with the HT-GPC

4.3.Importance of describing quaternary systems

The co- and anti-solubility effects are obviously going to be somewhat more complex in multicomponent mixtures, but once the kij have been identified (*Table 25*) can model the solubility to obtain some insight into the effect of gas phase composition in quaternary systems.

4.3.1. Effect of ICA on quaternary systems

A comparison between the ternary system of ethylene/1-butene/LLDPE-I and the quaternary system of ethylene/propane/1-butene/LLDPE-I at 80°C will be achieved in this section. The effect of propane as ICA will be highlighted, in order to see its effect on the overall quaternary solubility as well as on the partial solubility of the different components in the mixture. To do so, two simulations were performed: the first one was to keep ethylene molar fraction constant and the second one was to keep 1-butene molar fraction constant, by maintaining the same total pressure of the system, with respect to the ternary system. Therefore, the same molar fraction of propane, x_{C3a}=0.16, was used for both simulations. In order to simulate the quaternary system at 80°C with SL EoS. A temperature dependent correlation of the k_{ij} interaction parameter for ethylene/propane/1-butene/LLDPE-I system was obtained from ***Table 9,*** and gives k_{14}=-0.0992, k_{24}=0.0147 and k_{34}=0.0758. The k_{ij} for the ternary systems at 80°C were taken from the temperature correlations given in ***Table 20.***

Figure 75-Figure 77 show the overall and partial solubilities of ethylene and of 1-butene, respectively, for the ternary ethylene/1-butene/LLDPE-I and quaternary ethylene/propane/1-butene/LLDPE-I systems, at 80°C. ***Figure 75*** shows that adding propane to the ternary ethylene/1-butene/LLDPE-I system decreases the overall solubility. Besides, it is shown that higher fraction of ethylene and therefore smaller fraction of 1-butene leads to a lower overall solubility of the quaternary system, about 28% (i.e. green line) compared to 12% (i.e. orange line). In order to better interpret these trends, it is better to look at the partial solubilities of ethylene and 1-butene in order to understand the different interactions that occurs between the species in the quaternary system. ***Figure 76*** shows that adding propane to the ternary ethylene/1-butene/LLDPE-I system leads to a decrease of ethylene partial solubility. This is not an expected result as we have seen for ternary systems that heavier alkanes acts as co-solvents for the lighter ones (i.e. ethylene), and therefore increasing the solubility of the lighter component in the amorphous phase of the polymer. However, the trends in ***Figure 77*** follows what we have seen in the ternary systems concerning anti-solvent effect. ***Figure 77*** shows that adding propane to the ternary ethylene/1-butene/LLDPE-I system leads to a decrease in the partial solubility of 1-butene. This can be explained by the anti-solvent effect of propane (i.e. lighter component) on 1-butene (i.e. heavier component), leading to a decrease of the partial solubility of the heavier component in the system. To conclude, it has been shown that propane decreases both ethylene and 1-butene partial solubility when added in quaternary system,

leading to a decrease of the overall solubility of the quaternary mixture in the amorphous phase of the polymer.

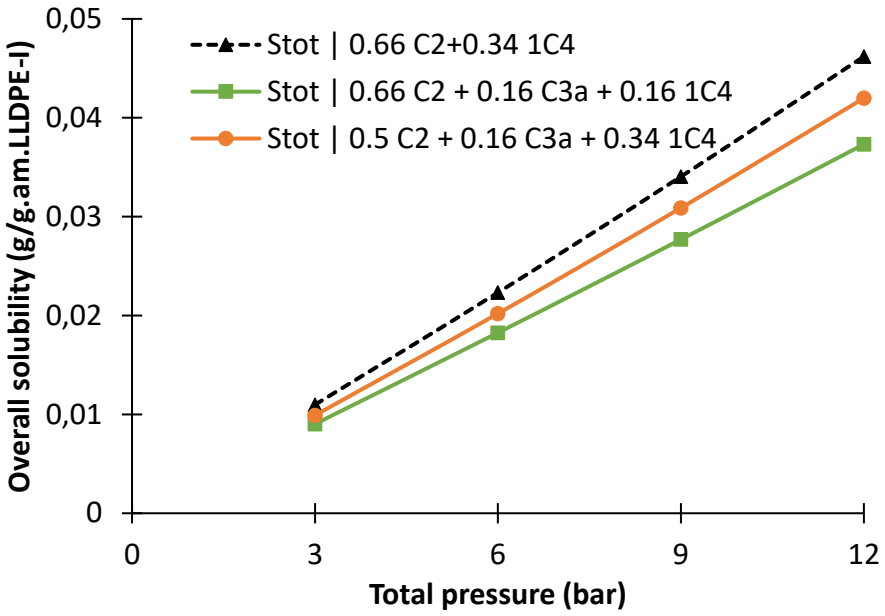

*Figure 75. Overall solubility calculated from SL EoS for ethylene/1-butene/LLDPE-I ternary system and for ethylene/propane/1-butene/LLDPE-I quaternary system at 80°C. k_{ij} for the ternary system was taken from **Table 20** and for the quaternary system from* **Table 25**

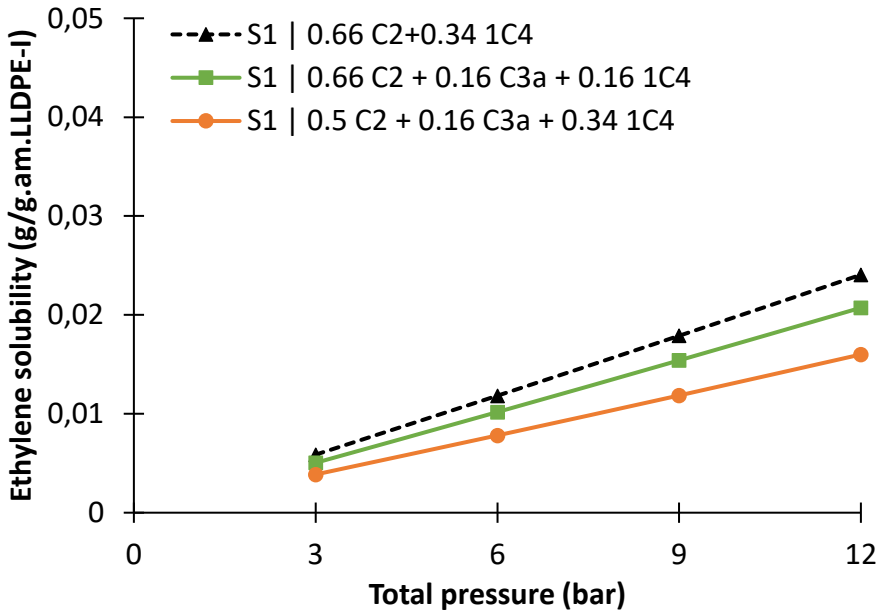

*Figure 76. Ethylene partial solubility calculated from SL EoS for ethylene/1-butene/LLDPE-I ternary system and for ethylene/propane/1-butene/LLDPE-I quaternary system at 80°C. k_{ij} for the ternary system was taken from **Table 20** and for the quaternary system from* **Table 25**

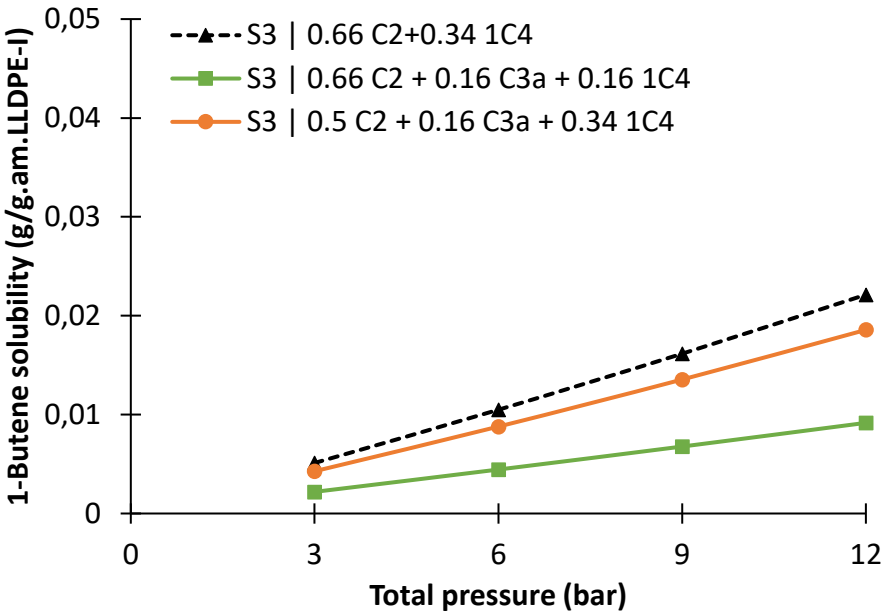

Figure 77. *1-Butene partial solubility calculated from SL EoS for ethylene/1-butene/LLDPE-I ternary system and for ethylene/propane/1-butene/LLDPE-I quaternary system at 80°C. k_{ij} for the ternary system was taken from* ***Table 20*** *and for the quaternary system from* **Table 25**

4.3.2. Effect of comonomer on quaternary systems

In this section, the comparison of the ternary system of ethylene/propane /LLDPE-I and the quaternary system of ethylene/propane/1-butene/LLDPE-I at 80°C will be examined. The effect of 1-butene as comonomer will be underlined. As in the previous section, the same simulations will be performed: keeping ethylene molar fraction constant first, and then keeping 1-butene molar fraction constant, by maintaining the same total pressure of the system, with respect to the ternary systems. The same mole fraction of 1-butene, x_{C3a}=0.16, is used for both simulations. The k_{ij} interaction parameter for ethylene/propane/1-butene/LLDPE-I system at 80°C are given in the previous section. The k_{ij} for the ternary systems at 80°C were taken from the temperature correlations given in ***Table 20.***

Figure 78-Figure 80 show the overall and partial solubilities of ethylene and of propane, respectively, for the ternary ethylene/propane /LLDPE-I and quaternary ethylene/propane/1-butene/LLDPE-I systems, at 80°C. ***Figure 78*** shows that adding 1-butene to the ternary ethylene/propane /LLDPE-I system leads to an increase in the overall solubility of the quaternary system to about 18% for the simulated system having higher fraction of ethylene (i.e. green line) and 30% for a higher fraction of propane (i.e. orange line). Contrarily to propane behavior shown in the previous section, adding 1-butene to the ternary system leads a significant increase of the overall solubility. This increase can be explained by looking at the

partial solubility of the different component in the gaseous mixture. ***Figure 79*** demonstrates the effect of adding 1-butene in the ternary system on the partial solubility of ethylene in the amorphous phase of the polymer. It is shown that adding 1-butene leads to an increase of the partial solubility of ethylene, demonstrating the co-solvent effect of 1-butene on ethylene. ***Figure 80*** shows the effect of adding 1-butene in the ternary system on the partial solubility of propane. It is shown that, when keeping ethylene molar fraction constant, adding 1-butene to the ternary system decreases propane partial solubility in the amorphous phase of the polymer to about 54%. This is not what we expected to see, as we would suppose that 1-butene which is the heavier component acts as a co-solvent towards propane, whereas the results shows that 1-butene acts as an anti-solvent to propane, decreasing its partial solubility in the amorphous phase of the polymer. However, adding 1-butene to the ternary system and decreasing ethylene molar fraction in the quaternary system leads to an increase of the partial solubility of propane.

It is clear that as we increase the number of components in the system (i.e. quaternary and higher order systems), the competing co- and anti-solvent effects make it difficult to estimate the impact of each component on the solubility *à priori*. In fact, this demonstrates the need for the type of thermodynamic model proposed here, and also suggests that more extensive measurements need to be made.

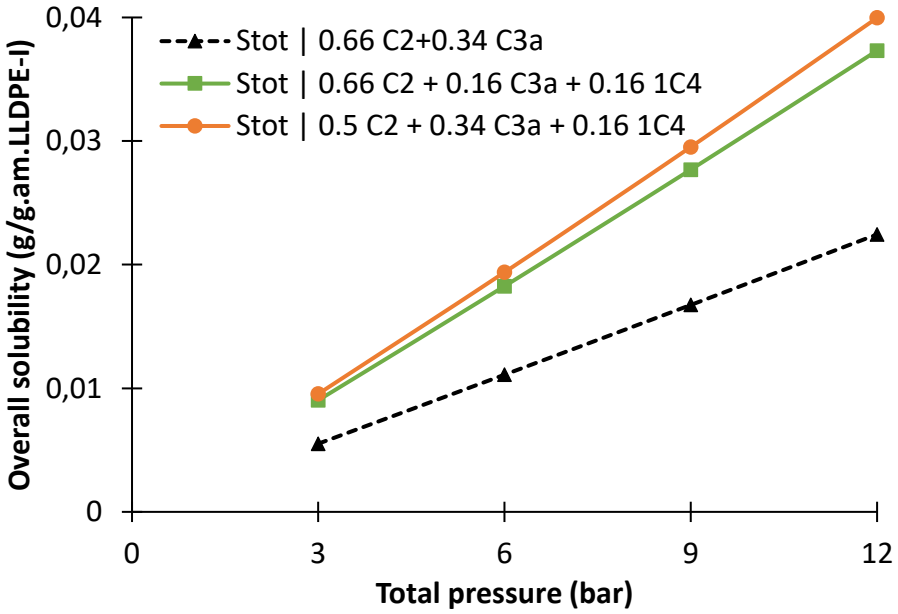

Figure 78. *Overall solubility calculated from SL EoS for ethylene/propane /LLDPE-I ternary system and for ethylene/propane/1-butene/LLDPE-I quaternary system at 80°C. k_{ij} for the ternary system was taken from* ***Table 20*** *and for the quaternary system from* **Table 25**

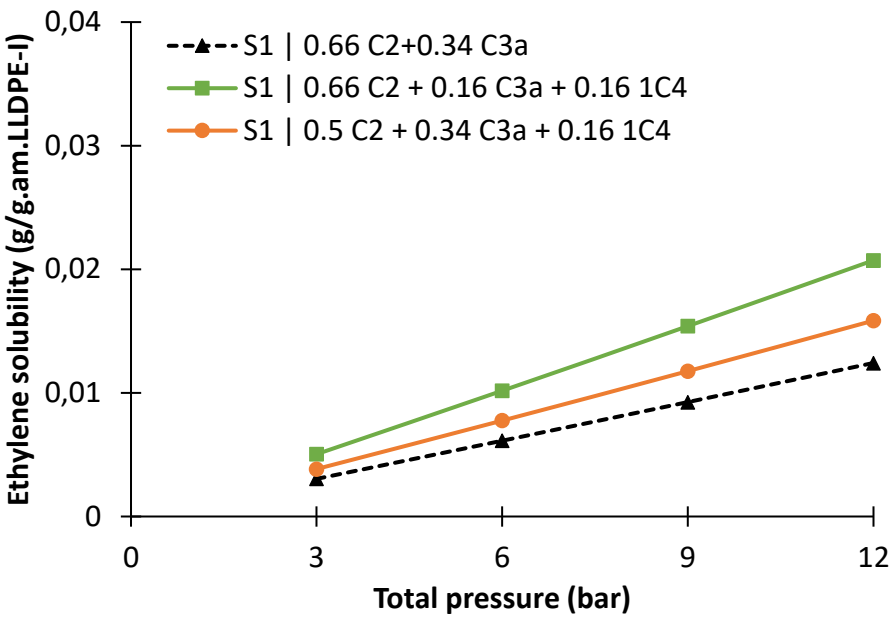

Figure 79. *Ethylene partial solubility calculated from SL EoS for ethylene/propane /LLDPE-I ternary system and for ethylene/propane/1-butene/LLDPE-I quaternary system at 80°C. k_{ij} for the ternary system was taken from* ***Table 20*** *and for the quaternary system from* **Table 25**

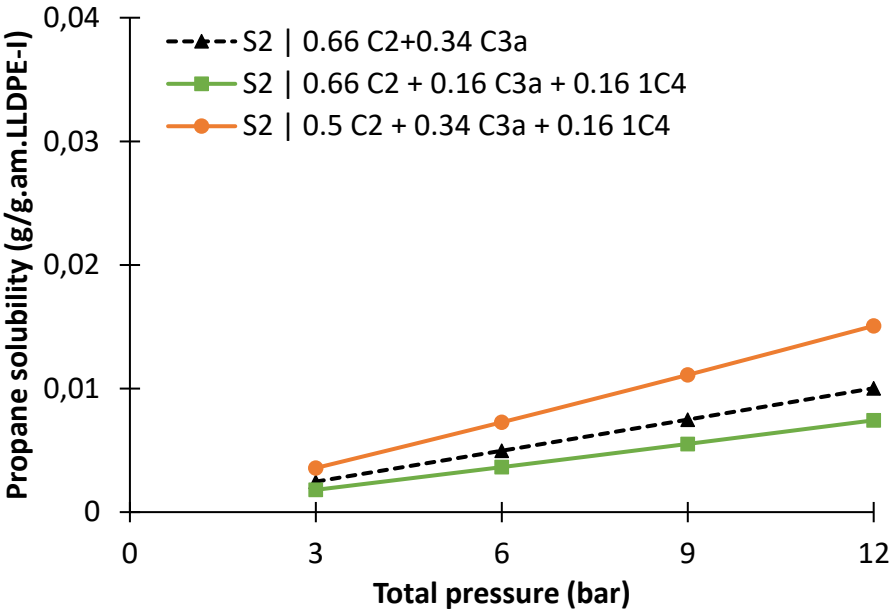

Figure 80. *Propane partial solubility calculated from SL EoS for ethylene/propane /LLDPE-I ternary system and for ethylene/propane/1-butene/LLDPE-I quaternary system at 80°C. k_{ij} for the ternary system was taken from* ***Table 20*** *and for the quaternary system from* **Table 25**

5. Conclusion

The solubility of ternary and quaternary polyolefin systems has been studied experimentally and theoretically. The solubility of ternary systems of ethylene/propane/LLDPE, ethylene/propylene/LLDPE and ethylene/1-butene/LLDPE have been measured experimentally using the pressure decay method at temperatures between 68 - 90°C and a total pressure up to 8 bars. The quaternary system of ethylene/propane/1-butene in different PE grades and at temperatures between 69 - 84°C and a total pressure up to 7 bars have been studied using pressure decay and gravimetric methods. The Sanchez-Lacombe EoS have been used in order to interpret the experimental results. An important data base of the solubilities of the ternary and more importantly the quaternary systems, as well as the k_{ij} interaction parameters from SL EoS, have been provided in this Chapter. It is important to note that these interaction parameters are valid for the range of pressure and temperature used during this study, and some changes might occur if very low temperatures and/or high pressures are used to describe the studied systems. Besides, the quaternary studied sorption represents an important contribution to the modelling of olefin polymerizations since it is the first time in the open literature that the solubilities of quaternary polyolefin systems are studied under conditions approaching those found in industry.

For ternary systems, it was demonstrated that, as expected, the heavier component acts as a co-solvent to the lighter one, and that the lighter component acts as an anti-solvent to the heavier one. Furthermore, it has been shown that the heavier the component is, the stronger is its co-solvent effect. It has also been revealed that the co-solvent effect has a more significant impact than the anti-solvent effect on the overall solubility. Finally, it has been shown that the heavier the component is, the stronger is its co-solvent effect, leading therefore to an important increase in the overall solubility of the system in the amorphous phase of the polymer.

Concerning quaternary systems, it has been shown that the overall solubility of the quaternary system of ethylene/propane/1-butene/LLDPE is higher than the one in the ternary system of ethylene/propane/LLDPE and lower than the one in the ternary system of ethylene/1-butene/LLDPE at the same temperature and total pressure. The obtained results from the quaternary studied systems demonstrate that the complexity of the changes in the gas phase composition needs to be interpreted by an accurate thermodynamic model. To do so, more experimental data is needed in order to be able to identify the SL interaction parameters. It would therefore be interesting to look at the effect of other quaternary systems involving for example other ICAs (i.e. isobutane, n-hexane) and other comonomers (i.e. 1-hexene) in order

to compare the effect of the different ICAs and co-monomers, and their combination, on the overall solubility in quaternary systems. Besides, it would be helpful to study the ternary system of propane/1-butene/LLDPE in order to better understand the effect of ethylene on the studied quaternary system.

As expected, the crystallinity of the polymer used in the solubility study has at least as much impact on the solubility of penetrants in the amorphous phase as the composition of the vapour phase mixture does. However, we unexpectedly found that for polymers with the same overall crystallinity, one can observe significant differences in the overall solubility of a gas mixture. In the current study, it was observed that polymers having a significantly broader MWD had higher solubilities than did polymers of similar crystallinity but with narrow MWD. It was postulated that this difference in solubility might be attributable to differences in the chain architecture, attributable to the catalyst used to make the polymers. However, it should be made clear that there is not yet any strong evidence to support this proposition, so it should be viewed more as a testable hypothesis for future studies than a real explanation.

6. References

1. Yao, W., Hu, X. & Yang, Y. Modeling the solubility of ternary mixtures of ethylene,iso-pentane,n-hexane in semicrystalline polyethylene. *J. Appl. Polym. Sci.* **104**, 3654–3662 (2007).

2. McKenna, T. F. Solubility and crystallinity data for ethylene/polyethylene systems. *European Polymer Journal* **34**, 1255–1260 (1998).

3. Novak, A. *et al.* Ethylene and 1-hexene sorption in LLDPE under typical gas-phase reactor conditions: Experiments. *J. Appl. Polym. Sci.* **100**, 1124–1136 (2006).

4. Chmelař, J., Haškovcová, K., Podivinská, M. & Kosek, J. Equilibrium Sorption of Propane and 1-Hexene in Polyethylene: Experiments and Perturbed-Chain Statistical Associating Fluid Theory Simulations. *Ind. Eng. Chem. Res.* **56**, 6820–6826 (2017).

5. Yao, W., Hu, X. & Yang, Y. Modeling solubility of gases in semicrystalline polyethylene. *J. Appl. Polym. Sci.* **103**, 1737–1744 (2007).

6. Moore, S. J. & Wanke, S. E. Solubility of ethylene, 1-butene and 1-hexene in polyethylenes. *Chemical Engineering Science* **56**, 4121–4129 (2001).

7. Savatsky, B. J., Moebus, J. A. & Greenhalgh, Brian. R. Parameterization of Models for Vapor Solubility in Semicrystalline Polyethylene. *Macromol. React. Eng.* **13**, 1900003 (2019).

8. Kanellopoulos, V., Mouratides, D., Pladis, P. & Kiparissides, C. Prediction of Solubility of α-Olefins in Polyolefins Using a Combined Equation of State Molecular Dynamics Approach. *Ind. Eng. Chem. Res.* **45**, 5870–5878 (2006).

9. Yoon, J.-S., Yoo, H.-S. & Kang, K.-S. Solubility of α-olefins in linear low density polyethylenes. *European Polymer Journal* **32**, 1333–1336 (1996).

10. Moebus, J. A. & Greenhalgh, B. R. Modeling Vapor Solubility in Semicrystalline Polyethylene. *Macromol. React. Eng.* **12**, 1700072 (2018).

11. Bashir, M. A., Kanellopoulos, V., Al-haj Ali, M. & McKenna, T. F. L. Applied Thermodynamics for Process Modeling in Catalytic Gas Phase Olefin Polymerization Reactors. *Macromol. React. Eng.* **14**, 1900029 (2020).

12. Sato, Y. *et al.* Vapor–liquid equilibrium ratios for hexane at infinite dilution in ethylene+impact polypropylene copolymer and propylene+impact polypropylene copolymer. *Fluid Phase Equilibria* **170**, 49–67 (2000).

13. Kröner, T. & Bartke, M. Sorption of Olefins in High Impact Polypropylene – Experimental Determination and Mass Transport Modeling. *Macromolecular Reaction Engineering* **7**, 453–462 (2013).

14. Cancelas, A. J. *et al.* Solubility and Diffusivity of Propylene, Ethylene, and Propylene-Ethylene Mixtures in Polypropylene. *Macromol. Chem. Phys.* **219**, 1700565 (2018).

15. Sato, Y. *et al.* Solubility and Diffusion Coefficient of Carbon Dioxide in Biodegradable Polymers. *Ind. Eng. Chem. Res.* **39**, 4813–4819 (2000).

16. Alizadeh, A. *et al.* Modeling Condensed Mode Operation for Ethylene Polymerization: Part I. Thermodynamics of Sorption. *Ind. Eng. Chem. Res.* **56**, 1168–1185 (2017).

17. Sanchez, I. C. & Lacombe, R. H. An elementary molecular theory of classical fluids. Pure fluids. *J. Phys. Chem.* **80**, 2352–2362 (1976).

18. Bashir, M. A., Ali, M. A., Kanellopoulos, V. & Seppälä, J. Combined EoS and elastic constraints models to predict thermodynamic properties for systems involving semi-crystalline polyolefins. *Fluid Phase Equilibria* **388**, 107–117 (2015).

19. Pedrosa, N., Vega, L. F., Coutinho, J. A. P. & Marrucho, I. M. Phase Equilibria Calculations of Polyethylene Solutions from SAFT-Type Equations of State. *Macromolecules* **39**, 4240–4246 (2006).

20. Lacombe, R. H. & Sanchez, I. C. Statistical thermodynamics of fluid mixtures. *J. Phys. Chem.* **80**, 2568–2580 (1976).

21. Chmelar, J., Haškovcová, K., Podivinská, M. & Kosek, J. Equilibrium sorption of propane and 1-hexene in polyethylene: experiments and PC-SAFT simulations. *Industrial & Engineering Chemistry Research* **56**, (2017).

22. Banaszak, B. J. *et al.* Ethylene and 1-Hexene Sorption in LLDPE under Typical Gas Phase Reactor Conditions: A Priori Simulation and Modeling for Prediction of Experimental Observations. *Macromolecules* **37**, 9139–9150 (2004).

23 Bashir, M.A.; Monteil, V.; Kanellopoulos, V.; Al-Haj Ali, M.; McKenna, T.F.L. Estimating Partial Molar Volumes of Penetrants and Polymers in Macromolecular Mixtures using Mixture Densities Predicted by Sanchez-Lacombe Equation of State, *Ind. Eng. Chem. Res.*, **2013**, *52*, 16491

Chapter 4

Diffusivity of Multicomponent Gas Mixtures in Polyethylene

1. Introduction

As was discussed in the previous chapters, there is a significant lack of data concerning both solubility and diffusivity of multicomponent gas phase mixtures. This information is crucial for a better understanding of mass transfer and concentrations of reactive species in the growing polymer particles during gas phase ethylene polymerization. It has been shown in the literature[1,2] that accounting for the co-solubility and co-diffusivity effects can help to explain the increase in the productivity. The sorption of multiple species can change the way that they interact with the amorphous phase of the polymer. Furthermore, the solubility of the different species will have an impact on the free volume of the amorphous phase of the polymer, which in turn can influence the diffusivities of the penetrants in the system. Indeed, it has also been shown that taking into account the interactions between the different species when calculating the diffusion coefficients improves the capacity of single particle models to explain high initial rates of polymerization in the presence of ICAs[1]. It is therefore crucial to have more experimental and theoretical studies about the diffusion of mixtures of penetrants in the polymer amorphous phase since it has a great importance in ethylene polymerization reaction in gas phase.

For this reason, the diffusivity of binary, ternary and quaternary systems will be studied experimentally and theoretically in the current Chapter. The overall diffusivity of ternary systems such as ethylene/propane/LLDPE-B, ethylene/isobutane/LLDPE-B and ethylene/1-butene/LLDPE-B at 70°C will be studied and compared to the binary ethylene/LLDPE-B system. Then, the quaternary overall diffusivity of ethylene/propane/1-butene/LLDPE-B and ethylene/isobutane/1-butene/LLDPE-B will be investigated at 70°C and compared to ternary diffusivity. These studies will therefore help to understand the interactions between the different penetrants in order to have a more realistic description of the diffusivity when modeling ethylene polymerization in gas phase. To the best of our knowledge, this is the first time that the diffusivity is investigated for such ternary and quaternary systems.

2. Diffusivity measurements

2.1.Gravimetric method

A gravimetric method is used to measure the overall diffusivity of the different studied systems. The experimental set-up is briefly described in Chapters 2 and 3. From the pressure, temperature, time and sample mass that are acquired during the sorption experiments, we can obtain the sorption curve as a function of time, as can be shown in ***Figure 81***. The equilibrium solubility of the penetrant(s) can be obtained from the sorbed mass at steady state. The rate of sorption during the transient initial phase can be used to estimate the total diffusivity of the same system.

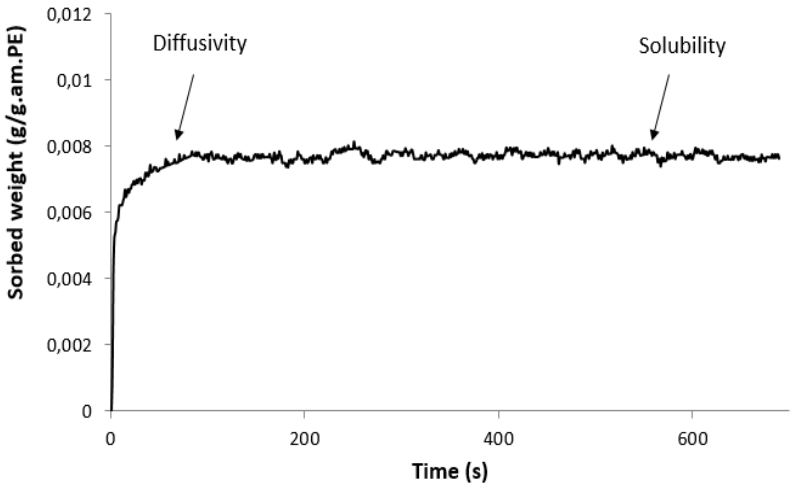

Figure 81.*Sorbed weight measured with a magnetic suspension balance*

2.2. Fickian diffusion in spherical particles

One way of interpreting the transient portion of the sorption curve is to use Crank's solution to the dynamic form of Fick's law[12]. Indeed, it has been shown that this model predicts well the shape of the experimentally measured degassing curves for compact polyolefin particles (in other words, homogeneous spheres). Crank's solution to Fick's law in spherical coordinates is written as:

$$\frac{M_t}{M_\infty} = 1 - \frac{6}{\pi^2}\sum_{n=1}^{\infty}\frac{1}{n^2}exp\left(-Dn^2\pi^2\frac{t}{r^2}\right)$$

Where M_t is the mass sorbed at a given time t, M_∞ is the total mass sorbed at equilibrium, D is the diffusivity of the process gases, r is the average radius of the polymer powders. From an

experimental point of view, this means that if we know *D,* we can use the sorption experiments to calculate the characteristic length scale for diffusion, *r*. And of course, the reverse method is also true.

Bobak et al.[13] and Zubov et al.[14] noticed that applying this solution did not yield to satisfactory results for porous particles. Indeed, they found that Fick's law with a single value of *D* and of *r* was not capable of predicting the shape of the degassing curves. This approach could fit either the rapid rise in the mass sorbed, or the slower transition toward steady state, but not both. This was assumed to be due to the fact that the polymer particle is supposed to be an agglomerate of smaller granules having different sizes (so different surface areas). As an approximation of these properties, they proposed a particle model including two sizes of compact polymer granules, one with a small radius and one with a larger radius in order to better fit the experimental sorbed weight. This particle model with two sizes of granules will be used in this study. As we will see below, this is a satisfactory way to account for both the initial quick increase of the sorbed weight caused by the presence of a certain fraction of small granules of radius r_S with high exchange surface area, as well as the following slower increase of the sorbed weight caused by the big granules of radius r_B. This is of course not strictly true, as the size of particles is much more distributed and it is likely that the structure of particles in the powder is more complex (and can vary from particle to particle). However, as we will see, the aforementioned authors were correct to assume that a minimum of two "families" of particle substructures is required to be representative of mass transfer in these powders. We will assume for this study that mass transport resistance in the particle pores is negligible (so the pores are assumed to be at the bulk concentration instantaneously). Therefore, the experimental measured sorbed weight relates only to the sorbed mass of penetrants in the polymer phase.

In this case, assuming that small and big spheres have the same diffusivity, Crank's equation for the mass uptake in a heterogeneous particle is defined as follows:

$$\frac{M_t^{tot}}{M_\infty^{tot}} = w_1\left[1 - \frac{6}{\pi^2}\sum_{n=1}^{\infty}\frac{1}{n^2}exp\left(-Dn^2\pi^2\frac{t}{{r_S}^2}\right)\right] + (1-w_1)\left[1 - \frac{6}{\pi^2}\sum_{n=1}^{\infty}\frac{1}{n^2}exp\left(-Dn^2\pi^2\frac{t}{{r_B}^2}\right)\right]$$

Where r_S and r_B are the radii of small and big granules, respectively and w_1 and w_2 are the weight fractions of small and big granules, respectively. We will discuss below how the representative length scales and weight fractions of the substructures are identified.

3. Results and discussion

3.1. Binary systems

The binary system of ethylene in LLDPE-B of crystallinity of 48.3% was first studied because a good estimate of the pure components diffusivity can be obtained from the literature. The importance of this will become apparent below, but in short, this gives us a reference for the analysis of the sorption experiments. Alves et al.[11] studied the diffusivity of ethylene in LLDPE at 70°C and ethylene pressure varying from 3-15 bar. These experiments could be compared to the present work since ethylene pressures as well as the crystallinity of the polymer powders are close, with a value of 48.6% for Alves et al.[11]. The diffusivity data taken from Alves et al. [11] at 70°C at different ethylene pressures are given in ***Table 26***. The experimental sorbed weight were therefore fitted to Crank's diffusion equation for small particles for the first moments of the experiment and for big particles for the entire time of the sorption experiment. The fitting procedure minimizes the percent average relative deviation, ARD, between the experiments and Crank's diffusion model:

$$ARD = \left(\sum_{t=1}^{10} \frac{|M_{\text{norm}}^{\text{Crank}} - M_{\text{norm}}^{\text{exp}}|}{M_{\text{norm}}^{\text{exp}}} + \sum_{t=10}^{200} \frac{|M_{\text{norm}}^{\text{Crank}} - M_{\text{norm}}^{\text{exp}}|}{M_{\text{norm}}^{\text{exp}}} \right) \times 100$$

where $M_{\text{norm}}^{\text{Crank}}$ is the normalized sorbed weight calculated with Crank's diffusion model and $M_{\text{norm}}^{\text{exp}}$ is the experimental normalized sorbed weight. t is the time of the reaction in seconds.

From this fitting procedure, we can therefore identify the radii of the small and big granules, r_S and r_B, as well as the weight fraction of these granules, w_1 and w_2. In order to identify these values, we studied the sorption in four ethylene/LLDPE-B systems with varying pressures, using the data of Alves et al.[11] for the diffusivity. The identified parameters are given in ***Table 26*** and the sorption results are shown in ***Figure 85.*** Since the same powder is used for all the sorption experiments in the current paper, the identified parameters will then be used for the ternary and quaternary systems, and the solution to Crank's equation will be used to determine the total diffusivity for each gas mixture.

Table 26. *Identified radii of small and big granules, and their respective fractions in the polymer particle. Diffusivity data were taken from Alves et al.[11] at 70°C.*

P (bar)	**4.3**	**6.1**	**10.3**	**13.94**
D **(m² s⁻¹)**	7.71×10^{-11}	1.02×10^{-10}	1.22×10^{-10}	1.58×10^{-10}
r_S **(µm)**	100			
r_B **(µm)**	210			
w_1	0.48			
w_2	0.52			

Figure 82 to ***Figure 85*** show the sorbed weight of ethylene in LLDPE at 70°C at different pressures up to 14 bars. The diffusivity data was taken from Alves et al.[11] at 70°C for different ethylene pressures, as can be seen in ***Table 26***. The parameter *n* in Crank's equation was assumed equal to 50 as large value of n satisfies the analytical solution convergence criterion.

Figure 82 to ***Figure 85*** show that the Crank's diffusion model for polymer particles with two sizes of granules represents the experimental sorption curves correctly for the ethylene/LLDPE-B binary system. Crank's diffusion equation for small particle radius is in good agreement with the first moments of the experimental sorption curves and for big particle radius with the entire time of the reaction. This model has therefore been validated with our experimental data for the ethylene/LLDPE-B binary system at different pressures. Besides, from these simulations, the radii of the small and big granules, r_S and r_B, as well as the fractions of these granules, w_1 and w_2 were found to be identical for each pressure step of ethylene in LLDPE-B (c.f. ***Table 26***).

Based on this analysis, we will henceforth use r_S=100 µm and r_B=210 µm, and w_1=0.48 and w_2=0.52 in the rest of our analysis, since the same LLDPE-B powder is used for all the following ternary and quaternary systems.

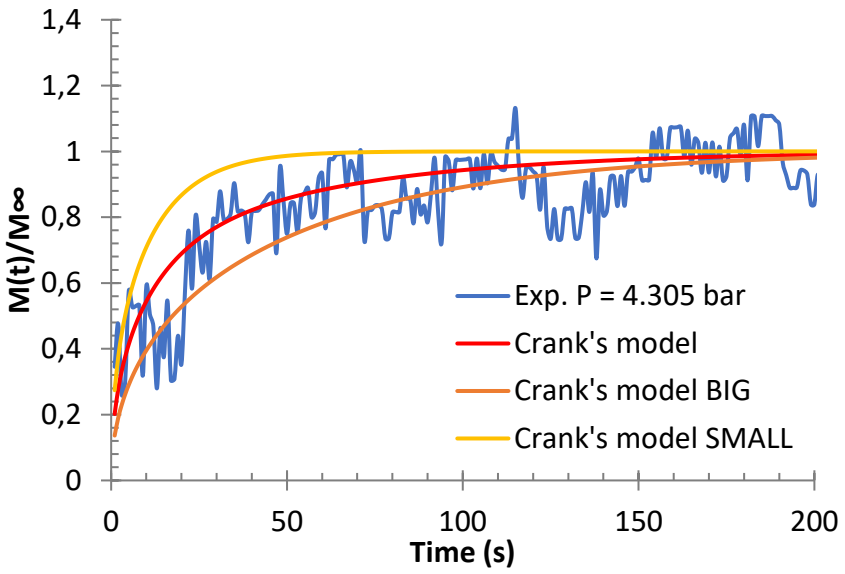

Figure 82.Sorption rates of ethylene/LLDPE-B binary system at a total pressure of 4.305 bar at 70°C obtained through gravimetric method and Crank's diffusion equation for particles with two sizes of granules

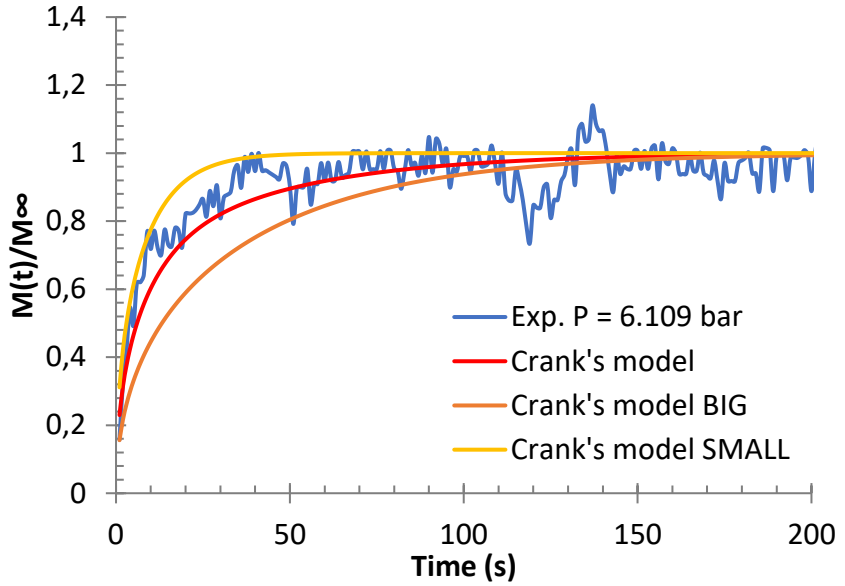

Figure 83. Sorption rates of ethylene/LLDPE-B binary system for a total pressure of 6.109 bar at 70°C obtained through gravimetric method and Crank's diffusion equation for particles with two sizes of granules

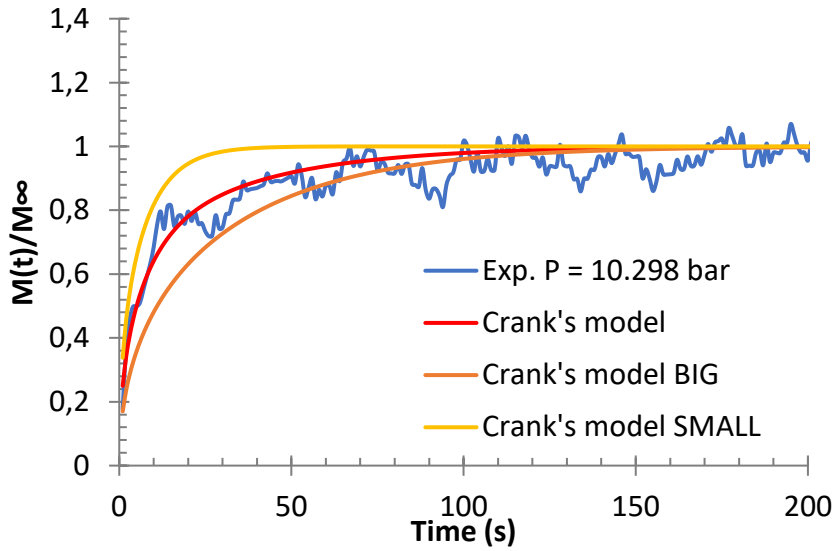

Figure 84. Sorption rates of ethylene/LLDPE-B binary system for a total pressure of 10.298 bar at 70°C obtained through gravimetric method and Crank's diffusion equation for particles with two sizes of granules

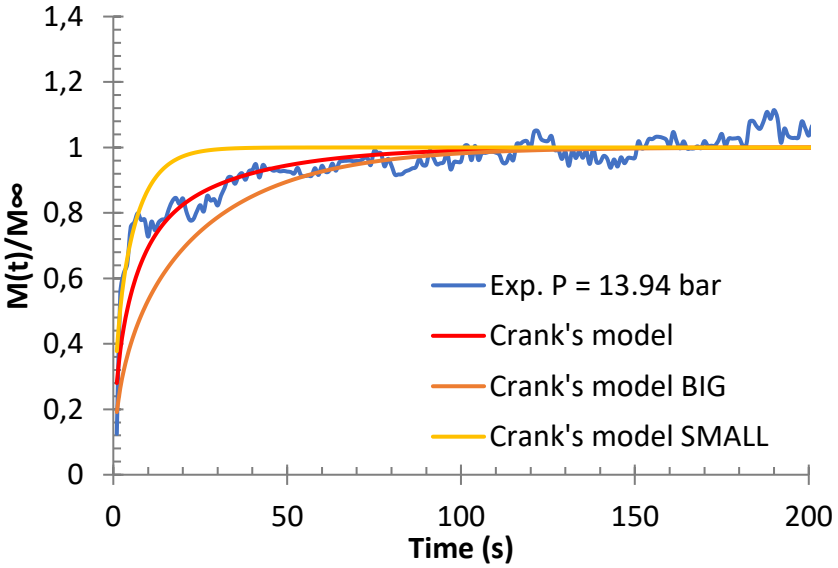

Figure 85. *Sorption rates of ethylene/LLDPE-B binary system for a total pressure of 13.94 bar at 70°C obtained through gravimetric method and Crank's diffusion equation for particles with two sizes of granules*

3.2. Ternary systems

The ternary systems of ethylene in LLDPE-B with different penetrants such as propane, isobutane and 1-butene were studied in this section. The overall diffusivity of these three systems will be measured for a pressure up to 5 bars and a constant temperature of 70°C. The gas phase composition of the different ternary systems is presented in ***Table 27***.

Table 27.*Gas-phase molar composition of the different studied ternary systems at 70°C*

System	Composition
Ethylene / Propane / LLDPE-B	$0 < P_{tot} < 5$ bar $x_{C2} = 0.509$ / $x_{C3} = 0.491$
Ethylene / Isobutane / LLDPE-B	$0 < P_{tot} < 5$ bar $x_{C2} = 0.485$ / $x_{iC4} = 0.515$
Ethylene / 1-butene / LLDPE-B	$0 < P_{tot} < 4$ bar $x_{C2} = 0.617$ / $x_{1C4} = 0.383$

The results of the experimental sorbed weight and Crank's diffusion model for polymer particles with two sizes of granules for ethylene/isobutane/LLDPE-B system are shown in ***Figure 86***-***Figure 87*** (at two different pressures), for ethylene/1-butene/LLDPE-B system in ***Figure 89***-***Figure 90***, and for the ethylene/propane/LLDPE-B system in ***Figure 91***-***Figure 93***. The fitting of the Crank's model with the experimental sorption rates will therefore yield the overall diffusivity of the two gases: ethylene and the added penetrant (i.e. propane, isobutane, 1-butene). The total diffusivities for these systems are shown in Figure ***Figure 94***.

Several observations can be made from these figures. First of all, the usefulness of the particle model with two sizes of granules can clearly be seen from ***Figure 89***-***Figure 93***; as the pressure increases, the rate of sorption at the beginning of the experiments increases quite quickly with respect to lower pressures. The use of large and small structures allows us to capture this quite precisely. Furthermore, it is important to point out that the same values of r_S and r_B are used in all of these fits, giving us confidence that this representation is reasonable.

First, ethylene/isobutane/LLDPE-B system is studied at 70°C and total pressures of 2.86 and 5.07 bar. Gas phase composition of ethylene and 1-butene is presented in ***Table 27***.

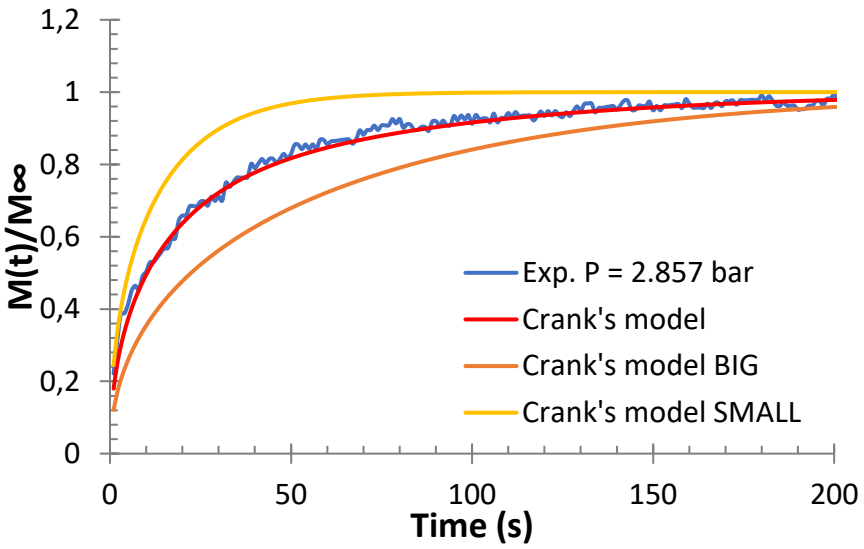

Figure 86. *Sorption rates of ethylene/isobutane/LLDPE-B ternary system at total pressure of 2.857 bars and 70°C obtained through gravimetric method and Crank's diffusion equation for particles with two sizes of granules. Molar composition is:* $x_{C2} = 0.485$ *and* $x_{iC4} = 0.515$.

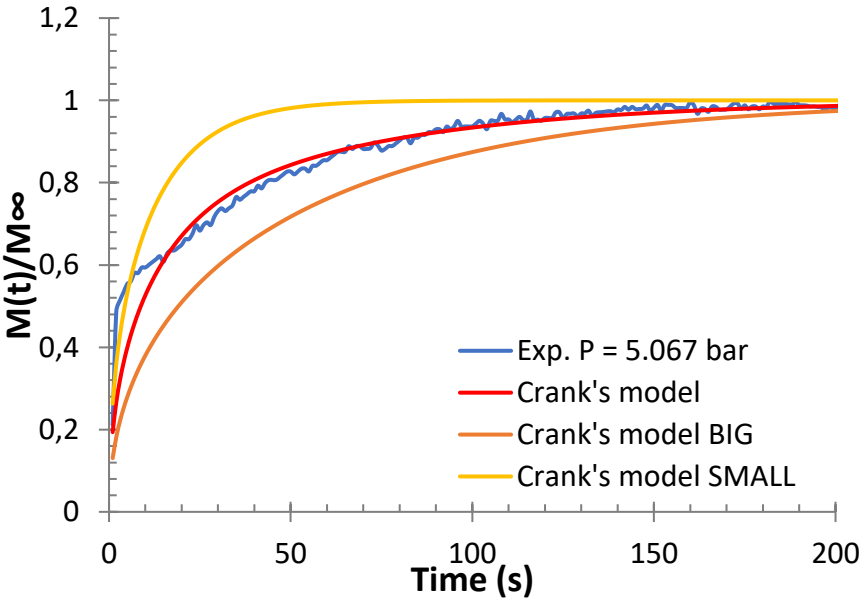

Figure 87. *Sorption rates of ethylene/isobutane/LLDPE-B ternary system at total pressure of 2.857 bars and 70°C obtained through gravimetric method and Crank's diffusion equation for particles with two sizes of granules. Molar composition is:* $x_{C2} = 0.485$ *and* $x_{iC4} = 0.515$.

In order to confirm the previous results, we compared the one level and two levels Crank's diffusion model for ethylene/isobutane/LLDPE-B ternary system. ***Figure 88*** compares the sorption curves, as well as the prediction of the mass uptake through Crank's equation using an optimized value for a single value of *r*, as well as the prediction for two substructure sizes. The value of the used diffusivity in ***Figure 88***, 8.52×10^{-11} m^2 s^{-1}, was identified through the fitting of the particle model with two sizes of granules with the experimental sorption curve, and was used for the fitting of the one size of granules particle model in order to identify the radius *r*. The calculated radius for the one level model is $r = 150$ μm. It can be seen that the particle model with two sizes of granules allows us to better predict the experimental sorption curves.

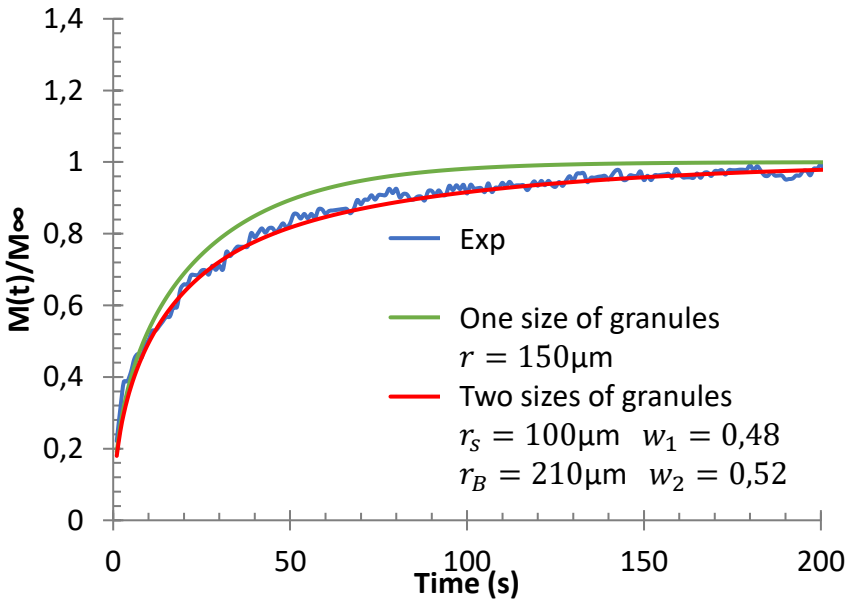

Figure 88. *Experimental sorption curves (blue lines) and Crank's solution for one level (green lines) and two levels (red line) particle morphology at 70°C, a total pressure of 2.86 bar and a total diffusivity of 8.52×10^{-11} m^2 s^{-1} for ethylene/isobutane/LLDPE-B system. r=150 μm for one size of granules model and r_S=100 μm, w_1=0.48, r_B=210 μm and w_2=0.52 for two sizes of granules model*

The second studied system is ethylene/1-butene/LLDPE-B at 70°C and total pressures of 2.6 and 3.93 bar. The gas phase composition of ethylene and 1-butene is presented in ***Table 27***.

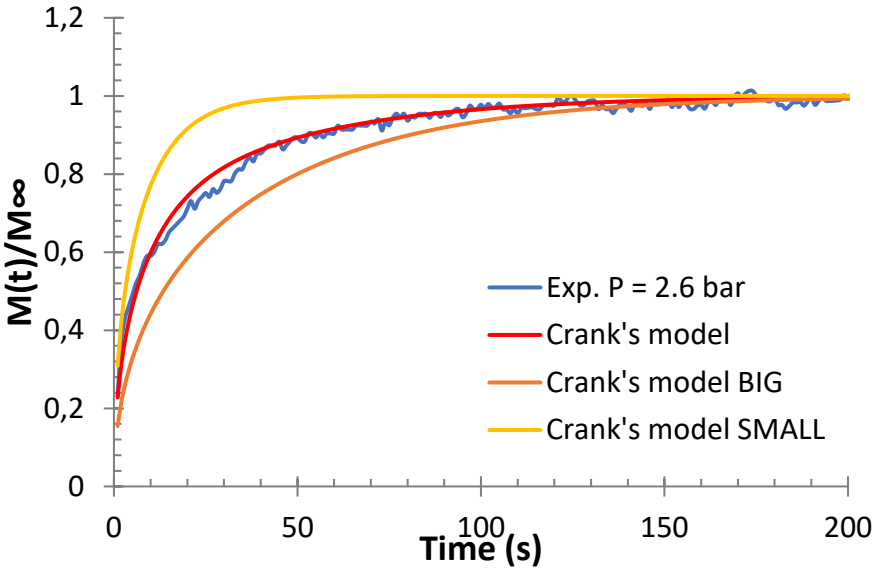

Figure 89. *Sorption rates of ethylene/1-butene/LLDPE-B ternary system at a total pressure of 2.6 bars and 70°C obtained through gravimetric method and Crank's diffusion equation for particles with two sizes of granules. Molar composition is:* $x_{C2} = 0.617$ *and* $x_{1C4} = 0.383$.

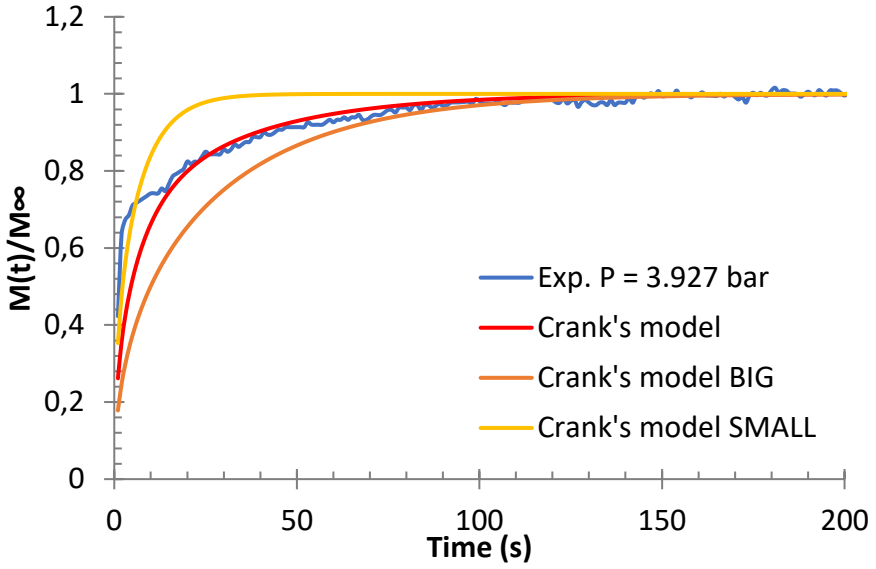

Figure 90. *Sorption rates of ethylene/1-butene/LLDPE-B ternary system at a total pressure of 3.927 bars and 70°C obtained through gravimetric method and Crank's diffusion equation for particles with two sizes of granules. Molar composition is:* $x_{C2} = 0.617$ *and* $x_{1C4} = 0.383$.

The last studied system is ethylene/propane/LLDPE-B at 70°C and total pressures of 2.56, 3.08 and 5.06 bar. Gas phase composition of ethylene and 1-butene is presented in ***Table 27***.

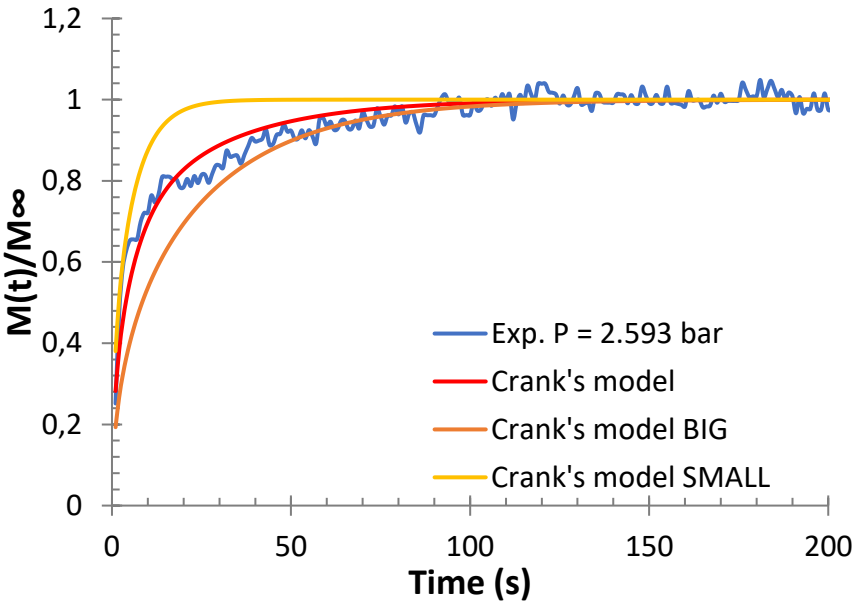

Figure 91. *Sorption rates of ethylene/propane/LLDPE-B ternary system at total pressure of 2.593 bars and 70°C obtained through gravimetric method and Crank's diffusion equation for particles with two sizes of granules. Molar composition is:* $x_{C2} = 0.509$ *and* $x_{iC4} = 0.491$.

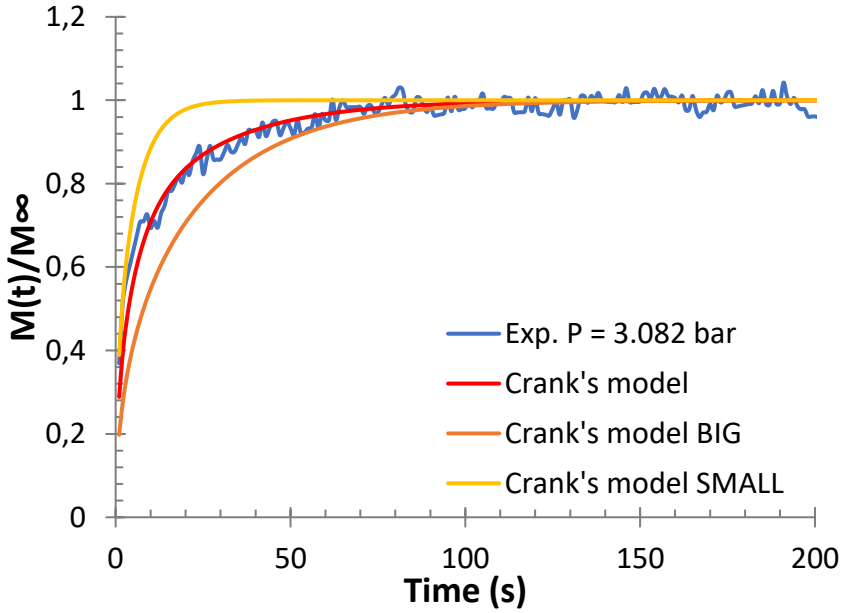

Figure 92. *Sorption rates of ethylene/propane/LLDPE-B ternary system at total pressure of 3.082 bars and 70°C obtained through gravimetric method and Crank's diffusion equation for particles with two sizes of granules. Molar composition is:* $x_{C2} = 0.509$ *and* $x_{iC4} = 0.491$.

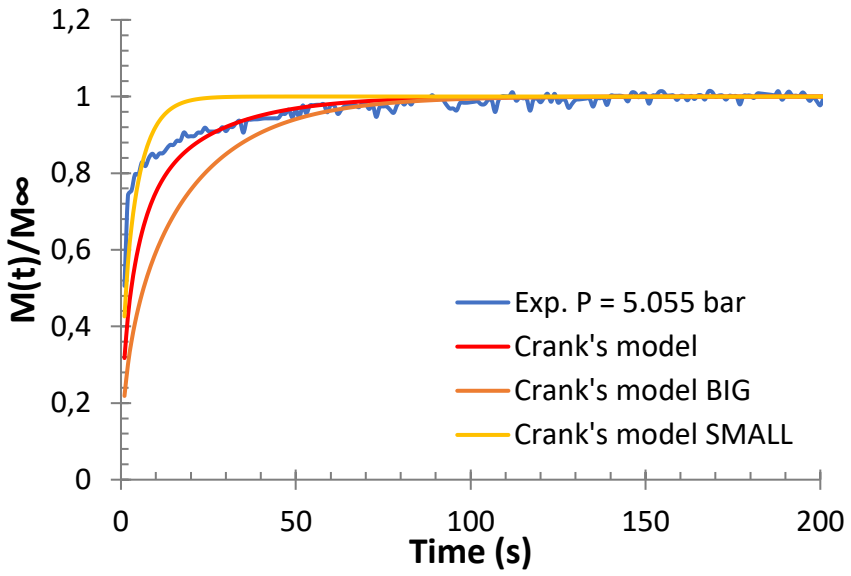

Figure 93. *Sorption rates of ethylene/propane/LLDPE-B ternary system at total pressure of 5.055 bars and 70°C obtained through gravimetric method and Crank's diffusion equation for particles with two sizes of granules. Molar composition is:* $x_{C2} = 0.509$ *and* $x_{iC4} = 0.491$.

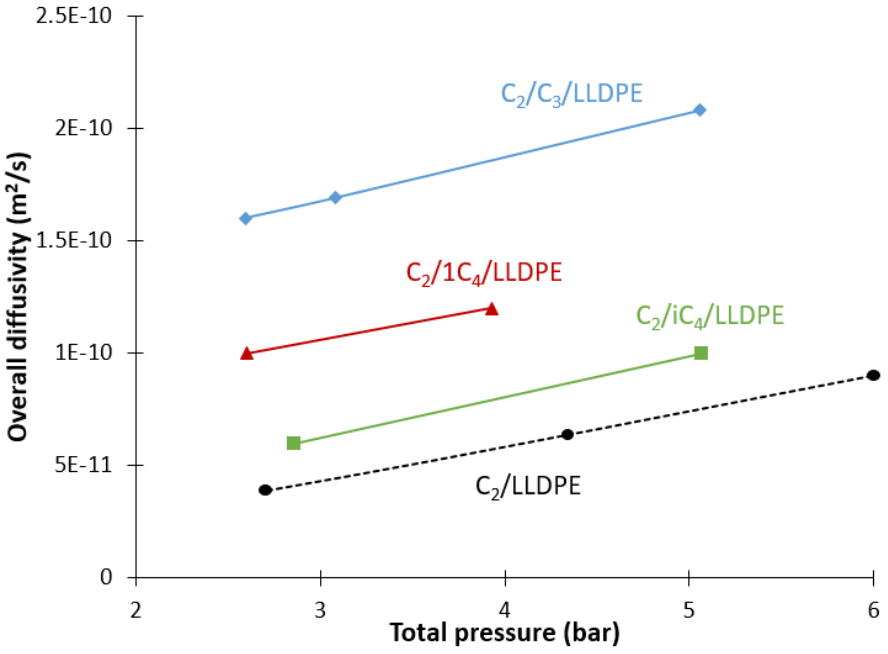

Figure 94. *Overall diffusivity of ethylene in LLDPE-B in binary system and in presence of propane, isobutane and 1-butene at 70°C with the molar fractions:* $x_{1C4}=0.383$, $x_{iC4}=0.515$ *and* $x_{C3}=0.491$.

Figure ***94*** compares the overall diffusivity of the binary system of ethylene/LLDPE-B and the different ternary systems (i.e. ethylene/propane/LLDPE-B, ethylene/isobutane/LLDPE-B, ethylene/1-butene/LLDPE-B) in order to show the effect of the gas phase composition on the

overall diffusivity. It can be seen that the overall diffusivity of all systems increases with increasing the total pressure of the mixture, as expected. Besides, it has been shown that the overall diffusivity of all ternary systems are higher than the binary system of ethylene/LLDPE. This can be explain by the co-diffusion effect leading to an increase of ethylene diffusivity in presence of different penetrants, leading therefore to an increase of the overall diffusivity of the system. The overall diffusivity of ethylene/1-butene/LLDPE-B is higher than ethylene/isobutane /LLDPE-B, as expected. The overall diffusivity of ethylene/propane /LLDPE-B appears to be higher than with isobutane and 1-butene. In order to have better explanations about the obtained results, a diffusivity model, capable of taking into account the interactions between the different species in a mixture, is needed.

3.3. Quaternary systems

The overall diffusivity of quaternary systems is studied in this section in order to show the effect of the gas phase composition in the system of ethylene/1-butene/ICA/LLDPE with different ICAs. To the best of our knowledge, this is the first time that quaternary overall diffusivity is experimentally measured and theoretically analyzed, especially at polyolefins industrial conditions.

Quaternary systems of ethylene as monomer, 1-butene as comonomer and both isobutane and propane as ICAs in LLDPE-B were studied in this section. The overall diffusivity of these systems will be measured for a pressure up to 6.2 bars at a constant temperature of 70°C, using Crank's diffusion equation for particles with two sizes of granules. Gas phase composition of the studied quaternary systems is given in Table ***28***.

Table 28. *Gas-phase molar composition of the different studied quaternary systems*

System	Composition
Ethylene / Propane / 1-butene / LLDPE-B	**$0 < P_{tot} < 6.2$ bar** $0.39 < x_{C3} < 0.42$ $0.17 < x_{1C4} < 0.23$
Ethylene / Isobutane / 1-butene / LLDPE-B	**$0 < P_{tot} < 6$ bar** $0.4 < x_{iC4} < 0.43$ $0.17 < x_{1C4} < 0.23$

3.3.1. Ethylene/Propane/1-butene/LLDPE-B

The first studied quaternary system is ethylene/propane/1-butene/LLDPE-B at 70°C and a total pressure up to 6.2 bars. The composition of the gas phase of the studied system is given in Table ***28***. Two cases will therefore be studied, with a slightly different composition of the gas phase:

- **Composition 1** : x_{C3}=0.39 ; x_{1C4}=0.23 ; x_{C2}=0.38
- **Composition 2** : x_{C3}=0.42 ; x_{1C4}=0.17 ; x_{C2}=0.41

As for ternary systems, the radii of small and big granules as well as their respective fractions that have been identified for ethylene/LLDPE-B binary system (c.f. ***Table 26***), and validated with different ternary systems, will be used for this study as the same PE powder is used.

Figure 95-Figure 97 show the overall quaternary diffusivity at 70°C for the mixture ethylene/propane/1-butene/LLDPE-B (**Composition 1)** at total pressures of 2.63, 4.83 and 6.21 bar, respectively. ***Figure 98-Figure 100*** show the mixture of ethylene/propane/1-butene/LLDPE-B (**Composition 2)** at total pressures of 2.61, 4.14 and 5.56 bar respectively. The gas phase composition of both systems are slightly different, with a very small increase of the fractions of ethylene and propane for the **Composition 2**, with respect to the **Composition 1**. However, we do not expect that this small differences will have an appreciable impact on the diffusivity estimates. The total diffusivity of these systems is shown in Figure ***101***.

First, it can be seen for both systems that increasing the total pressure of the mixture leads to faster diffusion through the amorphous phase of the polymer as the time to reach equilibrium decreases. Furthermore, it appears that at high pressures, sorption is almost instantaneous, as can be seen in ***Figure 96*** and ***Figure 97***. In the same manner, it is shown that the diffusivity of big particles is also quick, leading to more difficult fitting of the model to the experimental data, especially at higher pressures, as can be seen in ***Figure 97*** and ***Figure 100***. This could be an indication that the particle model with two sizes of granules is not correct. However, there is no apparent reason that it should work for the ternary systems and not here (as the powders are from the same batch). Furthermore, we noticed that the initial flow rate into the MSB could have an impact on the recorded sorption rate, especially if it was rapid. It is more likely that this is the cause for the poor fit of this portion of the curves.

The fitting of the experimental overall diffusivity of ethylene/propane/1-butene/LLDPE-B quaternary system with Crank's diffusion model for particles with two sizes of granules for the **Composition 1** is given in ***Figure 95-Figure 97***.

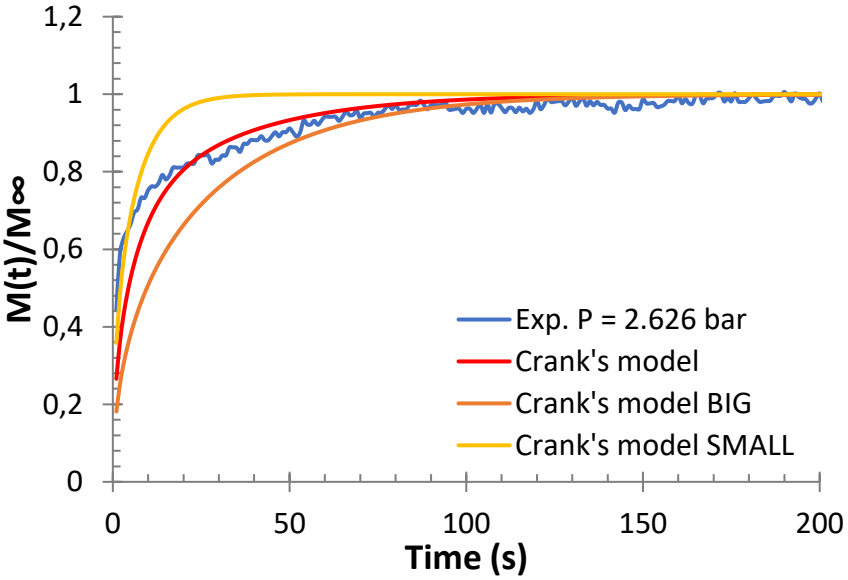

Figure 95. *Sorption rates of ethylene/propane/1-butene/LLDPE-B quaternary system at total pressure of 2.626 bars and 70°C obtained through gravimetric method and Crank's diffusion equation for particles with two sizes of granules for* ***Composition 1****. Molar composition is:* x_{C3}*=0.39,* x_{1C4}*=0.23 and* x_{C2}*=0.38.*

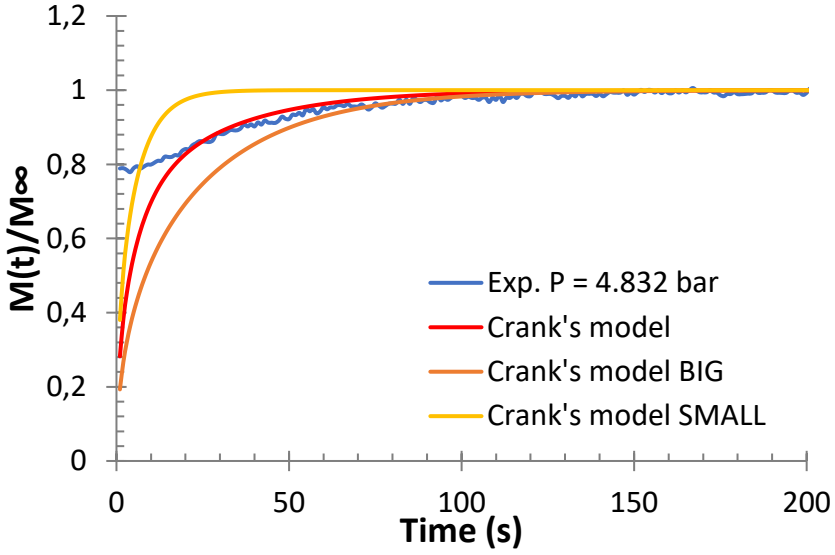

Figure 96. *Sorption rates of ethylene/propane/1-butene/LLDPE-B quaternary system at total pressure of 4.832 bars and 70°C obtained through gravimetric method and Crank's diffusion equation for particles with two sizes of granules for* ***Composition 1****. Molar composition is:* x_{C3}*=0.39,* x_{1C4}*=0.23 and* x_{C2}*=0.38.*

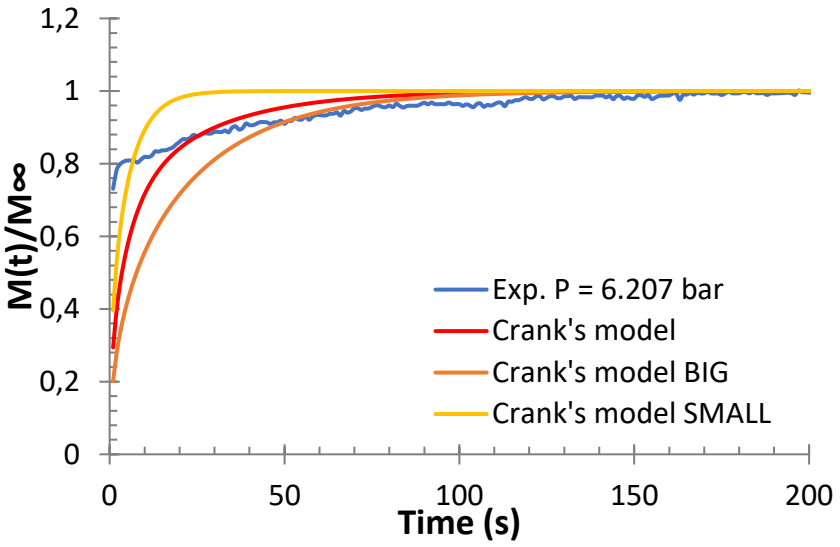

Figure 97. *Sorption rates of ethylene/propane/1-butene/LLDPE-B quaternary system at total pressure of 6.207 bars and 70°C obtained through gravimetric method and Crank's diffusion equation for* ***Composition 1****. Molar composition is:* x_{C3}*=0.39,* x_{1C4}*=0.23 and* x_{C2}*=0.38.*

The fitting of the overall diffusivity of ethylene/propane/1-butene/LLDPE-B quaternary system with Crank's diffusion model for particles with two sizes of granules for the **Composition 2** is given in ***Figure 98-Figure 100***.

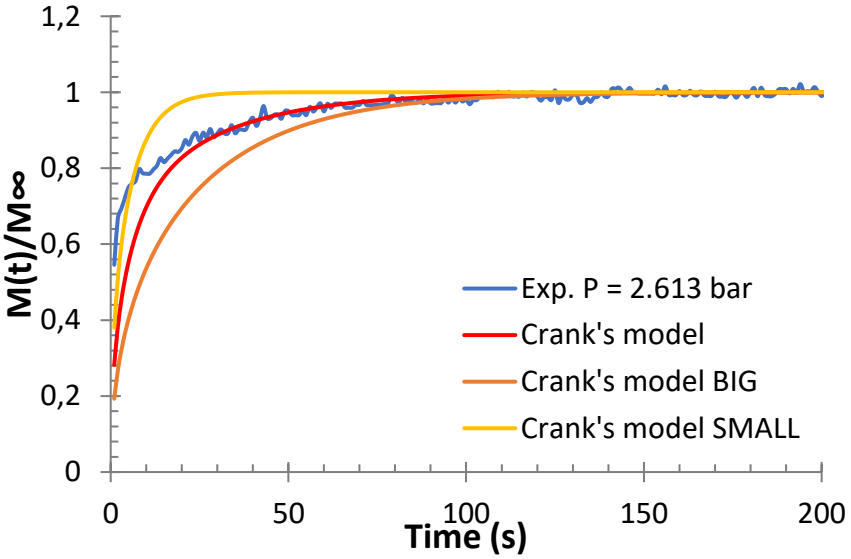

Figure 98. *Sorption rates of ethylene/propane/1-butene/LLDPE-B quaternary system at total pressure of 2.613 bars and 70°C obtained through gravimetric method and Crank's diffusion equation for particles with two sizes of granules for* ***Composition 2****. Molar composition is:* x_{C3}*=0.42,* x_{1C4}*=0.17 and* x_{C2}*=0.41*

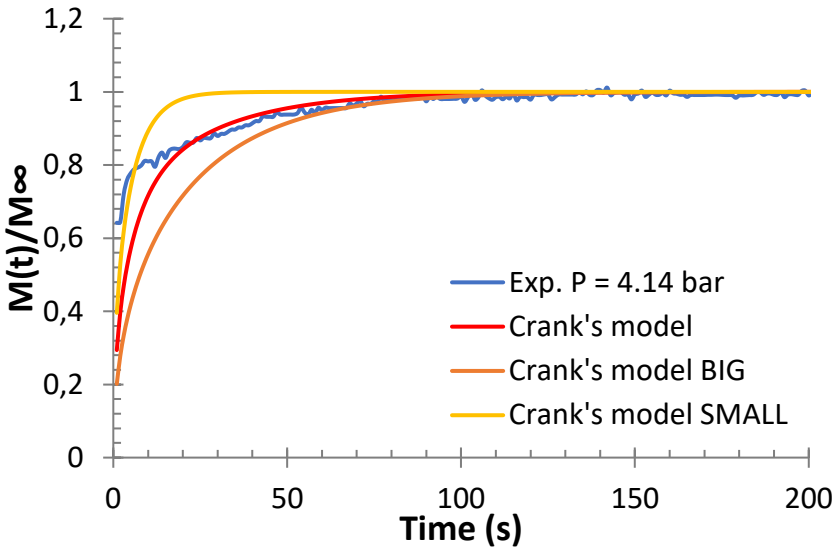

Figure 99. *Sorption rates of ethylene/propane/1-butene/LLDPE-B quaternary system at total pressure of 4.14 bars and 70°C obtained through gravimetric method and Crank's diffusion equation for particles with two sizes of granules for* ***Composition 2****. Molar composition is:* x_{C3}*=0.42,* x_{1C4}*=0.17 and* x_{C2}*=0.41*

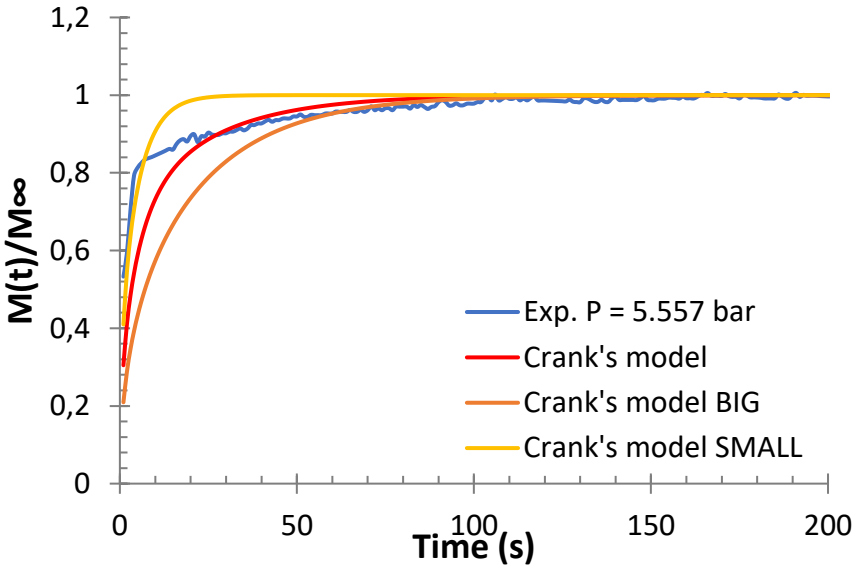

Figure 100. *Sorption rates of ethylene/propane/1-butene/LLDPE-B quaternary system at total pressure of 5.557 bars and 70°C obtained through gravimetric method and Crank's diffusion equation for particles with two sizes of granules for* ***Composition 2****. Molar composition is:* x_{C3}*=0.42,* x_{1C4}*=0.17 and* x_{C2}*=0.41*

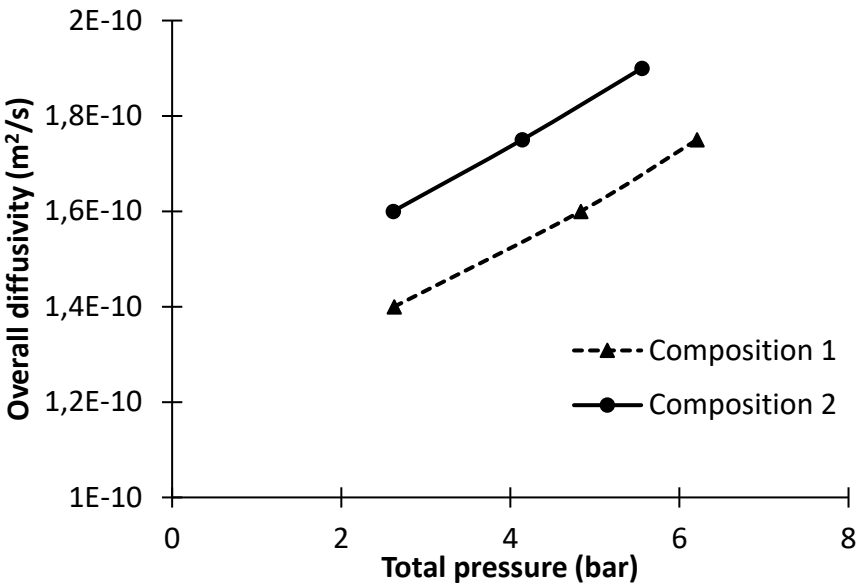

Figure 101. *Comparison of the diffusivity of ethylene/propane/1-butene/LLDPE-B quaternary system obtained from the fitting of Crank's diffusion equation for particles with two sizes of granules from* ***Composition 1*** *and* ***Composition 2****.*

Figure ***101*** presents the overall diffusivity of **Composition 1** and **Composition 2** with very little variation of the gas phase composition. A difference of 14% can be seen for both systems, which can be explained by the fact that **Composition 2** contains slightly more ethylene and propane compared to **Composition 1**, which might increase the overall diffusivity of the system. Note also that the experimental errors are higher when measuring diffusivity compared to the solubility since the diffusivity corresponds to the few moments after the injection whereas the solubility corresponds to the equilibrium. As we mentioned above, the way of injecting the gas (i.e. quick or slow) to the reactor might influence these diffusivity results. Nevertheless, these results lie between the values for the ternary systems ethylene/propane/LLPDE-B and ethylene/1-butene/LLDPE-B seen in Figure ***94***, suggesting that the estimates are reasonable despite the poor fit during the initial 5 or 10 seconds of the experiments.

3.3.2. Ethylene/Isobutane/1-butene/LLDPE-B

The second studied quaternary system is ethylene/isobutane/1-butene/LLDPE-B at 70°C and a total pressure up to 7 bars. The composition of the gas phase of the studied system is given in Table ***28***. Two cases will therefore be studied with a slightly different composition of the gas phase:

- **Composition 3** : x_{iC4}=0.37 ; x_{1C4}=0.23 ; x_{C2}=0.40
- **Composition 4** : x_{iC4}=0.43 ; x_{1C4}=0.17 ; x_{C2}=0.40

Figure 102-Figure 104 show the overall quaternary diffusivity at 70°C of ethylene/isobutane/1-butene/LLDPE-B **Composition 3** at total pressures of 2.86, 4.6 and 6.08 bar and ***Figure 105-Figure 107*** of ethylene/isobutane/1-butene/LLDPE-B **Composition 3** at total pressures of 2.5, 4.19 and 5.68 bar. The gas phase composition of both systems are slightly different, with an increase of isobutane and a decrease of 1-butene for **Composition 4**, with respect to **Composition 3**. Figure ***108*** shows the overall diffusivity of both systems.

The fit of the initial portions of the sorption curves is more satisfactory with this system. This is possibly due to paying particular attention to the feed rate to the MSB and to the fact that we expect that the diffusion process in these experiments to be slower than in the previously shown quaternary experiments. Indeed, at a total pressure of 2.86 bar, the diffusion of small particles lasts during the first 25 seconds compared to the previous quaternary system where the diffusion of small particles was almost instantaneous.

The fitting of the experimental overall diffusivity ethylene/isobutane/1-butene/LLDPE-B quaternary system with Crank's diffusion model for particles with two sizes of granules for **Composition 3** is given in ***Figure 102-Figure 104***.

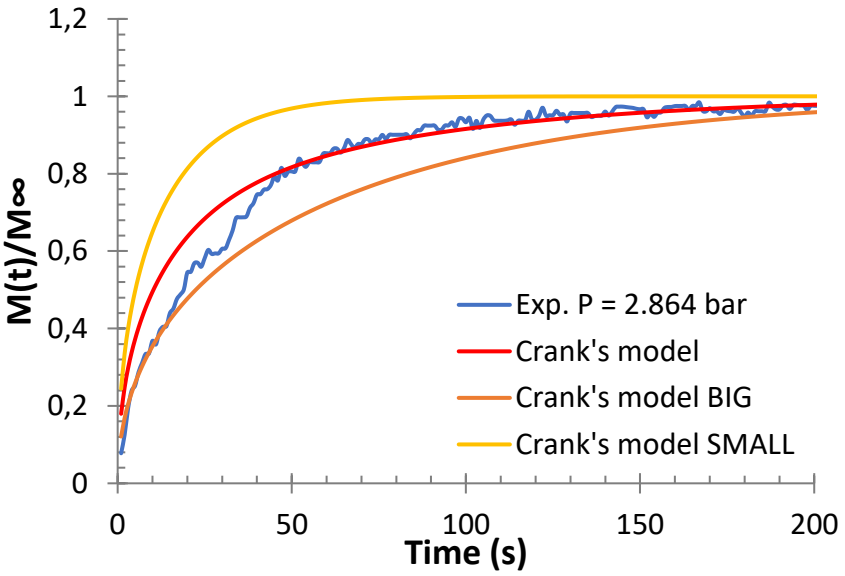

Figure 102. *Sorption rates of ethylene/isobutane/1-butene/LLDPE-B quaternary system at total pressure of 2.864 bars and 70°C obtained through gravimetric method and Crank's diffusion equation for particles with two sizes of granules for* ***Composition 3****. Molar composition is:* x_{iC4}*=0.37,* x_{1C4}*=0.23 and* x_{C2}*=0.40.*

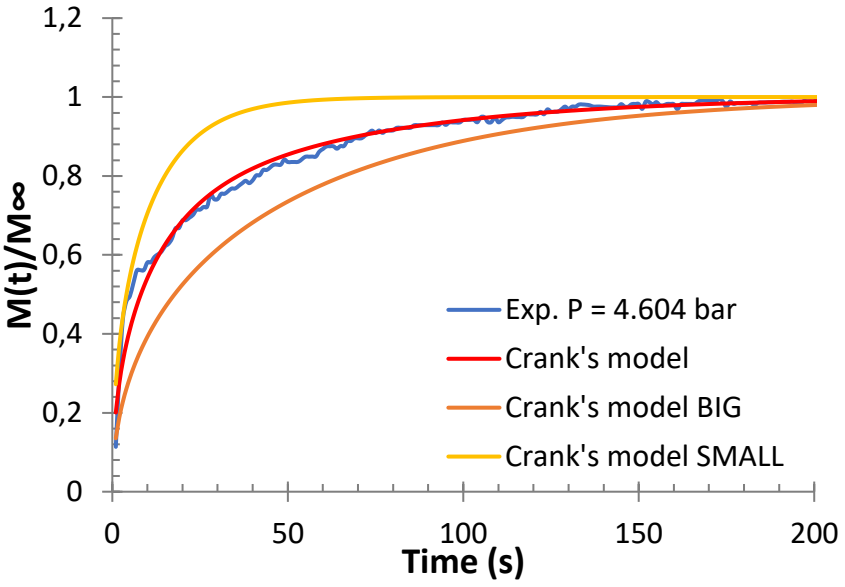

Figure 103. *Sorption rates of ethylene/isobutane/1-butene/LLDPE-B quaternary system at total pressure of 4.604 bars and 70°C obtained through gravimetric method and Crank's diffusion equation for particles with two sizes of granules equation for* ***Composition 3****. Molar composition is:* x_{iC4}*=0.37,* x_{1C4}*=0.23 and* x_{C2}*=0.40.*

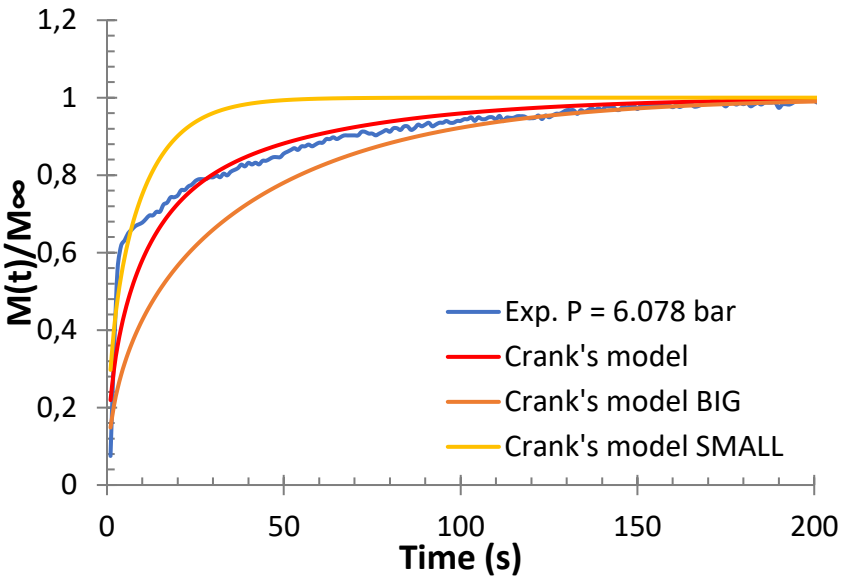

Figure 104. Sorption rates of ethylene/isobutane/1-butene/LLDPE-B quaternary system at total pressure of 6.078bars and 70°C obtained through gravimetric method and Crank's diffusion equation for particles with two sizes of granules for ***Composition 3****. Molar composition is:* x_{iC4}*=0.37,* x_{1C4}*=0.23 and* x_{C2}*=0.40.*

The fitting of the experimental overall diffusivity ethylene/isobutane/1-butene/LLDPE-B quaternary system with Crank's diffusion model for particles with two sizes of granules for **Composition 4** is given in ***Figure 105-Figure 107***.

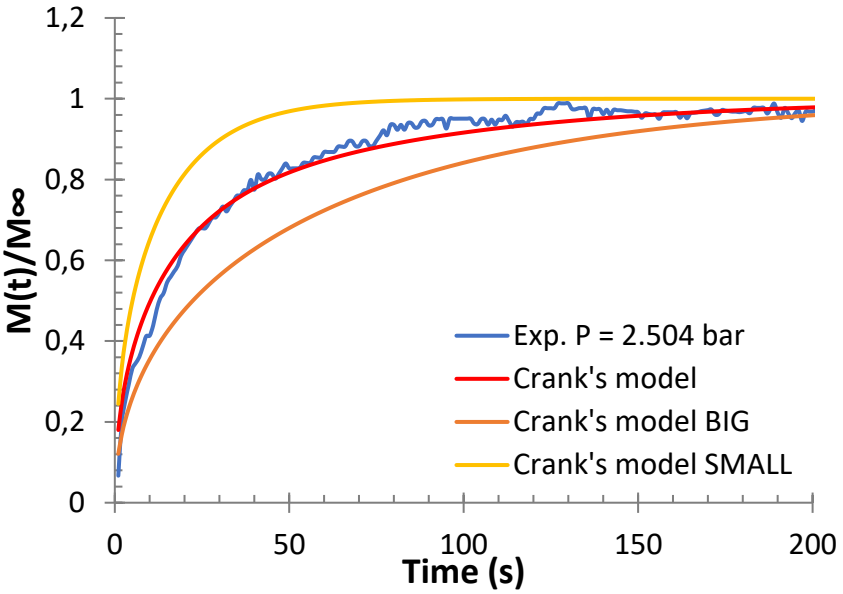

Figure 105. Sorption rates of ethylene/isobutane/1-butene/LLDPE-B quaternary system at total pressure of 2.504 bars and 70°C obtained through gravimetric method and Crank's diffusion equation for particles with two sizes of granules for ***Composition 4****. Molar composition is:* x_{iC4}*=0.43,* x_{1C4}*=0.17 and* x_{C2}*=0.40*

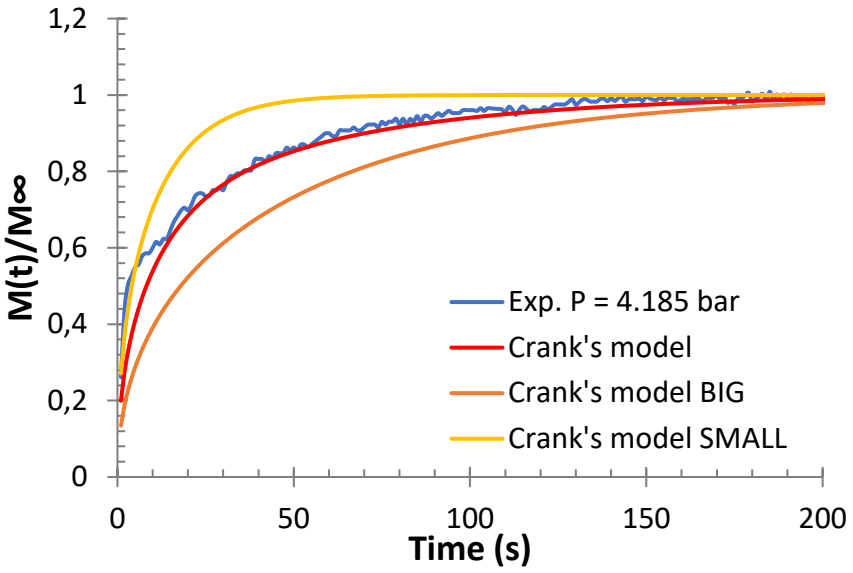

Figure 106. *Sorption rates of ethylene/isobutane/1-butene/LLDPE-B quaternary system at total pressure of 4.185 bars and 70°C obtained through gravimetric method and Crank's diffusion equation for particles with two sizes of granules for* ***Composition 4****. Molar composition is:* x_{iC4}*=0.43,* x_{1C4}*=0.17 and* x_{C2}*=0.40*

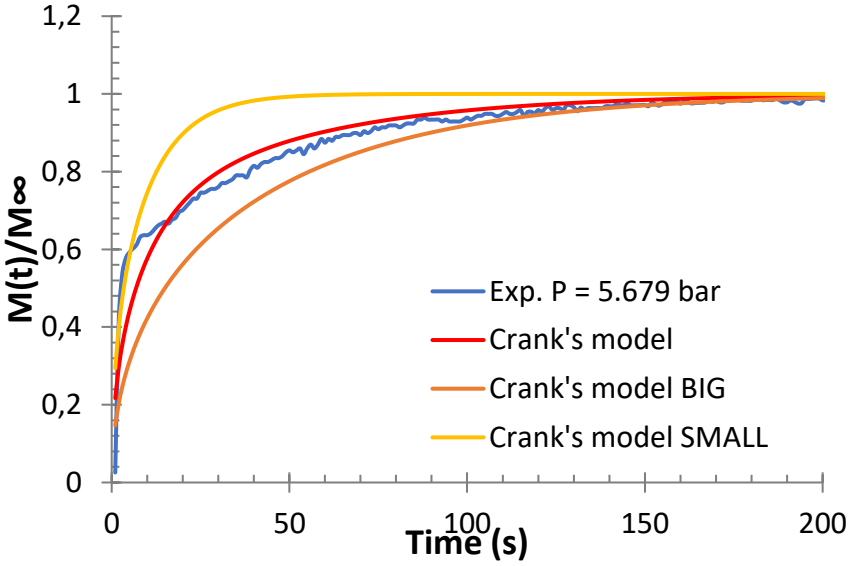

Figure 107. *Sorption rates of ethylene/isobutane/1-butene/LLDPE-B quaternary system at total pressure of 5.679 bars and 70°C obtained through gravimetric method and Crank's diffusion equation for particles with two sizes of granules for* ***Composition 4****. Molar composition is:* x_{iC4}*=0.43,* x_{1C4}*=0.17 and* x_{C2}*=0.40*

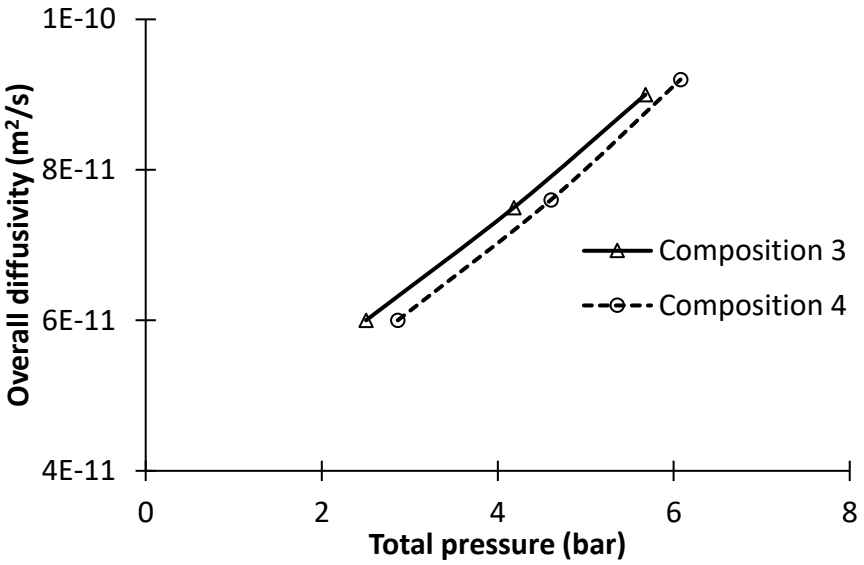

Figure 108. *Comparison of the diffusivity of ethylene/isobutane/1-butene/LLDPE-B quaternary system obtained from the fitting of Crank's diffusion equation for particles with two sizes of granules from* ***Composition 3*** *and* ***Composition 4****.*

Figure ***108*** compares the overall diffusivity of **Composition 3** and **Composition 4**, having a slight variation in the gas phase composition of the quaternary system. Indeed, the slight variation corresponds to an increase of isobutane fraction and a decrease of 1-butene fraction, which leads to very close overall diffusivity values, with a difference of 3%. This very small variation of isobutane and 1-butene composition in the gas phase might be considered equivalent. More experimental data with bigger variation of the gas phase composition might help explain these results.

3.4. Comparison of multicomponent systems

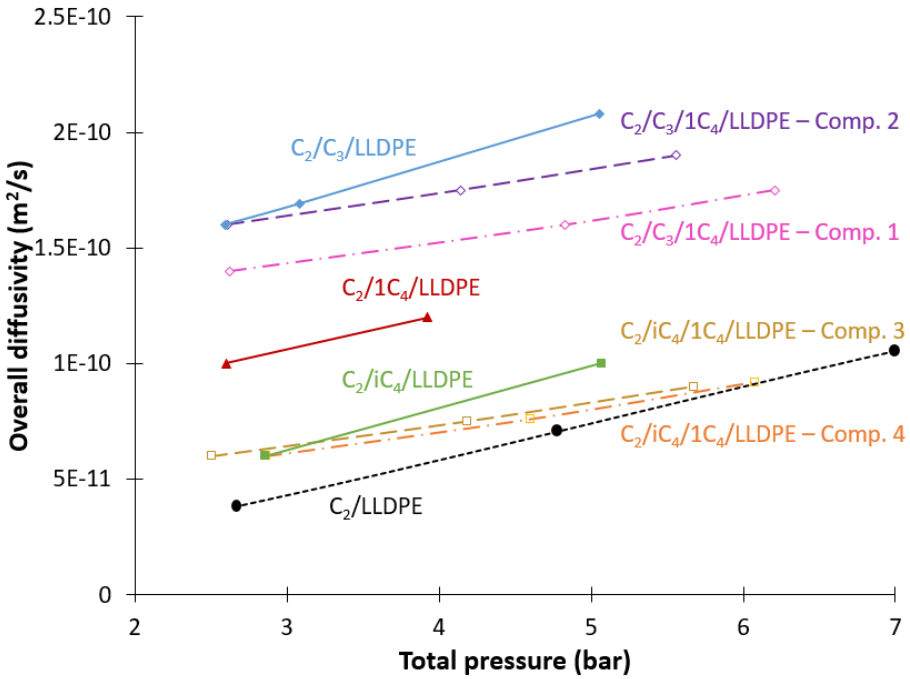

Figure 109. *Overall diffusivities of all studied systems (i.e. binary, ternary and quaternary) at 70°C and different total pressures. Gas phase composition are given in Tables 3 and 4.*

Binary (i.e. ethylene/LLDPE-B), ternary (i.e. ethylene/propane/LLDPE-B, ethylene/isobutane/LLDPE-B and ethylene/1-butene/LLDPE-B) and quaternary (i.e. ethylene/propane/1-butene/LLDPE-B and ethylene/isobutane/1-butene/LLDPE-B) overall diffusivities have been compared in Figure ***109***. It can be seen from this figure that, as expected, the diffusivity increases with increasing the total pressure of all systems. Furthermore, it can be seen that adding an ICA or comonomer increases the total diffusivity of the ternary systems with respect to the diffusivity of ethylene alone. The overall diffusivity of ethylene/propane/LLDPE-B appears to be higher than the diffusivity with isobutane and 1-butene. The overall diffusivities of both quaternary systems of ethylene/ICA/1-butene/LLDPE-B are lower than their respective ternary diffusivities of ethylene/ICA/LLDPE-B. Indeed, for lower total pressure up to 3 bar, the quaternary and ternary diffusivities are almost the same. Increasing the total pressure leads to higher slope of increase of diffusivity of ternary systems (i.e. ethylene/ICA/LLDPE-B) compared to quaternary systems (ethylene/ICA/1-butene/LLDPE-B). Besides, it might be interesting to see that the quaternary diffusivity of ethylene/isobutane/1-butene/LLDPE-B is very low, and is equal to the binary diffusivity of ethylene in LLDPE-B at a total pressure around 6 bar. This might explain that the diffusivity of small particles when fitting to Crank's diffusion model was very slow for ethylene/isobutane/1-butene/LLDPE-B.

4. Conclusion

Binary (i.e. ethylene/LLDPE-B), ternary (i.e. ethylene/propane/LLDPE-B, ethylene/isobutane/LLDPE-B and ethylene/1-butene/LLDPE-B) and quaternary (i.e. ethylene/propane/1-butene/LLDPE-B and ethylene/isobutane/1-butene/LLDPE-B) overall diffusivities at 70°C have been measured experimentally through gravimetric method and validated with Crank's diffusion model.

It has first been shown that the simple Crank's model for porous particle was not capable of predicting correctly the shape of the sorption curves. A particle model based on two sizes of compact polymer granules was used and showed good agreement with the experimental data. This model could estimate the size as well as the fractions of the small and large compact granules in the polymer particle, giving important information about the polymer particle morphology. The fast initial increase in the sorption curves was explained by the presence of a significant amount of small granules, whereas the following slower increase of the sorbed weight is caused by the presence of a certain amount of big granules.

Besides, it has been presented that the overall diffusivity of the ternary systems (i.e. ethylene/penetrant/LLDPE) were higher than the binary system of ethylene/LLDPE. This was explain by the co-diffusion effect leading to an increase of ethylene diffusivity in presence of different penetrants, leading therefore to an increase of the overall diffusivity of the system. Moreover, it has been seen that the overall diffusivity of the ternary systems in presence of propane is higher than in presence of 1-butene which is higher than in presence of isobutane. This might be explained by the fact that the lighter the penetrant, the easier its diffusion in the amorphous phase of the polymer. More experimental diffusivity studies with other penetrants would be useful in order to better understand the diffusion phenomena that occurs inside the polymer particle.

Finally, the overall diffusivity of the quaternary systems of ethylene/ICA/1-butene/LLDPE with propane and isobutane as ICA were also investigated in this chapter. It has been shown that the overall diffusivity of both quaternary systems is close to their respective ternary systems (i.e. ethylene/ICA/LLDPE) at the studied temperature and pressure. Besides, it is interesting to see that the quaternary overall diffusivity of ethylene/isobutane/1-butene/LLDPE is very low compared to the overall diffusivity of ethylene/propane/1-butene/LLDPE at 70°C. This is an important information for modeling quaternary systems in gas-phase polyolefin systems. More experimental studies are needed if one needs to better understand the diffusivity of quaternary

systems in polyethylene, such as different compositions of the gaseous mixture and different ICAs and comonomers.

The particle model including two sizes of compact polymer granules might be improved by taking into account the changes in the radius of both the big and small granules in function of the reaction time as well as their fraction since distributions of sizes and shapes remain in real porous particles. It is well known that the particle morphology changes rapidly during the course of the polymerization reaction, especially at the beginning of the reaction, where we would expect to see an important change in the distributions of sizes and fractions of big and small granules.

5. References

1. Alizadeh, A., Sharif, F., Ebrahimi, M. & McKenna, T. F. L. Modeling Condensed Mode Operation for Ethylene Polymerization: Part III. Mass and Heat Transfer. *Ind. Eng. Chem. Res.* **57**, 6097–6114 (2018).

2. Alves, R., Bashir, M. A. & McKenna, T. F. L. Modeling Condensed Mode Cooling for Ethylene Polymerization: Part II. Impact of Induced Condensing Agents on Ethylene Polymerization in an FBR Operating in Super-Dry Mode. *Ind. Eng. Chem. Res.* **56**, 13582–13593 (2017).

3. Kröner, T. & Bartke, M. Sorption of Olefins in High Impact Polypropylene – Experimental Determination and Mass Transport Modeling. *Macromol. React. Eng.* **7**, 453–462 (2013).

4. Sato, Y. *et al.* Solubility and Diffusion Coefficient of Carbon Dioxide in Biodegradable Polymers. *Ind. Eng. Chem. Res.* **39**, 4813–4819 (2000).

5. Yoon, J.-S. & Chung, C.-Y. Solubility and diffusion coefficient of gaseous ethylene and α-olefin in ethylene/α-olefin random copolymers. 6.

6. Dimos, V. & Kanellopoulos, N. Hybrid model for the diffusion of simple and complex penetrants in polymers. *J. Appl. Polym. Sci.* **104**, 2877–2885 (2007).

7. Kiparissides, C., Dimos, V., Boultouka, T., Anastasiadis, A. & Chasiotis, A. Experimental and theoretical investigation of solubility and diffusion of ethylene in semicrystalline PE at elevated pressures and temperatures. *J. Appl. Polym. Sci.* **87**, 953–966 (2003).

8. Chen, M., Wang, J., Jiang, B. & Yang, Y. Diffusion measurements of isopentane, 1-hexene, cyclohexane in polyethylene particles by the intelligent gravimetric analyzer. *J. Appl. Polym. Sci.* **127**, 1098–1104 (2013).

9. Raharjo, R. D., Freeman, B. D., Paul, D. R., Sarti, G. C. & Sanders, E. S. Pure and mixed gas CH4 and n-C4H10 permeability and diffusivity in poly(dimethylsiloxane). *J. Membr. Sci.* **306**, 75–92 (2007).

10. Cancelas, A. J. *et al.* Solubility and Diffusivity of Propylene, Ethylene, and Propylene-Ethylene Mixtures in Polypropylene. *Macromol. Chem. Phys.* **219**, 1700565 (2018).

11. Alves, R. F. & McKenna, T. F. L. Estimation of diffusion coefficients for multiple penetrant/polyolefin systems based on sorption data. *Chem. Eng. J.* **383**, 123114 (2020).

12. Crank, J. & Crank, E. P. J. *The Mathematics of Diffusion*. vol. Chap. 6 (Clarendon Press, 1979).

13. Bobak, M., Gregor, T., Bachman, B. & Kosek, J. Estimation of Morphology Characteristics of Porous Poly(propylene) Particles from Degassing Measurements. *Macromol. React. Eng.* **2**, 176–189 (2008).

14. Zubov, A., Pechackova, L., Seda, L., Bobak, M. & Kosek, J. Transport and reaction in reconstructed porous polypropylene particles: Model validation. *Chem. Eng. Sci.* **65**, 2361–2372 (2010).

Chapter 5

A Single Particle Model to Predict the Impact of Induced Condensing Agents on Polymerizing Particles

1. Introduction

A growing polymer particle can be thought of as a dynamically evolving microreactor, which exchanges heat and mass with the continuous phase of the main reactor, and where the polymer is formed. Upon injection into a reactor, the catalyst particle will change rapidly, first by undergoing fragmentation, and then growing by expansion[1,2,3,4]. The rate at which this expansion occurs is of course linked to the rate of production of polymer, and thus to both the intrinsic activity of the used catalyst, as well as to the concentration of reactive species and the local temperature at the active sites; the same is true for the molecular weight[5]. The monomer concentration at an active site will be a trade-off between the rate at which it is consumed at a given point in the particle, and the rate at which it diffuses through the particle. During ethylene polymerization, monomer diffuses from the continuous phase of the reactor, and into the pores of the supported particle, where it sorbs in, then diffuses through the amorphous phase of the polymer surrounding the active sites. Heat is produced when the monomer reacts at the active site, and this heat must be transported out of the particle to avoid overheating. Thus, to describe the polymerization reaction, it is imperative to be able to predict the dynamics of mass and heat transfer in the growing particle.

Most modelling studies now employ a version of the polymer flow model (PFM)[6–8] to describe particle growth and estimate the concentration and temperature gradients. These models assume that transport is by Fickian diffusion. The choice of which model to use has been extensively discussed in the literature[2,5,9–11], so interested readers may refer to these references for further information. In the current work we choose to use the Random Pore Polymer Flow Model (RPPFM) to describe the single particle behavior since it combines a certain amount of geometric simplicity with a mechanistic description of the diffusion process[12]. This model takes into account the transport phenomena through the pore phase and the mass transfer through the semicrystalline polymer phase.

In that sense, Alizadeh et al.[13] extended the work of Kanellopoulos et al.[12] to include an accurate thermodynamic description through the Sanchez-Lacombe EoS as sorption model and Vrentas and Duda[14,15] as diffusion model. They suggested that combined cosolubility and codiffusion effects had a noticeable impact on the mass and heat transfer, as well as on the polymerization rate. They used the SL EoS model to account for the co-solubility effects with n-hexane, but did not try to link the reaction rate to the molecular weight data.

In this chapter, a comprehensive mathematical particle growth model, accounting for mass and heat transfer limitations appearing during the early growth of a Ziegler-Natta catalyst in gas phase olefin polymerization is developed. The RPPFM model will be adapted in order to estimate the overall particle polymerization rate as well as mass balances of the different species (i.e. monomer, ICA, "live" and "dead" polymer chains) and energy balance, in order to predict the temporal-spatial evolution of concentration and temperature profiles in the growing polymer particle and the evolution of molecular weight distribution. However, the accurate determination of both the penetrants concentration at the catalyst active site and the effective penetrant diffusion coefficient is crucial in any particle growth modeling study. This study will therefore show the importance of having an accurate thermodynamic model when developing a particle growth model. The Sanchez-Lacombe EoS for multicomponent systems (i.e. monomer, penetrants), as thermodynamic model, is incorporated in this particle model, in order to calculate the equilibrium concentration of penetrants in the amorphous phase of the polymer. Vrentas and Duda diffusivity model is applied to calculate the diffusivity of penetrant molecules in the semicrystalline polymer. Finally, a kinetic model for homopolymerization is included to predict the changes in molecular weights in the growing particle as a function of the gas phase composition.

2. Model Development

2.1.Single Particle Model (SPM) - RPPFM

In the present study, the Random-Pore Polymer Flow Model (RPPFM)[12,16] has been adapted to predict the spatial-temporal evolution of monomer and ICA concentrations, temperature, polymerization rate and polymer molecular weight of gas-phase ethylene polymerization. For the purposes of modelling, the following assumptions have been made:

- The particle is assumed to be spherical;
- The particle is considered to be a pseudo-homogeneous medium;
- The active sites are uniformly dispersed throughout the particle;
- The fragmentation process is completed instantaneously;
- The crystallinity as well as the porosity of the produced polymer are assumed constant during the reaction;
- The hydrogen concentration in the polymer is very low compared to the other penetrants (i.e. ethylene, n-pentane) and is therefore assumed constant.

These assumptions simplify the numerical calculations, but as discussed in the literature[2,5,9–11], a good number of them are not entirely true. We know that the morphology of the particles evolves rapidly during the first minutes of the polymerization, and that the porosity changes with particle size and time. During the initial times, the crystallinity, critical length scale for diffusion, and perhaps even the number and nature of the active sites also change. Furthermore, it is possible that the relatively high ICA concentrations with respect to polymer during the initial phases of the reaction can retard crystallization, which in turn could have an impact on the diffusion of monomer to the active sites. Moreover, swelling of the amorphous phase by a penetrant might not be uniform in the whole particle, as it can be affected by the tie molecules. As the main purpose of this paper is to quantify the impact of the gas phase composition (i.e. monomer, ICA, hydrogen) on the reaction rate and molecular weight distributions, we will not attempt to model the start-up of the polymerization. Rather, we choose to fit the kinetic parameters (see below) to the experimental data after 5 minutes or so of the polymerization. This will allow us to calculate the mass and heat transfer in the growing polymer particle for a long time, and let us approximate the impact of the ICA on the rate and molecular weight data reasonably well.

The RPPFM consists of a system of partial differential equations (PDEs) combining material and energy balances over space and time. The full set of material and energy balances with their corresponding initial and boundary conditions is presented in ***Table 29***.

Table 29. *Material and energy balance with initial and boundary conditions of the single particle model*

	Initial condition	**Boundary conditions**
Ethylene mass balance:		
$\frac{\partial[M_1]}{\partial t} = \frac{1}{r^2}\frac{\partial}{\partial r}\left(D_{1,\mathrm{ov}} r^2 \frac{\partial[M_1]}{\partial r}\right) - R_{\mathrm{v}}$	$[M_1]_{(r,0)} = 0$	$[M_1]_{(R,t)} = [M_1]^{\mathrm{eq}}$ $\frac{\partial[M_1]_{(0,t)}}{\partial r} = 0$
ICA mass balance:		
$\frac{\partial[M_2]}{\partial t} = \frac{1}{r^2}\frac{\partial}{\partial r}\left(D_{2,\mathrm{ov}} r^2 \frac{\partial[M_2]}{\partial r}\right)$	$[M_2]_{(r,0)} = 0$	$[M_2]_{(R,t)} = [M_2]^{\mathrm{eq}}$ $\frac{\partial[M_2]_{(0,t)}}{\partial r} = 0$
Energy balance:		
$\rho_{\mathrm{ov}} C_{\mathrm{p,ov}} \frac{\partial T}{\partial t} = \frac{k_{\mathrm{c,p}}}{r^2}\frac{\partial}{\partial r}\left(r^2 \frac{\partial T}{\partial r}\right) + \left(-\Delta H_{\mathrm{p}}\right) R_{\mathrm{v}}$	$T_{(r,0)} = T_{\mathrm{b}}$	$-k_{\mathrm{c,p}} \frac{\partial T_{(R,t)}}{\partial r} = h(T - T_{\mathrm{b}})$ $\frac{\partial T_{(0,t)}}{\partial r} = 0$
Particle growth		
$\frac{\partial r_{\mathrm{pol}}}{\partial t} = \frac{R_{\mathrm{v}}\, r_{\mathrm{pol}}\, \mathrm{MW}_1}{3\rho_{\mathrm{ov}}}$	$r_{\mathrm{pol}_{(r,0)}} = r_{\mathrm{cat}}$	$\frac{\partial r_{\mathrm{pol}_{(R,t)}}}{\partial r} = 0$ $\frac{\partial r_{\mathrm{pol}_{(0,t)}}}{\partial r} = 0$

In all of the balance equations, *t* and *r* represent the time and radial position inside the particle, respectively. 1 represents ethylene, 2 is the ICA. *R* is the radius of the pseudohomogeneous particle at each moment during its growth.

In the material balance, $D_{i,\mathrm{ov}}$ is the overall diffusion coefficient of penetrant molecules in the polymeric particle, $[M_i]$ is the overall concentration of penetrant molecules and $[M_i]^{\mathrm{eq}}$ is the overall equilibrium concentration of penetrant molecules in the particle calculated from Sanchez-Lacombe EoS.

In the energy balance, T, ΔH_{p}, $k_{\mathrm{c,p}}$, ρ_{ov}, and $C_{\mathrm{p,p}}$ represent the temperature, the enthalpy of ethylene polymerization, the thermal conductivity of the polymer phase, the overall particle density calculated from $\rho_{\mathrm{ov}} = \rho_{\mathrm{p}}(1-\varepsilon)$ where ρ_{p} is the density of the polymer phase, and the heat capacity of the polymer phase, respectively. In the boundary condition, h, and T_b are the heat transfer coefficient and the bulk temperature of the reactor, respectively.

The use of the Ranz-Marshall correlation for the calculation of the external film heat transfer coefficient has been critically examined, as it can result in an overestimation of the particle temperature[12]. Nevertheless, we will use it here as the polymerization rates of the experiments serving as a basis for the estimation of the model parameters are moderate so no large temperature excursions are expected. In addition, it is worth underlining once again that the purpose of this chapter is to provide a quantitative analysis of the impact of the ICA on gas phase polymerization, not to do an "exact fit" model of a specific system.

As has been shown in ***Table 29***, the present particle model consists of a system of non-linear partial differential equations as well as a number of algebraic equations like the polymerization rate, the external mass and heat transfer and the diffusivity. The partial differential equations, which are the energy balance equation, the material balance equations and the particle growth equation, and their boundary and initial conditions must be solved simultaneously. This will lead to a prediction of the concentration and the temperature profiles within the growing particle during ethylene polymerization in gas phase. However, in order to do that, one must have an accurate description of both the equilibrium concentration of the different penetrants as well as the diffusion of these penetrants in the amorphous phase of the polymer.

2.2.Thermodynamics

2.2.1. Sanchez-Lacombe equation of state

A number of papers have shown that Henry's law is not applicable to polymer-penetrant systems involving heavy penetrants vapors and high pressures[17,18]. It is therefore essential to use a more sophisticated thermodynamic model in order to be able to have a realistic thermodynamic description of the system, by taking into account the interactions between the different penetrants and the polymer. In the present study, the Sanchez-Lacombe equation of state (SL EoS) is employed to calculate the equilibrium concentration of the different species (i.e. monomer, penetrants) in the amorphous phase of the polymer. SL EoS is a lattice-fluid model in which pure components are assumed to be broken into parts and placed into a lattice structure. The SL EoS introduces the concept of vacant lattice sites or holes to account for the compressibility and the density changes. Thus, the system volume or density can vary by changing the fraction of holes in the lattice structure[19]. The main equation of state is given by

$$\bar{\rho}^2 + \bar{P} + \bar{T}\left[ln(1-\bar{\rho}) + \left(1-\frac{1}{r}\right)\bar{\rho}\right] = 0$$

where $\bar{T}$, $\bar{P}$ and $\bar{\rho}$ are the reduced temperature, pressure, and density respectively. Three lattice parameters describe the thermodynamic properties of a pure component: the mer-mer interaction energy, the closed-packed molar volume of a mer and the number of mers a molecule occupies in the lattice. Three reduced parameters are defined from these three lattice parameters as follows

$$\bar{T} = {}^{T}/_{T^*} \qquad \bar{P} = {}^{P}/_{P^*} \qquad \bar{\rho} = {}^{\rho}/_{\rho^*}$$

where T^*, P^*, and ρ^* are the scale factors known as the characteristic temperature, pressure, and density respectively, which are used to characterize each pure component in the mixture. These parameters of SL EoS for each pure component used in the present study are given in the ***Table 30***.

Table 30. *Pure component parameters used in SL EoS*

Component	T^* (K)	P^* (bar)	ρ^* (kg m^{-3})	Reference
Ethylene	283	3395	680	[20]
n-pentane	445	3060	755	[20]
n-hexane	476	2979.1	775	[20]
LLDPE	653	4360	903	[20]

The development of SL EoS has been described in more details in Chapter 2 and in other papers, so will not be described here. For more details, the reader is referred to references[21,22].

The only adjustable parameters from SL EoS are the interaction parameters between the different species in the mixture, k_{ij}. We believe that the interaction parameters between small molecules are equal to zero due to low chemical affinity between like molecules, which leaves us the interaction parameters between vapor species and the polymer to be identified. (1) represents ethylene, (2) the ICA and (3) the polymer, meaning that k_{13} and k_{23} are the only adjustable parameters for ternary systems. These parameters are identified by fitting SL EoS to experimental solubility data from Yao et al.[23]. They measured experimentally the solubility of ethylene/n-pentane in semicrystalline PE of crystallinity of 48.6% at temperatures between 70-90°C and total pressure of 20 bar with n-pentane partial pressure of 0.8-1.8 bar. These identified k_{ij} can therefore be used in the present particle model since the produced PE has a crystallinity

of 45% and n-pentane partial pressure are between 1-2 bar which are close to the experimental conditions of Yao et al.[23]. k_{ij} used in the different simulations are given in ***Table 31***.

Table 31. *Binary and ternary interaction parameters of ethylene/alkane /LLDPE system from Sanchez-Lacombe EoS at 80°C.*

System	k_{ij}	Ref
Ethylene/LLDPE	k_{13} = -0.022	24
n-pentane/LLDPE	k_{13} = 0.024	24
n-hexane/LLDPE	k_{13} = 0.010	13
Ethylene/n-pentane/LLDPE	k_{13} = -0.027, k_{23} = 0.0501	23
Ethylene/n-hexane/LLDPE	k_{13} = -0.022, k_{23} = 0.029	13

The equilibrium concentration of the different species in the polymer calculated from SL EoS for ternary systems have been incorporated in the RPPFM model as boundary conditions of the material balances. The implementation of an accurate sorption model will allow a better description of the thermodynamics during ethylene polymerization in gas-phase, especially since a large number of papers have shown that the gas phase composition has a great impact on the reaction rate, as well as on the concentration and temperature gradients inside a growing polymer particle[13,25,26].

Since the solubility of hydrogen in the amorphous phase of the polymer is quite low compared to that of ethylene or n-pentane, the presence of hydrogen is assumed to have no effect on the solubility or diffusivity of ethylene in the particle model (and vice versa). The concentration of hydrogen, calculated with Henry's law, is therefore assumed to be constant in the whole particle over time, and not influencing the concentration/diffusion of ethylene[27].

$$[H_2] = k_{\mathrm{He,H_2}} P_{\mathrm{H_2}} \frac{\rho_{\mathrm{p}}}{MW_{\mathrm{H_2}}} \quad (1)$$

with $k_{\mathrm{He,H_2}} = 8.2533 \times 10^{-5}$ g Pa^{-1} g^{-1} amorphous polymer.

2.2.2. Vrentas and Duda diffusion model

The knowledge of the overall diffusion coefficient is also important in calculating the material balances of the RPPFM. However, the Sanchez-Lacombe EoS only gives equilibrium concentrations, while the system is not at equilibrium due to the high reaction rate. The diffusion of species is considered to take place from the bulk phase to the catalyst active sites

through the pores and the amorphous polymer that make up the pseudo-homogeneous medium supposed by the RPPFM. This phenomena has been described in the random-pore model proposed by Wakao and Smith[28] and has then been applied by Kanellopoulos et al.[34,44] and Yiagolopoulos et al.[27] in order to show its applicability for olefin polymerization. The effective (or overall) diffusion coefficient depends not only on the temperature and concentration of the penetrants in the amorphous phase of the polymer, but also on the particle porosity. Based on these works, the overall diffusion coefficient of species (i) can be expressed as follows:

$$D_{i,\mathrm{ov}} = \frac{\varepsilon}{\tau_\mathrm{f}^2} D_{i,\mathrm{g}} + (1-\varepsilon)(1+3\varepsilon) D_{i,\mathrm{pol}}$$

in which τ_f denotes the tortuosity factor and is introduced to take into account the tortuous nature of the pore phase present in the particle. The value of τ_f is assumed to be equal to 10, as this value has been approximated elsewhere[13,16]. The first term on the right-hand side of this equation represents the transport of the penetrants through the pores while the second term accounts for mass transfer through the semicrystalline polymer phase. The diffusion in the porous polymer particle is calculated from Chapman-Enskog correlation, and details on calculating this can be found elsewhere[29]. $D_{i,\mathrm{pol}} = D_{i,\mathrm{am}}^{\mathrm{ter}}/(\tau\beta_i)$, with β_i the chain immobilization factor accounting for the reduction in amorphous chain segmental mobility due to the proximity of crystallites and τ denotes the tortuosity factor corresponding to the magnitude of extension in the diffusion path associated with bypassing impermeable crystallites by the penetrant[13].

The diffusion of small molecules in the semicrystalline polymer has been studied extensively and has shown that the free volume theory refined by Vrentas and Duda[14,30,31] correlates accurately the diffusion coefficient at various temperatures and over a large concentration range. According to the free-volume theory[15], the diffusion coefficient of ethylene (1) and an ICA (2) in the amorphous PE (3) in the ternary system is given by:

$$D_{1,\mathrm{am.pol}}^{\mathrm{ternary}} = D_{01} exp\left(\frac{-(\omega_1 \hat{V}_1^* + \omega_2 \hat{V}_2^* \xi_{13}/\xi_{23} + \omega_3 \hat{V}_3^* \xi_{13}}{\omega_1 \left(\frac{K_{11}}{\gamma}\right)\left(K_{21} + T - T_{\mathrm{g1}}\right) + \omega_2 \left(\frac{K_{12}}{\gamma}\right)\left(K_{22} + T - T_{\mathrm{g2}}\right) + \omega_3 \left(\frac{K_{13}}{\gamma}\right)\left(K_{23} + T - T_{\mathrm{g3}}\right)} \right)$$

and

$$D_{2,\mathrm{am.pol}}^{\mathrm{ternary}} = D_{02} exp\left(\frac{-(\omega_2 \hat{V}_2^* + \omega_1 \hat{V}_1^* \xi_{23}/\xi_{13} + \omega_3 \hat{V}_3^* \xi_{23}}{\omega_1 \left(\frac{K_{11}}{\gamma}\right)\left(K_{21} + T - T_{g1}\right) + \omega_2 \left(\frac{K_{12}}{\gamma}\right)\left(K_{22} + T - T_{g2}\right) + \omega_3 \left(\frac{K_{13}}{\gamma}\right)\left(K_{23} + T - T_{g3}\right)}\right)$$

in which D_{0i} is the pre-exponential term for component (i), ω_i is the weight fraction of component (i) in the amorphous polymer phase calculated from SL EoS, $\hat{V}_i^*$ is the specific hole free volume of component (i) required for a diffusion jump, K_{1i} and K_{2i} are the free-volume parameters for component (i), T_{gi} is the glass transition temperature of species (i) and γ is the overlap factor introduced because the same free volume is available for more than one molecule.

Table 32 shows the free-volume theory parameters for the current ethylene/n-pentane/LLDPE studied system. The ξ parameter is the ratio of polymer and solvent molar jumping units[32], defined as follows:

$$\xi_{i3} = \frac{\bar{V}_i^0(0)}{\bar{V}_{3j}^*} = \frac{\mathrm{MW}_i * \widehat{V_i^*}}{\bar{V}_{3j}^*}$$

Where $\bar{V}_i^0(0)$is the penetrant molar volume at 0 K (m^3 mol^{-1}), $\bar{V}_{3j}^*$ is the critical molar volume of the polymer jumping unit (j) (m^3 mol^{-1}) and MW_i is the molecular weight of penetrant (i). The detailed calculation of the parameter ξ is proposed in references[20,30].

Table 32. *Parameters of the free-volume theory*

	ethylene	***n*-pentane**	**n-hexane**	**PE**	Units
D_{0i}	2.96×10^{-7}	3.11×10^{-8}	3.50×10^{-8}	—	m^2 s^{-1}
$\hat{V}_i^*$	1.341	1.158	1.133	1.006	cm^3 g^{-1}
K_{1i}/γ	1.97×10^{-3}	2.41×10^{-3}	1.96×10^{-3}	1.02×10^{-3}	cm^3 g^{-1} K^{-1}
$K_{2i} - T_{gi}$	42.38	-38.89	-41.08	-228.70	K
MW_i	28.05	72.15	86.18	—	g mol^{-1}
ξ_{i3}	0.4548	0.95664	0.9184	—	(—)
References	13,32	30	13	33	

2.3.Kinetic Model

2.3.1. Polymer Molecular Weight Data and Deconvolution

It is well accepted that Ziegler-Natta (ZN) catalysts are multi-site catalysts; in other words, each catalyst particle will contain a certain number of "families" of active sites. Each family will propagate at different rates, insert comonomer at different rates and eventually respond to hydrogen differently. One can use MWD deconvolution to identify the minimum number of (families) of active sites needed to describe the behavior of a catalyst system. We used the method described by Soares and McKenna[34] to deconvolute the molecular weight distributions of a series of ethylene polymerizations in the presence of n-pentane and hydrogen over a commercial ZN catalyst. The used experimental conditions are given in ***Table 33*** and the detailed experimental set-up is given in Appendix B.

Table 33. *Ethylene, n-pentane and hydrogen partial pressure for each polymerization experiment. All pressures are in bar.*

	R_{p1}	R_{p2}	R_{p3}	R_{p4}	R_{p5}
P_{C_2}	7				
P_{C_5}	0	1	2	0	2
P_{H_2}	0			3	

Figure 110 shows the experimental MWD and the results of the deconvolution. It appears from this analysis that the MWD can be adequately described with four distributions corresponding to the four site types, for experiments Rp_4 and Rp_5. This fit gives the fraction of each site; then the average of the fraction of each site for both experimental MWD was calculated and is presented in ***Table 34***. This average weight fraction of each site type was then used to identify the polymerization parameters by fitting the measured reaction rate and MWD to the experiments in the following sections.

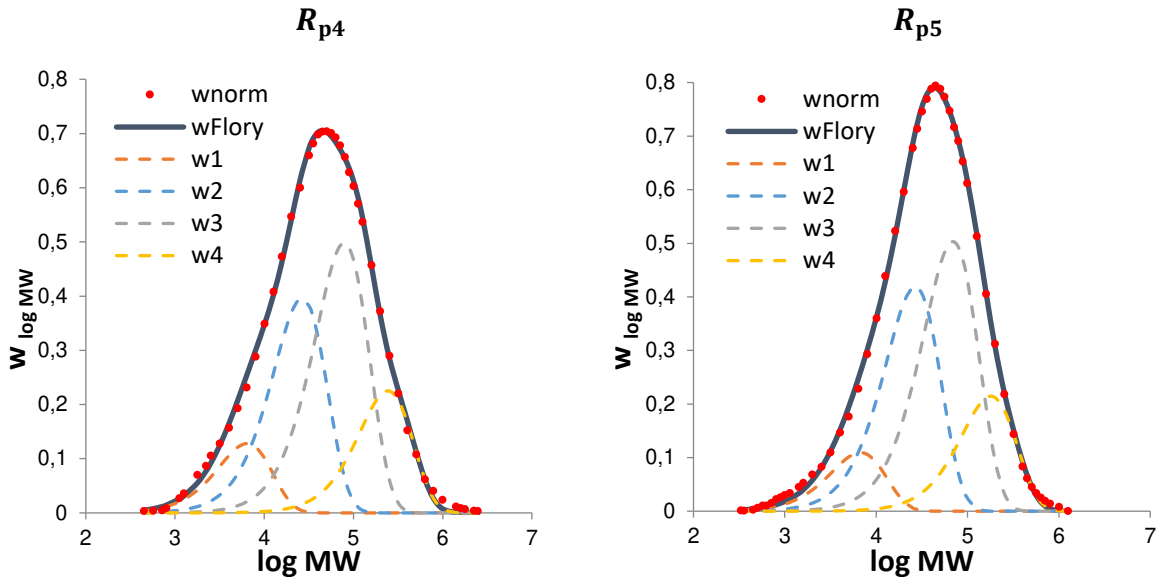

Figure 110. *The deconvolution of the experimental molecular weight distributions (red dots, w_{norm}) for R_{p_4} and R_{p_5} suggests that it is reasonable to use a minimum of 4 site types to describe this catalyst, designated by 1, 2, 3 and 4, respectively. w_{Flory} represents the calculated MWD.*

Table 34. *Fraction of each catalyst active site obtained from the deconvolution*

	Site 1	**Site 2**	**Site 3**	**Site 4**
R_{p_4}	0.1	0.32	0.40	0.18
R_{p_5}	0.09	0.34	0.40	0.17
w_{m_i}	**0.095**	**0.33**	**0.4**	**0.175**

The initial concentration of active sites, that is used as an initial condition for the calculation of the active site concentration, is considered as follow:

$$C^*_{0,k} = w^k_{m_i}\, C^* = w^k_{m_i}\, f_{\text{cat}} C^*_{\text{max}} = w^k_{m_i}\, f_{\text{cat}} \frac{w_{\text{Ti}}}{MW_{\text{Ti}}} \rho_{\text{cat}}$$

Where C^* is the active site concentration, MW_{Ti} is the molecular weight of titanium, ρ_{cat} is the density of the catalyst and f_{cat} is the efficiency factor of the catalyst. C^*_{max}, the maximum concentration of active site for the TiCl4 supported on MgCl2 Ziegler-Natta catalyst, was calculated using the amount of Titanium in the catalyst, w_{Ti}. Since the same catalyst was used by Andrade[35], w_{Ti} was taken equal to 2.8 wt%.

2.3.2. Kinetic Parameters

Following from the deconvolution analysis, a four-site kinetic model is employed in the present study to describe ethylene polymerization in multicomponent system (i.e. ethylene, n-pentane) over a Ziegler-Natta catalyst. The kinetic mechanism shown in ***Table 35*** comprises a classic series of elementary reactions including initiation and propagation reactions, transfer to monomer, molecular weight control reactions (i.e. initiation of P_H^k, transfer to H_2), and a first order spontaneous deactivation reaction. We assume that site activation is instantaneous.

As a result, the particle model combined with the kinetic model can be used to predict not only the polymerization rate, but also the evolution of the temperature and concentration gradients, and the molecular weight distribution as a function of the gas phase composition during ethylene polymerization in gas phase.

Table 35. *Kinetic mechanism of ethylene homopolymerization over a Ziegler-Natta 4 sites catalyst (k = 1 – 4)*

Description	**Chemical equations**	**Rate constants**
Initiation	$C_k^* + \mathrm{M} \longrightarrow P_r^k$	k_{i}^k
Propagation	$P_r^k + \mathrm{M} \longrightarrow P_{r+1}^k$	k_{p}^k
Transfer to H_2	$P_r^k + H_2 \longrightarrow P_{\mathrm{H}}^k + D_r^k$	k_{tH}^k
Initiation of P_H	$P_H^k + M \longrightarrow P_1^k$	k_{iH}^k
Transfer to monomer	$P_r^k + M \longrightarrow P_1^k + D_r^k$	k_{tM}^k
Spontaneous chain transfer	$P_r^k \longrightarrow C_k^* + D_r^k$	k_{tsp}^k
Deactivation	$P_r^k \longrightarrow C_{\mathrm{d}}^k + D_r^k$	k_{d}^k

In ***Table 35***, C_k^* is the concentration of vacant catalyst active sites, M is the monomer concentration, P_r^k is the concentration of "live" polymer chains, P_H^k is the concentration of the activated vacant catalyst sites occupied by a hydrogen, D_r^k is the concentration of dead polymer chains, H_2 is the hydrogen concentration in the bed, C_d^k is the concentration of deactivated catalyst site. The symbol *k* denotes the four catalyst active sites: *1, 2, 3* and *4*.

Based on the proposed kinetic scheme in ***Table 35*** and the definition of the moments of "live" (μ_i^k) and "dead" (η_i^k) total number chain length distributions, we obtain the moment equations summarized in *Erreur ! Source du renvoi introuvable.*.

Table 36. *Mass balances of active sites and moments of chain lengths, with the initial conditions:* $\boldsymbol{\mu_i^k(r,0) = \eta_i^k(r,0) = 0,\ P_H^k(r,0) = 0,\ C_k^*(r,0) = C_{0,k}^*,\ i = 0,1,2,\ k = 1,2\ ,3,4.}$

Description	Equations	Initial conditions
0th moment of living chains	$\frac{d\mu_0^k}{dt} = \left(k_{\mathrm{i}}^k C_k^* + k_{\mathrm{iH}}^k P_{\mathrm{H}}^k\right)[M] - (k_{\mathrm{tH}}^k[H_2] + k_{\mathrm{d}}^k + k_{\mathrm{tsp}}^k)\mu_0^k$	$\mu_0^k(0) = 0$
1st moment of living chains	$\frac{d\mu_1^k}{dt} = (k_{\mathrm{i}}^k C_k^* + k_{\mathrm{iH}}^k P_{\mathrm{H}}^k + (k_{\mathrm{p}}^k + k_{\mathrm{tM}}^k)\mu_0^k)[M] - \left(k_{\mathrm{tH}}^k[H_2] + k_{\mathrm{d}}^k + k_{\mathrm{tM}}^k[M] + k_{\mathrm{tsp}}^k\right)\mu_1^k$	$\mu_1^k(0) = 0$
2nd moment of living chains	$\frac{d\mu_2^k}{dt} = (k_{\mathrm{i}}^k C_k^* + k_{\mathrm{p}}^k\left(2\mu_1^k + \mu_0^k\right) + k_{\mathrm{iH}}^k P_{\mathrm{H}}^k + k_{tM}^k\mu_0^k)[M] - \left(k_{\mathrm{tH}}^k[H_2] + k_{\mathrm{d}}^k + k_{\mathrm{tM}}^k[M] + k_{\mathrm{tsp}}^k\right)\mu_2^k$	$\mu_2^k(0) = 0$
0th moment of dead chains :	$\frac{d\eta_0^k}{dt} = \left(k_{\mathrm{tH}}^k[H_2] + k_{\mathrm{d}}^k + k_{\mathrm{tM}}^k[M] + k_{\mathrm{tsp}}^k\right)\mu_0^k$	$\eta_0^k(0) = 0$
1st moment of dead chains	$\frac{d\eta_1^k}{dt} = \left(k_{\mathrm{tH}}^k[H_2] + k_{\mathrm{d}}^k + k_{\mathrm{tM}}^k[M] + k_{\mathrm{tsp}}^k\right)\mu_1^k$	$\eta_1^k(0) = 0$
2nd moment of dead chains	$\frac{d\eta_2^k}{dt} = \left(k_{\mathrm{tH}}^k[H_2] + k_{\mathrm{d}}^k + k_{\mathrm{tM}}^k[M] + k_{\mathrm{tsp}}^k\right)\mu_2^k$	$\eta_2^k(0) = 0$
Active site concentration	$\frac{dC_k^*}{dt} = k_{\mathrm{tsp}}^k\mu_0^k - (k_{\mathrm{i}}^k[M] + k_{\mathrm{d}}^k)C_k^*$	$C_{0,k}^*$
Catalyst sites bearing hydrogen, P_H	$\frac{dP_{\mathrm{H}}^k}{dt} = k_{\mathrm{tH}}^k\,\mu_0^k[H_2] - k_{\mathrm{iH}}^k P_{\mathrm{H}}^k[M] - k_{\mathrm{d}}^k P_{\mathrm{H}}^k$	$P_{\mathrm{H}}^k(0) = 0$

The rate of ethylene polymerization at the active site, R_p, for multiple catalyst active sites, is defined as follow:

$$R_{\mathrm{p}} = \sum_{k=1}^{N_{\mathrm{S}}} k_{\mathrm{p}}^{k} \mu_0^k [M_1] = (k_{\mathrm{p}}^1 \, \mu_0^1 + k_{\mathrm{p}}^2 \, \mu_0^2 + k_{\mathrm{p}}^3 \, \mu_0^3 + k_{\mathrm{p}}^4 \, \mu_0^4)[M_1]$$

Where N_{S} is the number of catalyst sites and k is the catalyst site type.

The volumetric rate of ethylene polymerization, R_{v}, is calculated by:

$$R_{\mathrm{v}} = R_{\mathrm{p}} \left(\frac{1 - \epsilon}{\varphi^3} \right)$$

And φ is the overall growth factor defined as:

$$\varphi = \frac{R_{\mathrm{pol}}}{r_{\mathrm{cat}}}$$

where R_{pol} is the equivalent radius particle only, excluding the volume of pore phase, at each time step during the reaction and r_{cat} is the radius of initial catalyst particle.

All the rate constants are described by the Arrhenius law as follow:

$$k = k_0 \exp \left(-\frac{E}{R\,T} \right)$$

in which T, E and R are the temperature, the activation energy and the universal gas constant, respectively.

The cumulative number average molecular weight of the polymer:

$$\bar{M}_{\mathrm{n}}(r,t) = \frac{\sum_{k=1}^{N_{\mathrm{S}}} \left(\mu_1^k + \eta_1^k \right)}{\sum_{k=1}^{N_{\mathrm{S}}} \left(\mu_0^k + \eta_0^k \right)} \mathrm{MW}_1$$

The cumulative weight average molecular weight of the polymer:

$$\bar{M}_{\mathrm{w}}(r,t) = \frac{\sum_{k=1}^{N_{\mathrm{S}}} \left(\mu_2^k + \eta_2^k \right)}{\sum_{k=1}^{N_{\mathrm{S}}} \left(\mu_1^k + \eta_1^k \right)} \mathrm{MW}_1$$

This method of moments gives the cumulative weight and number average molecular weight as well as the individual ones for each active site.

The MWD was reconstructed from these average values assuming that each catalyst site type produces a polymer where the chain lengths follow a lognormal distribution:

$$w(k, M_\mathrm{w}) = \frac{1}{M_\mathrm{w}\sigma_\mathrm{ln}(k)\sqrt{2\pi}} \exp\left(-\frac{\left(\ln M_\mathrm{w} - \ln \bar{M}_\mathrm{n,ov}(k)\right)^2}{2\sigma_\mathrm{ln}^2(k)}\right)$$

Where M_w is the polymer molecular weight, the variance is $\sigma_\mathrm{ln}(k) = \sqrt{\ln \frac{\bar{M}_\mathrm{w,ov}(k)}{\bar{M}_\mathrm{n,ov}(k)}}$, $w(k, M_\mathrm{w})$ is a density distribution as a function of $\ln M_\mathrm{w}$, and $\bar{M}_\mathrm{n,ov}(k)$ is the average value of $\bar{M}_\mathrm{n}(r,t)$ over the whole particle. The total MWD is then the sum of the MWD produced by the different catalyst sites, which is then normalized and transformed to a molar mass density to permit comparison with the experimental MWD given from the HT-GPC:

$$w_\mathrm{tot}(t, M_\mathrm{w}) = M_w \sum_{k=1}^{4} \frac{w(k, M_\mathrm{w}) w_{\mathrm{m}_k}}{\int_0^\infty w(k, M_\mathrm{w})\mathrm{d}M_\mathrm{w}}$$

The measured polymerization rate with time, and the measured final polymer MWD have been fitted to the model in order to identify a set of representative kinetic parameters, using the following minimization criterion:

$$J = \frac{|\bar{m}_\mathrm{w,m} - \bar{m}_\mathrm{w,exp}|}{\bar{m}_\mathrm{w,exp}} + \sum_{t=5,10,15,20\ \mathrm{min}} \frac{|R_\mathrm{p}(t) - R_\mathrm{p}^\mathrm{exp}(t)|}{R_\mathrm{p}^\mathrm{exp}(t)}$$

Where $\bar{m}_\mathrm{w,m}$ and $\bar{m}_\mathrm{w,exp}$ are the modes of the final model MWD, $w_\mathrm{tot}(M_\mathrm{w})$, and experimental $w_\mathrm{logM_w}^\mathrm{exp}(M_\mathrm{w})$, respectively.

Some parameters were taken from literature, such as the rate constants of transfer to monomer, k_tm0, spontaneous termination, k_tsp0, as well as the activation energy of the different constants[36]. The parameter k_iH0 was considered to be equal to k_i0, as was assumed by McAuley et al. for instance[37]. For the sake of simplicity, the kinetic parameters were taken the same for all catalyst site types, except for transfer to hydrogen, k_tH0. In order to be able to predict the experimental width of the MWD, it was found that the transfer to hydrogen parameters of the different active sites can be related as follows: $k_\mathrm{tH0}^1 = 8k_\mathrm{tH0}^4$, $k_\mathrm{tH0}^2 = 6k_\mathrm{tH0}^4$ and $k_\mathrm{tH0}^3 = 4k_\mathrm{tH0}^4$. Once again, the goal of this modelling study is to show realistic values of the impact of the ICA on the polymerization process, and not to accurately model the reaction precisely for this catalyst. These parameters give us however a reasonable approximation of ZN kinetics so that the thermodynamic effects can be highlighted independently.

***Table 37**. Values of the kinetic parameters used for the model of ethylene polymerization in gas-phase. The same parameters are used for all sites, except transfer to hydrogen (a the given value is for catalyst site type n° 4).*

	Pre-exponential factor (m^3 mol^{-1} s^{-1})	**Activation energy (J mol^{-1})**	**Reference**
Initiation	94	37656	This work
Reinitiation of sites bearing hydrogen	94	37656	This work
Propagation	1.4×10^6	37656	This work
Transfer to H_2	20.6 [a]	33472	This work
Transfer to monomer	0.186	33472	[36]
Spontaneous chain transfer	8.84	33472	[36,37]
Deactivation	33	33472	This work

This leaves us with 5 parameters that need to be identified by fitting the experimental data: k_{i0}, k_{p0}, k_{d0}, k_{tH0}^4 and f_{cat}. In order to do so, the experiments without hydrogen were first fitted to the model in order to identify k_{i0}, k_{p0}, k_{d0} and f_{cat}. The parameters k_{p0} and f_{cat} were used to adjust the level of $R_{\mathrm{p}_i}^{\mathrm{model}}$ during the entire period of the reaction, while k_{i0} was used to tune the initial amplitude of $R_{\mathrm{p}_i}^{\mathrm{model}}$ and k_{d0} was used to adapt the slope of $R_{\mathrm{p}_i}^{\mathrm{model}}$. Then, the experiments with hydrogen were fitted to the model by keeping the previously identified parameters constant, and by changing only k_{tH0}^4 which serves to adjust the MWD with $R_{\mathrm{p}_i}^{\mathrm{model}}$. Some adjustment of k_{p0} and f_{cat} were needed when fitting to experiments with hydrogen. These two parameters have the same impact on the reaction rate, and so they might not be identifiable based on the measurement of R_{p} alone. However, they do not have the same impact on the molecular weight (as f_{cat} does not influence the polymer molecular weight), therefore using both measurements may improve their identification. The adjusted value of f_{cat} was taken equal to 0.9.

Figure 111, ***Figure 113*** and ***Figure 113*** compare the experimental rates of polymerization without hydrogen, with 3 bar of hydrogen and the molecular weight distributions with the model predictions, respectively. These results shows that the predicted model and the experimental

reaction rates and MWDs are in good agreements at different compositions of the gas phase (i.e. n-pentane, hydrogen). The model can capture well the effect of n-pentane (as ICA) and hydrogen on the reaction rate and MWD. To the best of our knowledge, this is the first time that a detailed SPM, containing accurate thermodynamic models, is associated to a kinetic model in order to show the impact of the gas phase composition on the dynamics of polymerization of ethylene in gas-phase reactors.

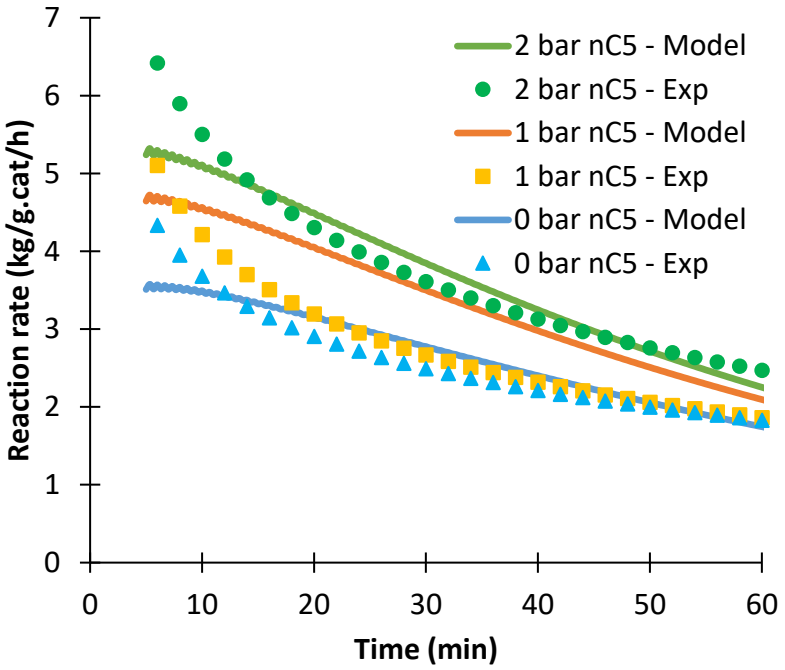

***Figure 111**. Polymerization rate calculated with the PFM and the experimental data of 7 bar of ethylene, with different amounts of n-pentane, and without hydrogen, at 80°C*

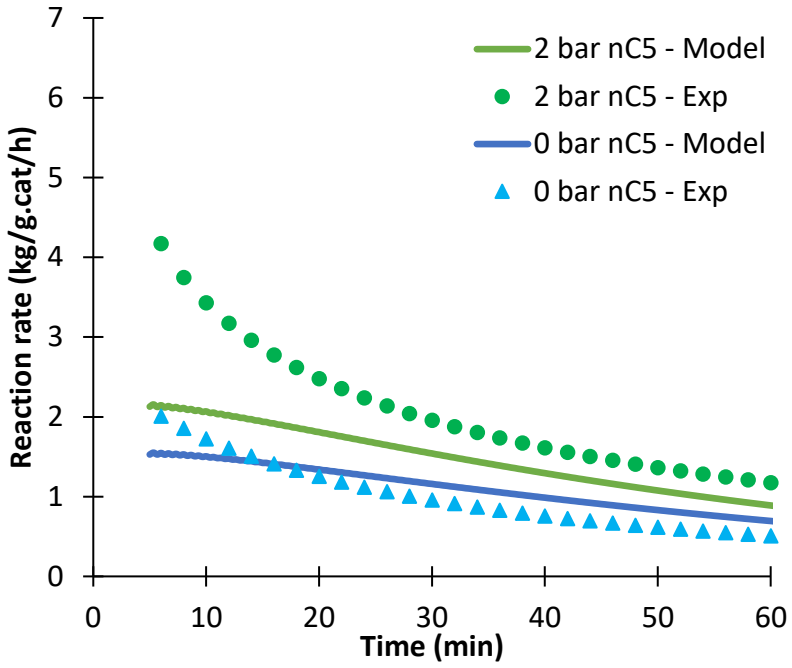

Figure 112. Polymerization rate calculated with the PFM and the experimental data of 7 bar of ethylene, with 3 bar of hydrogen and different amounts of n-pentane, at 80°C

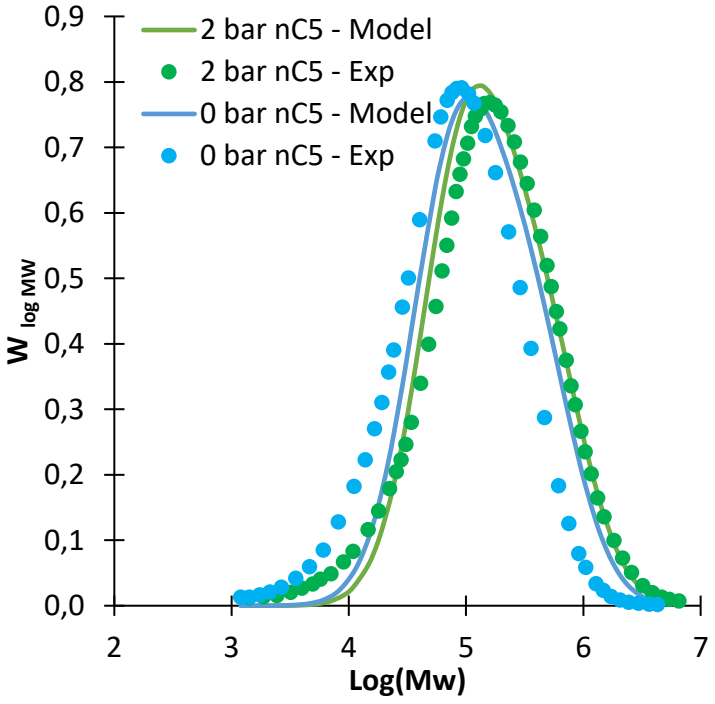

Figure 113. Molecular weight distribution calculated with the PFM and the experimental data measured with high temperature GPC of 7 bar of ethylene, 3 bar of hydrogen and 0 and 2 bar of n-pentane at 80°C

3. Results and discussion

The development of a single particle model associated with a kinetic model was employed to analyze the change in the gas phase composition (i.e. n-pentane, hydrogen) on the evolution of the concentration profiles, the reaction rate, the growth and overheating of the polymer particle, as well as the molecular weight distribution. This model was validated with the previous experimental data on reaction rates and molecular weight distributions (c.f. ***Figure 111***, ***Figure 113*** and ***Figure 113***). The temperature and ethylene partial pressure were kept constant (i.e. 7 bar of ethylene and 80°C, respectively) and only the partial pressures of n-pentane and hydrogen are changing between each experiment $R_{\mathrm{p}i}$.

3.1.Effect of thermodynamic and diffusion models

To the best of our knowledge, with the exception of a recent paper from Alizadeh et al.[13], virtually all single particle modelling studies appear to rely on binary solubility and diffusion models to describe ternary systems. However, it has been shown that the interactions between the two penetrants in ternary systems are crucial and lead to important changes when describing ethylene polymerization in gas phase. Adding ICA to the gas phase composition improves the heat capacity of the gas phase but also increases ethylene diffusion through the polymer phase which will lead to higher concentration of ethylene in the amorphous phase of the polymer. The instantaneous rate of ethylene polymerization is therefore higher in presence of ICA, as can be seen in ***Figure 114***. This was partly attributed to the co-solubility effect and to co-diffusion effects. Adding ICA to the gas phase composition leads to a co-solubility effect of ICA on ethylene and an anti-solvent effect of ethylene on ICA and to an enhanced diffusivity of ethylene. Accurate sorption and diffusion models are therefore important tools when modeling a single particle model in order to better analyze the influence of the gas phase composition on the polymerization rate.

Figure 114 compares the reaction rate as well as ethylene concentration gradients at 7 bar of ethylene, 1 bar of hydrogen and 1 (i.e. Rp_8) and 2 (i.e. Rp_9) bar of n-pentane. The binary model corresponds to the use of binary diffusivity and concentration of ethylene and n-pentane using SL EoS for binary systems, without taking into account the interactions between these two penetrants. The ternary corresponds to the use of ternary diffusivity and concentration of the gas phase mixture in the polymer, estimated by ternary Sanchez Lacombe EoS It can be seen that using the binary thermodynamic model leads to an underestimation of the concentration of

ethylene, leading to an underestimation of the polymerization rate. In the binary model, changing the concentration of ICA may only affect the temperature gradients inside the particle. However, the thermal effect was found to be negligible in this case, so no effect of the ICA is observed on the reaction rate when using the binary model.

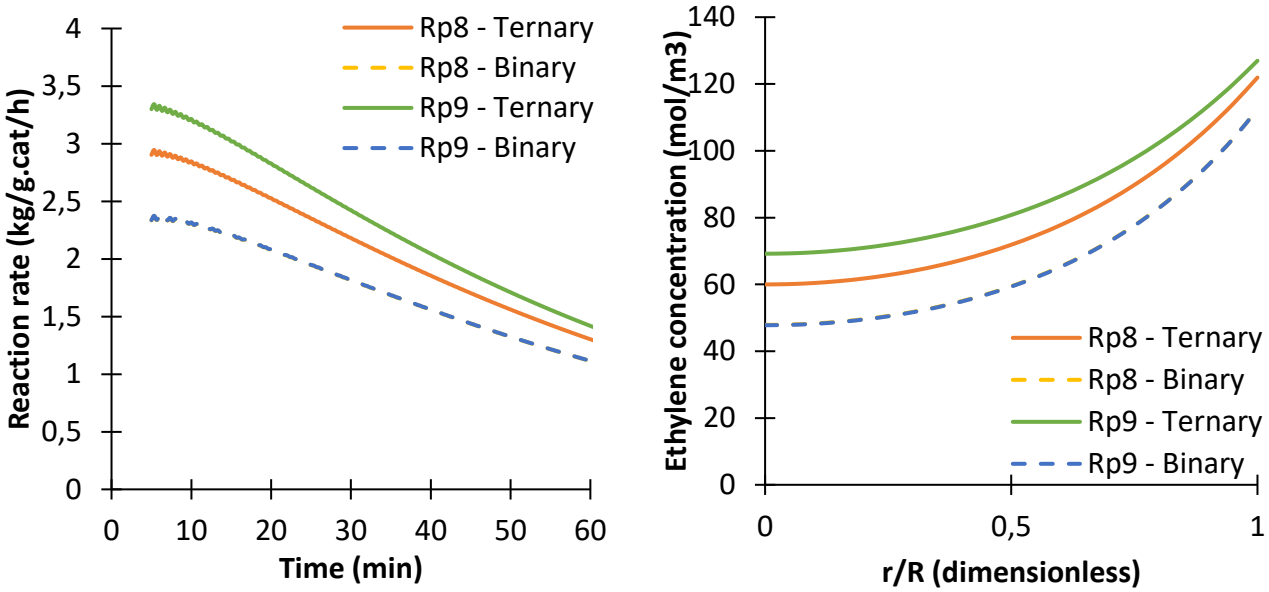

Figure 114. *Effect of thermodynamic model (i.e. binary, ternary) on the polymerization rate during the reaction and ethylene concentration gradients as a function of the normalized particle radius. The gas phase composition of Rp_8 (1 bar C_5, 1 bar H_2) and Rp_9 (2 bar C_5, 1 bar H_2) is described in Table 33. The concentration are taken at 40 minutes of the reaction. The porosity is ε=0.05.*

Note that the equilibrium concentration (i.e. the concentration of ethylene at the surface of the particle), is higher when ICA pressure is higher due to the co-solubility effect estimated by SL EoS. It is shown that the concentration of ethylene at the surface of the particle is about 121.92 mol m^{-3} with 1 bar of C_5 (i.e. Rp_8) and 126.96 mol m^{-3} with 2 bar of C_5 (i.e. Rp_9); so about 3.97% increase. It can be seen that higher amount of ICA leads to higher concentration of ethylene at the center of the particle, with an increase of 17% when adding 1 bar of n-pentane, and of 31% when 2 bars of n-pentane are added. This difference does not explain alone the observed effect of ICA on R_p which increases from about 3.23 to 3.65 kg g^{-1} h^{-1} from 1 to 2 bar of ICA, at 10 minutes of the reaction; so about 13% increase. Therefore, the co-diffusion effects are playing an important role too.

3.2.Effect of particle porosity

The overall diffusion coefficient of a given system depends on the temperature and concentration of the different gases in the amorphous phase of the polymer, but also on the particle porosity. However, the porosity of the produced polymer has not been measured

experimentally. The effect of particle porosity on ethylene diffusivity in ethylene/n-pentane/LLDPE ternary system calculated with the parameters given in ***Table 32*** is shown in ***Figure 115***.

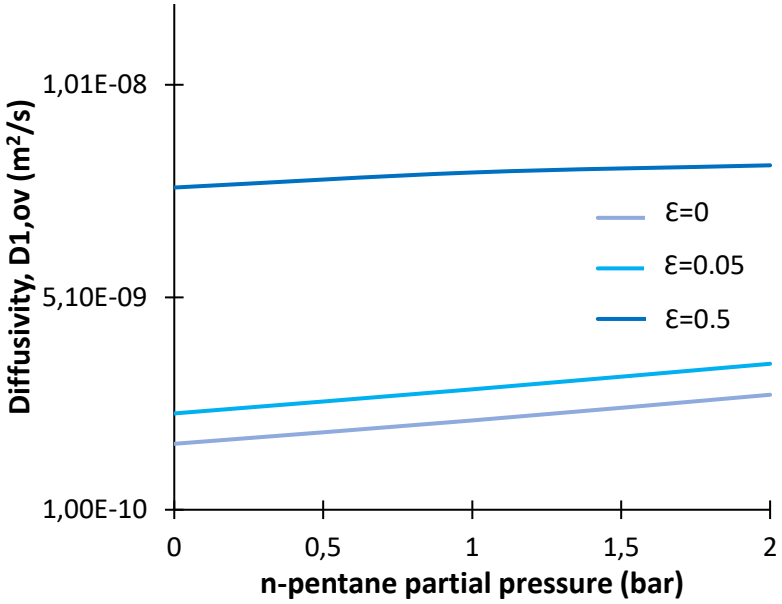

Figure 115. *Ethylene diffusion coefficient in ethylene/n-pentane/LLDPE at 80°C as a function of n-pentane partial pressure for different polymer porosity.*

The diffusion coefficient of ethylene increases with n-pentane partial pressure for a particle having a low degree of porosity (up to ε=0.5). It is shown that for a highly compact particle, increasing n-pentane partial pressure increases ethylene diffusion in the amorphous phase of the polymer, due an increase in the free volume available to of the amorphous phase of the polymer and therefore higher diffusion coefficient of ethylene.

The observed effect of the particle porosity on ethylene diffusivity, especially at higher n-pentane partial pressure, will have an impact on ethylene concentration gradients inside the growing polymer particle. ***Figure 116*** shows ethylene concentration as a function of the normalized particle radius for different polymer porosities and ICA pressures, 1 (i.e. Rp_8) and 2 bar (i.e. Rp_9) of n-pentane. It is shown that increasing the polymer porosity has a noticeable effect on ethylene concentration gradient inside the particle. Furthermore, increasing n-pentane partial pressure from 1 bar to 2 bar increases ethylene concentration gradient for all particle porosities because of the co-diffusion effect. However, the co-diffusion effect is stronger for a particle having a lower degree of porosity (as co-diffusion concerns diffusion into the

amorphous polymer, not in the pores). As one would expect, faster diffusion corresponds to less significant gradients.

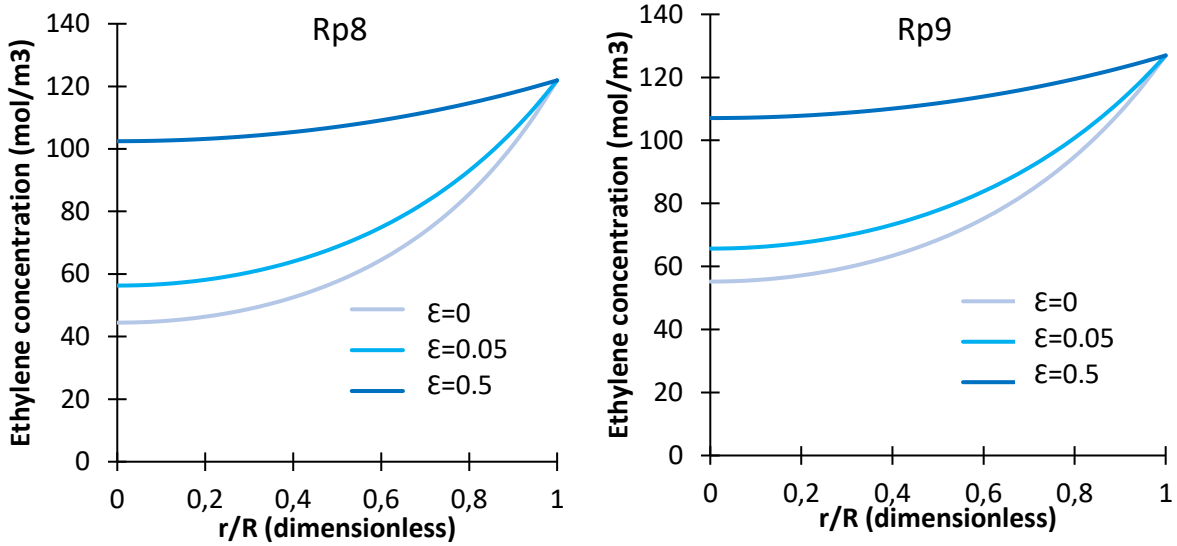

Figure 116. *Effect of polymer porosity on ethylene concentration gradient at 40 minutes of the reaction as a function of the normalized particle radius for 7 bar of ethylene, 1 bar of hydrogen and 1 (R_{p8}) and 2 bar (R_{p9}) of n-pentane*

The porosity of the polymer was chosen ε=0.05 as we do not have this information about the used polymer, and all the next simulations will use this value of porosity.

3.3.Effect of the gas phase composition on ethylene polymerization

3.3.1. Effect of the gas phase composition on the polymerization rate

As have been showed in the previous sections, adding ICA will lead to co-solubility and co-diffusion effects. ***Figure 117*** shows the simulated polymerization rate with respect to the polymerization time, for different amounts of hydrogen and n-pentane; 0-2 bar for n-pentane and 0-3 bar for hydrogen. We can see that the difference between the polymerization rate in the absence of n-pentane (binary) and with 1 bar of n-pentane is higher than the difference between 1 and 2 bar of n-pentane, for all hydrogen pressures, due to the co-solubility and co-diffusion effects in ternary systems.

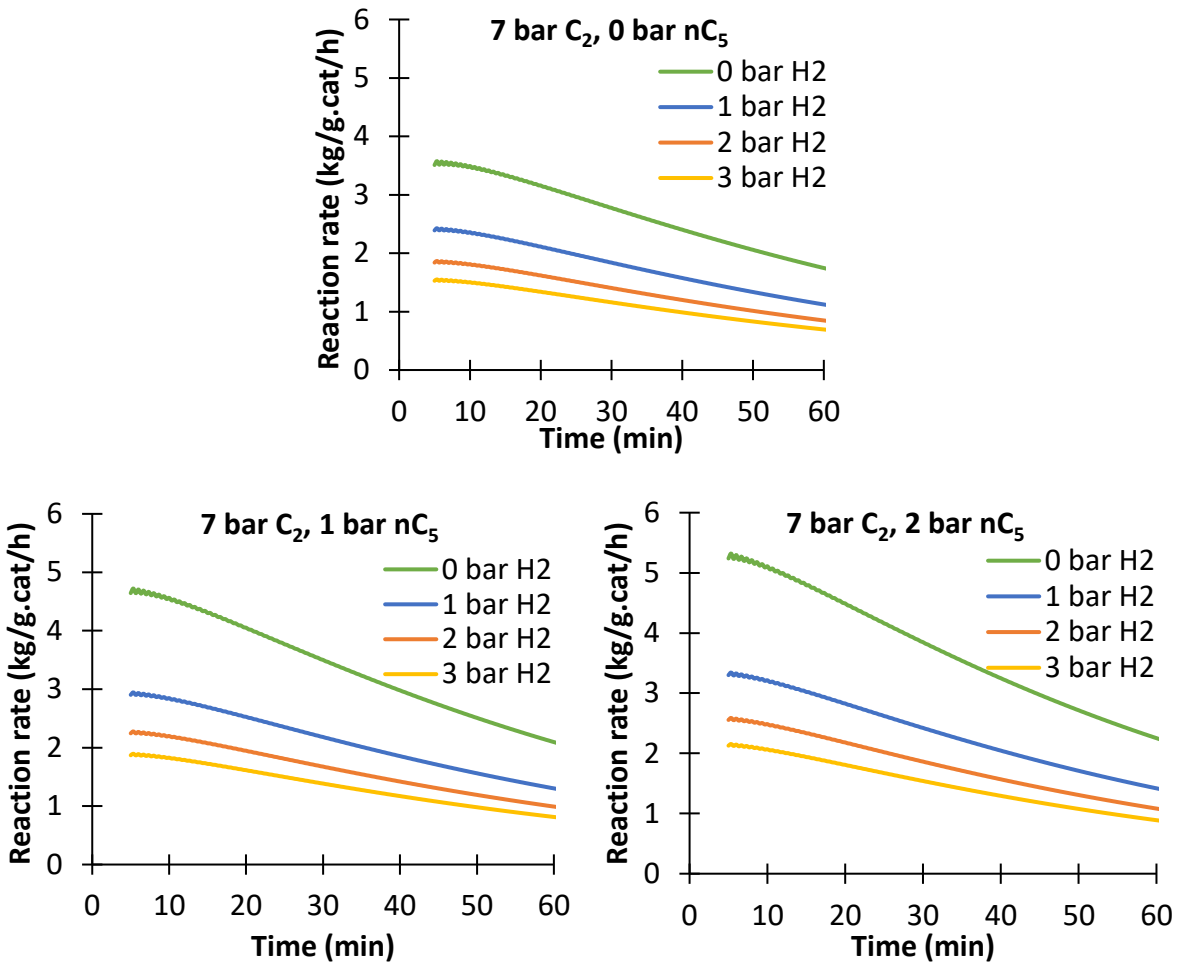

Figure 117. Polymerization rate during the reaction time for 7 bar of ethylene, 0, 1 and 2 bar of n-pentane and different amounts of hydrogen, at 80°C

Figure 117 also shows the effect of hydrogen on the polymerization rate. A great difference can be seen without hydrogen and with 1-3 bar of hydrogen at the beginning of the reaction, from 5.3 kg/g.cat/h without hydrogen to 2.7 kg/g.cat/h with 3 bar of hydrogen, with 1 bar of n-pentane. This difference is mainly due to the fact that chain transfer to hydrogen stops the reaction on the active site until P_H is reinitiated, and this reinitiation is slower than the initiation of vacant sites. Note that the solubility of hydrogen in the amorphous phase of the polymer is quite low compared to that of ethylene or n-pentane, the concentration of hydrogen is therefore assumed to be constant in the whole particle over time, and not influence the concentration/diffusion of ethylene in the amorphous phase of the polymer.

3.3.2. Effect of the gas phase composition on ethylene concentration gradient

Figure 118 shows ethylene concentration gradients inside the polymer particle, from the surface to the center of the particle. Different amounts of ICA as well as hydrogen are used; 0-2 bar for n-pentane and 0-3 bar for hydrogen. The concentration of ethylene at the surface is the equilibrium concentration calculated from SL EoS for ternary system of ethylene/n-pentane/LLDPE (c.f. ***Table 30*** and ***Table 31***).

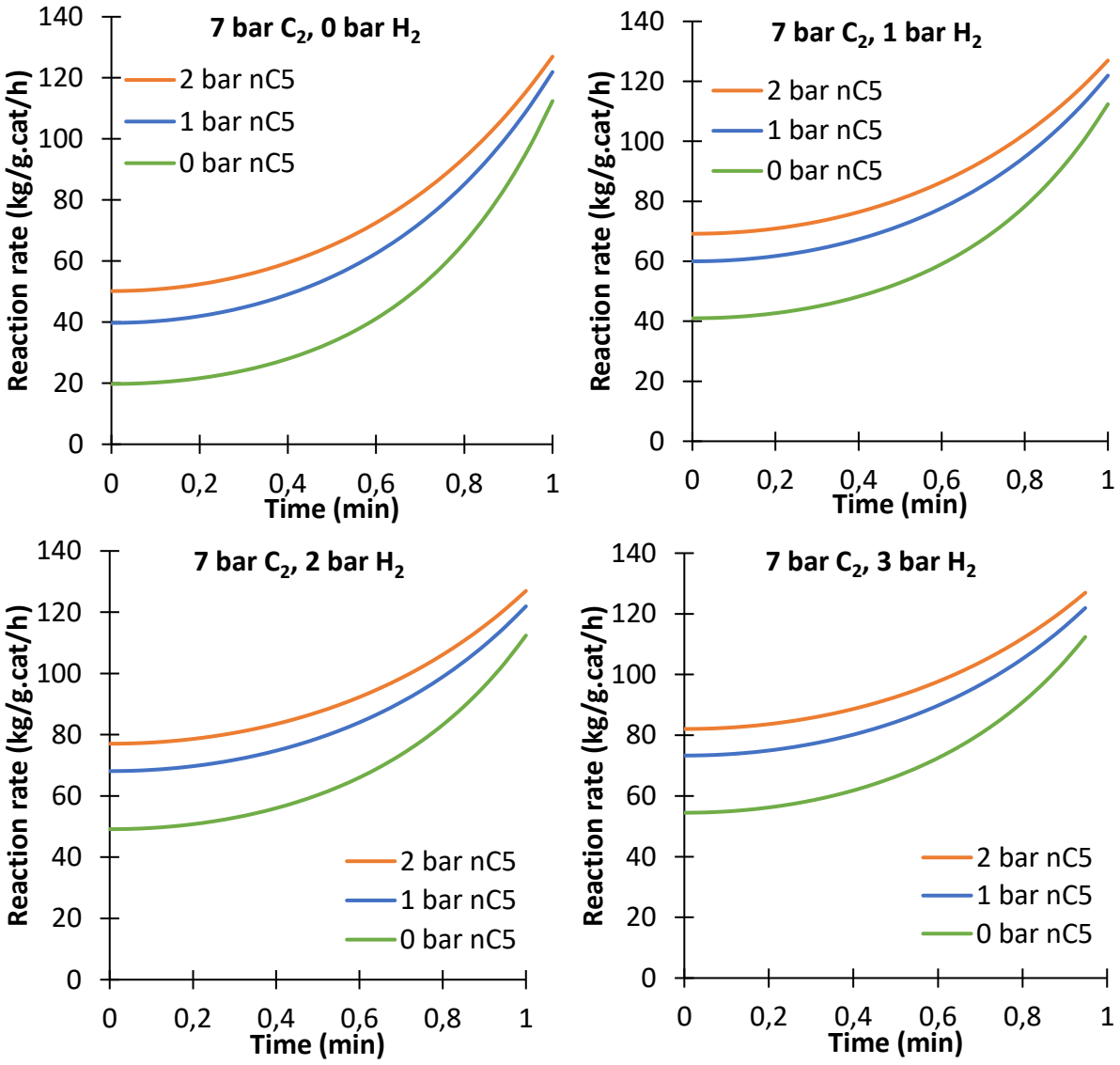

Figure 118. *Ethylene concentration gradients as a function of the normalized particle radius at 40 minutes of the reaction for 7 bar of ethylene, 0-2 bar of n-pentane and 1-3 bar of hydrogen at 80°C*

Figure 118 shows that ethylene concentration at the surface is not the same for the different amounts of ICA used. The concentration of ethylene at the surface is not only function of ethylene pressure, as one would expect from a basic particle model. This concentration is also

function of the amount of ICA injected into the reactor during ethylene polymerization in gas phase. The overall equilibrium concentration of ethylene at the surface increases as we increase ICA partial pressure. This is due to co-solubility effect; heavier alkanes increase the solubility of lighter ones. Also, increasing ICA partial pressure leads to less concentration gradients (between the particle surface and its center) which is due to co-diffusion effects; heavier alkanes increase the overall diffusivity of lighter ones through the growing particle.

The effect of hydrogen partial pressure can also be seen in ***Figure 118***. It is shown that increasing the hydrogen partial pressure decreases the gradient of concentration of ethylene inside the growing polymer particle, with an increase of almost 66% of ethylene concentration at the center of the particle from 0 to 3 bar of hydrogen with 1 bar of n-pentane. This can be explained by the lower reaction rate when adding more hydrogen.

3.3.3. Effect of the gas phase composition on the temperature gradient

The difference between the temperature of the particle surface T_s and the bulk temperature T_b represents the overheating of the particle. ***Figure 119*** shows the overheating of the polymer particle during reaction time at the same conditions as previous simulations. We can see that the particle temperature rises significantly at the beginning of the reaction and then declines at 20 minutes to a steady-state value. This is expected as the reaction rate is higher at the beginning, and the surface area for heat exchange is the lowest. These temperature gradients were calculated using the Ranz-Marshall correlation, so it is possible that they are larger than might be the case in a fluidized bed reactor. Nevertheless, the relative changes between the different cases will be similar regardless of the correlation chosen. Regarding the effect of ICA, we can see that adding ICA leads to a slight increase of the boundary layer temperature gradient at the beginning of the polymerization, which is due to the higher monomer concentration and reaction rate. With the kinetic parameters chosen here, the increased heat capacity of the gas phase is outweighed by the increase in rate due to the addition of the ICA. On the other hand, as shown in ***Figure 111***, ***Figure 112*** and ***Figure 118***, increasing the hydrogen partial pressure decreases the reaction rate which leads to a lower reaction rate.

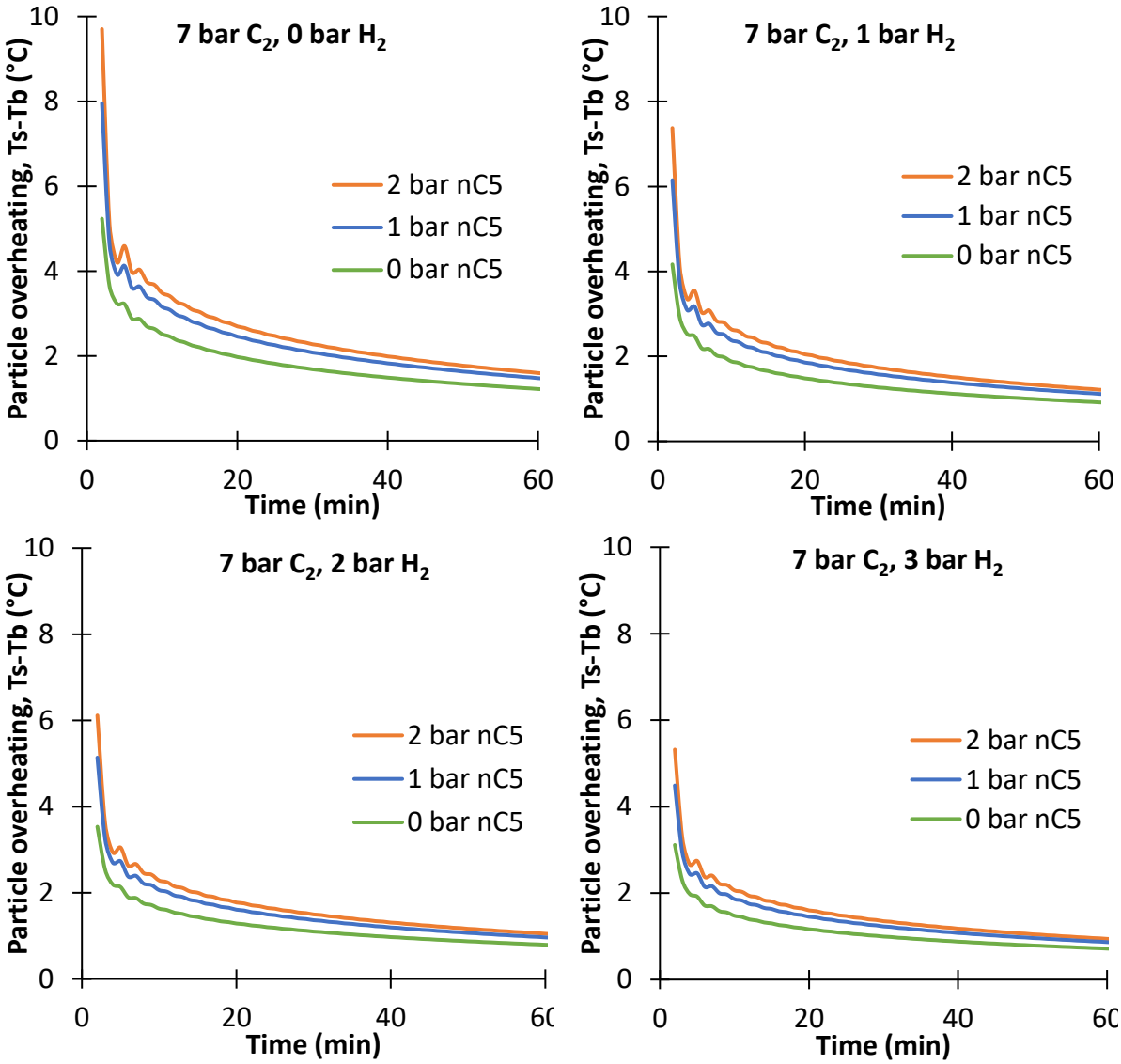

Figure 119. Particle overheating during ethylene polymerization 7 bar of ethylene, 0-2 bar of n-pentane and 1-3 bar of hydrogen at 80°C

Besides, the overheating of the polymer particle during ethylene polymerization in gas phase depends on hydrogen partial pressure. As can be seen in ***Figure 117*** and ***Figure 118***, increasing the hydrogen partial pressure decreases the reaction rate which leads to a reduction in the ethylene concentration inside the amorphous phase of the polymer. Producing less polymer leads to less overheating of the produced polymer particle, especially in presence of ICA that acts as heat dispersing agents. Nevertheless, the use of the Ranz-Marshall correlation to calculate the external film heat transfer coefficient may lead to an overestimation of the particle temperature. Thus the exact values of the temperature gradient reported here need to be taken with caution.

3.3.4. Effect of the gas phase composition on the molecular weight distribution

Figure 120 and ***Figure 121*** show the effect of hydrogen and n-pentane partial pressure, respectively, on the molecular weight distribution. Hydrogen is the most important factor for controlling the MWD, because chain transfer to hydrogen is the main reaction producing dead polymer, even though the temperature as well as ethylene concentration may impact importantly the MWD. Increasing the hydrogen concentration leads to lower MWD. However, increasing ICA partial pressure will lead to higher MWD since it will increase the concentration of ethylene in the amorphous phase of the polymer, producing longer chains. The effect of ICA partial pressure is nevertheless less significant than the effect of hydrogen partial pressure on the MWD, as can be seen in ***Figure 121***.

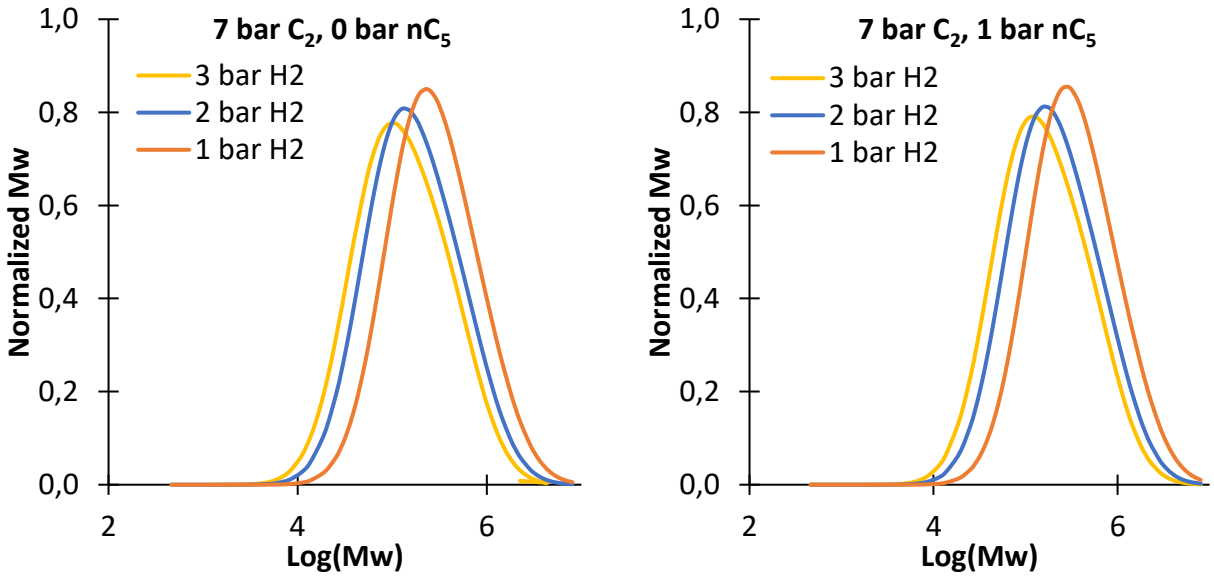

Figure 120. *Effect of hydrogen on the molecular weight distribution calculated with the method of moments at 7 bar of ethylene and 0 and 1 bar of n-pentane, at 80°C*

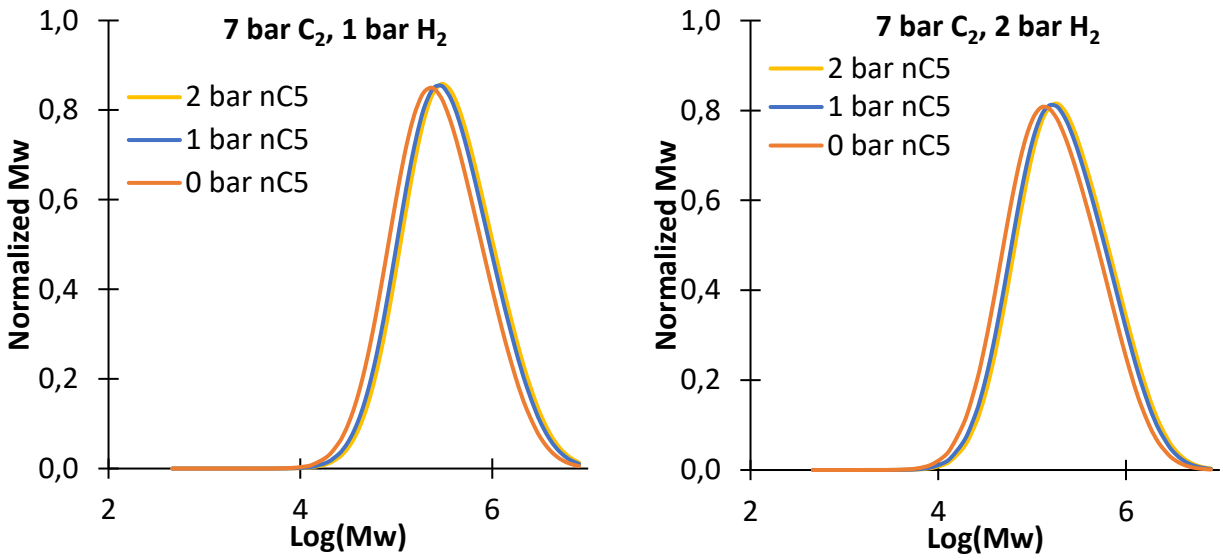

Figure 121. Effect of n-pentane on the molecular weight distribution calculated with the method of moments at 7 bar of ethylene and 1 and 2 bar of hydrogen, at 80°C

3.4.Effect of ICA type

As has been shown in previous papers[38-40], different ICA can influence the polymerization rate in different ways due to different co-solubility effects. One could therefore suspect that changing the ICA will lead to changes in the internal concentration gradients and MWD as well. To test this idea, simulations were run with the same kinetic parameters defined above, but with different parameters for the thermodynamic model (i.e. solubility and diffusivity). The SL parameters are given in Table 30 and Table 31 and the Vrentas and Duda parameters for the diffusivity are given in Table 32 for both n-pentane and n-hexane at 80°C. The interaction parameters for the ethylene/n-hexane/HDPE system were taken from Alizadeh et al.[13]. Note that the crystallinity of the polymer made in the presence of n-pentane in this work is 45%, whereas that of Alizadeh et al. was 60%. For this reason the simulation results are shown as normalized polymerization rates, normalized ethylene concentration gradient and normalized diffusivity to be able to quantify the change from the dry mode (pure ethylene) to the condensed mode in presence of n-hexane and n-pentane as ICAs.

***Figure* 122** compares the polymerization rate in presence of 7 bar of ethylene with either 1 bar of n-pentane or 1 bar of n-hexane normalized by the polymerization rate in dry mode (i.e. pure ethylene). This figure shows that the polymerization rate in presence of n-hexane is higher than in presence of an equivalent amount of n-pentane, with respect to the one with pure ethylene. The increase in the polymerization rate in condensed mode (i.e. in presence of ICA) is about

1.4 for n-pentane compared to 1.62 for n-hexane. This trend was validated with Alizadeh et al.[38] who compared the polymerization rate in presence of 1 bar of n-pentane with 0.8 bar of n-hexane. They found out that the increase in the polymerization rate in presence of 1 bar of n-pentane was about 1.5 and in presence of n-hexane about 1.85. It is important to note that they found a higher increase of the polymerization rate in presence of n-hexane because their crystallinity is lower than the one used in the present study. It is also interesting to note that the slopes of the curves are different, showing that there are also diffusion effects involved, and that the higher diffusion coefficients for n-pentane and for n-hexane lead to faster rates at the beginning of the polymerization.

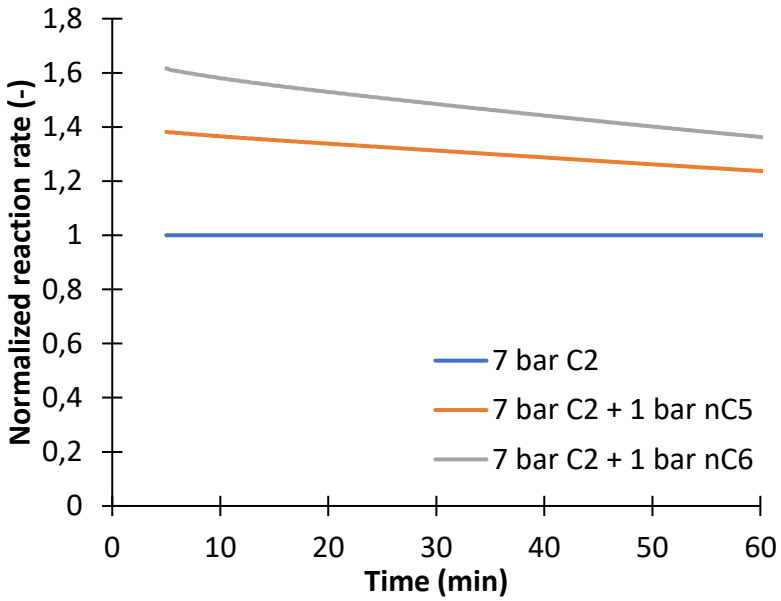

Figure 122. Polymerization rate during the reaction time for 7 bar of ethylene with 1 bar of n-pentane and n-hexane normalized by the polymerization rate without ICA at 80°C

This is due to the co-solubility and co-diffusion effects that are presented in ***Figure* 123** and ***Figure* 124**. shows the diffusivity of ethylene in the ternary system of ethylene/ICA/PE normalized by the diffusivity of ethylene in the binary system as a function of ICA partial pressure for 1 bar of n-pentane and 1 bar of n-hexane as ICA at 80°C. It is shown that adding 1 bar of n-hexane leads to a higher increase of ethylene diffusivity with respect to 1 bar of n-pentane. This is explained by the co-diffusion effect, where adding ICA increases ethylene diffusivity and the heavier the ICA is, the higher the diffusivity will be. ***Figure* 124** shows ethylene concentration gradient at 40 minutes of the reaction with either 1 bar of n-pentane or 1 bar of n-hexane normalized by the concentration gradient of ethylene in dry mode as a function of the normalized particle radius. This figure shows that the equilibrium concentration

calculated from SL EoS is slightly higher in presence of n-hexane than in presence of n-pentane. The difference is expected to be higher, but the crystallinity of LLDPE in presence of n-hexane is about 60% compared to 45% in presence of n-pentane. However, it demonstrates that the concentration of ethylene at the surface is function of ethylene pressure but also on the type and amount of ICA used during the polymerization reaction. Besides, it is shown that adding ICA leads to higher concentration gradient of ethylene inside polymer particle due to co-solubility effect of ICA increasing ethylene concentration in the amorphous phase of the polymer. Furthermore, heavier ICA lead to higher concentration gradient of ethylene due to the co-diffusion effect of ICA increasing the diffusivity of ethylene through the growing polymer particle.

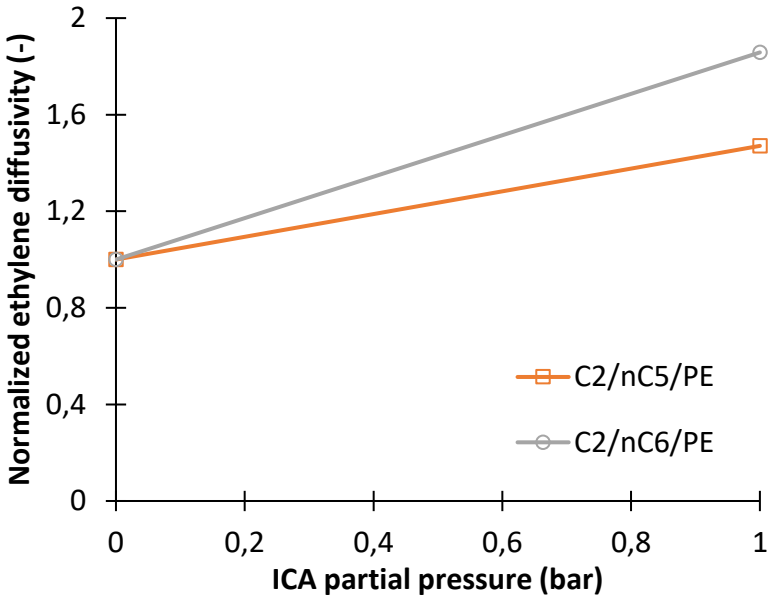

Figure 123.*Ethylene diffusivity in the ternary system of ethylene/ICA/PE normalized by ethylene diffusivity in the binary system of ethylene/PE as a function of ICA partial pressure at 80°C.*

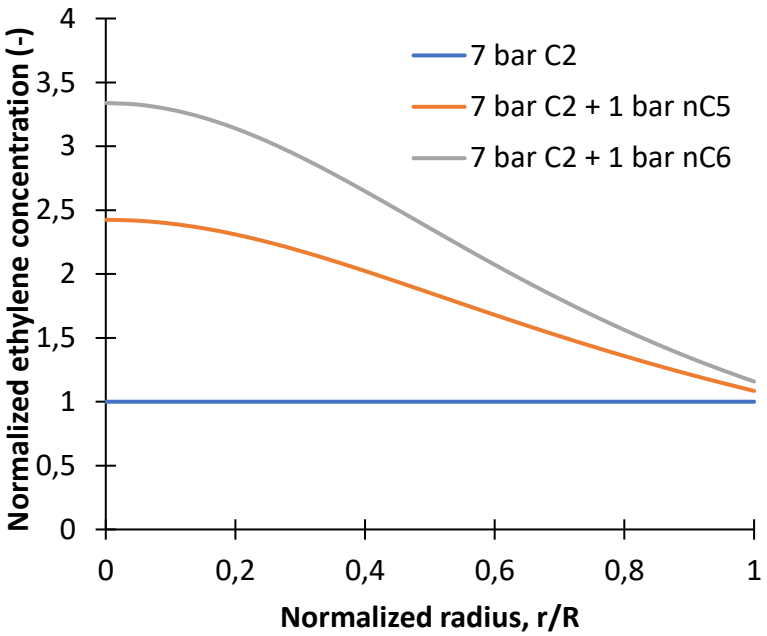

Figure 124.*Ethylene concentration gradient as a function of the normalized particle radius at 40 minutes of the reaction for 7 bar of ethylene with 1 bar of n-pentane and n-hexane normalized by ethylene concentration gradient without ICA at 80°C*

4. Conclusion

A single particle model, based on the RPPFM has been developed in this chapter in order to describe describe the polymerization of ethylene in presence of n-pentane and hydrogen at 80°C. The RPPFM model was adapted to quantify the impact of the gas phase composition (i.e. monomer, n-pentane, hydrogen) on the reaction rate, the concentration and temperature gradients and the molecular weight distribution. 0-2 bar of n-pentane have been used, and 0-3 bar of hydrogen, with a constant pressure of 7 bar of ethylene. The particle model was therefore validated with experimental reaction rate data as well as the measure of the molecular weight distribution through the HT-GPC.

The importance of using an accurate thermodynamic model describing both the equilibrium concentration of the different penetrants as well as the diffusion of these penetrants in the amorphous phase of the polymer, has been highlighted. The Sanchez-Lacombe EoS have been used as sorption model, and Vrentas and Duda, as diffusion model. It is important to note that the concentration of hydrogen being very low compared to ethylene concentration in the polymer, it was considered constant over time and particle radius and not influencing the concentration/diffusivity of ethylene. Model predictions showed that the use of binary systems leads to an underestimation of ethylene concentration and therefore of the polymerization rate, because of co-solubility and co-diffusion effects. Furthermore, the use of different type of ICAs (i.e. n-pentane, n-hexane) demonstrates that accurate thermodynamic models are crucial when describing their effects on the polymerization reaction.

The effect of the gas phase composition has been evaluated through the polymerization rate, ethylene concentration gradients inside the polymer particle, the growth and overheating of the polymer particle, and finally the molecular weight distribution. In all the results, the higher the partial pressure of hydrogen is, the lower is the productivity and the molecular weight of the polymer, whereas increasing n-pentane partial pressure increases the productivity and the polymer molecular weight.

5. References

1. McKenna, T. F. L. Growth and Evolution of Particle Morphology: An Experimental & Modelling Study. *Macromol. Symp.* **260**, 65–73 (2007).

2. McKenna, T. F. L., Di Martino, A., Weickert, G. & Soares, J. B. P. Particle Growth During the Polymerisation of Olefins on Supported Catalysts, 1 - Nascent Polymer Structures. *Macromol. React. Eng.* **4**, 40–64 (2010).

3. van Grieken, R., Carrero, A., Suarez, I. & Paredes, B. Effect of 1-Hexene Comonomer on Polyethylene Particle Growth and Kinetic Profiles. *Macromol. Symp.* **259**, 243–252 (2007).

4. Estenoz, D. A. & Chiovetta, M. G. A structural model for the catalytic polymerization of ethylene using chromium catalysts. Part II: Thermal effects. *Polym. Eng. Sci.* **36**, 2229–2240 (1996).

5. Alizadeh, A. & McKenna, T. F. L. Particle Growth during the Polymerization of Olefins on Supported Catalysts. Part 2: Current Experimental Understanding and Modeling Progresses on Particle Fragmentation, Growth, and Morphology Development. *Macromol. React. Eng.* **12**, 1700027 (2018).

6. Debling, J. A. & Ray, W. H. Heat and Mass Transfer Effects in Multistage Polymerization Processes: Impact Polypropylene. *Ind. Eng. Chem. Res.* **34**, 3466–3480 (1995).

7. Hutchinson, R. A., Chen, C. M. & Ray, W. H. Polymerization of olefins through heterogeneous catalysis X: Modeling of particle growth and morphology. *J. Appl. Polym. Sci.* **44**, 1389–1414 (1992).

8. Hatzantonis, H., Yiannoulakis, H., Yiagopoulos, A. & Kiparissides, C. Recent developments in modeling gas-phase catalyzed olefin polymerization fluidized-bed reactors: The effect of bubble size variation on the reactor's performance. *Chemical Engineering Science* 23 (2000).

9. Polyolefin Microstructural Modeling. in 187–269 (Wiley-VCH Verlag GmbH & Co. KGaA, 2012). doi:10.1002/9783527646944.ch6.

10. McKenna, T. F. L. & Bashir, M. A. Fragmentation, Particle Growth and Single Particle Modelling. in *Multimodal Polymers with Supported Catalysts: Design and Production* (eds. Albunia, A. R., Prades, F. & Jeremic, D.) 81–114 (Springer International Publishing, 2019). doi:10.1007/978-3-030-03476-4_3.

11. McKenna, T. F. & Soares, J. B. P. Single particle modelling for olefin polymerization on supported catalysts: A review and proposals for future developments. *Chemical Engineering Science* **56**, 3931–3949 (2001).

12. Kanellopoulos, V., Dompazis, G., Gustafsson, B. & Kiparissides, C. Comprehensive Analysis of Single-Particle Growth in Heterogeneous Olefin Polymerization: The Random-Pore Polymeric Flow Model. *Ind. Eng. Chem. Res.* **43**, 5166–5180 (2004).

13. Alizadeh, A., Sharif, F., Ebrahimi, M. & McKenna, T. F. L. Modeling Condensed Mode Operation for Ethylene Polymerization: Part III. Mass and Heat Transfer. *Ind. Eng. Chem. Res.* **57**, 6097–6114 (2018).

14. Vrentas, J. S., Duda, J. L. & Ling, H. C. Free-volume equations for polymer-penetrant diffusion. *Journal of Membrane Science* **40**, 101–107 (1989).

15. Vrentas, J. S., Duda, J. L. & Ling, H.-C. Self-diffusion in polymer-solvent-solvent systems. *J. Polym. Sci. Polym. Phys. Ed.* **22**, 459–469 (1984).

16. Kanellopoulos, V., Tsiliopoulou, E., Dompazis, G., Touloupides, V. & Kiparissides, C. Evaluation of the Internal Particle Morphology in Catalytic Gas-Phase Olefin Polymerization Reactors. *Ind. Eng. Chem. Res.* **46**, 1928–1937 (2007).

17. Weickert, G., Meier, G. B., Pater, J. T. M. & Westerterp, K. R. The particle as microreactor: catalytic propylene polymerizations with supported metallocenes and Ziegler–Natta catalysts. *Chemical Engineering Science* **54**, 3291–3296 (1999).

18. McKenna, T. F., Dupuy, J. & Spitz, R. Modeling of transfer phenomena on heterogeneous Ziegler catalysts: Differences between theory and experiment in olefin polymerization (an introduction). *J. Appl. Polym. Sci.* **57**, 371–384 (1995).

19. Sanchez, I. C. & Lacombe, R. H. An elementary equation of state for polymer liquids. *J. Polym. Sci. B Polym. Lett. Ed.* **15**, 71–75 (1977).

20. Alves, R. F. & McKenna, T. F. L. Estimation of diffusion coefficients for multiple penetrant/polyolefin systems based on sorption data. *Chemical Engineering Journal* **383**, 123114 (2020).

21. Alizadeh, A. *et al.* Modeling Condensed Mode Operation for Ethylene Polymerization: Part I. Thermodynamics of Sorption. *Ind. Eng. Chem. Res.* **56**, 1168–1185 (2017).

22. Alizadeh, A. Study of sorption, heat and mass transfer during condensed mode operation of gas phase ethylene polymerization on supported catalyst. (Departement of Chemical Engineering, Queen's University, 2014).

23. Yao, W., Hu, X. & Yang, Y. Modeling the solubility of ternary mixtures of ethylene,iso-pentane,n-hexane in semicrystalline polyethylene. *J. Appl. Polym. Sci.* **104**, 3654–3662 (2007).

24. Yao, W., Hu, X. & Yang, Y. Modeling solubility of gases in semicrystalline polyethylene. *J. Appl. Polym. Sci.* **103**, 1737–1744 (2007).

25. Andrade, F. N. & McKenna, T. F. L. Condensed Mode Cooling for Ethylene Polymerization: Part IV. The Effect of Temperature in the Presence of Induced Condensing Agents. *Macromol. Chem. Phys.* **218**, 1700248 (2017).

26. Ishola, N., Andrade, F. N., Machado, R. & McKenna, T. F. L. Condensed Mode Cooling for Ethylene Polymerization: Part VI. Impact of Induced Condensing Agents on Comonomer Incorporation.

27. Sun, J. *et al.* Solubility measurement of hydrogen, ethylene, and 1-hexene in polyethylene films through an intelligent gravimetric analyzer. *J. Appl. Polym. Sci.* **134**, (2017).

28. Wakao, N. & Smith, J. M. Diffusion and Reaction in Porous Catalysts. https://pubs.acs.org/doi/pdf/10.1021/i160010a007 (2002) doi:10.1021/i160010a007.

29. Yiagopoulos, A., Yiannoulakis, H., Dimos, V. & Kiparissides, C. Heat and mass transfer phenomena during the early growth of a catalyst particle in gas-phase olefin polymerization : the effect of prepolymerization temperature and time. *Chemical Engineering Science* **56**, 3979–3995 (2001).

30. Zielinski, J. M. & Duda, J. L. Predicting polymer/solvent diffusion coefficients using free-volume theory. *AIChE J.* **38**, 405–415 (1992).

31. Vrentas, J. S., Duda, J. L., Ling, H.-C. & Hou, A.-C. Free-volume theories for self-diffusion in polymer–solvent systems. II. Predictive capabilities. *J. Polym. Sci. Polym. Phys. Ed.* **23**, 289–304 (1985).

32. Gonzalez, A., Eceolaza, S., Etxeberria, A. & Iruin, J. J. Diffusivity of ethylene and propylene in atactic and isotactic polypropylene: Morphology effects and free-volume simulations. *Journal of Applied Polymer Science* **104**, 3871–3878 (2007).

33. Kanellopoulos, V., Mouratides, D., Tsiliopoulou, E. & Kiparissides, C. An Experimental and Theoretical Investigation into the Diffusion of Olefins in Semi-Crystalline Polymers: The Influence of Swelling in Polymer-Penetrant Systems. *Macromolecular Reaction Engineering* **1**, 106–118 (2007).

34. Polyolefin Reaction Engineering. in (Wiley-VCH Verlag GmbH & Co. KGaA, 2012). doi:10.1002/9783527646944.ch6.

35. Andrade, F. N. de. Effect of condensable materials during the gas phase polymerization of ethylene on supported catalysts. (Université de Lyon, 2019).

36. Chatzidoukas, C., Perkins, J. D., Pistikopoulos, E. N. & Kiparissides, C. Optimal grade transition and selection of closed-loop controllers in a gas-phase olefin polymerization fluidized bed reactor. *Chemical Engineering Science* **58**, 3643–3658 (2003).

37. McAuley, K. B., MacGregor, J. F. & Hamielec, A. E. A kinetic model for industrial gas-phase ethylene copolymerization. *AIChE Journal* **36**, 837–850 (1990).

38. Alizadeh, A., Namkajorn, M., Somsook, E. & McKenna, T. Condensed Mode Cooling for Ethylene Polymerization: Part II. The Effect of Different Condensable Comonomers and Hydrogen on Polymerization Rate. *Macromolecular Chemistry and Physics* **216**, (2015).

Chapter 6

Sorption and Swelling of liquid diluents in polyethylene

1. Introduction

As have been discussed in the previous chapters, the sorption of pure gases in polyolefins has been widely studied. However, it turns out that very few studies have been performed concerning the sorption of liquid diluents in polyethylene. This is crucial thermodynamic data for slurry polymerization, where the growing polymer particles are dispersed in a liquid diluent in which the monomer is dissolved. Obviously, the swelling of the polymer by the diluent, and the eventual dissolution of the polymer in the continuous phase are both going to be important points when developing an in-depth understanding of a slurry process. The temperature sensitivity of these two phenomena will also be important, and it is expected that slurries will exhibit a different temperature response than gas phase systems.

As with gas phase reactions, increasing temperature can lead to higher catalyst productivity, but unlike in the gas phase, this also enhances the risk of polymer swelling since the latter tends to become more soluble in the continuous phase at higher temperatures[1]. If the temperature reaches a critical point, polymer particles might swell significantly and this in turn can lead to the production of a more viscous or adhesive polymer slurry that can slow down recirculation in the reactor or lead to deposition on the reactor wall[2,3]. As an example, Zhou et al.[4] calculated the swelling of dodecane-PE using mass transfer rate measurements and developed a swelling-based fluid dynamic model in order to quantify the aggregation behavior of the swollen particles, and found out that solid accumulation appears at the bottom of the slurry loop reactors. Reactor fouling by polymer adhesion is often linked to the swelling of the amorphous phase of the polymer due to the sorption of diluents like isobutane, or n-hexane.

Knowledge of this thermodynamic data is crucial if one needs to control the molecular weight of the produced polymer or to optimize the degassing process. Besides, this is all the more important since these liquid diluents will change the physical properties of the produced polymer as they cause its swelling and softening due to their high solubility in the amorphous phase of the polymer. Up to now, only a limited number of studies of phase equilibria for PE/liquid diluent systems can be found in the literature[5–11]. Recently, Krajakova et al.[10] studied the sorption of liquid diluents (i.e. n-octane, n-hexane, n-pentane) in different PE samples of varying density from 902 to 967 kg m^{-3}. They showed that longer hydrocarbons diluents have higher solubility in all PE samples. They also showed a partial dissolution of PE samples in the liquid diluents using GPC analysis, but this dissolution was not quantified.

This chapter is built upon these previous studies in order to quantify the solubility of diluents in different PE grades, the swelling of the PE in presence of different diluents, and the dissolution of PE in these diluents. The sorption and swelling of the amorphous phase of the polymer are investigated in presence of different liquid diluents (i.e. n-pentane to n-decane) at temperature between 25-100°C and various PE grades with densities from 925-960 $kg.m^{-3}$.

2. Materials and Methods

Part of the experiments described in this Chapter were carried out by an intern in the C2PM, M. Léo Mermet.

2.1. Materials

Normal alkanes with carbon numbers 4 through 10 with a minimum purity of 99% were used as received from Air Liquide France. All seven alkanes were used for the swelling experiments, but only the n-pentane and heavier alkanes were used in the solubility experiments.

HDPE granules and LLDPE powders were graciously supplied by Ineos (HDPE-I, LLDPE-I), and HDPE and MDPE powders were graciously supplied by Borealis (HDPE-B, MDPE-B).

The crystallinity of the polymer samples was measured using differential scanning calorimetry (DSC 3+ by Mettler Toledo). Polyethylene samples were weighed (i.e. around 5-7 mg) and placed in an aluminium capsule with a volume of 40 µL. The sample was first cooled to -20°C and then heated from −20 to 180 °C at a heating rate of 10°C min^{-1}, held for 5 minutes at that temperature and then cooled from 180 to −20 °C at a rate of 10°C min^{-1}. This temperature was maintained for 5 minutes, and the sample was reheated to 180°C at a rate of 10°C min^{-1}. The melting behavior of the samples was studied in the second heating cycle in order to detect the melting point and the melting enthalpy of the samples. The ratio of the heat of fusion of the sample to that of the completely crystallized polyethylene was used to calculate the degree of crystallization. A heat of fusion of 293 J g^{-1} for completely crystallized polyethylene was used for the calculation. The STARe software was used for data acquisition and data analysis. Polymer densities and crystallinities are summarized in ***Table 38***.

LLDPE-I, HDPE-B and MDPE-B were hot-pressed at 180°C for about 2 hours, and then cooled, in order to produce a thin film. The final cylindrical film has a diameter of 20 mm and a thickness of 1 mm.

Table 38. *Density and crystallinity characteristics of the studied polymer samples*

	Density (kg.m^{-3})	**Crystallinity (%)**
HDPE-I	960	75
HDPE-B	945	65.7
MDPE-B	935	59
LLDPE-I	926	52.6

2.2.Dissolution of polyethylene in liquid solvents

It is known that amorphous PE and low molecular weight fractions of polymer can dissolve in liquid alkanes, and that the amount of polymer that dissolves will be a function of the temperature and alkane chain length.[9] Furthermore, if we wish to study the swelling of PE by liquid alkanes, it is necessary to know what fraction of that PE actually dissolves in the liquid diluents.

The PE solubility in alkanes is measured as following: 5g of polymer is added to 15 mL of diluent in a test tube. This is the same ratio of polymer to solvent as was used in the reactor for the swelling experiments. A magnetic stirrer bar is inserted in the tube. The tube is then closed and kept at the desired temperature for 48 hours. After 48 hours, we would expect a partial dissolution of the polymer in the solvent, and therefore a supernatant solution of solvent and polymer. This solution is then withdrawn with a syringe and weighted. The solution is left to dry under the hood for 24 hours and then in an oven at 100°C for an additional 24 hours and weighted again, as can be seen in ***Figure 125***. Each experiment was repeated 2-3 times.

The amount of dissolved polymer (g of polymer dissolved / g of solvent) is calculated as follows:

$$S_{\mathrm{PE}}^{\mathrm{diss}} = \frac{m_4 - m_1}{m_2 - m_4}$$

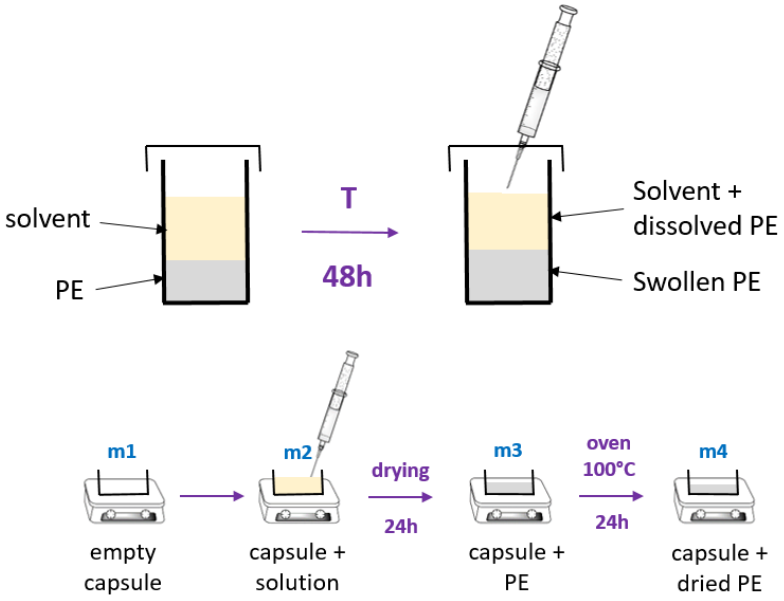

Figure 125. *Experimental scheme of the dissolution of polyethylene powders in liquid diluents at different temperatures*

2.3.Solubility of Alkanes in PE

2.3.1. Room temperature sorption

PE granules and films were used for the sorption experiments as they are more easily recovered than powder from the liquid phase. Desorption experiments were performed as follows (c.f. ***Figure 126***): a PE film or granule is weighted and placed into different liquid solvents at room temperature for 48 hours, during which the sorption equilibrium was established (it was found that increasing the sorption time to 72 hours does not have any measurable difference). After reaching equilibrium, the polymer sample is removed from the liquid, any droplets present on the surface of the film/granule are rapidly removed by sponging with a filtration paper, and the polymer sample is placed on an analytical balance. The rate of decrease of the mass of the polymer at room temperature was recorded manually until a stable value was observed.

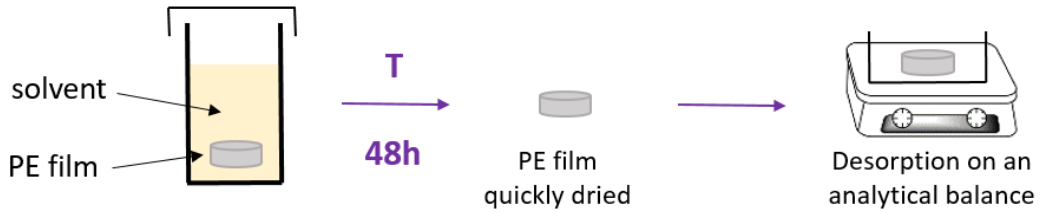

Figure 126. *Scheme of the desorption experiments of PE films and granules at room temperature.*

The solubility of the liquid diluent in the polymer is calculated as follows:

$$S = \frac{m(t=0) - m_{\mathrm{PE_{end}}}}{m_{\mathrm{PE_{end}}}}$$

Where $m(t=0)$ is the mass of the swollen polymer measured at zero time before the desorption and $m_{\mathrm{PE_{end}}}$ is the mass of the dry polymer after the desorption experiment.

Generally, the dry polymer mass after the experiment is found to be lower than the mass of the dry polymer before the experiment. The reason is that a fraction of the polymer partially dissolves into the liquid diluent during the sorption experiment, as have been seen in the previous section. The dissolution of the amorphous phase of the polymer in the different diluents is therefore taken into account when calculating the solubility of the different liquid diluents in the polymer.

2.3.2. High temperature sorption

Only HDPE-I was evaluated in this manner. The experiment is shown schematically in ***Figure 127***. For each experiment, one granule was introduced into different liquid diluents at different temperatures for 48 hours as previously. After reaching equilibrium, the granule (approximately 11 mg) is pulled out of the liquid, its surface is quickly dried by a filtration paper and placed in a 40 µL steel capsule used for thermogravimetric analysis (TGA). The decrease of the mass of the capsule as a function of temperature was measured using a TGA 2 by Mettler Toledo. The advantage of this technique is that if the solid sample is transferred to the capsule rapidly enough, the desorption is carried out at the same temperature as the sorption. Isothermal analysis at the temperature of interest without any nitrogen atmosphere flow was performed. The values obtained in the desorption analysis were treated using STARe Software.

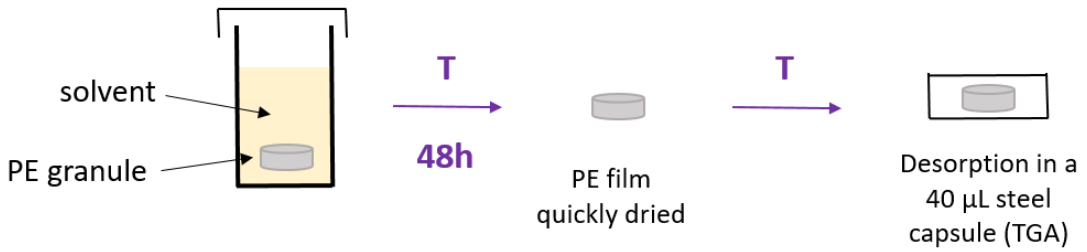

Figure 127. *Schema of the desorption experiments of PE granules at high temperature*

All the experiments were carried out three times at the same conditions (identical temperature, PE granules) and were found to be quite repeatable. The solubility S is calculated as for solubility experiments at room temperature:

$$S = \frac{m(t=0) - m_{\mathrm{PE_{end}}}}{m_{\mathrm{PE_{end}}}}$$

Where $m(t=0)$ is the mass of the swollen polymer measured at zero time before the desorption and $m_{\mathrm{PE_{end}}}$ is the mass of the dry polymer after the desorption experiment. At high temperatures, the dry polymer mass after the experiments is very different from the mass of the polymer before the desorption experiment since the dissolution of the polymer in the solvents is greater with temperature. It is therefore crucial to take into account PE dissolution in the solvents when measuring the solubility at high temperatures.

2.4.Swelling Experiments

HDPE-B, MDPE-B and LLDPE-I powders were used for the swelling experiments in order to show the effect of the crystallinity of the PE sample on its degree of swelling, as well as the temperature of the reactor. The reactor used for the swelling experiments is shown in ***Figure 128***.

Figure 128. *Experimental set-up for the swelling experiments in slurry*

A 2 liter stirred reactor heated by circulating water in an external jacket is used for the swelling experiments. A sapphire window is available on this reactor in order to see the volume change due to the polymer swelling during the sorption experiment. A known amount of polyethylene powder (± 300 g of polymer) and diluent (± 900 mL) are introduced in the reactor. The height of the powder phase is measured right away. The volume of solvent has to be more than sufficient to saturate the powders in liquid. We choose to work with 1/4 of solid and 3/4 of liquid for all the swelling experiments. The reactor is then closed and heated to the desired temperature. The reactor is stirred at a constant temperature for 90 minutes (the time it was found to reach equilibrium) and the value of the height of the powder is then taken once again. The experimental temperature dependent swelling is then calculated in % of volume change, as follows:

$$SW_{\text{exp}}\ (\%) = \frac{h(T) - \text{h}(T_i)}{\text{h}(T_i)} \times 100$$

Where $h(T)$ is the height of polymer powder inside the reactor at different temperature steps taken from the sapphire window and $\text{h}(T_i)$ is the height of polymer powders inside the reactor at the beginning of the experiment at room temperature taken from the sapphire window.

However, the swelling of the polymer has to be corrected for the partial dissolution of the amorphous phase of the polymer in the liquid solvents, especially for light solvents (i.e. n-pentane, n-hexane), as have been seen in Section 2.2. This correction is achieved by adding the volume of polymer dissolved in the solvent, $V_{\text{PE}}^{\text{diss}}$, to the volume of swollen polymer measured during swelling experiments, V_{PE}^{i}. Besides, this volume of swollen polymer measured experimentally has to be corrected for polymer expansion due to temperature increase, $V_{\text{PE,corr}}^{\text{i}}$.

$$V_{PE,corr} = \left(V_{\text{PE,corr}}^{\text{i}} + V_{\text{PE}}^{\text{diss}}\right)\left(\frac{SW_{\text{exp}}}{100} + 1\right)$$

$$V_{\text{PE,corr}}^{\text{i}} = V_{\text{PE}}^{\text{i}} \times \frac{\rho_{\text{PE}}^{\text{am}}(T_i)}{\rho_{\text{PE}}^{\text{am}}(T)}$$

$$V_{\text{PE}}^{\text{diss}} = \frac{S_{\text{PE}}^{\text{diss}}}{\rho_{\text{PE}}^{\text{am}}(T)} m_{solvent}$$

Where $S_{\text{PE}}^{\text{diss}}$ is the mass of dissolved polymer per gram of solvent used during the swelling experiment, and $\rho_{\text{PE}}^{\text{am}}(T)$ is the amorphous density of the polymer corrected for the thermal expansion.

The corrected swelling for polymer dissolution in solvents and polymer thermal expansion is given by:

$$SW_{\text{corr}}(\%) = \frac{V_{PE,corr} - V^{\text{i}}_{\text{PE,corr}}}{V^{\text{i}}_{\text{PE,corr}}} \times 100$$

It is important to note that the maximum temperature in each experiment varies as a function of the solvents. For heavier solvents, temperature steps were performed up to 100°C for the swelling experiments. However, for some of the lighter solvents (i.e. n-butane, n-pentane, n-hexane) which can strongly plasticize the polymer at lower temperatures than heavier solvents, and can cause the particles to lose their integrity, the maximum temperature achieved was around 80°C. ***Figure 129*** shows an example of plasticization of MDPE powders in presence of n-hexane at temperature of 90°C. When this occurred, the swelling experiments were stopped.

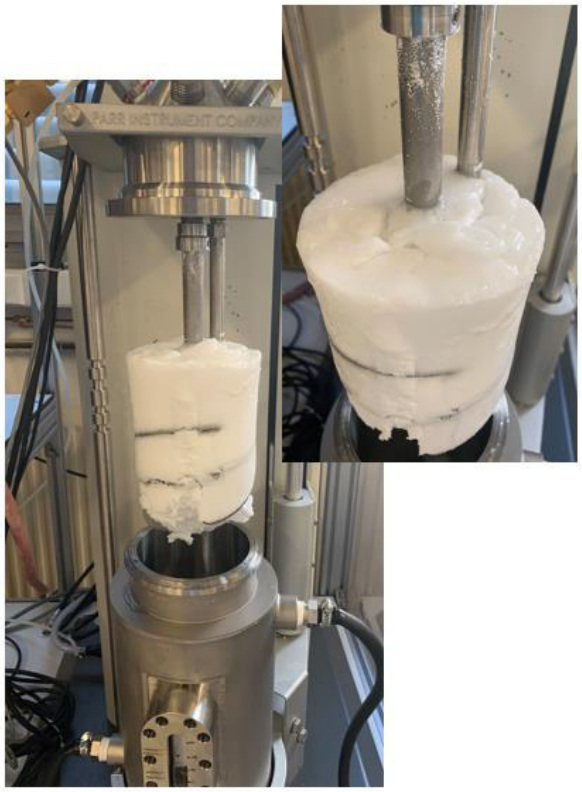

Figure 129. *Example of plasticization of MDPE-B powders in presence of n-hexane at 90°C*

3. Results and Discussion
   3.1. Polymer solubility in alkanes

In order to properly interpret the sorption and swelling experiments presented in the next sections, it is necessary first to know how much polymer can dissolve into the continuous phase during the experiments. Therefore, a correction is achieved by introducing a temperature dependent correlation of the mass of dissolution of the amorphous phase of the polymer with respect to the mass of solvent used during the swelling experiments, as can be seen in ***Table 40***, ***Table 41*** and ***Table 42***. The same method is performed for HDPE-B, MDPE-B and LLDPE-I samples.

The data in ***Table 39*** appears to be roughly linear over the studied range of temperature, as can be seen from the plots in ***Figure 130***. The correlations used to estimate the solubility of HDPE-B in the different alkanes as a function of temperature are given in ***Table 40***. The results of similar experiments for LLDPE-I are shown in ***Figure 131*** and ***Table 41***, and MDPE in ***Figure 132*** and ***Table 42***.

Table 39. *Percent mass dissolved of HDPE-B powders in the presence of different solvents and at different temperatures.*

T (°C)	80	60	40
nC_{10}	2.48	1.67	0.99
nC_9	2.52	1.72	1.24
nC_8	2.65	1.72	1.26
nC_7	2.59	1.83	1.26
nC_6	2.94	2.09	1.4
nC_5	4.16	3.48	1.56

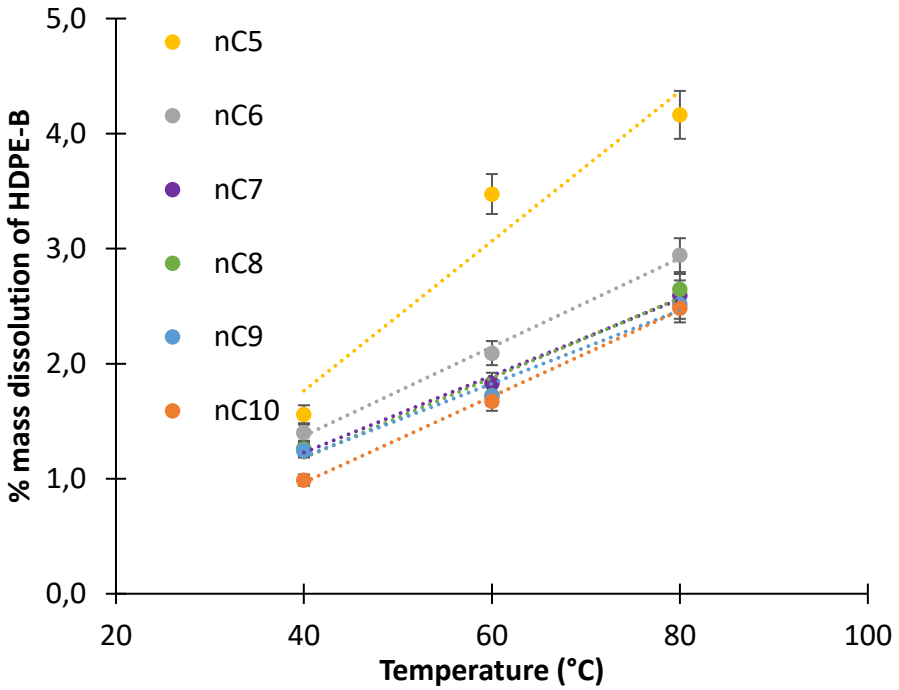

Figure 130. *Percent mass dissolved of HDPE-B powders in the presence of different solvents and at different temperatures.*

Table 40. *Temperature dependence correlation for the mass of dissolution of HDPE-B powders in presence of different solvents*

Solvents	Correlation for HDPE-B dissolution
nC10	$\%_{mass}^{diss} = 0.0374 \times T - 0.528$
nC9	$\%_{mass}^{diss} = 0.0317 \times T - 0.079$
nC8	$\%_{mass}^{diss} = 0.0347 \times T - 0.206$
nC7	$\%_{mass}^{diss} = 0.0333 \times T - 0.107$
nC6	$\%_{mass}^{diss} = 0.0386 \times T - 0.171$
nC5	$\%_{mass}^{diss} = 0.065 \times T - 0.838$

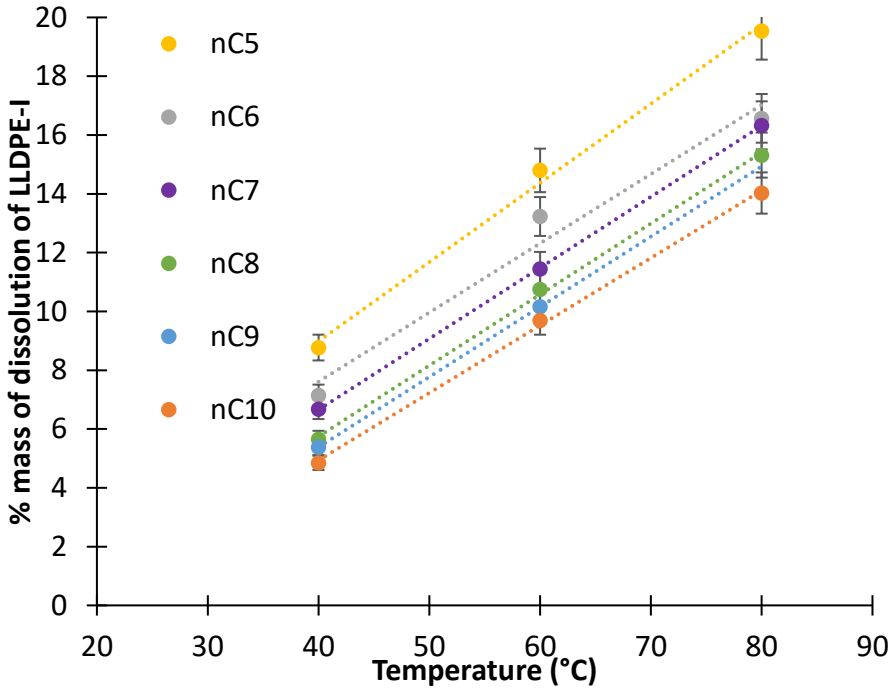

Figure 131. *Percent mass dissolved of LLDPE-I powders in the presence of different solvents and at different temperatures.*

Table 41. *Temperature dependence correlation for the mass of dissolution of LLDPE-I powders in presence of different solvents*

Solvents	Correlation for LLDPE-I dissolution
nC10	$\%_{mass}^{diss} = 0.229 \times T - 4.247$
nC9	$\%_{mass}^{diss} = 0.239 \times T - 4.169$
nC8	$\%_{mass}^{diss} = 0.241 \times T - 3.916$
nC7	$\%_{mass}^{diss} = 0.241 \times T - 3$
nC6	$\%_{mass}^{diss} = 0.235 \times T - 1.807$
nC5	$\%_{mass}^{diss} = 0.269 \times T - 1.787$

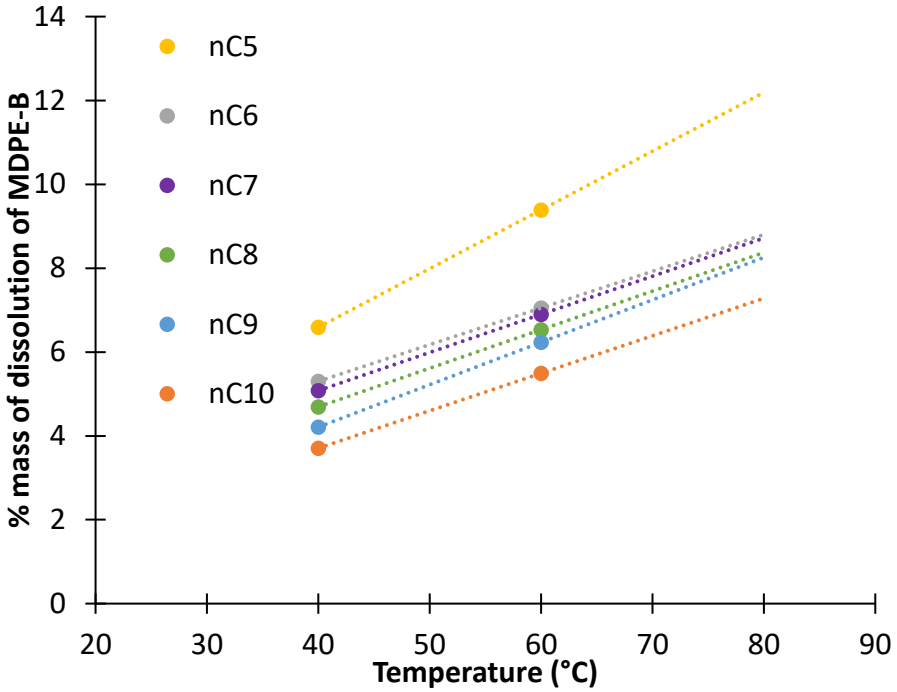

Figure 132. *Percent mass dissolved of MDPE-B powders in the presence of different solvents and at different temperatures.*

Table 42. *Temperature dependence correlation for the mass of dissolution of MDPE-B powders in presence of different solvents*

Solvents	Correlation for MDPE-B dissolution
nC_{10}	$\%_{mass}^{diss} = 0.0893 \times T + 0.132$
nC_9	$\%_{mass}^{diss} = 0.1012 \times T + 0.163$
nC_8	$\%_{mass}^{diss} = 0.0919 \times T + 1.016$
nC_7	$\%_{mass}^{diss} = 0.0909 \times T + 1.444$
nC_6	$\%_{mass}^{diss} = 0.0875 \times T + 1.802$
nC_5	$\%_{mass}^{diss} = 0.14 \times T + 0.989$

We can see from these experimental results that the polymer dissolution increases with increasing the temperature from 40 to 80°C, and with lighter solvents. nC_5 dissolves more polymer per gram than does nC_{10} for all types of polyethylene. Besides, the polymer dissolution in the different solvents depends on the polymer type. Indeed, LLDPE dissolves more than MDPE which in turn dissolves more than HDPE with the same solvent and under the same conditions. Increasing the crystallinity of the polymer (i.e. HDPE) decreases the amount of

polymer dissolved in liquid diluents because only the amorphous phase of the polymer partially dissolves in the solvent.

These experimental results have shown that the partial dissolution of the amorphous phase of the polymer is not negligible, and can reach almost 20% of dissolution of the polymer, with respect to the mass of solvent used during swelling experiments. This data is therefore crucial in order to correct the experimental sorption of liquid diluents in polyethylene and the swelling of the latter when exposed to these diluents.

3.2.Alkane sorption in polymers – Room Temperature Experiments

The solubility of n-pentane, n-hexane, n-heptane, n-octane, n-nonane and n-decane in PE granules (i.e. HDPE-I) and films (i.e. HDPE-B, MDPE-B, LLDPE-I) was first measured at room temperature. The desorption time was constant for each granule and film in order to have reproducible results. Each desorption experiment was repeated at least 3 times under the same conditions in order to show the repeatability of these experiments. **Figure 133** and **Figure 134** show good repeatability with a difference at time zero of the desorption curve of 1.2% between each sorption experiment in presence of n-hexane in HDPE-I granules, and a maximum difference of 5% between each sorption experiment in presence of n-pentane in HDPE-I granules, respectively.

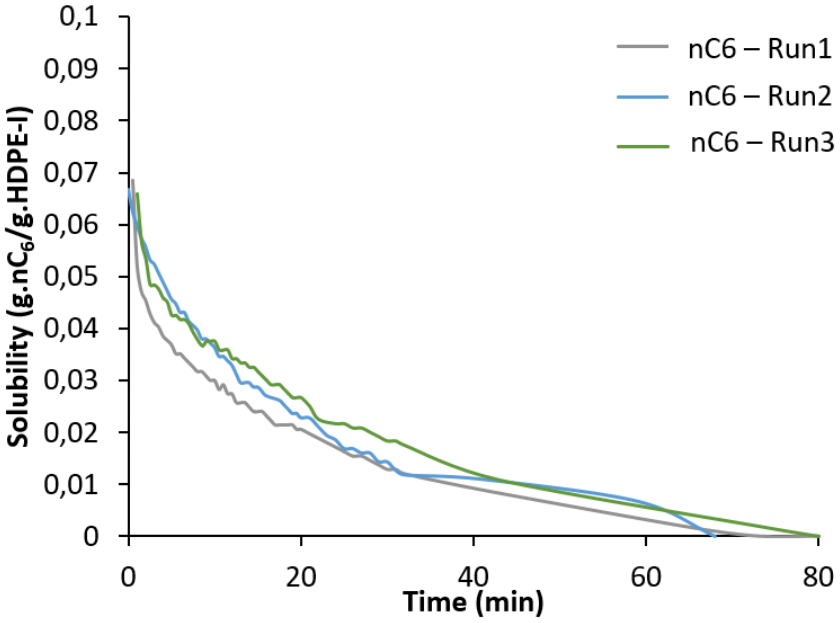

Figure 133. *Solubility of n-hexane in HDPE-I granules at room temperature (the same experiment at the same conditions was repeated three times)*

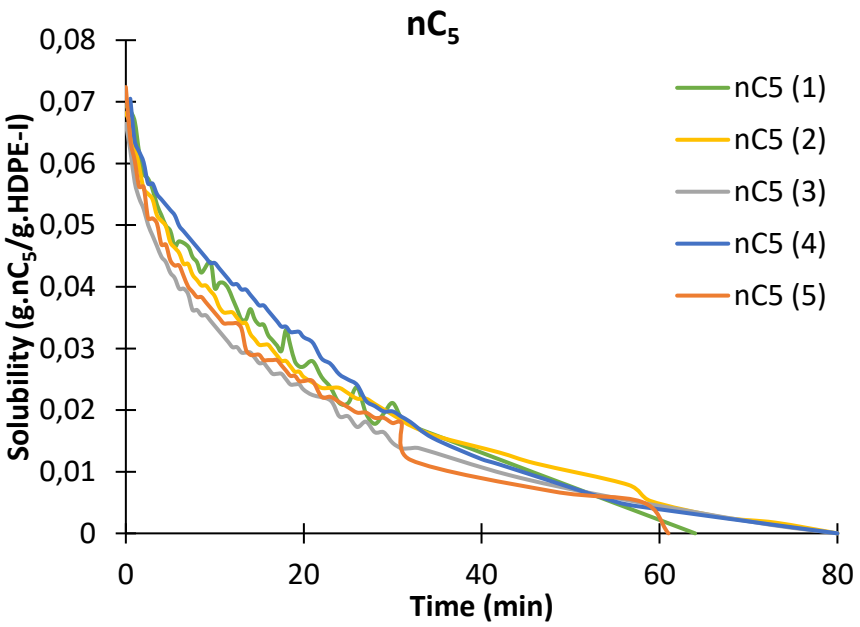

Figure 134. *Solubility of n-pentane in HDPE-I granules at room temperature (the same experiment at the same conditions was repeated five times)*

In the same manner, the desorption experiments on PE films (i.e. HDPE-B, MDPE-B, LLDPE-I) were repeated two to three times, as can be seen in ***Figure 135, Figure 136*** and ***Figure 137***. The solubility of each alkane presented in ***Table 6*** was taken as the average of all the experiments repeated at the same conditions.

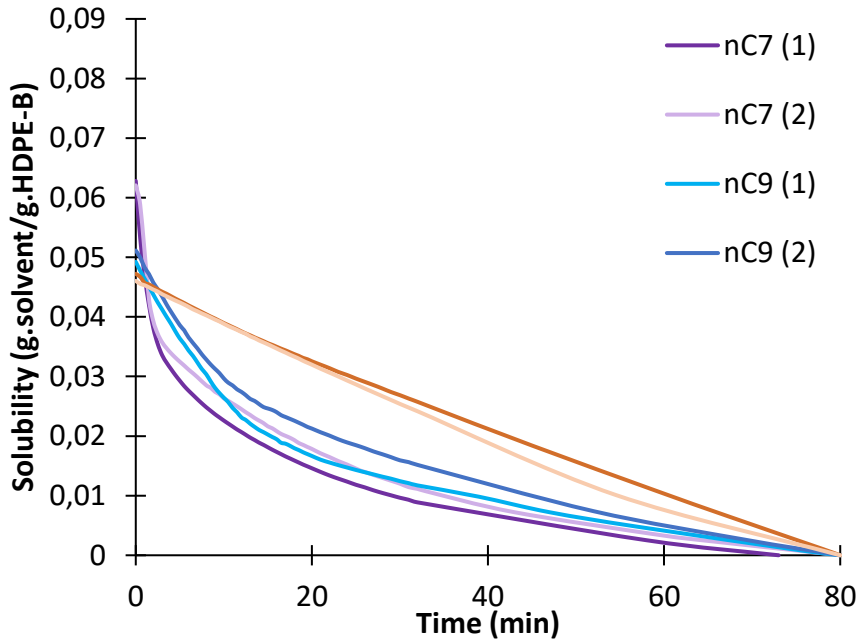

Figure 135. *Solubility of n-heptane, n-nonane and n-decane in HDPE-B films at room temperature (the same experiment at the same conditions was repeated 2 times)*

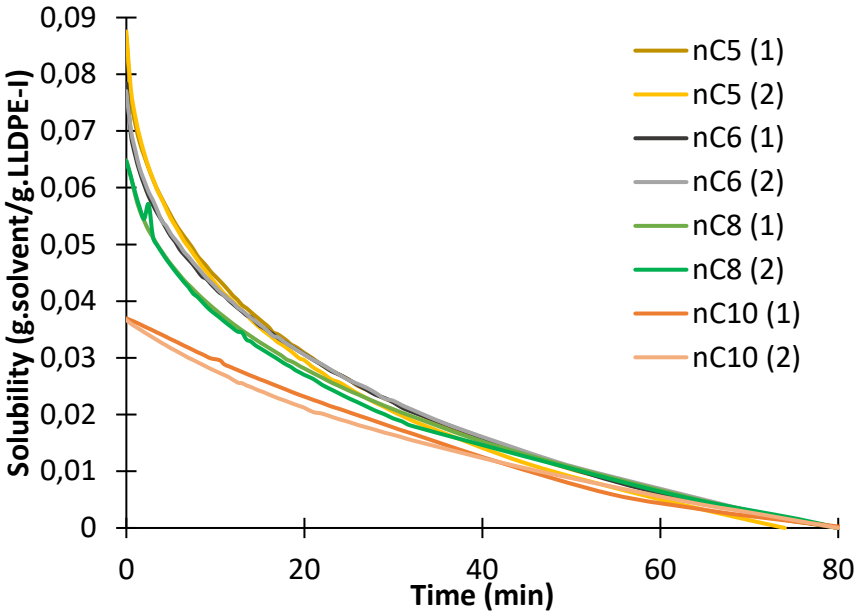

Figure 136. *Solubility of n-pentane, n-hexane, n-octane and n-decane in LLDPE-I films at room temperature (the same experiment at the same conditions was repeated 2 times)*

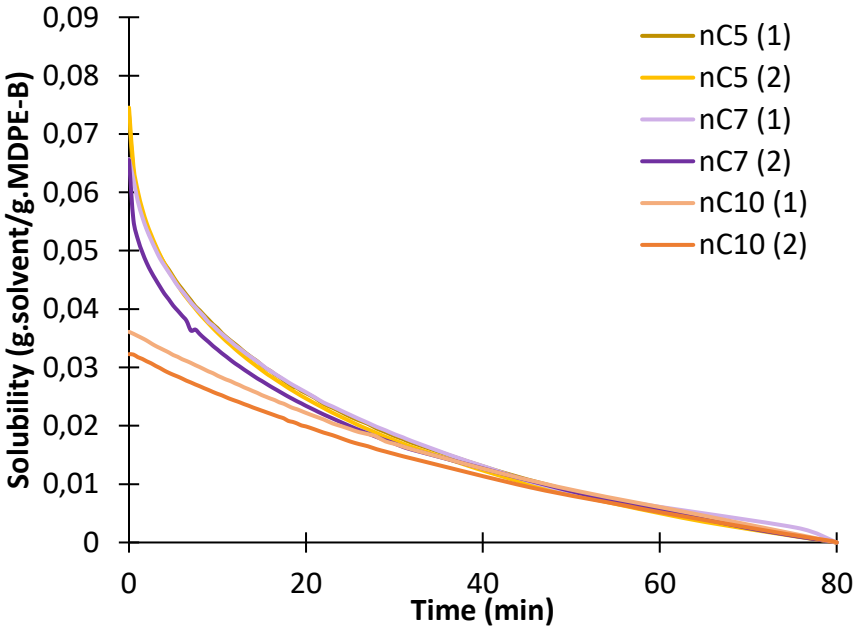

Figure 137. *Solubility of n-pentane, n-heptane and n-decane in MDPE-B films at room temperature (the same experiment at the same conditions was repeated 2 times)*

Table 43. Comparison of the solubility of different liquid solvents in all PE samples

	HDPE-I (granule)	HDPE-B (film)	MDPE-B (film)	LLDPE-I (film)
nC_5	0.069	0.071	0.075	0.087
nC_6	0.067	0.069	0.072	0.078
nC_7	0.063	0.062	0.066	0.069
nC_8	0.059	0.06	0.061	0.065
nC_9	0.049	0.05		
nC_{10}	0.044	0.047	0.034	0.037

Figure 138 shows the solubility per gram of different alkanes in the different PE samples with respect to the solvent chain length (N.B. this is total polymer mass, not with respect to the amorphous phase). It is shown that increasing the solvent chain length decreases its solubility in the polymer. The difference of solubility between the heavier (i.e. n-decane) and the lighter (i.e. n-pentane) solvent in HDPE-B and HDPE-I is about 55%. Smaller solvents have higher solubility in the semicrystalline polymer as they are small enough to diffuse inside the amorphous phase of the polymer.

Furthermore, since n-butane is in a gaseous state at room temperature, it is hard to evaluate the solubility of this diluent. In order to correct for the solubility of polymer in n-butane during the swelling experiments, we approximated the solubility by extrapolating the results in ***Figure 138*** to a chain length of 4. While inexact, we can most likely use these values as an approximation.

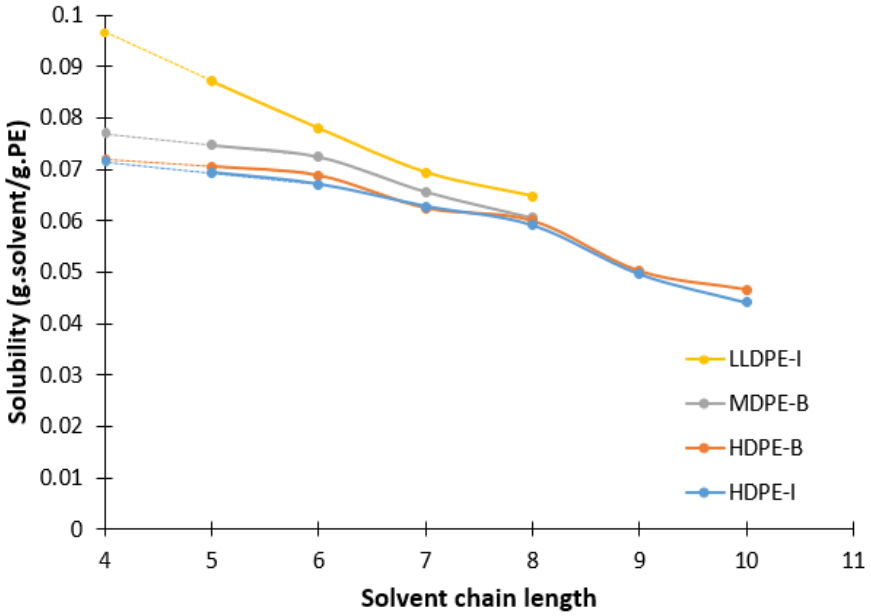

Figure 138. *Solubility (g of solvent / g of polyethylene) at room temperatures in the different PE samples with respect to the solvent chain length.*

Figure 139 shows the solubility of n-pentane, n-hexane, n-heptane and n-octane in different polyethylene samples (i.e. HDPE, MDPE and LLDPE). We can see that the solubility of all solvents in polyethylene at room temperature decreases with increasing the polymer density and crystallinity. This trend is expected since these solvents can only penetrate into the amorphous phase of the semicrystalline polymer, and increasing polymer density leads to a decrease of the amorphous phase fraction. Besides, it is shown that the solubility of the different solvents at room temperature can be considered constant for polyethylene densities up to 935 kg m^{-3}. This trend was confirmed by Krajakova et al.[11] who studied the solubility of n-hexane in different polyethylene samples of densities from 900 to 970 kg m^{-3}. They explained this trend by the new morphological model of free and constrained amorphous phase in polyethylene introduced by Chmelar et al.[12] . They assumed that polyethylene consists of the crystalline phase (rigid), constrained amorphous phase inside the lamellar stacks (semirigid) and the free amorphous phase outside the stacks (mobile). The free amorphous phase, which is not present for PE having crystallinities above 62 wt.%, corresponding to a density of 940 kg m^{-3} (i.e. HDPE), can sorb more penetrants than the constrained amorphous phase which is affected by the surrounding crystalline lamellar stacks.

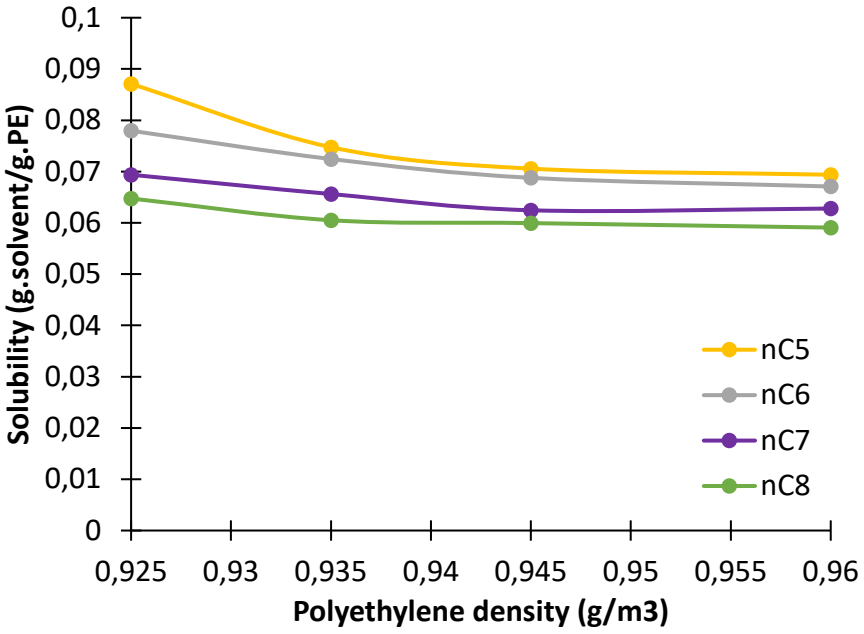

Figure 139. *Solubility (g of solvent / g of polyethylene) at room temperature of the different solvents in three different PE samples having different densities.*

Knowing that the liquid diluents can only sorb in the amorphous phase of the polymer, we can relate the solubility to the mass of the polymer amorphous phase as follows:

$$S_{\mathrm{am}} = \frac{S}{(1-\omega_{\mathrm{c}})}$$

Where ω_{c} is the crystallinity of the different polymers given in ***Table 1***.

The solubility of the different solvents with respect to the amorphous phase of the polymer is therefore presented in ***Figure 140***. This figure shows that converting the overall solubility presented in ***Figure 139*** into the solubility with respect to the amorphous phase of the polymer gives the same tendency. The solubility in the amorphous phase of the polymer is still almost constant for polyethylene density above 935 kg.m^{-3}. This observed trend confirms that the amorphous phase of the polymer does not sorb equally for all measured PE samples.

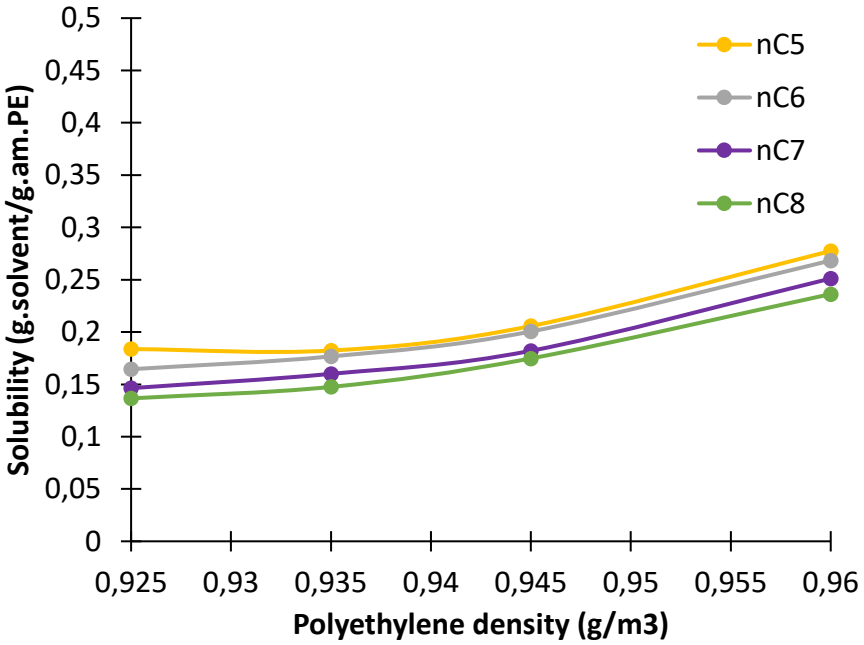

Figure 140. *Solubility (g of solvent / g of amorphous polyethylene) at room temperature of the different solvents in three different PE samples having different densities*

3.3.Alkane sorption in polymers – TGA Method

Figure 141, Figure 142 and ***Figure 143*** show the solubility of different solvents (nC_5, nC_6, nC_7, nC_8, nC_9, nC_{10}) in HDPE-I granules at different temperatures (25, 40, 60 °C) as measured with the TGA method.

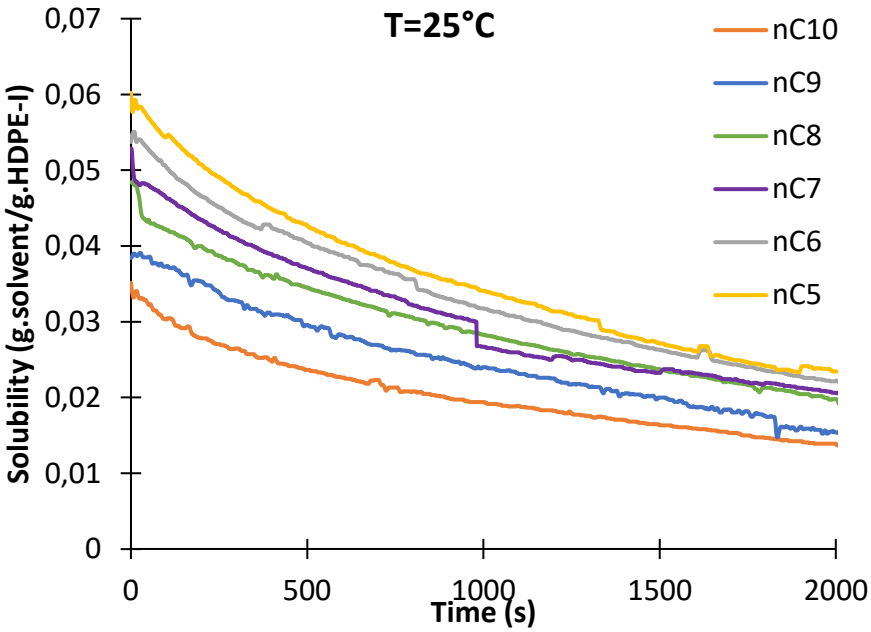

Figure 141. *Solubility of different solvents (nC_5, nC_6, nC_7, nC_8, nC_9, nC_{10}) in HDPE-I granules at 25°C (Each experiment was repeated at least two times under the same conditions)*

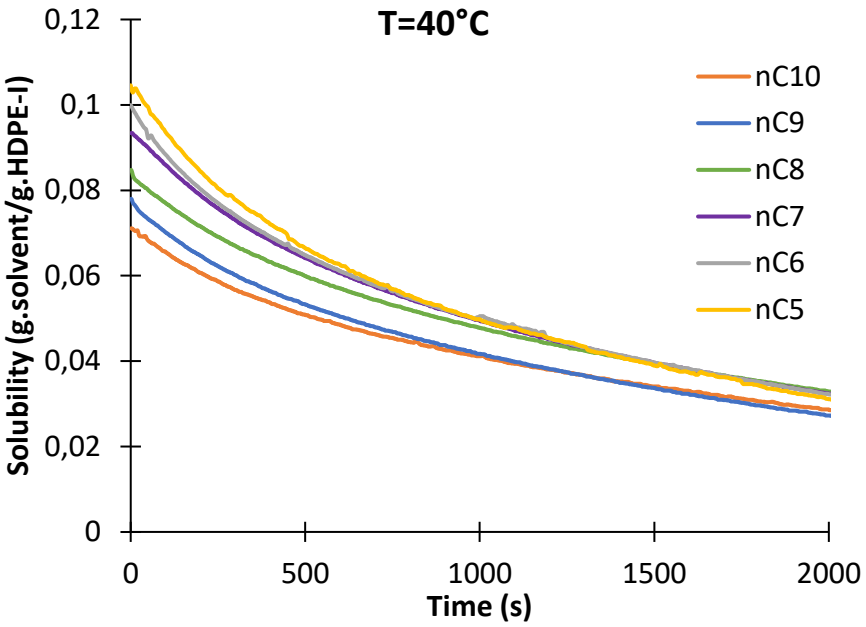

Figure 142. Solubility of different solvents (nC_5, nC_6, nC_7, nC_8, nC_9, nC_{10}) in HDPE-I granules at 40°C (Each experiment was repeated at least two times under the same conditions)

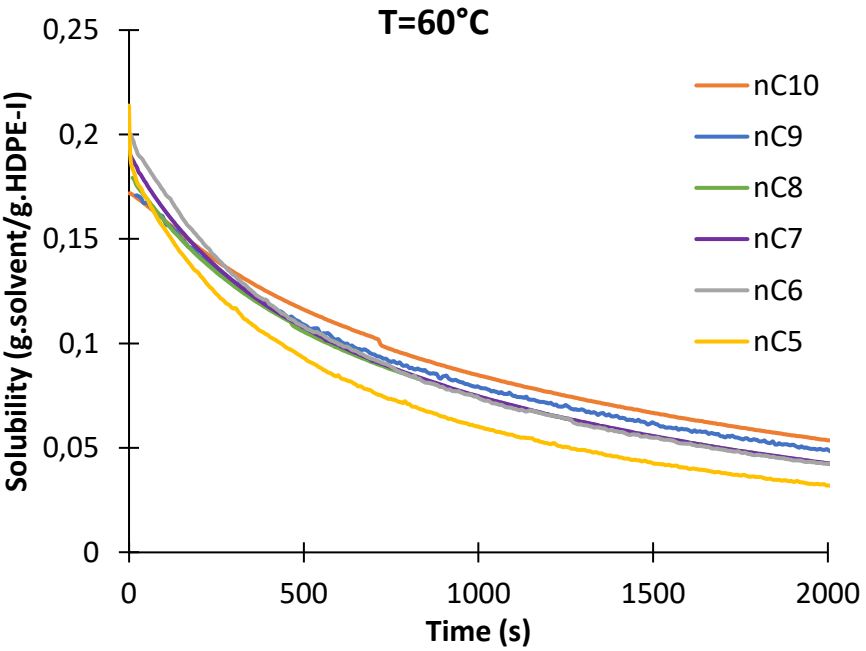

Figure 143. Solubility of different solvents (nC_5, nC_6, nC_7, nC_8, nC_9, nC_{10}) in HDPE-I granules at 60°C (Each experiment was repeated at least two times under the same conditions)

These figures show the desorption of different solvents measured with a TGA balance at different temperatures between 25-60°C. The results show that the solubility increases with increasing the temperature and with decreasing the number of carbons of the penetrant, as can

be seen in ***Figure 141, Figure 142*** and ***Figure 143***. The enhancement of the solubility of lighter solvents (i.e. n-pentane, n-hexane, n-heptane) is bigger at higher temperature than with heavier solvents. However, this significant increase of the solubility of light solvents at high temperature can cause the polymer to swell considerably, leading to reactor fouling by polymer adhesion and plasticization.

In the same manner as ***Figure 138***, the solubility of liquid n-butane in function of temperature up to 60°C can be extrapolated from ***Figure 20*** since the solubilites for n-pentane, n-hexane and n-heptane follow the same trend. Indeed, the solubility of liquid n-butane extrapolated with the experiments at room temperatures and the ones with TGA method are in good agreements, with a difference of 10% between both methods. Once again these values have to be taken with caution.

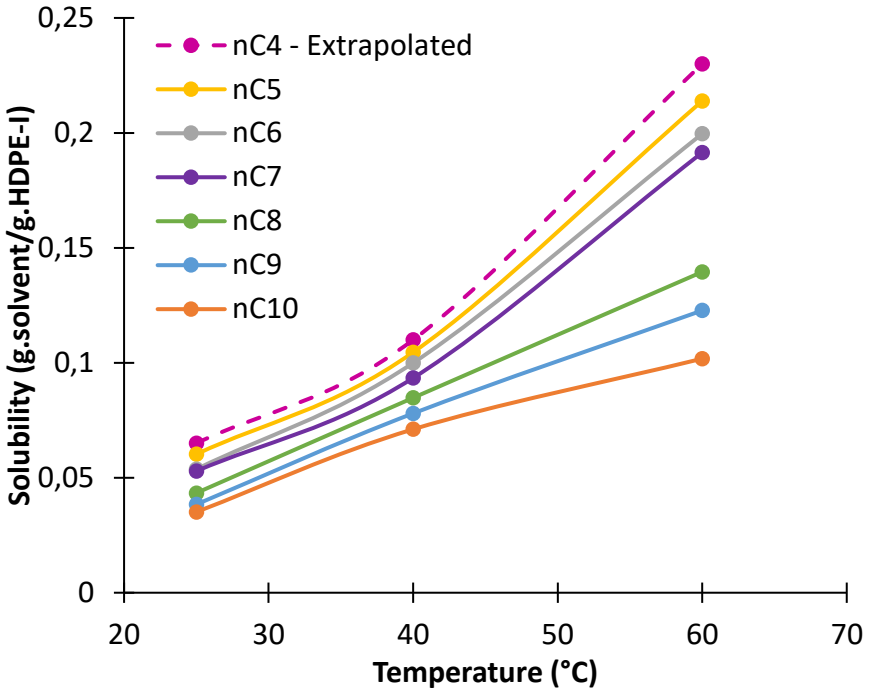

Figure 144. *Solubility of different solvents (nC_5, nC_6, nC_7, nC_8, nC_9, nC_{10}) in HDPE-I granules as a function of temperature*

3.4.Swelling experiments

Swelling experiments were run with different solvents (i.e. n-butane, n-pentane, n-hexane, n-heptane, n-octane, n-nonane and n-decane) at temperatures between 30-100°C. All the experiments were carried out at least two times at the same conditions (temperature, identical agitation and PE powders).

Swelling of HDPE-B in presence of liquid solvents such as n-decane, n-nonane, n-octane, n-heptane, n-hexane, n-pentane and n-butane expressed in volume percent units at different temperatures will be presented in this section.

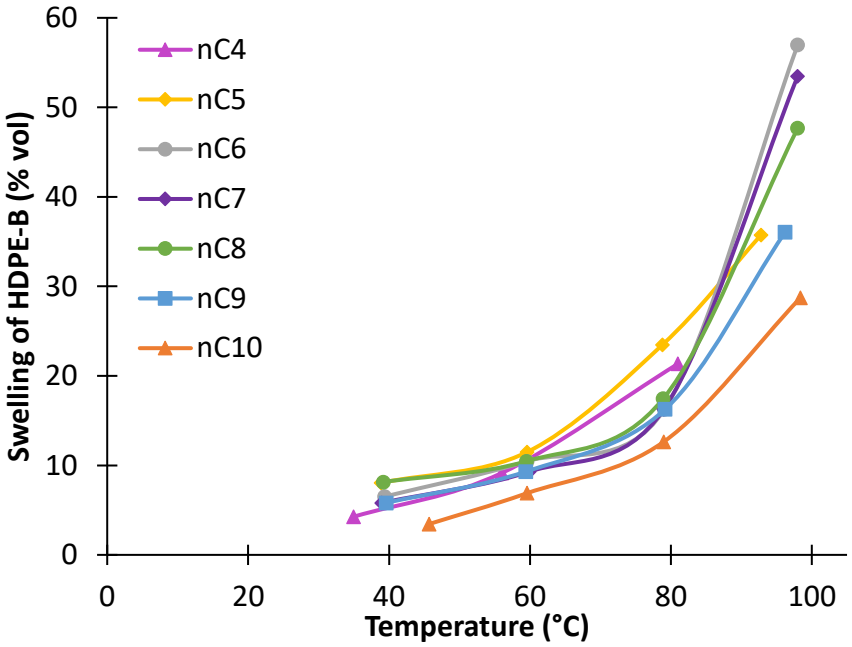

Figure 145. *Swelling of HDPE-B (in % vol) powders in presence of different solvents at different temperatures. (Each experiment was repeated at least twice under the same conditions)*

Figure 145 shows that the swelling of HDPE-B in all solvents is almost the same at temperature below 70°C, except for nC_{10}. Then, the swelling increases considerably between 70 and 100°C, which corresponds to the breakthrough curve. Indeed, the difference of the degree of swelling of the polymer in presence of the different solvents can be seen for temperatures above 70°C. The breakthrough curve corresponds to a temperature where solvents start increasing the swelling drastically. The swelling of the amorphous phase of the polymer can therefore increase in 90 minutes from 15 %vol to 57 %vol for a temperature increase of 10°C for the lighter solvent (i.e. n-pentane). This significant increase of swelling is very important to control in an industrial

reactor, and this data, especially for butane and hexane, is therefore crucial for reactor model development.

The swelling of LLDPE-I in presence of liquid solvents such as n-decane, n-octane, n-heptane, n-hexane and n-pentane expressed in volume percent units at different temperatures will be presented in this section.

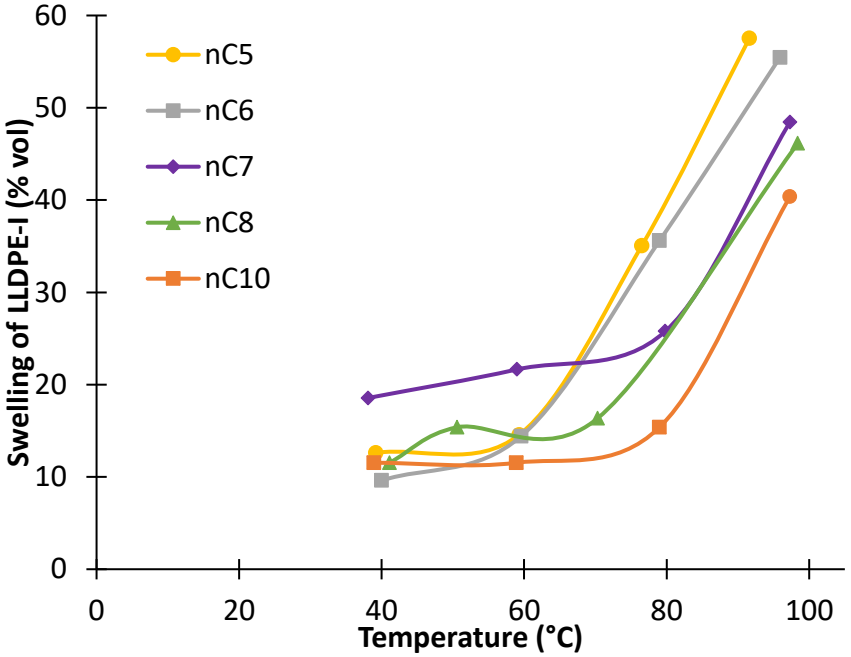

Figure 146. *Swelling of LLDPE-I (in % vol) powders in presence of different solvents at different temperatures. (Each experiment was repeated at least twice under the same conditions)*

Figure 146 shows the same tendency for LLDPE-I as can be seen in Figure 145 for HDPE-B. Increasing the temperature increases the swelling of the polymer and the swelling is higher for lighter solvents. Note that the swelling of the polymer has been corrected for n-pentane and n-hexane. Besides, the swelling is almost constant for temperature lower than 60°C, expect for n-heptane which is higher than all other solvents.

The swelling of MDPE-B in presence of liquid solvents such as n-decane, n-octane, n-heptane, n-hexane and n-pentane expressed in volume percent units at different temperatures will be presented in this section.

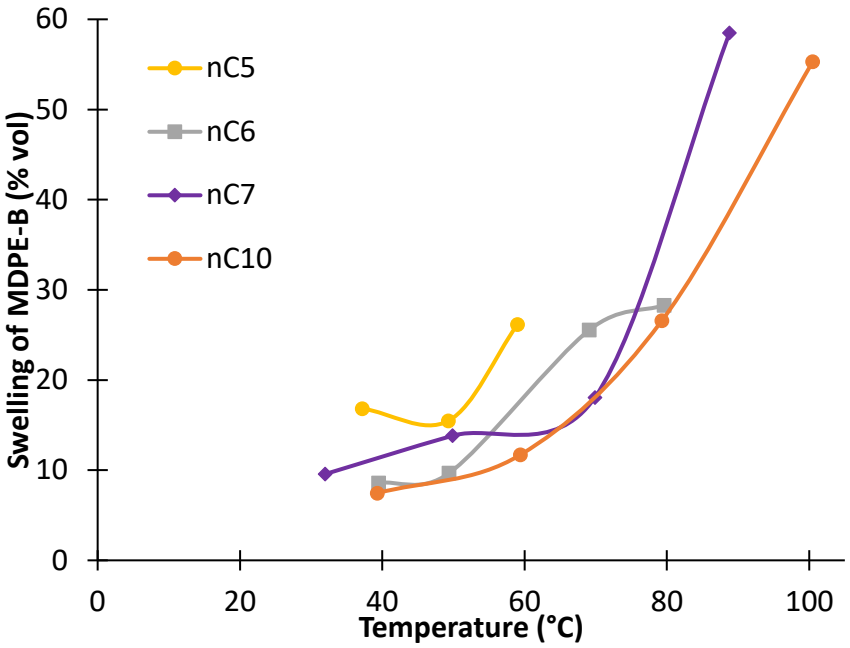

Figure 147. Swelling of MDPE-B (in % vol) powders in presence of different solvents at different temperatures. (Each experiment was repeated at least twice under the same conditions).

Figure 147 shows the same tendency as for LLDPE-I and HDPE-B. Increasing the temperature increases the swelling of the polymer and higher degree of swelling can be seen for lighter solvents. Note that the swelling of the polymer has been corrected for n-pentane and n-hexane, since lighter solvents leads to higher degree of polymer dissolution. Besides, swelling experiments for lighter solvents (i.e. n-pentane, n-heptane) were stopped at lower temperatures; around 60°C for n-pentane and 80°C for n-hexane because MDPE-B powders starts plasticizing, as shown in ***Figure 5***.

Taking into account the amount of polymer dissolved in the solvents when calculating the swelling of the polymer is crucial in order to have a realistic description of the swelling phenomena. Indeed, ***Figure 148*** and ***Figure 149*** compare the swelling measured directly from the experimental set-up and the corrected swelling with the mass of dissolution of LLDPE-I and MDPE-B in solvents, respectively. An important difference is observed, especially at higher temperatures and for lighter solvents; where polymer dissolution is higher. A difference of 80% of the swelling can be seen for n-pentane in MDPE-B at 60°C and of 320% for n-pentane in LLDPE-I at 90°C.

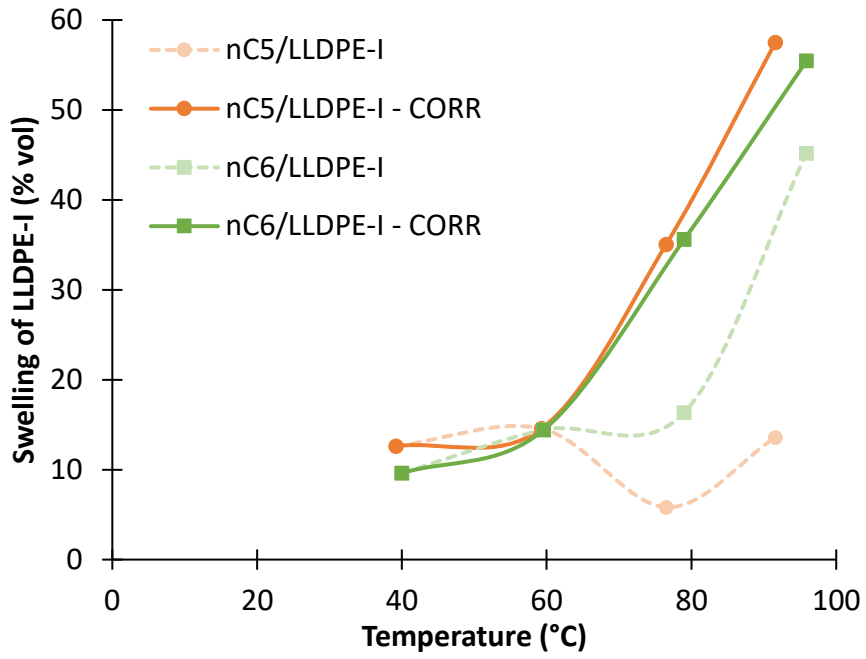

Figure 148. *Swelling measured experimentally and corrected with LLDPE-I dissolution in the solvent given in* ***Table 41***

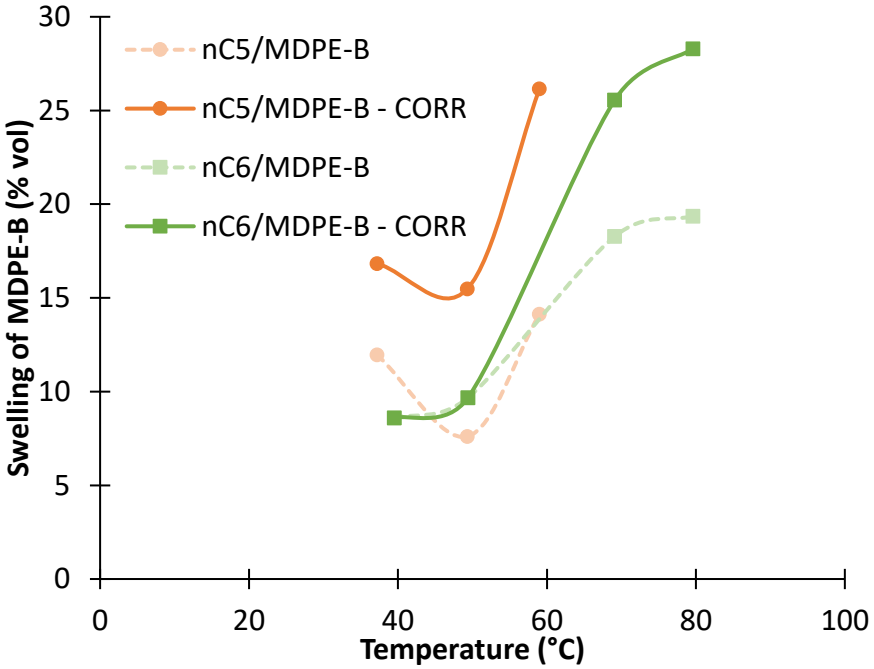

Figure 149*. Swelling measured experimentally and corrected with MDPE-B dissolution in the solvent given in* ***Table 42***

4. Conclusion

The sorption of liquid diluents in PE samples as well as the swelling and the dissolution of PE samples was studied in this chapter. Indeed, a profound lack of data concerning phase equilibria for PE/liquid diluent systems can be found in the open literature. The thermodynamic of liquid diluents in PE samples was therefore studied at relevant industrial conditions; temperatures up to 100°C and isobutane to n-decane as liquid diluents. To the best of our knowledge, this is the first time in the literature that the swelling of different PE samples with varying density from 925-960 $kg.m^{-3}$ are studied at such conditions.

Nevertheless, we were able to show that the smaller the hydrocarbon is, the higher is its solubility in the amorphous phase of the polymer. This implies that the swelling of PE samples in presence of light hydrocarbons is also higher than with heavier hydrocarbons. It was also shown that increasing the temperature increases the solubility of the different liquid diluents in the amorphous phase of the polymer. However, this significant increase of the solubility at high temperature can cause the polymer to swell considerably, leading to reactor fouling by polymer adhesion and plasticization. It was shown that the swelling of PE samples is almost constant for temperatures below 70°C for all types of polymer, and then increases significantly; corresponding to the breakthrough curves where polymer starts to plasticize. This drastic increase of swelling is a very important property that needs to be controlled in industrial reactors, and is therefore crucial for reactor model development. Moreover, the effect of density and crystallinity of PE samples was also studied in this chapter. Indeed, it was shown that the solubility decreases with increasing polymer density and crystallinity for all PE samples, as expected since the crystalline phase of the polymer is impenetrable to liquid diluents. However, the solubility is assumed constant for PE densities up to 935 $kg.m^{-3}$, which was explained by the new morphological model comprising free and constrained amorphous phase in polyethylene. Finally, the dissolution of PE samples was also studied in order to correct swelling experiments.

It would be interesting to push the limits on these experiments to test the swelling of the polymer in supercritical propane (also used in slurry processes) and liquid propylene. Ideally, it would be useful to adapt the Sanchez-Lacombe or PC-SAFT equations of state to predict swelling (which is the ultimate goal here) in diluents used in commercial slurry processes. This data will then be used in reactor models to predict the impact of process conditions, not just on polymer properties, but also to explore operating limits on polymer loading, slurry viscosity and heat transfer. Furthermore, it would also be useful to combine swelling and solubility experiments.

5. References

1. McGrath, P. J., Morris, R. J. & Kreitz, R. W. Cascaded boiling pool slurry reactors for producing bimodal low to medium density polyethylene polymers. (2004).

2. Fouarge, L., Lewalle, A., Auwera, M. V. D. & Brande, F. V. D. Swell control in slurry loop reactor. (2005).

3. Siraux, D. Optimisation of the ethylene polymerisation process. (2010).

4. Zhou, R. *et al.* Modeling of complex liquid-solid flow of particle swelling in slurry loop reactors. *Chemical Engineering Science* **176**, 476–490 (2018).

5. Schnell, M., Stryuk, S. & Wolf, B. A. Liquid/Liquid Demixing in the System n-Hexane/Narrowly Distributed Linear Polyethylene. *Ind. Eng. Chem. Res.* **43**, 2852–2859 (2004).

6. de Loos, Th. W., de Graaf, L. J. & de Swaan Arons, J. Liquid - liquid phase separation in linear low density polyethylene - solvent systems. *Fluid Phase Equilibria* **117**, 40–47 (1996).

7. Pochivalov, K. V., Lebedeva, T. N., Ilyasova, A. N., Basko, A. V. & Kudryavtsev, Y. V. A new look at the semicrystalline polymer – liquid systems: Phase diagrams low-density polyethylene – n-alkanes. *Fluid Phase Equilibria* **471**, 1–7 (2018).

8. Hamada, F., Fujisawa, K. & Nakajima, A. Lower Critical Solution Temperature in Linear Polyethylene–n-Alkane Systems. *Polym J* **4**, 316–322 (1973).

9. Nakajima, A. & Hamada, F. Estimation of thermodynamic interactions between polyethylene and n-alkanes by means of melting point measurements. *Kolloid-Z.u.Z.Polymere* **205**, 55–61 (1965).

10. Aminabhavi, T. M. & Naik, H. G. Sorptionrdesorption, diffusion, permeation and swelling of high density polyethylene geomembrane in the presence of hazardous organic liquids. 12 (1999).

11. Krajakova, L., Laskova, M., Chmelar, J., Jindrova, K. & Kosek, J. Sorption of Liquid Diluents in Polyethylene: Comprehensive Experimental Data for Slurry Polymerization. *Ind. Eng. Chem. Res.* **58**, 7037–7043 (2019).

12. Chmelař, J. *et al.* Free and constrained amorphous phases in polyethylene: Interpretation of 1H NMR and SAXS data over a broad range of crystallinity. *Polymer* **58**, 189–198 (2015).

General Conclusion and Perspectives

1. General conclusion

The focus of the current thesis was to show the importance of an accurate description of penetrant-polymer thermodynamics in order to obtain a realistic model for the solubility, the diffusion and the swelling of the polymer particles in multicomponent systems. We have shown that a good thermodynamic model allows us to predict the impact of process conditions on the rate of polymerization and on the properties of the polymer produced from the gas phase polymerization of ethylene.

The primary objective of this thesis was to overcome the lack of experimental data available in the literature concerning the sorption and diffusion in multicomponent systems, especially in ternary and quaternary systems. Gravimetric and pressure decay methods were used to measure the overall solubility and diffusivity (gravimetry) and the overall and partial solubility (pressure decay) of penetrants in multicomponent systems at conditions relevant to those found in industrial processes.

The ternary systems were first studied for ethylene/propane/PE, ethylene/isobutane/PE and ethylene/1-butene/PE in order to show the impact of the different penetrants on ethylene polymerization in gas phase. The overall solubility of these systems was measured using the gravimetric method. The measured solubilities were then fitted to the Sanchez-Lacombe EoS and combined with the Peng-Robinson EoS (SL-PR). This novel approach used the experimental overall solubility as well as the compressibility factor of the gas mixture calculated with the Peng-Robinson EoS as second data source to estimate the two necessary interaction parameters for the SL EoS. The advantage of this method is that it leads to the identification of the interaction parameters with a measurement of only the overall solubility of the system. This approach was first validated with experimental available data and showed reasonable results, leading to its application to the experimental overall solubility measured with the magnetic suspension balance (MSB). Capturing partial solubilities of the different penetrants in ternary system leads to a better understanding of the thermodynamic phenomena that occurs during ethylene polymerization in gas phase. The co-solubility effect was observed when adding ICAs/comonomer to the gas mixture containing ethylene. This means that adding heavier components increases the solubility of ethylene in the amorphous phase of the polymer. An anti-solvent effect was also highlighted, where lighter components like ethylene decrease the solubility of heavier ones. These thermodynamic properties are very important in the sense that it has been proved that using binary thermodynamic data for ternary system is not correct,

as the interactions between the different components in ternary system have to be taken into account.

The SL EoS was extended to quaternary systems containing three penetrants and a polymer. These quaternary solubility studies represent an important contribution to the modelling of olefin polymerizations since it is the first time in the open literature that solubilities involving polyolefin quaternary systems are studied under conditions approaching those found in industry. Ethylene/propane/1-butene/PE and ethylene/isobutane/1-butene/PE were studied experimentally using the gravimetric and pressure decay methods in order to validate both approaches. It has been shown that the overall solubility of the quaternary system of ethylene/propane/1-butene/LLDPE is higher than that of the ternary system of ethylene/propane/LLDPE and lower than that of ethylene/1-butene/LLDPE at the same temperature and total pressure. However, the results obtained from the quaternary systems demonstrate that the complexity of the changes in the gas phase composition needs to be interpreted by an accurate thermodynamic model, and therefore more experimental data is needed.

As was the case for the solubility, diffusion in multicomponent polymeric systems is so far not completely understood, especially in ternary and more importantly in quaternary systems. Experimental overall diffusivity in ternary and quaternary systems was measured using the gravimetric method. Crank's solution to the Fickian diffusion model in spheres based on two sizes of compact polymer granules was used in order to theoretically interpret the experimental data, and showed good agreement with the latter. This model was capable of estimating the size as well as the fractions of the small and large compact granules in the polymer particle, giving important information about the polymer particle morphology. The rapid initial increase in the sorption curves was explained by the presence of a significant amount of small granules, whereas the following slower increase of the sorbed weight is caused by the presence of a certain amount of big granules. It has been shown that the overall diffusivity of the different studied ternary systems were higher than the binary system of ethylene/LLDPE. This was explained by the co-diffusion effect of heavy penetrants increasing ethylene partial diffusivity in the amorphous phase of the polymer. Furthermore, it has been shown that the quaternary overall diffusivities were found to be close to their respective ternary overall diffusivity at a given temperature and total pressure. However, this observation needs a more detailed thermodynamic analysis based on the changes in the partial molar volumes for example, in order to better understand the diffusion effects occurring in multicomponent systems.

Once all this thermodynamic data acquired, the main goal was to investigate the effect of accurate thermodynamic description on ethylene polymerization in gas phase reactors. This study explored the impact of changes in the gas phase composition (i.e. ICA, hydrogen) through the polymerization rate, ethylene concentration gradients inside the polymer particle, the growth and overheating of the polymer particle, and finally the molecular weight distribution. In all the results, the higher the partial pressure of hydrogen is, the lower the productivity and the molecular weight of the polymer are, whereas increasing n-pentane partial pressure increases the productivity and the polymer molecular weight. In order to do so, the Sanchez-Lacombe EoS was used to describe the solubility of the different penetrants in the amorphous phase of the polymer and the diffusivity was modelled using this data and the free volume model of Vrentas and Duda.

As in gas phase systems, a profound lack of data concerning phase equilibria for PE/liquid diluent systems related to slurry polymerization was found in the open literature. These liquid diluents are expected to change the physical properties of the produced polymer as they cause its swelling and softening due to their high solubility in the amorphous phase of the polymer. The thermodynamic of liquid diluents in PE samples was therefore studied at relevant industrial conditions; temperatures up to 100°C and isobutane to n-decane as liquid diluents. The sorption and swelling of the amorphous phase of the polymer in presence of these liquid diluents were experimentally studied with different grades of polyethylene (i.e. density varying from 925-960 $kg.m^{-3}$). To the best of our knowledge, this is the first time in the literature that the swelling of different PE samples is studied at such conditions. It was found that the solubility of alkanes in the amorphous phase of the polymer was greater for lighter hydrocarbons than for heavier ones. This implies that the swelling of PE samples in presence of light hydrocarbons is also higher than with heavier hydrocarbons. It was also shown that the solubility could be considered constant for polyethylene densities up to 940 kg m^{-3} because the free amorphous phase is not present for these PE grades (i.e. HDPE) and it can sorb more penetrants. Finally, increasing the temperature increases the solubility of liquids in the polymer, and therefore the swelling of the amorphous phase of the polymer. However, a significant increase of the swelling at high temperatures, especially with light hydrocarbons (i.e. n-pentane, n-hexane) can cause the polymer to plasticize, leading therefore to reactor fouling, which is an important parameter to take into account when modeling slurry reactors.

Pertinent thermodynamic data have been presented in this thesis, which represents an important tool for understanding the evolution of the growing polymer particle during ethylene

polymerization, in gas and slurry phase. This thermodynamic data is crucial if one needs to obtain more accurate models describing ethylene polymerization in industrial reactors.

2. Perspectives and future work

The current thesis focused on important thermodynamic and kinetic effects related to industrial polyolefin issues. However, some questions are still not resolve, or might lead to further studies. This could lead to new and very interesting research topics, concerning the impact of the thermodynamics in gas and slurry phase reactors producing polyethylene.

The RPPFM developed in the present thesis highlighted the importance of using an accurate thermodynamic model able to describe the solubility and the diffusivity of multicomponent systems. However, due to the level of complexity of the physical and chemical phenomena that occurs simultaneously during ethylene polymerization in gas phase, a more precise description of the evolution of the morphology of the polymer particle would be needed, as the catalyst/polymer particle evolves rapidly in terms of structure and morphology (i.e. porosity, crystallinity), especially during the initial steps of the polymerization reaction. The measure of the porosity of the polymer particle during the first time of the reaction would be an important parameter to take into account. The crystallinity of the polymer as a function of time would also be a crucial parameter to take into account since the amorphous phase of the polymer changes due to the solubility of the different species in the latter. Besides, it has been shown that the use of the Ranz-Marshall correlation to calculate the external film heat transfer coefficient leads to an overestimation of the particle temperature. Another correlation should be used in order to better predict the change in the overheating of the polymer particle, as this will also have an important impact on the productivity. In the present RPPFM model, ethylene polymerization in presence of n-pentane and hydrogen has been shown. However, the use of only ternary system of ethylene/n-pentane/PE have been used in this study. The concentration of hydrogen have been calculated with Henry's law. It would be more useful to measure the solubility of ethylene/n-pentane/hydrogen/PE in order to take into account the possible interactions between ethylene and n-pentane with hydrogen, in order to have a more accurate kinetic model. Finally, this model can be extended to copolymerization reaction by integrating quaternary solubility and diffusivity data. The measured quaternary solubility and diffusivity data from gravimetric

and pressure decay method could be used in order to describe the polymerization of the mixture of ethylene/isobutane/1-butene/PE or ethylene/propane/1-butene/PE.

One of the main concern in the field of polyolefin reaction engineering is the lack of experimental thermodynamic data. In order to overcome these issues, two approaches have been used in order to measure the overall and partial solubility of the different components in a mixture, as well as the overall diffusivity; gravimetric and pressure decay methods. The gravimetric method measures the overall solubility and diffusivity data whereas the pressure decay method measures the overall and partial solubility of multicomponent systems. Significantly more data for gas mixtures and polymers of different densities and molecular weight distributions needs to be collected in order to refine our thermodynamic models and to eventually help explain the relationship between solubility/swelling and polymer structure.

The same is true for diffusion. Concerning the diffusivity experiments, we have shown that the two level Crank's model is capable of predicting the shape of the degassing experiments. However, we have seen that some systems (i.e. ethylene/propane/1-butene/LLDPE) lead to more difficult fitting of this model to the experimental data. An improvement of this model might be to take into account the changes in the radius of both the big and small granules as a function of time, as well as their fractions in the polymer particle. In that sense, we would expect to have different fractions of big and small granules during ethylene polymerization. Indeed, the particle morphology changes rapidly, especially at the beginning of the reaction by undergoing a fragmentation step where smaller particles are produced followed by the expansion of the polymer particles through the diffusion and sorption of the different penetrants. The effect of the evolution of the radius of the big and small granules on the productivity of the polymerization could therefore be analyzed. Besides, this two-level model could be integrated inside the RPPFM in order to have a better description of the diffusivity of the different penetrants inside the amorphous phase of the polymer.

The quaternary experiments performed (i.e. ethylene/propane/1-butene/PE and ethylene/isobutane/1-butene/PE) have shown the impact of different ICAs on the solubility of the mixture. It would be interesting to look at the effect of other quaternary systems involving for example other ICAs (i.e. isobutane, n-pentane, n-hexane) and other comonomers (i.e. 1-hexene) in order to compare the effect of different ICAs and co-monomers, and their combination, on the overall solubility in quaternary systems. Furthermore, the study of structurally close ICA and comonomer could be interesting in order to show the impact of the

interactions between them and with ethylene on the overall solubility in quaternary sytems. As an example, the systems of ethylene/isobutane/1-butene/PE and ethylene/n-hexane/1-butene/PE could be compared. Finally, the study of the solubility in different polymer grades, using different catalyst (i.e. metallocene, Ziegler-Natta) could be achieved in order to show the impact of the interaction parameters k_{ij} on the different polymer samples. The interaction parameters, k_{ij}, being temperature dependent, broader temperature could be performed in order to have more reliable correlations of these interaction parameters, that are crucial when modeling thermodynamic behaviors with SL EoS. Finally, quintary system could also be realized using the pressure decay method in order to show the impact of hydrogen on the solubility of the quaternary systems. The SL EoS could be extended to quintary systems in order to model systems that are closer to the industrial polymerization conditions.

Concerning the experiments in slurry phase, the effect of crystallinity changes during the experiments would be a useful characteristic to analyze. It would be expected to see a change in the crystallinity of the polymer due to a high degree of solubility and swelling of the amorphous phase of the polymer in presence of liquid diluents. It would be interesting as well to push the limits on these experiments to test the swelling of the polymer in supercritical propane (also used in Borstar slurry processes) and liquid propylene. Ideally, it would be useful to adapt the Sanchez-Lacombe or PC-SAFT equations of state to predict swelling (which is the ultimate goal here) in diluents used in commercial slurry processes. This data could be used in reactor models to predict the impact of process conditions (i.e. Hostalen and Innovene processes), not just on polymer properties, but also to explore operating limits on polymer loading, slurry viscosity and heat transfer. Furthermore, it would also be useful to combine solubility experiments in slurry and gas phase. This study would explore the influence of liquid diluent on the solubility of gaseous components in the polymer.

Appendix A

Application of the Sanchez-Lacombe Equation of State for quaternary systems

Model Development

The details of the mathematical equations derived from the Sanchez-Lacombe Equation of State in order to describe quaternary systems is presented in this Appendix.

1. Description of Sanchez-Lacombe EoS model

The Sanchez-Lacombe Equation of State (SL EoS) is defined by

$$\bar{\rho}^2 + \bar{P} + \bar{T}\left[ln(1-\bar{\rho}) + \left(1-\frac{1}{r}\right)\bar{\rho}\right] = 0 \qquad (1)$$

where $\bar{T}, \bar{P}$ and $\bar{\rho}$ are the reduced temperature, pressure, and density respectively which are defined as follows

$$\bar{T} = T/T^*, \qquad T^* = \varepsilon^*/R_g \qquad (2)$$

$$\bar{P} = P/P^*, \qquad P^* = \varepsilon^*/v^* \qquad (3)$$

$$\bar{\rho} = \rho/\rho^* = V^*/V, \qquad V^* = N(rv^*) \text{ and } \rho^* = MW/(rv^*) \qquad (4)$$

where ε^* is the mer-mer interaction energy, v^*, is the closed packed molar volume of a mer, *MW* is molecular weight, *N* is number of molecules, *r* is the number of sites (mers) a molecule occupies in the lattice, $\bar{T}$ is the reduced volume and R_g is the universal gas constant. The parameters ε^*,v^* and *r* are used to define T^*, P^*, and ρ^* which are the characteristic temperature, pressure, and close-packed mass density.

For a mixture of components, defining combining rules for the estimation of $\varepsilon^*_{\text{mix}}$, v^*_{mix}, and r_{mix} is necessary to be able to use the equation of state to calculate the properties of mixture. The Van der Waals mixing rule is chosen and applied in our study.

For characteristic closed-packed molar volume of a “mer” of the mixture, the "Van der Waals" mixing rule, v^*_{mix}, is defined as

$$v^*_{mix} = \sum_{i=1}^{N_c}\sum_{j=1}^{N_c} \phi_i \phi_j v^*_{ij} \qquad (5)$$

with

$$v_{ij}^{*} = \frac{v_{ii}^{*} + v_{jj}^{*}}{2}\left(1 - n_{ij}\right) \tag{6}$$

Where ϕ is the volume fraction of the i^{th} and j^{th} component in the mixture, N_{c} is the number of component in the mixture and n_{ij} corrects the possible deviation of v_{ij}^{*} from the arithmetic mean value of v_{ii}^{*} and v_{jj}^{*} of the pure component.

The closed-packed volume fraction of the i^{th} component at the limit of zero temperature or incompressible state, ϕ_i^{gas} is defined as

$$\phi_i^{\text{gas}} = \frac{\omega_i^{\text{gas}}}{\rho_i^{*} v_i^{*}} \Bigg/ \sum_{j=1}^{N_{\text{c}}} \left(\frac{\omega_j^{\text{gas}}}{\rho_j^{*} v_j^{*}}\right) \tag{7}$$

where ω_i^{gas} is the mass fraction of the component *i* in the gas phase, defined as follows:

$$\omega_i^{\text{gas}} = \frac{\rho_i^{\text{gas}}}{\sum_{i=1}^{N_{\text{c}}} \rho_i^{\text{gas}}}$$

The mixing rule for the characteristic interaction energy for the mixture, $\varepsilon_{\text{mix}}^{*}$, is defined as

$$\varepsilon_{\text{mix}}^{*} = \frac{1}{v_{\text{mix}}^{*}} \sum_{i=1}^{N_{\text{c}}} \sum_{j=1}^{N_{\text{c}}} \phi_i \phi_j \varepsilon_{ij}^{*} v_{ij}^{*} \tag{8}$$

Where the cross-energy parameter between mers of component *i* and component *j*, ε_{ij}^{*}, is introduced in order to take into account the interactions between the different components in the mixture, as follows

$$\varepsilon_{ij}^{*} = \left(\varepsilon_{ii}^{*} \varepsilon_{jj}^{*}\right)^{0.5}\left(1 - k_{ij}\right) \tag{9}$$

where ε_{ii}^{*} and ε_{jj}^{*} are the characteristic mer-mer interaction energies for components *i* and *j*, and k_{ij} is an adjustable parameter that accounts for the interactions between components *i* and *j*.

Finally, the mixing rule for the number of sites (mers) occupied by a molecule of the mixture, r_{mix}, is given by

$$\frac{1}{r_{\mathrm{mix}}} = \sum_{j=1}^{N_c} \frac{\phi_j}{r_j} \tag{10}$$

where r_j is the number of sites occupied by molecule *j* in the lattice.

For the calculation of sorption equilibrium for polymer-solvent system, the chemical potential of the i^{th} component in each phase of the mixture of multicomponent species can be expressed as:

$$\mu_i = \mathrm{R}\,T\left[\ln\phi_i + \left(1 - \frac{r_i}{r_{\mathrm{mix}}}\right)\right] + \tag{11}$$

$$+r_i\left\{-\overline{\rho_{\mathrm{mix}}}\left[\frac{2}{\upsilon^*_{\mathrm{mix}}}\left(\sum_{j=1}^{Nc}\phi_j\upsilon^*_{ij}\varepsilon^*_{ij} - \varepsilon^*_{\mathrm{mix}}\sum_{j=1}^{Nc}\phi_j\upsilon^*_{ij}\right) + \varepsilon^*_{\mathrm{mix}}\right]\right.$$

$$\left. + \frac{\mathrm{R}\,T}{\overline{\rho_{\mathrm{mix}}}}\left[(1-\overline{\rho_{\mathrm{mix}}})\ln(1-\overline{\rho_{\mathrm{mix}}}) + \frac{\overline{\rho_{\mathrm{mix}}}}{r_i}ln\overline{\rho_{\mathrm{mix}}}\right] + \frac{P}{\overline{\rho_{\mathrm{mix}}}}\left(2\sum_{j=1}^{Nc}\phi_j\upsilon^*_{ij} - \upsilon^*_{\mathrm{mix}}\right)\right\}$$

In order to solve SL EoS, we consider that the chemical potential of each penetrant at equilibrium is equal to the chemical potential of the polymer as follows:

$$\mu_i^{\mathrm{polymer}} = \mu_i^{\mathrm{gas}} \qquad i=1,2,3,4 \tag{12}$$

As an example, in binary system composed of a gaseous specie with a polymer, we will have two phase in equilibrium: the gas phase composed of the gaseous specie only and the polymer phase, which is constituted of both polymer and the gaseous specie.

2. Sanchez-Lacombe EoS for quaternary systems

We consider here a quaternary system containing a monomer (1), an ICA (2), a comonomer (3) and a polymer (4). The corresponding interaction parameters in order to solve SL EoS are : k_{12}, k_{13}, k_{14}, k_{23}, k_{24}, k_{34} which are the interaction parameters between the monomer and the ICA, the monomer and the comonomer, the monomer and the polymer, the ICA and the comonomer, the ICA and the polymer and the comonomer and the polymer, respectively. Only k_{14}, k_{24}, k_{34} parameters are estimated by fitting SL EoS to experimental data, while k_{12}, k_{13} and k_{24} are equal to zero because we assume that there is no interaction between small olefin molecules.

The first objective here is to calculate the solubility of the different component in the mixture in the polymer phase, knowing their partial pressure in the mixture (*i.e.* P_1, P_2, P_3) at a specific

temperature, *T*. All of the other properties will therefore be calculated from the extent of the solubility of the different component in the polymer.

First, it is necessary to calculate the chemical potential of component *1*, 2 and *3* in the gas phase. These values will later be used in the equilibrium condition, in which the chemical potential of each of the components are equal in all phases. In other words, $\mu_1^{gas} = \mu_1^{pol}$, $\mu_2^{gas} = \mu_2^{pol}$ and $\mu_3^{gas} = \mu_3^{pol}$.

Knowing the partial pressure of component *1, 2* and *3* in the gas phase at the specific temperature, the reduced density of each component in the gas phase is calculated from the SL EoS, (1) by solving equation (13), (14) and (15), respectively, as follow

$$\bar{\rho}_1{}^{gas} = 1 - \exp\left(-\frac{(\bar{\rho}_1{}^{gas})^2}{\bar{T}_1} - \frac{\bar{P}_1}{\bar{T}_1} - \left(1 - \frac{1}{r_1}\right)\bar{\rho}_1{}^{gas}\right) \quad (13)$$

$$\bar{\rho}_2{}^{gas} = 1 - \exp\left(-\frac{(\bar{\rho}_2{}^{gas})^2}{\bar{T}_2} - \frac{\bar{P}_2}{\bar{T}_2} - \left(1 - \frac{1}{r_2}\right)\bar{\rho}_2{}^{gas}\right) \quad (14)$$

$$\bar{\rho}_3{}^{gas} = 1 - exp\left(-\frac{(\bar{\rho}_3{}^{gas})^2}{\bar{T}_3} - \frac{\bar{P}_3}{\bar{T}_3} - \left(1 - \frac{1}{r_3}\right)\bar{\rho}_3{}^{gas}\right) \quad (15)$$

The density of component *1, 2* and *3* in the gas phase will be equal to

$$\rho_1{}^{gas} = \rho_1^*\bar{\rho}_1{}^{gas} \quad (16)$$

$$\rho_2^{gas} = \rho_2^*\bar{\rho}_2{}^{gas} \quad (17)$$

$$\rho_3^{gas} = \rho_3^*\bar{\rho}_3{}^{gas} \quad (18)$$

At given volume of the gas phase mixture, the mass fraction of component *1, 2* and *3* in the gas phase is given by

$$\omega_1^{gas} = \frac{\rho_1^{gas}}{\rho_1^{gas} + \rho_2^{gas} + \rho_3^{gas}} \quad (19)$$

$$\omega_2^{gas} = \frac{\rho_2^{gas}}{\rho_1^{gas} + \rho_2^{gas} + \rho_3^{gas}} \quad (20)$$

$$\omega_3^{gas} = \frac{\rho_3^{gas}}{\rho_1^{gas} + \rho_2^{gas} + \rho_3^{gas}} \quad (21)$$

As a result, according to the equation (7), the closed packed volume fraction of components in the gas phase can be found by

$$\phi_1^{\text{gas}} = \frac{\frac{\left(\rho_1{}^{gas}/(\rho_1^{gas}+\rho_2^{gas}+\rho_3^{gas})\right)}{\rho_1^* v_1^*}}{\frac{\left(\rho_1{}^{gas}/(\rho_1^{gas}+\rho_2^{gas}+\rho_3^{gas})\right)}{\rho_1^* v_1^*}+\frac{\left(\rho_2{}^{gas}/(\rho_1^{gas}+\rho_2^{gas}+\rho_3^{gas})\right)}{\rho_2^* v_2^*}+\frac{\left(\rho_3{}^{gas}/(\rho_1^{gas}+\rho_2^{gas}+\rho_3^{gas})\right)}{\rho_3^* v_3^*}} \quad (22)$$

$$\phi_2^{\text{gas}} = \frac{\frac{\left(\rho_2{}^{gas}/(\rho_1^{gas}+\rho_2^{gas}+\rho_3^{gas})\right)}{\rho_2^* v_2^*}}{\frac{\left(\rho_1{}^{gas}/(\rho_1^{gas}+\rho_2^{gas}+\rho_3^{gas})\right)}{\rho_1^* v_1^*}+\frac{\left(\rho_2{}^{gas}/(\rho_1^{gas}+\rho_2^{gas}+\rho_3^{gas})\right)}{\rho_2^* v_2^*}+\frac{\left(\rho_3{}^{gas}/(\rho_1^{gas}+\rho_2^{gas}+\rho_3^{gas})\right)}{\rho_3^* v_3^*}} \quad (23)$$

Assuming that there is no polymer molecules in the gas phase, $\phi_3^{\text{gas}} = 1 - \phi_1^{\text{gas}} - \phi_2^{\text{gas}}$

The reduced gas phase density, $\bar{\rho}^{gas}$, is calculated base on (1) as follow

$$\bar{\rho}^{gas} = 1 - \exp\left(-\frac{\bar{\rho}^{gas2}}{\bar{T}_{mix}^{gas}} - \frac{\bar{P}_{mix}^{gas}}{\bar{T}_{mix}^{gas}} - \left(1 - \frac{1}{r_{\text{mix}}^{\text{gas}}}\right)\bar{\rho}^{gas}\right) \quad (24)$$

in which

$$\bar{T}_{mix}^{gas} = \frac{R_g T}{\varepsilon^{*\text{gas}}_{\text{mix}}} \quad (24.1)$$

$$\bar{P}_{mix}^{gas} = \frac{P\, v^{*\text{gas}}_{\text{mix}}}{\varepsilon^{*\text{gas}}_{\text{mix}}} \quad (24.2)$$

$$\frac{1}{r_{\text{mix}}^{\text{gas}}} = \frac{\phi_1^{gas}}{r_1} + \frac{\phi_2^{gas}}{r_2} + \frac{\phi_3^{gas}}{r_3} \quad (24.3)$$

in which $v^{*\text{gas}}_{\text{mix}}$ and $\varepsilon^{*\text{gas}}_{\text{mix}}$ are calculated based on (5) and (8), respectively, as follow

$$v^{*\text{gas}}_{\text{mix}} = \alpha\phi_1^{gas} + \beta\phi_2^{gas} + \Upsilon \quad (25)$$

$$\varepsilon^{*\text{gas}}_{\text{mix}} = \frac{A\phi_1^{gas2} + B\phi_2^{gas2} + C\phi_1^{gas}\phi_2^{gas} + D\phi_1^{gas} + E\phi_2^{gas} + F}{\alpha\phi_1^{gas} + \beta\phi_2^{gas} + \Upsilon} \quad (26)$$

The parameters α, β, Υ , A, B, C, D, E and F are defined as follow

$$\alpha = v_1 - v_3 \tag{26.1}$$

$$\beta = v_2 - v_3 \tag{26.2}$$

$$\Upsilon = v_3 \tag{26.3}$$

$$A = \varepsilon_1^* v_1^* + \varepsilon_3^* v_3^* - 2\varepsilon_{13}^* v_{13}^* \tag{26.4}$$

$$B = \varepsilon_2^* v_2^* + \varepsilon_3^* v_3^* - 2\varepsilon_{23}^* v_{23}^* \tag{26.5}$$

$$C = 2(\varepsilon_{12}^* v_{12}^* - \varepsilon_{13}^* v_{13}^* - \varepsilon_{23}^* v_{23}^* + \varepsilon_3^* v_3^*) \tag{26.6}$$

$$D = 2\varepsilon_{13}^* v_{13}^* - 2\varepsilon_3^* v_3^* \tag{26.7}$$

$$E = 2\varepsilon_{23}^* v_{23}^* - 2\varepsilon_3^* v_3^* \tag{26.8}$$

$$F = \varepsilon_3^* v_3^* \tag{26.9}$$

After the calculation of the closed-packed volume fraction of the different components in the gas phase (ϕ_1^{gas}, ϕ_2^{gas} and ϕ_3^{gas}) and the reduced gas phase density ($\bar{\rho}^{\text{gas}}$), it is possible to calculate chemical potential of components *1, 2* and 3 in the gas phase following equation (11) as follow

$$\mu_1^{\text{gas}} = R_g T \left[ln\phi_1^{\text{gas}} + 1 - \frac{r_1}{r_{\text{mix}}^{\text{gas}}} \right] \tag{27}$$

$$+ r_1 \left\{ \begin{array}{c} -\bar{\rho}_{\text{gas}} \left[\frac{2}{v^{*\text{gas}}_{\text{mix}}} \left(\begin{array}{c} \left(\phi_1^{\text{gas}} v_1^* \varepsilon_1^* + \phi_2^{\text{gas}} v_{12}^* \varepsilon_{12}^* + \phi_3^{\text{gas}} v_{13}^* \varepsilon_{13}^*\right) \\ -\varepsilon^{*\text{gas}}_{\text{mix}} \left(\phi_1^{\text{gas}} v_1^* + \phi_2^{\text{gas}} v_{12}^* + \phi_3^{\text{gas}} v_{13}^*\right) \end{array} \right) + \varepsilon^{*\text{gas}}_{\text{mix}} \right] + \\ \frac{R_g T}{\bar{\rho}_{\text{gas}}} \left[\left(1 - \bar{\rho}_{\text{gas}}\right) \ln\left(1 - \bar{\rho}_{\text{gas}}\right) + \frac{\bar{\rho}_{\text{gas}}}{r_1} ln\bar{\rho}_{\text{gas}} \right] + \frac{P}{\bar{\rho}_{\text{gas}}} \left[2\left(\phi_1^{\text{gas}} v_1^* + \phi_2^{\text{gas}} v_{12}^* + \phi_3^{\text{gas}} v_{13}^*\right) - v^{*\text{gas}}_{\text{mix}} \right] \end{array} \right\}$$

$$\mu_2^{\text{gas}} = R_g T \left[ln\phi_2^{\text{gas}} + 1 - \frac{r_2}{r_{\text{mix}}^{\text{gas}}} \right] \tag{28}$$

$$+ r_2 \left\{ \begin{array}{c} -\bar{\rho}_{\text{gas}} \left[\dfrac{2}{v^{*\text{gas}}_{\text{mix}}} \left(\begin{array}{c} \left(\phi_1^{\text{gas}} v_{12}^* \varepsilon_{12}^* + \phi_2^{\text{gas}} v_2^* \varepsilon_2^* + \phi_3^{\text{gas}} v_{23}^* \varepsilon_{23}^*\right) \\ -\varepsilon^{*\text{gas}}_{\text{mix}} \left(\phi_1^{\text{gas}} v_{12}^* + \phi_2^{\text{gas}} v_2^* + \phi_3^{\text{gas}} v_{23}^*\right) \end{array} \right) + \varepsilon^{*\text{gas}}_{\text{mix}} \right] + \\ \dfrac{R_g T}{\bar{\rho}_{\text{gas}}} \left[\left(1 - \bar{\rho}_{\text{gas}}\right) \ln\left(1 - \bar{\rho}_{\text{gas}}\right) + \dfrac{\bar{\rho}_{\text{gas}}}{r_2} ln\bar{\rho}_{\text{gas}} \right] + \dfrac{P}{\bar{\rho}_{\text{gas}}} \left[2\left(\phi_1^{\text{gas}} v_{12}^* + \phi_2^{\text{gas}} v_2^* + \phi_3^{\text{gas}} v_{23}^*\right) - v^{*\text{gas}}_{\text{mix}} \right] \end{array} \right\}$$

$$\mu_3^{\text{gas}} = R_g T \left[ln\phi_3^{\text{gas}} + 1 - \frac{r_3}{r_{\text{mix}}^{\text{gas}}} \right] \qquad (29)$$

$$+ r_3 \left\{ \begin{array}{c} -\bar{\rho}_{\text{gas}} \left[\dfrac{2}{v^{*\text{gas}}_{\text{mix}}} \left(\begin{array}{c} \left(\phi_1^{\text{gas}} v_{13}^* \varepsilon_{13}^* + \phi_2^{\text{gas}} v_{23}^* \varepsilon_{23}^* + \phi_3^{\text{gas}} v_3^* \varepsilon_3^*\right) \\ -\varepsilon^{*\text{gas}}_{\text{mix}} \left(\phi_1^{\text{gas}} v_{13}^* + \phi_2^{\text{gas}} v_{23}^* + \phi_3^{\text{gas}} v_3^*\right) \end{array} \right) + \varepsilon^{*\text{gas}}_{\text{mix}} \right] + \\ \dfrac{R_g T}{\bar{\rho}_{\text{gas}}} \left[\left(1 - \bar{\rho}_{\text{gas}}\right) \ln\left(1 - \bar{\rho}_{\text{gas}}\right) + \dfrac{\bar{\rho}_{\text{gas}}}{r_3} ln\bar{\rho}_{\text{gas}} \right] + \dfrac{P}{\bar{\rho}_{\text{gas}}} \left[2\left(\phi_1^{\text{gas}} v_{13}^* + \phi_2^{\text{gas}} v_{23}^* + \phi_3^{\text{gas}} v_3^*\right) - v^{*\text{gas}}_{\text{mix}} \right] \end{array} \right\}$$

Once the gas phase system and its characteristics defined, it is necessary to define the characteristic parameters for the polymer phase as the mixture of solute (*1*, *2, 3*) and polymer (*4*) components. By considering that $\phi_1^{\text{pol}} + \phi_2^{\text{pol}} + \phi_3^{\text{pol}} + \phi_4^{\text{pol}} = 1$, the characteristic closed-packed molar volume of "mer" of polymer phase mixture can be written, based on (5) as follow

$$v^{*\text{pol}}_{\text{mix}} = \sigma_1 \phi_1^{\text{pol}} + \sigma_2 \phi_2^{\text{pol}} + \sigma_3 \phi_3^{\text{pol}} + \sigma_4 \qquad (30)$$

in which

$$\sigma_1 = v_1^* - v_4^* \qquad (30.1)$$

$$\sigma_2 = v_2^* - v_4^* \qquad (30.2)$$

$$\sigma_3 = v_3^* - v_4^* \qquad (30.3)$$

$$\sigma_4 = v_4^* \qquad (30.4)$$

Similarly, it is possible to obtain the characteristic mer-mer interaction energy of the polymer phase mixture, by expanding equation (8), as follow

$$\begin{aligned} \varepsilon^{*\text{pol}}_{\text{mix}} = \frac{1}{\sigma_1 \phi_1^{\text{pol}} + \sigma_2 \phi_2^{\text{pol}} + \sigma_3 \phi_3^{\text{pol}} + \sigma_4} (& A_1 {\phi_1^{\text{pol}}}^2 + A_2 {\phi_2^{\text{pol}}}^2 + A_3 {\phi_3^{\text{pol}}}^2 \\ & + A_{12} \phi_1^{\text{pol}} \phi_2^{\text{pol}} + A_{23} \phi_2^{\text{pol}} \phi_3^{\text{pol}} + A_{13} \phi_1^{\text{pol}} \phi_3^{\text{pol}} + B_1 \phi_1^{\text{pol}} \\ & + B_2 \phi_2^{\text{pol}} + B_3 \phi_3^{\text{pol}} + C_1) \end{aligned} \qquad (31)$$

in which

$$A_1 = \varepsilon_1^* v_1^* + \varepsilon_4^* v_4^* - 2\varepsilon_{14}^* v_{14}^* \quad (31.1)$$

$$A_2 = \varepsilon_2^* v_2^* + \varepsilon_4^* v_4^* - 2\varepsilon_{24}^* v_{24}^* \quad (31.2)$$

$$A_3 = \varepsilon_3^* v_3^* + \varepsilon_4^* v_4^* - 2\varepsilon_{34}^* v_{34}^* \quad (31.3)$$

$$A_{12} = 2(\varepsilon_{12}^* v_{12}^* - \varepsilon_{14}^* v_{14}^* - \varepsilon_{24}^* v_{24}^* + \varepsilon_4^* v_4^*) \quad (31.4)$$

$$A_{23} = 2(\varepsilon_{23}^* v_{23}^* - \varepsilon_{24}^* v_{24}^* - \varepsilon_{34}^* v_{34}^* + \varepsilon_4^* v_4^*) \quad (31.5)$$

$$A_{13} = 2(\varepsilon_{13}^* v_{13}^* - \varepsilon_{14}^* v_{14}^* - \varepsilon_{34}^* v_{34}^* + \varepsilon_4^* v_4^*) \quad (31.6)$$

$$B_1 = 2\varepsilon_{14}^* v_{14}^* - 2\varepsilon_4^* v_4^* \quad (31.7)$$

$$B_2 = 2\varepsilon_{24}^* v_{24}^* - 2\varepsilon_4^* v_4^* \quad (31.8)$$

$$B_3 = 2\varepsilon_{34}^* v_{34}^* - 2\varepsilon_4^* v_4^* \quad (31.9)$$

$$C_1 = \varepsilon_4^* v_4^* \quad (31.10)$$

Finally the number of sites (mers) occupied in the lattice by a molecule of polymer phase mixture will be given assuming $r_4 >> r_1$, r_2, r_3, as follow

$$\frac{1}{r_{\text{mix}}^{\text{pol}}} = \frac{\phi_1^{\text{pol}}}{r_1} + \frac{\phi_2^{\text{pol}}}{r_2} + \frac{\phi_3^{\text{pol}}}{r_3} \quad (32)$$

The Sanchez-Lacombe EoS for polymer phase is obtained by substituting equations (30), (31), (32) into the equation (1) as follow

$$\bar{\rho}^{\text{pol}^2} + P\frac{\left(\sigma_1\phi_1^{\text{pol}} + \sigma_2\phi_2^{\text{pol}} + \sigma_3\phi_3^{\text{pol}} + \sigma_4\right)^2}{\begin{matrix} A_1\phi_1^{\text{pol}^2} + A_2\phi_2^{\text{pol}^2} + A_3\phi_3^{\text{pol}^2} + A_{12}\phi_1^{\text{pol}}\phi_2^{\text{pol}} + A_{23}\phi_2^{\text{pol}}\phi_3^{\text{pol}} + A_{13}\phi_1^{\text{pol}}\phi_3^{\text{pol}} \\ +B_1\phi_1^{\text{pol}} + B_2\phi_2^{\text{pol}} + B_3\phi_3^{\text{pol}} + C_1 \end{matrix}} \quad (33)$$

$$+R_gT\frac{\sigma_1\phi_1^{\text{pol}}+\sigma_2\phi_2^{\text{pol}}+\sigma_3\phi_3^{\text{pol}}+\sigma_4}{A_1{\phi_1^{\text{pol}}}^2+A_2{\phi_2^{\text{pol}}}^2+A_3{\phi_3^{\text{pol}}}^2+A_{12}\phi_1^{\text{pol}}\phi_2^{\text{pol}}+A_{23}\phi_2^{\text{pol}}\phi_3^{\text{pol}}+A_{13}\phi_1^{\text{pol}}\phi_3^{\text{pol}}}*$$
$$+B_1\phi_1^{\text{pol}}+B_2\phi_2^{\text{pol}}+B_3\phi_3^{\text{pol}}+C_1$$

$$\left[ln\left(1-\bar{\rho}^{\text{pol}}\right)+\left(1-\frac{\phi_1^{\text{pol}}}{r_1}-\frac{\phi_2^{\text{pol}}}{r_2}-\frac{\phi_3^{\text{pol}}}{r_3}\right)\bar{\rho}^{\text{pol}}\right]=0$$

Following the thermodynamic rule for the equilibrium condition $\mu_1^{\text{gas}}=\mu_1^{\text{pol}}$, $\mu_2^{\text{gas}}=\mu_2^{\text{pol}}$ and $\mu_3^{\text{gas}}=\mu_3^{\text{pol}}$, the chemical potential in the polymer phase can therefore be calculated.

For component *1*, the equilibrium condition is given by

$$R_gT\left[ln\phi_1^{\text{pol}}+1-r_1\left(\frac{\phi_1^{\text{pol}}}{r_1}+\frac{\phi_2^{\text{pol}}}{r_2}+\frac{\phi_3^{\text{pol}}}{r_3}\right)\right] \qquad (34)$$

$$+r_1\left\{-\bar{\rho}^{\text{pol}}\left[\frac{2}{\sigma_1\phi_1^{\text{pol}}+\sigma_2\phi_2^{\text{pol}}+\sigma_3\phi_3^{\text{pol}}+\sigma_4}\left(\left(G_1\phi_1^{\text{pol}}+G_2\phi_2^{\text{pol}}+G_3\phi_3^{\text{pol}}+G_4\right)-\right.\right.\right.$$

$$\left(\frac{A_1{\phi_1^{\text{pol}}}^2+A_2{\phi_2^{\text{pol}}}^2+A_3{\phi_3^{\text{pol}}}^2+A_{12}\phi_1^{\text{pol}}\phi_2^{\text{pol}}+A_{23}\phi_2^{\text{pol}}\phi_3^{\text{pol}}+A_{13}\phi_1^{\text{pol}}\phi_3^{\text{pol}}+B_1\phi_1^{\text{pol}}+B_2\phi_2^{\text{pol}}+B_3\phi_3^{\text{pol}}+C_1}{\sigma_1\phi_1^{\text{pol}}+\sigma_2\phi_2^{\text{pol}}+\sigma_3\phi_3^{\text{pol}}+\sigma_4}\right)\left(g_1\phi_1^{\text{pol}}+\right.$$

$$\left.\left.g_2\phi_2^{\text{pol}}+g_3\phi_3^{\text{pol}}+g_4\right)\right)+$$

$$\left.\left.\left(\frac{A_1{\phi_1^{\text{pol}}}^2+A_2{\phi_2^{\text{pol}}}^2+A_3{\phi_3^{\text{pol}}}^2+A_{12}\phi_1^{\text{pol}}\phi_2^{\text{pol}}+A_{23}\phi_2^{\text{pol}}\phi_3^{\text{pol}}+A_{13}\phi_1^{\text{pol}}\phi_3^{\text{pol}}+B_1\phi_1^{\text{pol}}+B_2\phi_2^{\text{pol}}+B_3\phi_3^{\text{pol}}+C_1}{\sigma_1\phi_1^{\text{pol}}+\sigma_2\phi_2^{\text{pol}}+\sigma_3\phi_3^{\text{pol}}+\sigma_4}\right)\right]+\right.$$

$$\frac{R_gT}{\bar{\rho}^{\text{pol}}}\left[\left(1-\bar{\rho}^{\text{pol}}\right)\ln\left(1-\bar{\rho}^{\text{pol}}\right)+\frac{\bar{\rho}^{\text{pol}}}{r_1}ln\bar{\rho}^{\text{pol}}\right]+\frac{P}{\bar{\rho}^{\text{pol}}}\left[2\left(g_1\phi_1^{\text{pol}}+g_2\phi_2^{\text{pol}}+g_3\phi_3^{\text{pol}}+g_4\right)-\right.$$

$$\left.\left.\left(\sigma_1\phi_1^{\text{pol}}+\sigma_2\phi_2^{\text{pol}}+\sigma_3\phi_3^{\text{pol}}+\sigma_4\right)\right]\right\}-\mu_1^{\text{gas}}=0$$

in which the parameters G_1, G_2, G_3, G_4, g_1, g_2, g_3 and g_4 are given by

$$G_1=\upsilon_1^*\varepsilon_1^*-\upsilon_{14}^*\varepsilon_{14}^* \qquad (34.1)$$

$$G_2=\upsilon_{12}^*\varepsilon_{12}^*-\upsilon_{14}^*\varepsilon_{14}^* \qquad (34.2)$$

$$G_3=\upsilon_{13}^*\varepsilon_{13}^*-\upsilon_{14}^*\varepsilon_{14}^* \qquad (34.3)$$

$$G_4 = v_{14}^* \varepsilon_{14}^* \tag{34.4}$$

$$g_1 = v_1^* - v_{14}^* \tag{34.5}$$

$$g_2 = v_{12}^* - v_{14}^* \tag{34.6}$$

$$g_3 = v_{13}^* - v_{14}^* \tag{34.7}$$

$$g_4 = v_{14}^* \tag{34.8}$$

For component *2*, the equilibrium condition is given by

$$R_g T \left[ln\phi_2^{\text{pol}} + 1 - r_2 \left(\frac{\phi_1^{\text{pol}}}{r_1} + \frac{\phi_2^{\text{pol}}}{r_2} + \frac{\phi_3^{\text{pol}}}{r_3} \right) \right] \tag{35}$$

$$+ r_2 \left\{ -\bar{\rho}^{\text{pol}} \left[\frac{2}{\sigma_1\phi_1^{\text{pol}} + \sigma_2\phi_2^{\text{pol}} + \sigma_3\phi_3^{\text{pol}} + \sigma_4} \left(\left(H_1\phi_1^{\text{pol}} + H_2\phi_2^{\text{pol}} + H_3\phi_3^{\text{pol}} + H_4 \right) - \right. \right. \right.$$

$$\left(\frac{A_1\phi_1^{\text{pol}^2} + A_2\phi_2^{\text{pol}^2} + A_3\phi_3^{\text{pol}^2} + A_{12}\phi_1^{\text{pol}}\phi_2^{\text{pol}} + A_{23}\phi_2^{\text{pol}}\phi_3^{\text{pol}} + A_{13}\phi_1^{\text{pol}}\phi_3^{\text{pol}} + B_1\phi_1^{\text{pol}} + B_2\phi_2^{\text{pol}} + B_3\phi_3^{\text{pol}} + C_1}{\sigma_1\phi_1^{\text{pol}} + \sigma_2\phi_2^{\text{pol}} + \sigma_3\phi_3^{\text{pol}} + \sigma_4} \right) \left(h_1\phi_1^{\text{pol}} + \right.$$

$$\left. \left. h_2\phi_2^{\text{pol}} + h_3\phi_3^{\text{pol}} + h_4 \right) \right) +$$

$$\left. \left. \left(\frac{A_1\phi_1^{\text{pol}^2} + A_2\phi_2^{\text{pol}^2} + A_3\phi_3^{\text{pol}^2} + A_{12}\phi_1^{\text{pol}}\phi_2^{\text{pol}} + A_{23}\phi_2^{\text{pol}}\phi_3^{\text{pol}} + A_{13}\phi_1^{\text{pol}}\phi_3^{\text{pol}} + B_1\phi_1^{\text{pol}} + B_2\phi_2^{\text{pol}} + B_3\phi_3^{\text{pol}} + C_1}{\sigma_1\phi_1^{\text{pol}} + \sigma_2\phi_2^{\text{pol}} + \sigma_3\phi_3^{\text{pol}} + \sigma_4} \right) \right] + \right.$$

$$\frac{R_g T}{\bar{\rho}^{\text{pol}}} \left[\left(1 - \bar{\rho}^{\text{pol}} \right) \ln\left(1 - \bar{\rho}^{\text{pol}} \right) + \frac{\bar{\rho}^{\text{pol}}}{r_1} ln\bar{\rho}^{\text{pol}} \right] + \frac{P}{\bar{\rho}^{\text{pol}}} \left[2\left(h_1\phi_1^{\text{pol}} + h_2\phi_2^{\text{pol}} + h_3\phi_3^{\text{pol}} + h_4 \right) - \right.$$

$$\left. \left. \left(\sigma_1\phi_1^{\text{pol}} + \sigma_2\phi_2^{\text{pol}} + \sigma_3\phi_3^{\text{pol}} + \sigma_4 \right) \right] \right\} - \mu_2^{\text{gas}} = 0$$

in which the parameters H_1, H_2, H_3, H_4, h_1, h_2, h_3 and h_4 are given by

$$H_1 = v_{12}^* \varepsilon_{12}^* - v_{24}^* \varepsilon_{24}^* \tag{35.1}$$

$$H_2 = v_2^* \varepsilon_2^* - v_{24}^* \varepsilon_{24}^* \tag{35.2}$$

$$H_3 = v_{23}^* \varepsilon_{23}^* - v_{24}^* \varepsilon_{24}^* \tag{35.3}$$

$$H_4 = v_{24}^* \varepsilon_{24}^* \tag{35.4}$$

$$h_1 = v_{12}^* - v_{24}^* \tag{35.5}$$

$$h_2 = v_2^* - v_{24}^* \tag{35.6}$$

$$h_3 = v_{23}^* - v_{24}^* \tag{35.7}$$

$$h_4 = v_{24}^* \tag{35.8}$$

For component *3*, the equilibrium condition is given by

$$R_g T\left[ln\phi_3^{\text{pol}} + 1 - r_3\left(\frac{\phi_1^{\text{pol}}}{r_1} + \frac{\phi_2^{\text{pol}}}{r_2} + \frac{\phi_3^{\text{pol}}}{r_3}\right)\right] \tag{36}$$

$$+ r_3\left\{-\bar{\rho}^{\text{pol}}\left[\frac{2}{\sigma_1\phi_1^{\text{pol}}+\sigma_2\phi_2^{\text{pol}}+\sigma_3\phi_3^{\text{pol}}+\sigma_4}\left(\left(K_1\phi_1^{\text{pol}} + K_2\phi_2^{\text{pol}} + K_3\phi_3^{\text{pol}} + K_4\right) -\right.\right.\right.$$

$$\left(\frac{A_1\phi_1^{\text{pol}^2}+A_2\phi_2^{\text{pol}^2}+A_3\phi_3^{\text{pol}^2}+A_{12}\phi_1^{\text{pol}}\phi_2^{\text{pol}}+A_{23}\phi_2^{\text{pol}}\phi_3^{\text{pol}}+A_{13}\phi_1^{\text{pol}}\phi_3^{\text{pol}}+B_1\phi_1^{\text{pol}}+B_2\phi_2^{\text{pol}}+B_3\phi_3^{\text{pol}}+C_1}{\sigma_1\phi_1^{\text{pol}}+\sigma_2\phi_2^{\text{pol}}+\sigma_3\phi_3^{\text{pol}}+\sigma_4}\right)\left(k_1\phi_1^{\text{pol}} +\right.$$

$$\left.\left.\left.k_2\phi_2^{\text{pol}} + k_3\phi_3^{\text{pol}} + k_4\right)\right) +\right.$$

$$\left.\left.\left(\frac{A_1\phi_1^{\text{pol}^2}+A_2\phi_2^{\text{pol}^2}+A_3\phi_3^{\text{pol}^2}+A_{12}\phi_1^{\text{pol}}\phi_2^{\text{pol}}+A_{23}\phi_2^{\text{pol}}\phi_3^{\text{pol}}+A_{13}\phi_1^{\text{pol}}\phi_3^{\text{pol}}+B_1\phi_1^{\text{pol}}+B_2\phi_2^{\text{pol}}+B_3\phi_3^{\text{pol}}+C_1}{\sigma_1\phi_1^{\text{pol}}+\sigma_2\phi_2^{\text{pol}}+\sigma_3\phi_3^{\text{pol}}+\sigma_4}\right)\right] +\right.$$

$$\left.\frac{R_g T}{\bar{\rho}^{\text{pol}}}\left[\left(1-\bar{\rho}^{\text{pol}}\right)\ln\left(1-\bar{\rho}^{\text{pol}}\right) + \frac{\bar{\rho}^{\text{pol}}}{r_1} ln\bar{\rho}^{\text{pol}}\right] + \frac{P}{\bar{\rho}^{\text{pol}}}\left[2\left(k_1\phi_1^{\text{pol}} + k_2\phi_2^{\text{pol}} + k_3\phi_3^{\text{pol}} + k_4\right) -\right.\right.$$

$$\left.\left.\left(\sigma_1\phi_1^{\text{pol}} + \sigma_2\phi_2^{\text{pol}} + \sigma_3\phi_3^{\text{pol}} + \sigma_4\right)\right]\right\} - \mu_3^{\text{gas}} = 0$$

in which K_1, K_2, K_3, K_4, k_1, k_2, k_3 and k_4 are clustered functions given by

$$K_1 = v_{13}^*\varepsilon_{13}^* - v_{34}^*\varepsilon_{34}^* \tag{36.1}$$

$$K_2 = v_{23}^*\varepsilon_{23}^* - v_{34}^*\varepsilon_{34}^* \tag{36.2}$$

$$K_3 = v_3^*\varepsilon_3^* - v_{34}^*\varepsilon_{34}^* \tag{36.3}$$

$$K_4 = v_{34}^*\varepsilon_{34}^* \tag{36.4}$$

$$k_1 = v_{13}^* - v_{34}^* \tag{36.5}$$

$$k_2 = v_{23}^* - v_{34}^* \tag{36.6}$$

$$k_3 = v_3^* - v_{34}^* \tag{36.7}$$

$$k_4 = v_{34}^* \tag{36.8}$$

The reduced polymer phase density, $\bar{\rho}^{pol}$, as well as the closed-packed volume fractions of solute components in the polymer phase, ϕ_1^{pol}, $\phi_2^{\text{pol}}$and ϕ_3^{pol} are calculated by solving simultaneously four non-linear equations, (33), (34), (35) and (36).

3. Solubility calculation from SL EoS

In order to calculate the solubility of the different species in the mixture in the polymer, the mass fraction of each specie in the polymer has to be calculated. According to equation (7), the mass fraction of solute *1*, 2 and *3* in the amorphous phase of the polymer can be calculated as follow

$$\omega_1^{\text{am}} = \frac{\rho_1^* v_1^* \phi_1^{\text{pol}}}{\rho_1^* v_1^* \phi_1^{\text{pol}} + \rho_2^* v_2^* \phi_2^{\text{pol}} + \rho_3^* v_3^* \phi_3^{\text{pol}} + \rho_4^* v_4^* \phi_4^{\text{pol}}} \tag{37}$$

$$\omega_2^{\text{am}} = \frac{\rho_2^* v_2^* \phi_2^{\text{pol}}}{\rho_1^* v_1^* \phi_1^{\text{pol}} + \rho_2^* v_2^* \phi_2^{\text{pol}} + \rho_3^* v_3^* \phi_3^{\text{pol}} + \rho_4^* v_4^* \phi_4^{\text{pol}}} = \left[\left(\frac{\rho_2^* v_2^*}{\rho_1^* v_1^*}\right)\left(\frac{\phi_2^{\text{pol}}}{\phi_1^{\text{pol}}}\right)\right]\omega_1^{\text{am}} \tag{38}$$

$$\omega_3^{\text{am}} = \frac{\rho_3^* v_3^* \phi_3^{\text{pol}}}{\rho_1^* v_1^* \phi_1^{\text{pol}} + \rho_2^* v_2^* \phi_2^{\text{pol}} + \rho_3^* v_3^* \phi_3^{\text{pol}} + \rho_4^* v_4^* \phi_4^{\text{pol}}} = \left[\left(\frac{\rho_3^* v_3^*}{\rho_1^* v_1^*}\right)\left(\frac{\phi_3^{\text{pol}}}{\phi_1^{\text{pol}}}\right)\right]\omega_1^{\text{am}} \tag{39}$$

Where the mass fraction of the polymer phase is defined as

$$\omega_4^{\text{am}} = 1 - \omega_2^{\text{am}} - \omega_2^{\text{am}} - \omega_3^{\text{am}} \tag{40}$$

It is important to note that the sorption of solute species is assumed to take place only in the amorphous phase of the polymer, while the crystalline phase is assumed to be impenetrable to the solute species.

The solubility of the different species in the mixture can therefore be calculated as follow

$$S_1^{\mathrm{am}} = \frac{\omega_1^{\mathrm{am}}}{\omega_4^{\mathrm{am}}} \quad (41)$$

$$S_2^{\mathrm{am}} = \frac{\omega_2^{\mathrm{am}}}{\omega_4^{\mathrm{am}}} \quad (42)$$

$$S_3^{\mathrm{am}} = \frac{\omega_3^{\mathrm{am}}}{\omega_4^{\mathrm{am}}} \quad (43)$$

$$S_{123}^{\mathrm{am}} = \frac{\omega_1^{\mathrm{am}} + \omega_2^{\mathrm{am}} + \omega_3^{\mathrm{am}}}{\omega_4^{\mathrm{am}}} \quad (44)$$

$$S_{123}^{\mathrm{tot}} = S_{12}^{\mathrm{am}}(1 - \chi) \quad (45)$$

Where S_i^{am} is the partial solubility of the i^{th} component in the mixture in the amorphous phase of the polymer, S_{123}^{am} and $S_{123}^{\mathrm{tot}}$are the overall solubility of all the species in the mixture in the amorphous phase of the polymer, and in the entire polymer phase (i.e. amorphous and crystalline), respectively.

Appendix B

Homopolymerization of ethylene and characterization of the produced polymer

Experimental set-up

1. Homopolymerization of ethylene

The experiments described in this Appendix were carried out by a phD student in our group research, M. Niyi B. Ishola.

1.1.Materials

Ethylene and hydrogen, with a minimum purity of 99.5%, were obtained from Air Liquide France. Ethylene was passed over columns of zeolite and active carbon for purifying. n-pentane, with a minimum purity of 99%, was obtained from Sigma-Aldrich ICN – Germany. Argon, with a minimum purity of 99.5%, was obtained from Air Liquide France and was used to keep the reaction environment free of oxygen and other impurities. A commercial TiCl4 supported on MgCl2 Zeigler-Natta catalyst was used as the catalytic system with a Ti content of 2.8 wt% for all polymerizations, and triethylaluminium (TEA) was used as co-catalyst. Sodium chloride (NaCl), with a minimum purity of 99.8%, was carefully dried and used as a seedbed to disperse the catalyst particles.

1.2.Experimental set-up

The gas-phase polymerization experiments are performed in a spherical stirred-bed semi-batch reactor. The reactor operates at a pressure up to 25 bar and temperatures up to 90°C. The reactor is heated by a circulating water through an external jacket, and is equipped with temperature and pressure sensors, vacuum pump and recording computer. This stirred-bed reactor operates in semi-batch mode, meaning that all components involved in the polymerization reaction (i.e. ICA, hydrogen, catalyst, salt) are added to the reactor, and only ethylene is supplied continuously to the reactor during the entire time of the reaction in order to maintain a constant pressure. The detailed experimental set-up and measuring procedure are given elsewhere[1–3].

The rate of polymerization was recorded by measuring the pressure drop of ethylene in the ballast, corresponding to the consumption of ethylene during the entire time of the polymerization. The pressure drop in the ballast was then converted into a molar flow rate using the Soave-Redlich-Kwong (SRK) cubic equation of state.

The experiments performed used 7 bar of ethylene, 0-2 bar of n-pentane and 0 and 3 bar of hydrogen, at 80°C. The experimental conditions of the different studied experiments are given

in Table 1. The experimental results for the homopolymerization without hydrogen are given in Figure 1 and with 3 bar of hydrogen in Figure 2.

Table 44. Ethylene, n-pentane and hydrogen partial pressure for each homopolymerization experiment. All pressures are in bar.

	R_{p1}	R_{p2}	R_{p3}	R_{p4}	R_{p5}
P_{C_2}	7				
P_{C_5}	0	1	2	0	2
P_{H_2}	0			3	

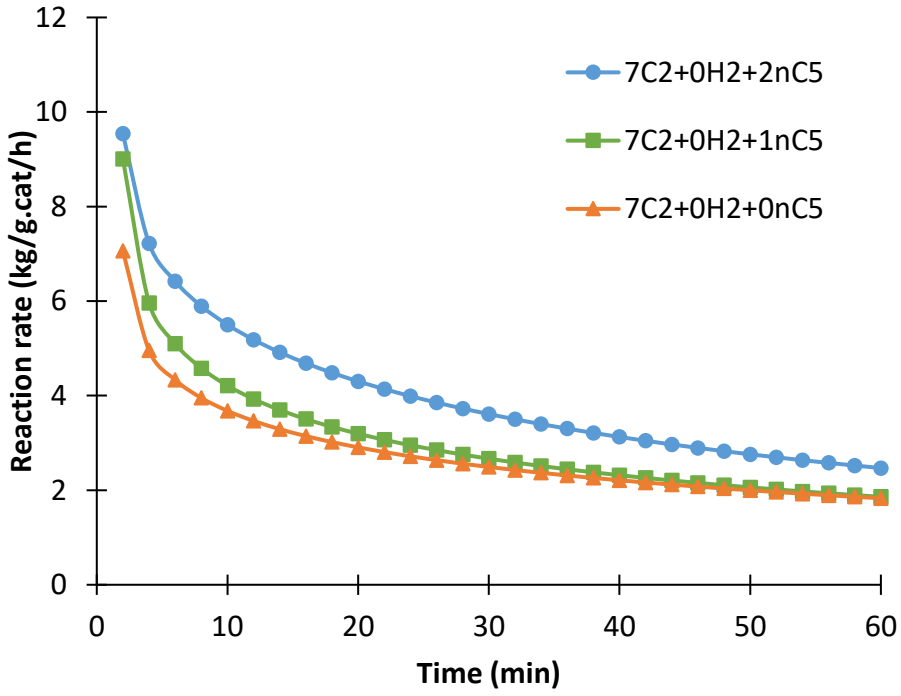

Figure 150. Polymerization rate duting the reaction time for 7 bar of ethylene, 0, 1 and 2 bar of n-pentane and without hydrogen, at 80°C

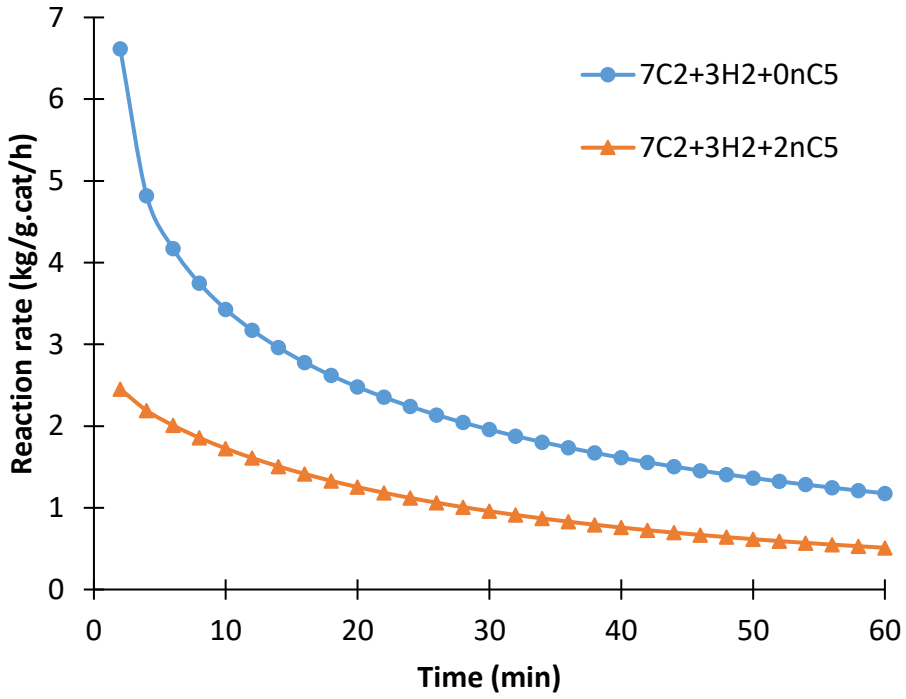

Figure 151. Polymerization rate duting the reaction time for 7 bar of ethylene, 0, 1 and 2 bar of n-pentane and 3 bar of hydrogen, at 80°C

2. Molecular weight distribution of the polymer

Molar mass measurements of polyethylene (PE) were performed using a Viscotek 350A High-Temperature Triple Detection GPC (HT-GPC) system (Malvern Instruments). The system is equipped with a differential refractive index, static light scattering RALS (90°) and LALS (7°) and a viscometer detector. The set of columns used comprises a pre-column, followed by three Waters Styragel HT6E columns in series having a mass detection range of 500 – 4,200,000 g/g mol (equivalent to Polystyrene - PDI = 1.01). Columns and detectors were maintained at 150 °C. 1,2,4-Trichlorobenzene (TCB) was used as the mobile phase at a flow rate of 0.6 mL min^{-1}. TCB was stabilized with 2,6-di(tert-butyl)-4-methylphenol. The volume of the samples used is 200 µL with concentrations of 3 mg mL^{-1}. The Omnisec software was used for data acquisition and data analysis. The molecular weight distributions (MWD) were calculated by means of a conventional calibration curve on the basis of linear polyethylene standards from 300 to 130 000 g mol^{-1} (Polymer Standards Service). The obtained MWDs of the produced polymer are shown in Figure 3.

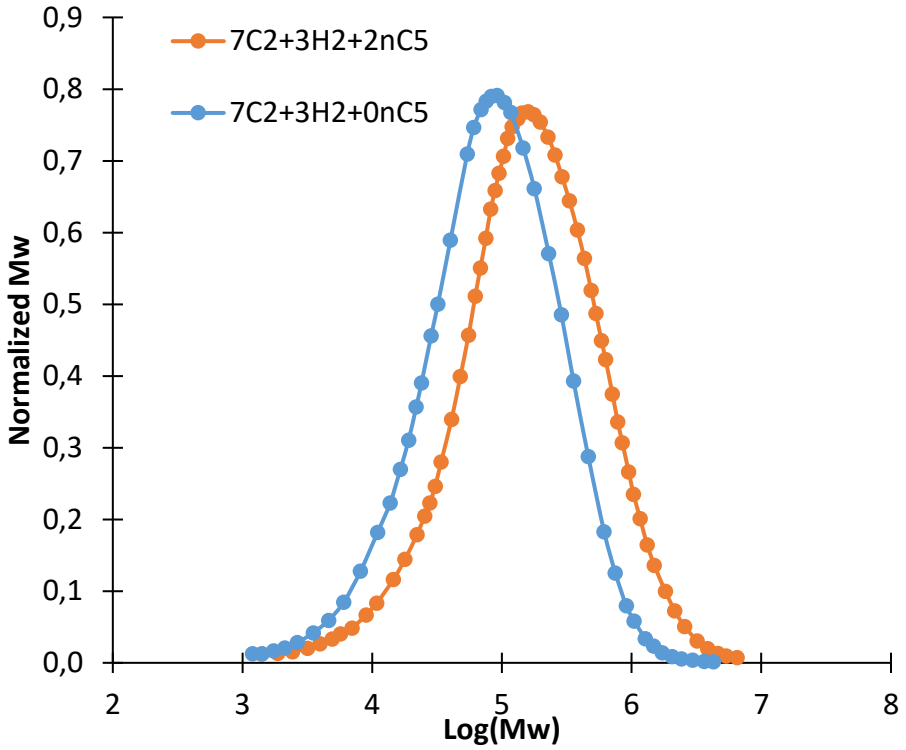

Figure 152. Molecular weight distribution calculated using HT-GPC for polymer produced with 7 bar of ethylene, 3 bar of hydrogen and 0 and 2 bar of n-pentane at 80°C.

2.1.Crystallinity of the polymer

The crystallinity of the polymer samples was measured using differential scanning calorimetry (DSC 3+ by Mettler Toledo). Polyethylene samples were weighed (i.e. around 5-7 mg) and placed in an aluminium capsule with a volume of 40 µL. The sample was first cooled to -20°C and then heated from −20 to 180 °C at a heating rate of 10°C min^{-1}, held for 5 minutes at that temperature and then cooled from 180 to −20 °C at a rate of 10°C min^{-1}. This temperature was also maintained for 5 minutes, and the sample was reheated to 180°C at a rate of 10°C min^{-1}. The melting behavior of the samples was studied in the second heating step in order to detect the melting point and the melting enthalpy of the sample. The ratio of the melting heat of the sample and the melting heat of the completely crystallized polyethylene was used to calculate the degree of crystallization. A melting heat of 293 J g^{-1} for completely crystallized polyethylene was used for the calculation. The STARe software was used for data acquisition and data analysis. The crystallinity of the produced PE from the homopolymerization of ethylene in presence of n-pentane was measured equal to 45%.

3. References

1. Andrade, F. N. de. Effect of condensable materials during the gas phase polymerization of ethylene on supported catalysts. (Université de Lyon, 2019).

2. Andrade, F. N. & McKenna, T. F. L. Condensed Mode Cooling for Ethylene Polymerization: Part IV. The Effect of Temperature in the Presence of Induced Condensing Agents. *Macromol. Chem. Phys.* **218**, 1700248 (2017).

3. Ishola, N., Andrade, F. N., Machado, R. & McKenna, T. F. L. Condensed Mode Cooling for Ethylene Polymerization: Part VI. Impact of Induced Condensing Agents on Comonomer Incorporation.